SUSTAINABILITY ASSESSMENT OF POWER

PRODUCTION BY CHEMICAL LOOPING

COMBUSTION

Miss Watchara Uraisakul

จุฬาลงกรณ์มหาวิทยาลัย
CHULALONGKORN UNIVERSITY

A Dissertation Submitted in Partial Fulfillment of the Requirements

for the Degree of Doctor of Philosophy in Chemical Technology

Department of Chemical Technology

FACULTY OF SCIENCE

Chulalongkorn University

Academic Year 2020

การประเมินความยั่งยืนของการผลิตไฟฟ้าโดยการเผาไหม้แบบเคมิคอลลูปิง

น.ส.วัชรา อุไรสกุล

วิทยานิพนธ์นี้เป็นส่วนหนึ่งของการศึกษาตามหลักสูตรปริญญาวิทยาศาสตรดุษฎีบัณฑิต
สาขาวิชาเคมีเทคนิค ภาควิชาเคมีเทคนิค
คณะวิทยาศาสตร์ จุฬาลงกรณ์มหาวิทยาลัย
ปีการศึกษา 2563

Thesis Title	SUSTAINABILITY ASSESSMENT OF POWER PRODUCTION BY CHEMICAL LOOPING COMBUSTION
By	Miss Watchara Uraisakul
Field of Study	Chemical Technology
Thesis Advisor	Professor PORNPOTE PIUMSOMBOON, Ph.D.
Thesis Co Advisor	Associate Professor BENJAPON CHALERMSINSUWAN, Ph.D.

Accepted by the FACULTY OF SCIENCE, Chulalongkorn University in Partial Fulfillment of the Requirement for the Doctor of Philosophy

.... Dean of the FACULTY OF SCIENCE

(Professor POLKIT SANGVANICH, Ph.D.)

DISSERTATION COMMITTEE

.... Chairman

(Associate Professor PRASERT REUBROYCHAROEN, Ph.D.)

.... Thesis Advisor

(Professor PORNPOTE PIUMSOMBOON, Ph.D.)

.... Thesis Co-Advisor

(Associate Professor BENJAPON CHALERMSINSUWAN, Ph.D.)

.... Examiner

(Associate Professor PRAPAN KUCHONTHARA, Ph.D.)

.... Examiner

(Professor SUTTICHAI ASSABUMRUNGRAT, Ph.D.)

.... External Examiner

(Associate Professor Thumrongrut Mungcharoen, Ph.D.)

วัชรา อุไรสกุล : การประเมินความยั่งยืนของการผลิตไฟฟ้าโดยการเผาไหม้แบบเคมิคอลลูปิง. (SUSTAINABILITY ASSESSMENT OF POWER PRODUCTION BY CHEMICAL LOOPING COMBUSTION) อ.ที่ปรึกษาหลัก : ศ. ดร.พรพจน์ เปี่ยมสมบูรณ์, อ.ที่ปรึกษาร่วม : รศ. ดร. เบญจพล เฉลิมสินสุวรรณ

งานวิจัยนี้ได้ศึกษาการปรับปรุงประสิทธิภาพของกระบวนการเคมิคอลลูปิงสำหรับการผลิตไฟฟ้า ซึ่งเป็นการพัฒนาใน 3 แนวทางนั่นคือ การจัดการพลังงาน อุทกพลศาสตร์ของเครื่องปฏิกรณ์ และความยั่งยืนของกระบวนการ ในส่วนแรก นำการออกแบบการทดลองแบบ 3^k แฟกทอเรียลมาใช้เพื่ออธิบายผลกระทบของตัวแปรดำเนินการที่มีต่อประสิทธิภาพเชิงความร้อนของกระบวนการเคมิคอลลูปิงที่ดำเนินการควบคู่กับวัฏจักรแก๊สอากาศชื้นอย่างเป็นระบบ โดยชุดตัวแปรดำเนินการอันประกอบด้วย A) ความดันของเครื่องปฏิกรณ์อากาศ B) จำนวนขั้นของการอัดอากาศ C) วิธีการดำเนินการของการอัดอากาศ และ D) อัตราการไหลของอากาศ จากการศึกษาพบว่า ค่าประสิทธิภาพความร้อนมีค่าสูงสุดที่ได้คือ 55.87 % ที่ภาวะของการดำเนินการ (A) 15 บรรยากาศ (B) 7 ขั้น (C) แบบที่ 3 และ (D) 61,000 กิโลโมล/ชั่วโมง นอกจากนั้นยังพบว่า สามารถเพิ่มค่าประสิทธิภาพเชิงความร้อนให้มีค่าสูงขึ้นเป็น 57.67% ด้วยการเพิ่มปริมาณของนิกเกิลบนตัวรองรับอะลูมินาเป็น 28% ในส่วนที่สอง เลือกใช้เครื่องปฏิกรณ์ฟลูอิไดซ์เบดหมุนเวียนแบบสองหอสำหรับกระบวนการเคมิคอลลูปิงและศึกษาการเดินกระบวนการผ่านการจำลองพลศาสตร์ของไหลเชิงคำนวณแบบ 2 มิติ ผลการศึกษาสำหรับเชื้อเพลิงของแข็งพบว่า ที่ภาวะอุณหภูมิต่ำและอัตราส่วนระหว่างความเร็วของถ่านหินต่อน้ำหนักของตัวพาออกซิเจนต่ำ เป็นภาวะที่ให้ประสิทธิภาพสูงที่สุด ส่วนผลของการศึกษาสำหรับเชื้อเพลิงแก๊ส พบว่า ตัวแปรพรีเอกซ์โพเนนเชียลที่มีค่าสูง อัตราส่วนโดยปริมาตรของของแข็งที่มีค่าต่ำ ความเร็วที่มีค่าต่ำ และอัตราส่วนโดยมวลของมีเทนในสายป้อนเข้าที่มีค่าต่ำ จะส่งผลให้อุณหภูมิและการเกิดปฏิกิริยามีค่าสูงขึ้น จากการศึกษาพบว่า ภาวะดำเนินการเป็นปัจจัยที่สำคัญอย่างมากต่อการเกิดอุทกพลศาสตร์ที่เหมาะสมภายในเครื่องปฏิกรณ์ ในส่วนสุดท้ายของงานวิจัย ทำการประเมินหากรณีศึกษาที่ดีที่สุดในมิติของความยั่งยืนของกระบวนการเคมิคอลลูปิง โดยใช้การวิเคราะห์ 3 แบบ ได้แก่ การประเมินทางประสิทธิภาพความร้อน การประเมินทางเศรษฐศาสตร์ และการประเมินความยั่งยืน กรณีศึกษาที่ทำการประเมินมีทั้งสิ้น 6 กรณี ซึ่งครอบคลุมอิทธิพลของรูปแบบของการเผาไหม้ (การเผาไหม้แบบปกติ และเคมิคอลลูปิง) และลักษณะกระบวนการ (จำนวนชั้นของเครื่องปฏิกรณ์ดักจับ CO_2 และภาวะดำเนินการ) จากการวิเคราะห์โดยเอเมอร์จีซึ่งเป็นเครื่องมือวิเคราะห์ในแบบองค์รวมมากกว่าวิธีการอีกสองวิธี กรณีที่ 4 ให้ค่าความยั่งยืนสูงสุด เมื่อพิจารณาการใช้ทรัพยากรพื้นถิ่น ในขณะที่กรณีที่ 5 ให้ค่าการใช้ทรัพยากรของโลกต่ำที่สุด

สาขาวิชา	เคมีเทคนิค	ลายมือชื่อนิสิต ....
ปีการศึกษา	2563	ลายมือชื่อ อ.ที่ปรึกษาหลัก ....
		ลายมือชื่อ อ.ที่ปรึกษาร่วม ....

5772886623 : MAJOR CHEMICAL TECHNOLOGY

KEYWORD: chemical looping combustion, thermal efficiency, hydrodynamic behavior, sustainability assessment, emergy

Watchara Uraisakul :
SUSTAINABILITY ASSESSMENT OF POWER PRODUCTION BY CHEMICAL LOOPING COMBUSTION. Advisor: Prof. PORNPOTE PIUMSOMBOON, Ph.D. Co-advisor: Assoc. Prof. BENJAPON CHALERMSINSUWAN, Ph.D.

This study investigated the chemical looping combustion (CLC) process improvement for power production from energy management, system hydrodynamics, and sustainability perspectives. In the first part, the 3^k factorial design was used for systematically investigating the operating variables that affect the thermal efficiency of the CLC combined with the humid air gas turbine (HAT) cycle. A set of operating variables, A) pressure of the air reactor, B) air compressor stages number, C) air compression methods, and D) air flow rate, were explored. The result showed that the highest thermal efficiency was at 55.87 % when operated at (A) 15 atm, (B) 7 stages, (C) method 3, and (D) 61,000 kmol/hr. Moreover, the efficiency could be improved further to 57.67% by increasing the Ni loading to 28% (by weight). The second part, the dual circulating fluidized bed reactor (DCFBR), was selected for the CLC system and investigated its operation by 2-D computational fluid dynamics (CFD) simulation. For the solid fuel, the result showed that the low value of temperature and ratio of coal velocity to the weight of an oxygen carrier provided the best performance. For the gaseous fuel, the high pre-exponential factor, the low initial solid volume fraction, velocity, and CH_4 mass fraction in feed increased temperature and conversion. The result also indicated that the operating conditions are crucial for suitable hydrodynamics achievement and the CO_2 capture efficiency. In the last part, three analyses, which were energy performance, economics, and sustainability, were evaluated to identify the best case by enhancing the process sustainability. Six case studies have been investigated the effects of the combustion types (conventional combustion (CC) and CLC) and system configuration (CO_2 capture stages and operating conditions). According to emergy analysis, which is the tool that gives a more holistic view of the solution than the others, Case 4 was the best case due to its emergy sustainability index (ESI), when local content was taken into consideration. However, Case 5 would be the best case from a global perspective.

Field of Study:	Chemical Technology	Student's Signature	
Academic Year:	2020	Advisor's Signature	
		Co-advisor's Signature	

ACKNOWLEDGEMENTS

TABLE OF CONTENTS

LIST OF TABLES

Pages

จุฬาลงกรณ์มหาวิทยาลัย
CHULALONGKORN UNIVERSITY

LIST OF FIGURES

Chapter 4

Chapter 6

จุฬาลงกรณ์มหาวิทยาลัย

CHULALONGKORN UNIVERSITY

Chapter 1
Sustainability assessment of power Production by chemical looping combustion

1.1.Background

A greenhouse gas, mostly CO_2, has been the most released gas from power production processes. Although the reduction of energy consumption is the true solution of this crisis, it is complicated to carry out because of the economic growth and population increase. Thus, one is searching for a technology that could provide power and heat with minimal impact to the environment. Chemical looping combustion (CLC) is a novel technology that could help the issue of CO_2 management. With this technology, the power generation will be more efficient and environmentally friendly. The CLC has two reacting units connecting each other, air and fuel reactors. In the air reactor, metal is oxidized by the air to produce metal oxide as an oxygen carrier. The oxygen carrier is transported from the air reactor to the fuel reactor and combusts directly with fuel. The products of the combustion are heat, steam, and carbon dioxide which is easily to separate. Carbon dioxide is separated from steam by condensation. Finally, the spent oxygen carrier is returned to regenerate in the air reactor. The carbon dioxide, which is high purity, will be sent to the storage. The power production system that is sustainable will not only supply to meet the demand, but also create positive impact to environment.

This study investigates operating conditions that will provide the highest efficiency of power production. The optimal operation condition of the CLC will increase the power production and worthiness of fuel usage. After obtaining the operating condition for the maximum power production, the hydrodynamics of CLC reactor was investigated further. The hydrodynamics data of the reactors were used to estimate the geometry of the reactors. However, the maximum thermal efficiency is not sufficient conclusion for sustainable investment. Eventually, the decision for construction and operation of a plant will have to consider both profit and environmental impact. The economic and sustainable analyses will be evaluated for the best decision. There are various methods for sustainability assessment. The emergy analysis is a novel method for sustainability assessment. The method considers the impacts of materials, energy, money, and manpower on producing a product or services.

1.2. Objectives

1.2.1. Study effect of operating conditions on power production with CLC process

1.2.2. Develop dual circulating fluidized bed reactor for CLC

1.2.3. Study economic feasibility and emergy analysis

1.3. Scope of the investigation

Part I

- The power production by chemical looping combustion with humid air gas turbine (HAT) cycle without CO_2 utilization

Part II

- The 2-dimensional model of the dual circulating fluidized bed reactor (DCFBR) with full loop simulation for chemical looping combustion

Part III

- The economic and sustainability analyses of a power plant at 50 MW (electrical) when it was located on Thailand

1.4. Benefit

Part I

- The guideline for operating significant parameters to obtain the highest thermal efficiency.
- The investigation of the multi-stage compressor operation on the thermal efficiency of the system.
- The investigation of the work and heat integration of the CLC process for power production.

Part II

- The complete-loop of DCFBR model for chemical looping combustion.
- The proper operating condition to obtain the suitable hydrodynamics behavior in DCFBR.

Part III

- The comparison of 3 analyses; thermal efficiency, economic analysis and sustainability analysis.

- The sustainability comparison between the conventional combustion and chemical looping combustion.
- The guideline of the operation condition to achieve high sustainability.

1.5. Methodology

The sustainability evaluation of chemical loping combustion for power production was divided into 3 parts.

Part I: The operation conditions for obtaining the optimal thermal efficiency of the system.

The 3^k factorial design was used to systematically conduct the experiment. All case studies were simulated by Aspen plus program version 8. 8 at steady state condition. The four independent parameters were investigated including of pressure of air reactor, number stages of air compressors, methods of air compression and air flow rate. Four responses to be observed were thermal efficiency, power production from air reactor, work of air compressors and air compressor discharge temperature. The result in this part will be used as preliminary data for obtaining the optimum thermal efficiency in power production. After that, the optimum conditions were used to in next part.

Part II: The hydrodynamics of dual fluidized bed reactor for chemical looping combustion reactor

The result from part I was the optimum operating condition of the investigated process. For this part, the hydrodynamics inside the CLC reactor were investigated. The DCFBR model was developed by using the Ansys Fluent version 19. 2. The model was used to gain the understanding of hydrodynamics and to estimate the size of chemical looping combustion reactor.

Part III: The economic analysis and sustainability evaluation of chemical looping combustion

The suitable case studies were selected from part I. The material and energy data from part I were used to conduct in economic and sustainability analyses. The capital and operating costs in economic analysis were calculated by using the process information obtained from part I. The emergy flow in sustainability analysis was also calculated by using the process information from part I. The size of reactor from part

II will affect to the purchased cost in this part. Furthermore, the sustainability evaluation of the CLC and conventional combustion were compared. The result from this part was the way to improve the chemical looping combustion process for power production.

Chapter 2
Literature reviews

Electricity is one of the public utilities. It is a form of energy that is convenient to utilize. As a result of the population increase and economic growth, the trend of electricity demand is continuously increased. [1] The United States Environmental Protection Agency (EPA) reported that CO_2 was the highest species of greenhouse gas of U.S. [2] In addition, the international energy agency (IEA) reported that the power production was the potent source of greenhouse gas emissions of Thailand and World as shown in Fig. 2.1. [3]
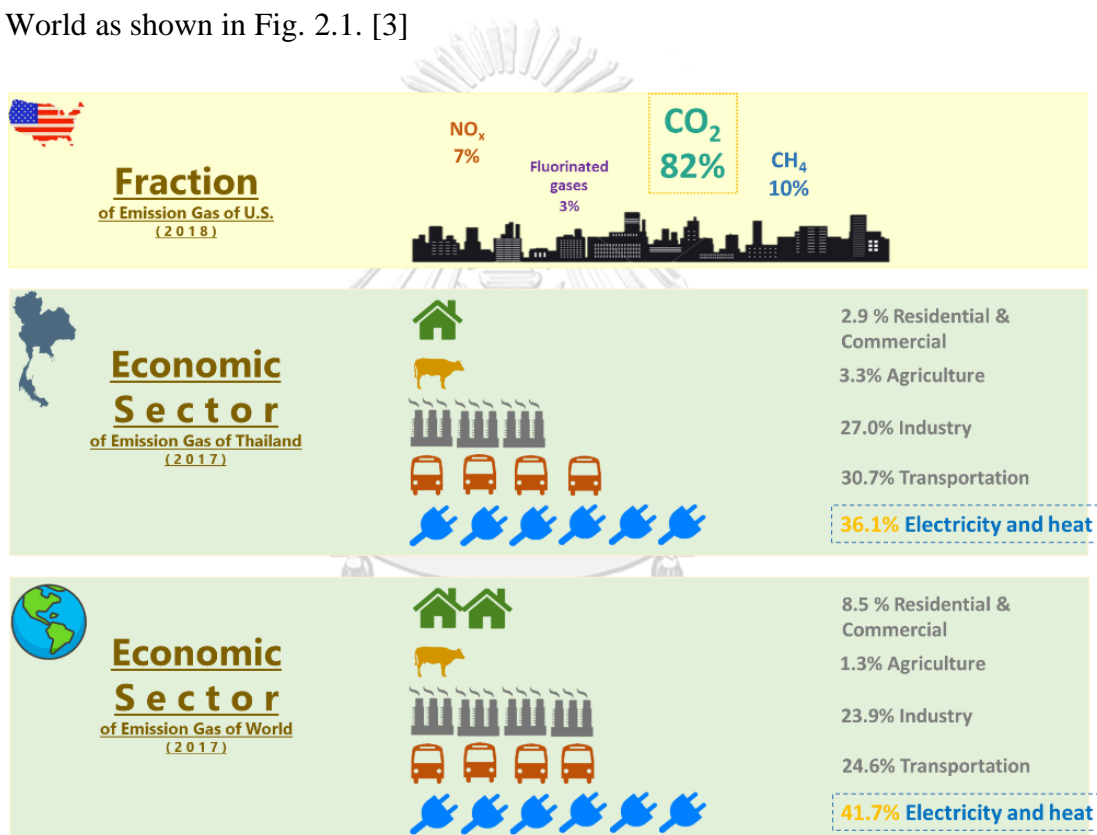
Fig. 2.1 Emission of greenhouse gas. [2, 3]

Accordingly, the power production for supporting the society demand is the reason of the global warming crisis. CO_2 is the highest fraction of the greenhouse gas. Electricity is directly produced by combusting a fuel (natural gas, coal, or fuel oil) with air in a combustion chamber to produce hot gas that is used to drive a gas turbine or to produce steam and use produced steam to drive turbine and a generator.

Therefore, the fuel combustion is typically the main source that releases large amount of CO_2 to the atmosphere and accelerates global warming effect. The quantity of the CO_2 in the flue gas that is released to the environment depends on the efficiency of a CO_2 capture process.

The environmental crisis and the natural resource depletion are key factors that stimulate the development of combustion technology and CO_2 mitigation technology. In the conventional combustion, fuel and air reacts with each other directly. For a power generation, its system efficiency without carbon capture and storage system (CCS) is only 25%.[4] Therefore, the thermal process to produce electricity should be improved to be more efficient and the process should also become a greener electricity production. There are several power production systems that have high energy conversion efficiency. The efficiency of the gas turbine combined cycle (GTCC) is 60%. After the post-combustion process, the efficiency is reduced by 8-10% due to energy penalty in CO_2 capture operation. [5]. The combined cycle of natural gas without the carbon capture and storage (CCS) has the efficiency of 58% , but the CCS process will reduce its efficiency by 10% [6] [7]. The technology for CCS is developed to reduce the CO_2 release to the environment. There are several CO_2 sequestrations available, such as pre-combustion, post-combustion and oxy-combustion technologies as shown in Fig. 2.2.

จุฬาลงกรณ์มหาวิทยาลัย
CHULALONGKORN UNIVERSITY
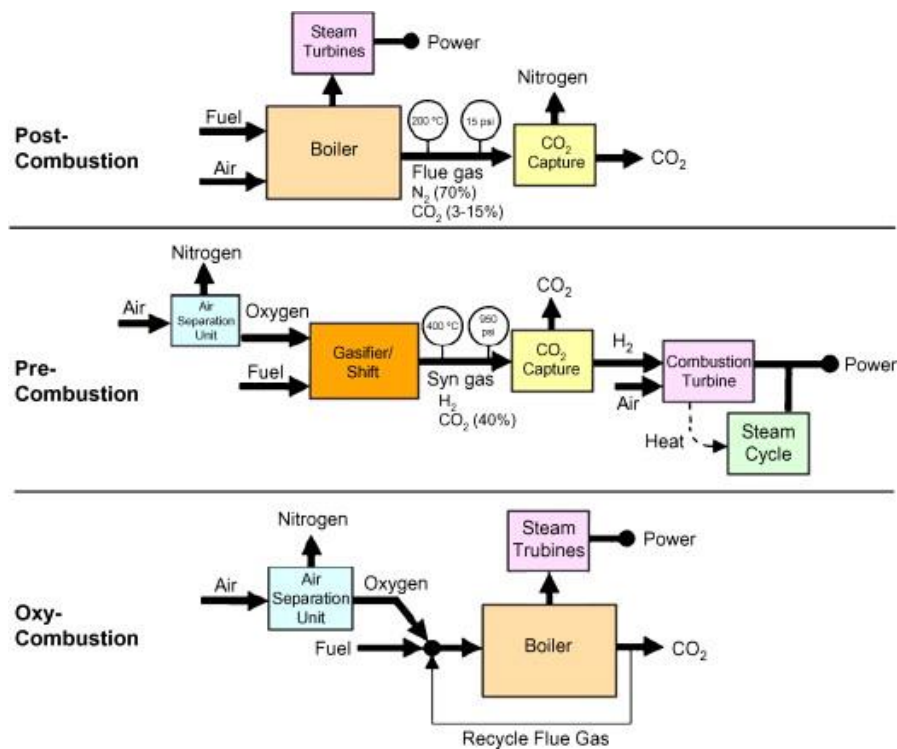
Fig. 2.2 The configuration of post-combustion, pre-combustion and oxy-combustion processes. [8]

2.1. The types of CO_2 sequestrations

2.1.1. Post-combustion processes

It is used to capture CO_2 in flue gas after combustion by sorbents such as K_2CO_3 and MEA. This process has high efficiency in capturing CO_2 (more than 90%) depending on conditions or operations and reactors. The advantages of this method are high efficiency in capturing CO_2, low cost investment, and no change of the original plant. [9] K_2CO_3 is a promising solid sorbent for CO_2 capture process from flue gas because of high economic performance and stable capture performance. In addition, K_2CO_3 requires low energy for regeneration. [10] The CO_2 is captured by K_2CO_3 at 60-80°C and the sorbent can be regenerated at 120-200°C. [11] When comparing monoethanolamine (MEA) and K_2CO_3 processes, it was found that the K_2CO_3 process was lower heat of absorption and lower cost of investment. [12] Even though, amine absorption process is the mature of CO_2 capture process, [13] its main disadvantages are high energy consumption and material corrosion. [13] On the contrary, K_2CO_3 was the good candidate of CO_2 capture process because of high CO_2

capture efficiency, high cyclic usage, and low energy requirement for the adsorption. [14, 15] In this study, solid sorbent CO2 capture process was selected for the power production case studies. because it was the best process in term of sustainability aspect for CO_2 capture process. [16]

The implement of a post-combustion CO_2 capture process with solid sorbents reduces the overall efficiency of power plants by 8.2–14.0%, mainly due to the solid sorbent regeneration section. [17] The type of post-combustion sequestration that provides the highest CO_2 capture efficiency is physical adsorption, because it is a reversible process. [16, 18, 19] The challenge of the post-combustion process is the operating condition at ambient pressure which is lower than the requirement of CO_2 compression. [8]

2.1.2. Pre-combustion processes

It is used to capture CO_2 of fuel gas before combustion. This method widely uses in integrated gasification combined cycle (IGCC) and hydrogen (H_2) production. There are two main unit operations: air separation unit (ASU) and gasification unit. ASU produces high purity of oxygen (O_2) and sends to a gasifier. Syngas is produced by the gasifier at high temperature and high pressure. H_2O is fed into a reactor for reacting with CO to produce H_2 and CO_2. After that CO_2 is separated from H_2 by acid gas removal system. H_2 is used as fuel for power generation or other processes. This method produces high purity of H_2, CO_2 and heat. The advantages of pre-combustion process are the high concentrated of CO_2 in syngas, operation condition at high pressure and lower energy consumption for CO_2 compression. [8] Moreover, the problem and challenge of pre-combustion process was to separate the undesired gases from syngas, especially CO_2. [20] In addition, this technology was suitable for a new plant more than apply to the existing plant. However, ASU and gasifier require high energy and high-cost investment. Accordingly, this technology was mostly investigated in a small-scale plant. [21]

2.1.3. Oxy-fuel combustion processes

It is used to capture pure CO_2 in flue gas by using pure O_2 to combust with a fuel instead of air. This method widely uses in a combustion process. The oxy fuel combustion has 3 main units of energy penalty installed : an air separation unit

(ASU), a compression unit and a purification unit (CPU). [22] ASU produces high purity of O_2 and sends to combustion chamber. The flue gas composes with CO_2 and H_2O. The 2/3 of total flue gas was recycle into combustion reactor for temperature maintaining because the material cannot be tolerated with high temperature from the combustion with pure O_2. [23] H_2O is separated from flue gas by condensation. Accordingly, it can separate very high CO_2 concentration from flue gas. [8] The efficiency of this system is reduced due to the energy consumed in these units by 10-12% . The challenge of oxy-fuel combustion process is high energy consumption and high cost investment in the ASU requirement. [8] Each type of the CO_2 capture process has different advantages and disadvantages.

The achievement of a CCS depends on the competence of the safety at the storage that it is not hazardous to the ecosystem. [23] The efficiency of a natural gas combined cycle before the CO_2 capture process was reported to be 60%, whereas the efficiency of the process with a post-combustion, pre-combustion and oxy-combustion processes are 50%, 46% and 48%, respectively, with 85–90% CO_2 removal. [7] In three technologies, it consumed additional energy which led to the reduction of the process efficiency.

2.2. Chemical looping combustion

Chemical looping combustion (CLC) is a novel technology that could help the issue of CO_2 management. With this technology, the power generation will be environmentally friendly and be more efficient due to less energy penalty for the CCS. The CLC was the oxy-fuel combustion process that was developed for commercialization. [8] The resemblance between CLC and oxy-fuel is the reaction between only O_2 and fuel. Oxygen carrier is the media that only carries the O_2 from the air to oxidize with the fuel.

Mostly, the CLC has two reactors connecting to each other, air and fuel reactors. The principal of the CLC was showed in Fig. 2.3. In the air reactor, a metal is oxidized by the air to produce metal oxide as an oxygen carrier. The oxygen carrier is transported from the air reactor to the fuel reactor and combusted directly with the fuel. The products of the combustion are heat, steam, carbon dioxide which is easily to separate from the combustion gas, as shown in Eq. 2.1 and Eq. 2.2. There are 2

main components in flue gas which are CO_2 and H_2O. The water is separated from the flue gas by condensation and the remainder is high purity of CO_2. Finally, the spent oxygen carrier is returned to regenerate in the air reactor and the process is continued as a cycle. The CLC process is a high thermal efficiency for the power production, not because pure O_2 is needed. It was because of the easiness of the CO_2 separation in the flue gas. [24] The CLC process that use H_2 as a fuel obtained very high thermal efficiency: 63.5%. [25] The efficiency of the CLC with combined cycle is 51% and increase to 53% when increased the temperature from 1,000 °C to 1,200 °C. [26] When increased the gas pressure by using multiple pressure levels of the turbines, one could utilize the heat in the exhausted gas from the turbines, reduce the loss of energy and increase the process efficiency. The maximum efficiency of Ibrahim's study was 55.2% [27] and Brandvoll's study was 55.9 [28]
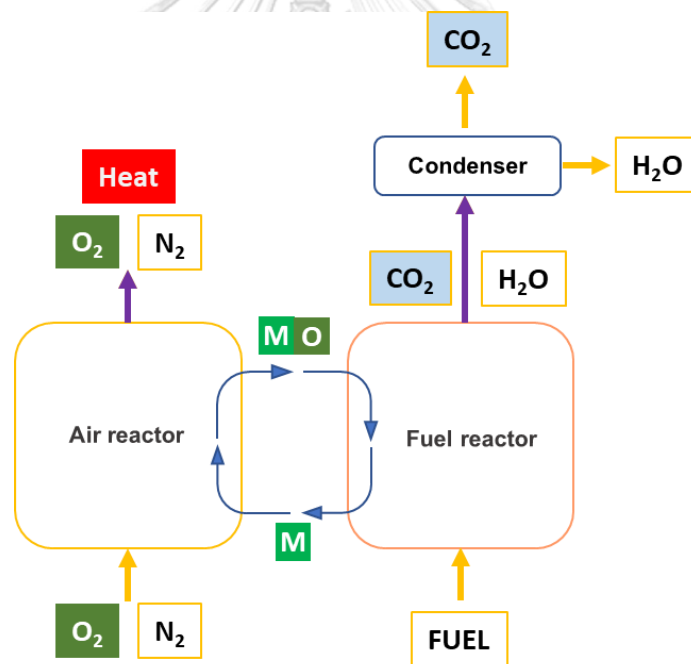
Fig. 2.3 Principle of Chemical looping combustion (CLC). [29]

Reaction in air reactor: $Ni + 0.5O_2 \rightarrow NiO$ (2.1)

Reaction in fuel reactor: $CH_4 + 4NiO \rightarrow CO_2 + 2H_2O + 4Ni$ (2.2)
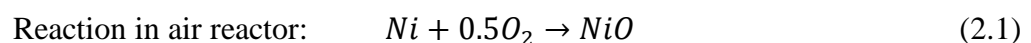
2.2.1. The classified CLC by number of main reactors.

When classified the CLC types by the number of the main reactors, there were 3 types; two, three and multi-reactors.

2.2.1.1. The two reactors system

The process consisted of air reactor and fuel reactor as mentioned above. The oxidation reaction occurred in the air reactor. The reduction reaction occurred in the fuel reactor, as shown in Fig. 2.4.
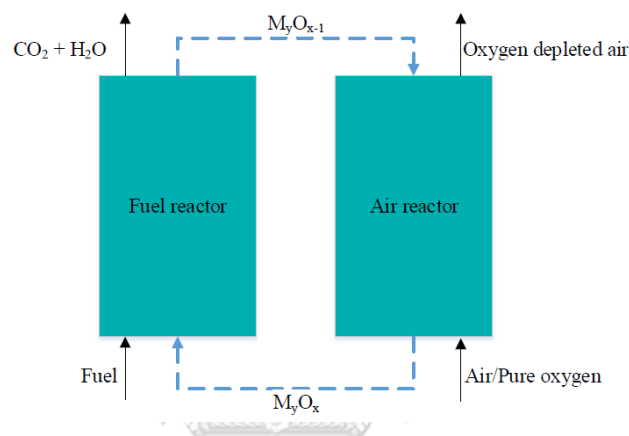
Fig. 2.4 The two reactors of the CLC system. [30]

2.2.1.2. The three reactors system

This system is consisted of air reactor, fuel reactor and steam reactor, as shown in Fig.2.5. The steam reactor was used to produce H_2. [31] Firstly, fuel was reacted with oxygen carrier (M_yO_x) in the fuel reactor. The products of the first step were CO_2, H_2O and spent oxygen carrier (M_yO_{x-2}). Next, steam was reacted with the spent oxygen carrier (M_yO_{x-2}) in the steam reactor. The products of this step were H_2, excess H_2O and partially oxidized oxygen carrier (M_yO_{x-1}). The last step, the partially oxidized oxygen carrier (M_yO_{x-1}) was reacted with compressed air in the air reactor. The products of this step were oxygen carrier (M_yO_x) and the excess air. After that the partially oxidized oxygen carrier (M_yO_{x-1}) was regenerated and was used in a cyclic system again. The H_2O from the fuel reactor and the steam reactor were separated by the condensation process. The high purity of CO_2 and H_2 were obtained. The iron was also used as an oxygen carrier that might be suitable for this process. [31]
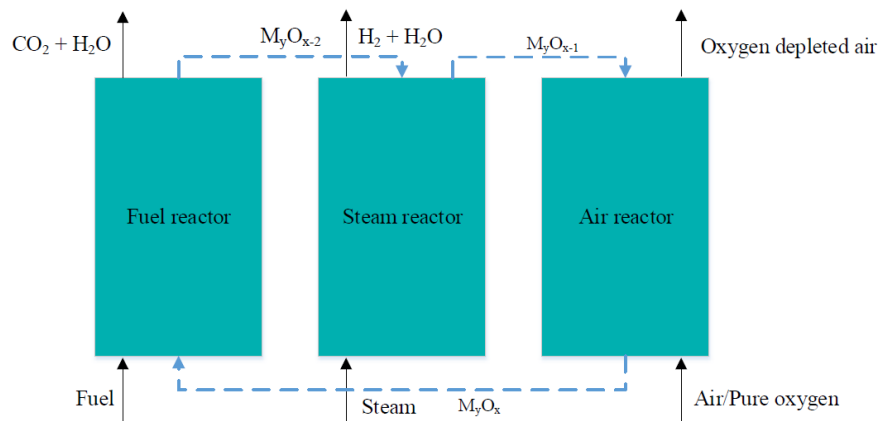
Fig. 2.5 The three reactors of a CLC system. [30]

2.2.1.3. The multi-reactors system

The configuration of this system was the repeat of two reactors system. For instance, there were 2 fuel reactors and 2 air reactors for combustion section. The configuration of reactors were parallel or series which it depended on the types of reactor. [30]

When classified the CLC types by the system of power production, there were 2 types; electro-chemical and thermo-mechanical.

2.2.2. The CLC using with a fuel cell

2.2.2.1. Solid oxide fuel cell (SOFC)/chemical looping-based system

Firstly, coal was gasified by gasification media; CO_2 and O_2 at gasifier reactor, when coal was used as the fuel of the system. The product of this process was syngas. After that, the syngas was introduced into the anode side of a SOFC. On the other hand, if the process was introduced by gaseous fuel; syngas or natural gas, the gaseous fuel would be introduced into the anode side of the SOFC without gasification step. The example of reactions at the anode were shown in Eqs. 2.3, 2.4 and 2.5, when the inlet gas including of CH_4, CO and H_2. [32, 33] The main reaction at the anode was the oxidation reaction of H_2 where H_2 lost its electrons and it became H_2O. H_2O was used as a reactant and reacted with CH_4 and CO. The products, consisting of H_2O, CO and CO_2, and were sent to the fuel reactor. Next, the compressed air was introduced into the cathode side of the SOFC. There was

oxidation reaction of O_2, as shown in Eq. 2.6. After that the compressed air and the depleted air were introduced into air reactor [32, 33]

The products of this step were mixed with the air that was sent to the air reactor.

Reactions in anode: $\qquad H_2 + O^{2-} \rightarrow H_2O + 2e^-$ $\qquad$ (2.3)

$\qquad CH_4 + H_2O \leftrightarrow CO + 3H_2$ $\qquad$ (2.4)

$\qquad CO + H_2O \leftrightarrow CO_2 + H_2$ $\qquad$ (2.5)

Reaction in cathode: $\qquad O_2 + 2e^{2-} \rightarrow 2O^{2-}$ $\qquad$ (2.6)
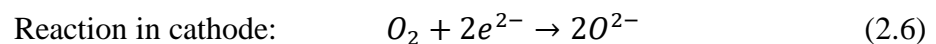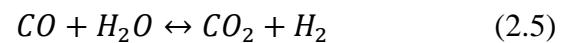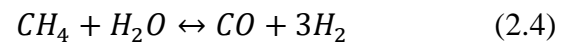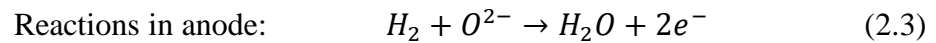
The discharge from the fuel and air reactors were sent to turbines for power production. The outlet streams from the turbines were used for heat recovery. The power was generated in 2 processes 1) SOFC and 2) turbines. The advantage of this process was the high thermal efficiency achievement, 72%. [34] The reason of high efficiency is that chemical energy was directly converted to electrical energy by the SOFC. In addition, the outlets of fuel and air reactors were used to produced power, as well. [35] The challenge of this process was the increased capacity for the power production. There was a pilot scale plant of a SOFC for H_2 and power production at 500 kWe. [35] The configuration of the SOFC with CLC was shown in Fig. 2.6.
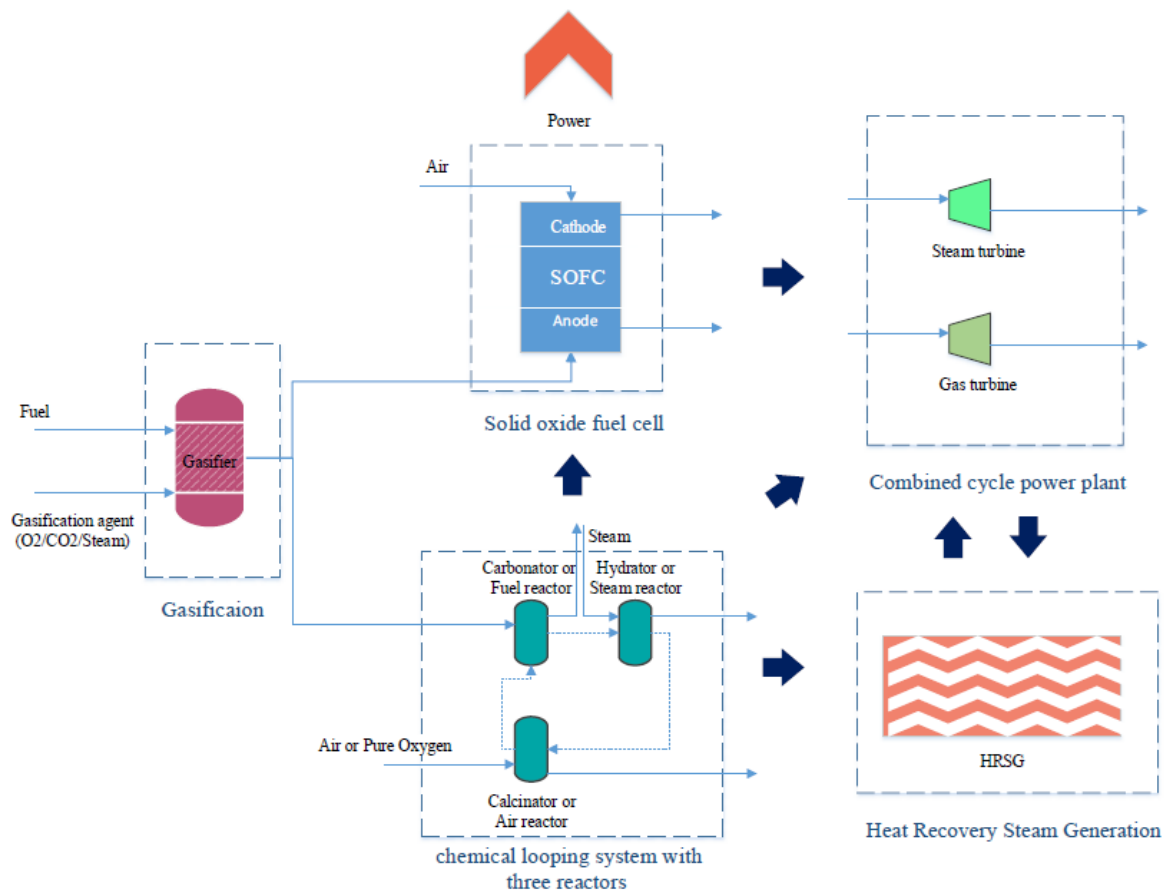
Fig. 2.6 The SOFC with CLC process. [30]

2.2.2.2. Proton-exchange membrane fuel cells (PEMFC)/chemical looping-based system

The PEMFC was operated with the three reactors of a CLC system. [36] Syngas was treated the acid gas, sulfur compound and particulate matter. Firstly, fuel was reacted with oxygen carrier (M_yO_x) in a fuel reactor. The products of the first step were CO_2, H_2O and spent oxygen carrier (M_yO_{x-2}). Next, steam was reacted with the spent oxygen carrier (M_yO_{x-2}) in a steam reactor. The main product of this step was H_2 and others were the excess H_2O and partially oxidized oxygen carrier (M_yO_{x-1}). H_2 from the steam reactor was purified. The CO might be found in low concentration (in PPM level). CO was eliminated by the oxidation process. CO_2 was eliminated by pressure swing adsorption process (PSA). Next, the partially oxidized oxygen carrier (M_yO_{x-1}) was reacted with the compressed air in air reactor. The products of this step

were oxygen carrier (M_yO_x) and the excess air. The gaseous outlet of the air reactor was used for power production. The purified H_2 from the steam reactor was introduced to the anode side of a PEMFC. The reaction at the anode was shown in Eq. 2.7. [37] Air was separated by an air separation unit. High purity of O_2 was obtained and it was introduced into the cathode side of the PEMFC. The product of the cathode side was hot water. The reaction at the cathode was shown in Eq. 2.8. [37]

$$\text{Reactions in anode:} \qquad 2H_2 \rightarrow 4H^+ + 4e^- \qquad (2.7)$$

$$\text{Reaction in cathode:} \qquad O_2 + 4H^+ + 4e^- \rightarrow 2H_2O \qquad (2.8)$$
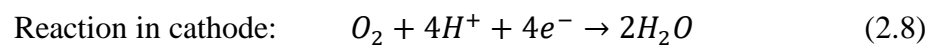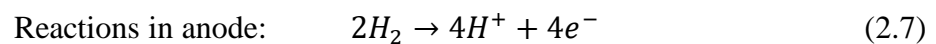
The net efficiency of a PEMFC was 43.6%. [36] The net efficiency of the PEMFC system was lower because the energy was highly consumed by ASU section. The economic analysis of Napoli et al. indicated that the net present value of the SOFC was higher than the PEMFC. [38] Even though, the investment cost of the SOFC was higher, the SOFC was preferable when it was operated for a long time (more than 6 years). [38]

2.2.3. The CLC for the utilization

Chemical looping processes were developed for other utilization such as chemical looping reforming (CLR), chemical looping hydrogen regeneration (CLHG), chemical looping air separation (CLAS) and chemical looping with oxygen uncoupling (CLOU).

2.2.3.1. Chemical looping reforming, CLR

The main product of a CLR is syngas. The essential property of an oxygen carrier in the CLR is the partially oxidation ability to obtain syngas. The product of fully oxidation is flue gas; CO_2 and H_2O. The NiO is an oxygen carrier that is suitable for the CLR because of the strong catalytic properties. [39] In addition, the other oxygen carrier that is suitable for this process is CeO_2 because it has high selectivity to produce syngas. [40] On the other hand, Fe-based, Mn-based and Cu-based oxygen carriers are the carriers that have low selectivity for syngas production. [41] The CLR principle is similar to the CLC principle. There are 2 main reactors; fuel reactor and air reactor, as shown in Fig. 2.7. Fuel is introduced into the fuel reactor and reacts with the oxygen carrier. The product of the fuel reactor was syngas; CO, H_2. By some

operation conditions, the H_2O and CO_2 are introduced into the fuel reactor for steam reforming and CO_2 reforming reaction. However, the steam reforming and CO_2 reforming reactions are strong endothermic reactor. [42] The ratio of H_2O and CO_2 is limited, otherwise the external energy is required which it is the reason of low net efficiency of the system. The spent oxygen carrier is regenerated in the air reactor. The fuel is introduced into the system more than the air stream for fully oxidation prevention.
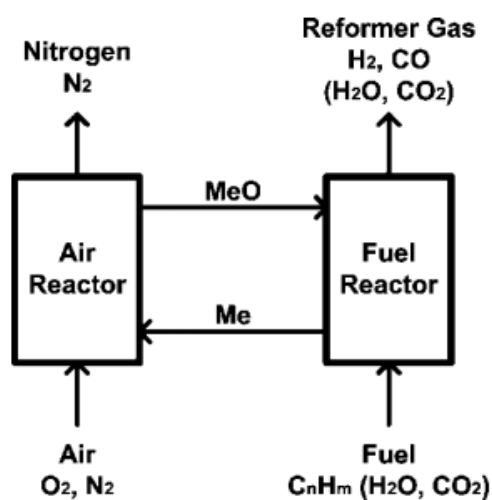
Fig. 2.7 The Flow diagram of CLR. [42]

2.2.3.2. Chemical looping hydrogen regeneration, CLHG

The CLHG is the three-reactor system. Accordingly, the principle of the CLHG and the three reactors of the chemical looping system are similar.

2.2.3.3. Chemical looping air separation, CLAS

The main product of a CLAS system is high purity O_2. [43] The CLAS process is usually applied with an oxy-fuel process and an integrated gasification combined cycle (IGCC). The CLAS process is included of 2 main reactors; an oxidation reactor and a reduction reactor, as shown in Fig. 2.8. The oxidation reaction occurs in an oxidation reactor as shown in Eq. 2.9. The spent oxygen carrier (Me_xO_{y-2}) is oxidized by O_2 in air to Me_xO_y which it is at the higher oxidation state. The reduction reaction takes place in a reduction reactor. The oxygen carrier (Me_xO_y) releases O_2 as shown in Eq. 2.10. It is at the lower oxidation state, Me_xO_{y-2}. The investigation of Shah

reported that Mn_2O_3/Mn_3O_4, CuO/Cu_2O, and Co_3O_4/CoO were good candidates as oxygen carrier type for the CLAS process. [44]

$$Me_xO_{y-2} + O_2 \rightarrow Me_xO_y \qquad (2.9)$$

$$Me_xO_y \rightarrow Me_xO_{y-2} + O_2 \qquad (2.10)$$
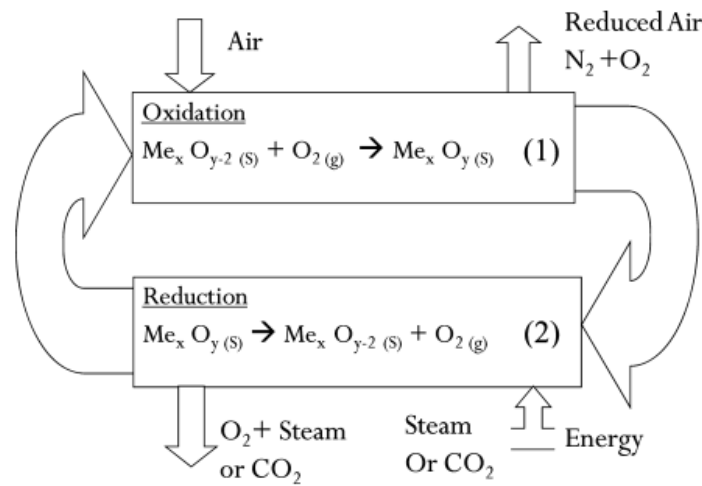
Fig. 2.8 The flow diagram of CLAS and ICLAS. [44]

2.2.3.4. Integrated chemical looping air separation, ICLAS

When a reduction medium is introduced into a reduction reactor of a CLAS system, the CLAS system becomes an integrated chemical looping air separation (ICLAS). When steam is used as the reduction medium, steam is the inert in the reduction reactor because it does not react with other species. [44] Even though, the inert does not directly affect the equilibrium reaction, the inert introduced into the reduction reactor increases the total pressure of the system. Then, the partial pressure of O_2 in the reduction reactor decreases. Accordingly, the equilibrium is pushed into forward direction. The products of reduction reaction are O_2 and H_2O. The O_2 was purified by the condensation process. The ICLAS is applied to oxy-fuel combustion, as shown in Fig. 2.9. When the pure O_2 from the reduction reactor is introduced into the combustion reactor, the temperature of the reactor is very high. Therefore, CO_2 or recycled flue gas will be introduced into the combustion reaction for controlling combustion temperature. [43] The cost for O_2 production by the CLAS process is lower than the cryogenic air separation unit (CASU).
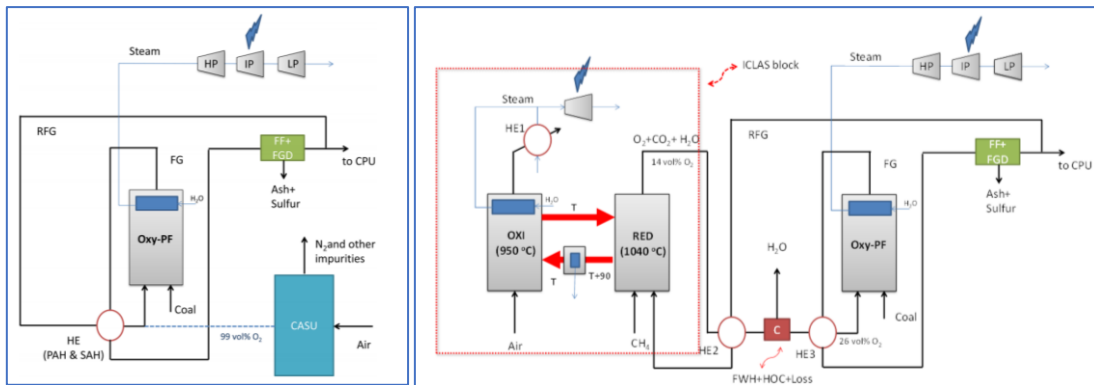
Fig. 2.9 The oxy-combustion process for power production (Left), the oxy-combustion with ICLAS process for power production. [45]

2.2.3.5. Chemical looping with oxygen uncoupling, CLOU

The main reactors of a CLOU are air reactor and fuel reactor, as shown in Fig. 2.10. The oxygen carrier (Me_xO_{y-2}) with low oxidation state reacts with O_2 in the air, as shown in Eq. 2.11. The product from the air reactor is the oxygen carrier (Me_xO_y) with higher oxidation state. Me_xO_y is transferred into the fuel reactor. O_2 is released from Me_xO_y as shown in Eq. 2.12 and reacts with fuel in the fuel reactor, as shown in Eq. 2.13. [46] The CLOU concept enhanced the overall rate of the reaction, especially solid fuel. For solid fuel as coal, the rate determining step is the coal gasification. Nonetheless, when the coal is the fuel for CLOU process, the O_2 releasing step is faster than the gasification. [47] Accordingly, the released O_2 will react with the coal without the gasification step in system.

The reaction in the air reactor $\qquad 2Me_xO_{y-1} + O_2 \rightarrow 2Me_xO_y \qquad$ (2.11)

The reactions in the fuel reactor $\qquad 2Me_xO_y \rightarrow 2Me_xO_{y-1} + O_2 \qquad$ (2.12)

$$Fuel + O_2 \rightarrow CO_2 + H_2O \qquad (2.13)$$
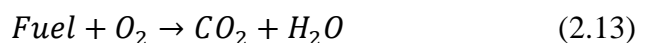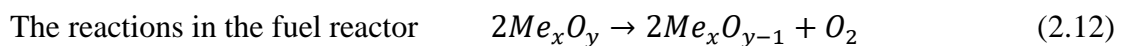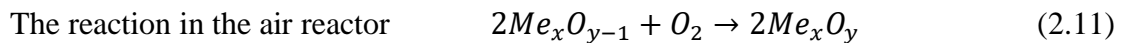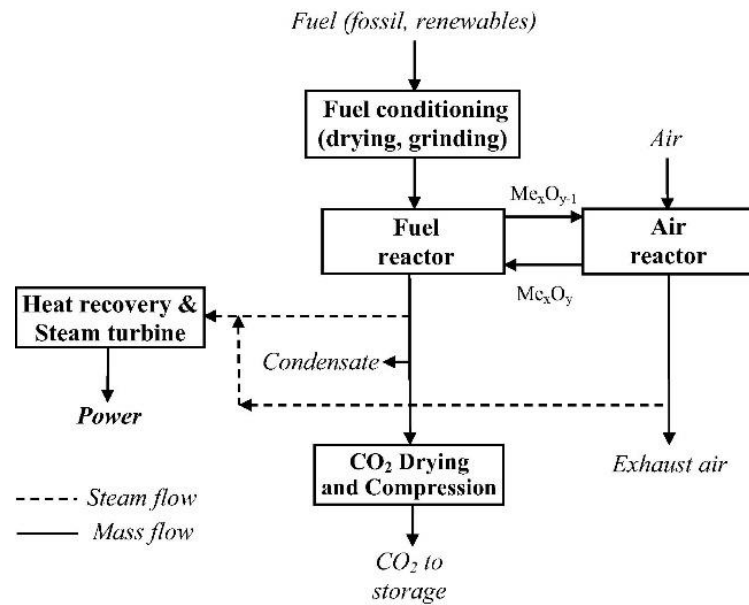
Fig. 2.10 The flow diagram of CLOU process. [46]

2.3. The oxygen carrier

Nickel-based oxygen carrier is also a good candidate for the oxygen carrier (OC) because of the high reactivity and high thermal stability. Therefore, the fuel conversion is completely combusted when methane is used as a fuel. [48] The reactivity of NiO is higher than CuO, Mn_2O_3, and Fe_2O_3. Iron-based OC is the most favorable OC because of its low cost and environment friendliness Besides, iron-based OC was investigated as the oxygen carrier in many pilot scales. However, the power plant using iron-based OC had higher cost than those using nickel-based OC, due to its lower reactivity. The comparison of NiO and CuO expressed that the operation condition of NiO-based OC was higher than CuO-based OC. There was not sintering in the NiO process. The comparison of Ni-based OC and Mn-based OC expressed that Mn-based OC exhibited lower conversion when it reacted with methane. Accordingly, the nickel-base OC was still a good candidate for an oxygen carrier. Therefore, it was selected as an OC in this study because of its high reactivity and high thermal stability.

2.4. The section for power production

In previous content, the combustion section was mentioned. In this section, the unit for power production would be reviewed. There are 4 significant processes for

power production, including conventional steam cycle (SC), combined cycle (CC), steam injected gas turbine cycle (STIG) and humid turbine cycle (HAT).

2.4.1. Conventional steam cycles, SC

The principle of this cycle is to extract energy from pressurized fluid and convert to power by a turbine. The process of steam cycle is shown in Fig. 2.11. The water was pumped to increase its pressure before feeding into a boiler. Water was boiled to steam in the boiler. The outlet steam from the boiler was high pressure and temperature. Then, the steam was used for power production by expanding in the turbine.
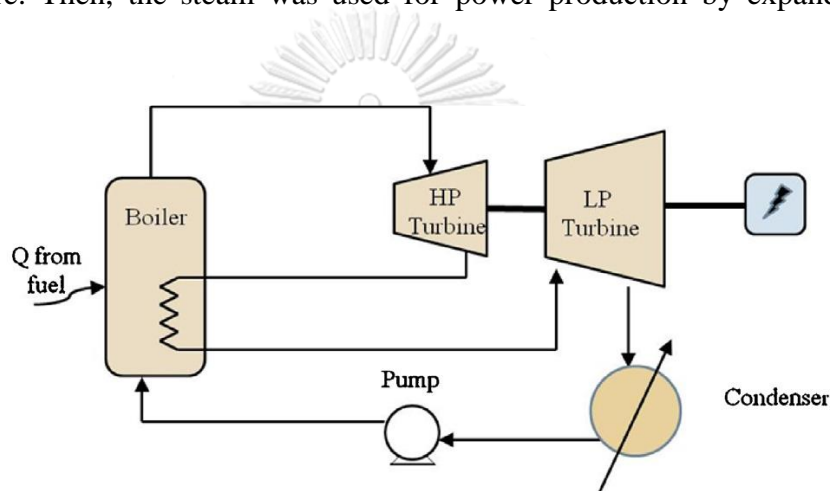
Fig. 2.11 Steam cycle [49]

2.4.2. Combined cycle, CC

The process of combined cycle is shown in Fig. 2.12. The steam is generated in a heat recovery steam generator (HRSG). Steam at high pressure and temperature is used to produce the power by a steam turbine which is similar to stem cycle. Nonetheless, the combined cycle has the supplementary section from steam cycle. The combined cycle also includes the combustion section. In the combustion section, air is compressed to obtain high pressure by a compressor. The fuel is combusted with the compressed air in combustion section. The flue gas from combustion section has high pressure and temperature. The flue gas is introduced into a gas turbine for power production. The remaining heat of flue gas after power production is used to preheat water at HRSG.
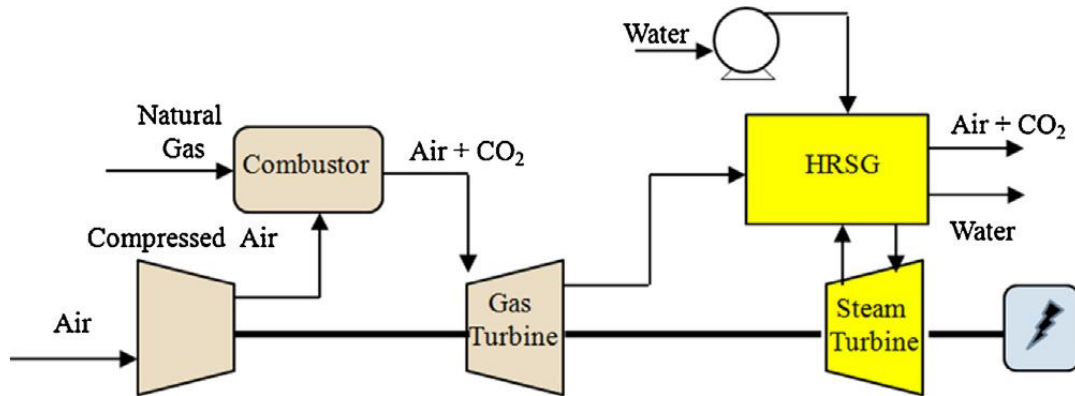
Fig. 2.12 Combined cycle [49]

2.4.3. Steam injected gas turbine cycle, STIG cycle

The STIG is similar to a combined cycle that the combustion section is included. The flow diagram of a STIG is shown in Fig. 2.13. Air is compressed by a compressor to increase its pressure. Water is pumped into a HRSG unit to produce superheated steam and introduce into a combustion reactor to combust with the compressed air and fuel. The product from the combustion reactor is flue gas which is sent to a turbine for power production. The superheated steam generation step includes 3 main processes; economizer, evaporator and superheater. [47] Water is pumped into an economizer for preheating. Then, it is evaporated to eliminate the condensed liquid water. The saturated steam is introduced into a superheater to increase the energy of the steam and obtain superheated steam. However, the amount of steam was limited by the heat at the HRSG unit.[50] The benefit of the superheated steam is 1) the NO_x reduction in the combustion section by decreasing the temperature in the reactor and 2) the increase of power production by increasing mass flowrate inlet to the turbine. In addition, the enthalpy of superheated steam is higher than that of air at the same temperature. Accordingly, the power production of this process was increased by superheated steam injection through the combustion section, leading to the increase of total efficiency of the power production process, as well.
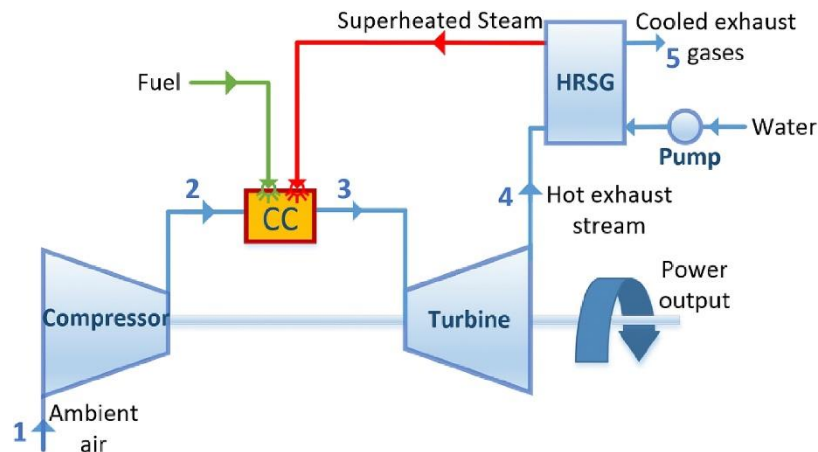
Fig. 2.13 STIG cycle [47]

2.4.4. Humid air turbine cycle, HAT cycle

The humid air turbine (HAT) cycle is the power production section that aims to offer higher thermal efficiency with a low-investment cost [51]. The flow diagram of a HAT cycle is shown in Fig. 2.14. This cycle is similar to the STIG that uses superheated steam in the combustion section. Nonetheless, the HAT cycle has the supplementary section from the STIG cycle. The HAT cycle includes the air compression section which it is divided to multi-stage compressor for reducing compression work. The 2 main processes of the HAT cycle are the multi-stage compressor and the humidifier. The multi-stage compressor has the inter-cooler or heat exchanger installed between each stage of the compressor.

Air is compressed in the first stage of the compressor. The compressed air has higher pressure and temperature. Then the compressed air is cooled by the intercooler and fed to next compressor. Due to lower temperature of the compressed air, the work required by the air compressor becomes less. The heat from the compressor was transferred to the cooling water at the inter-cooler. Air was alternately compressed and reduced heat, until the last stage of compressor. Then, the compressed air and the hot water were introduced to a humidifier. The hot water is evaporated into the air until it reaches the saturated condition. [52] Therefore, the humidifier was the unit that eliminated the condensed liquid water and produced the humid air. Then, the humid air is preheated by the recuperation reactor. The humid air is fed into the

combustion reactor. The flue gas is at high pressure and temperature and it is sent to a turbine for power production.

The benefits of a HAT cycle include 1) the increase of power production by increasing the mass of working fluid passed through a turbine and 2) the increase of net power production by reducing the turbine work consumption. This cycle is the best gas turbine cycle. [52] Moises et. al. reported the comparison of 3 types of power production unit of a CLC process which was comprised of SC, STIG cycle and HAT cycle. The study indicated that the net plant efficiency of CLC-SC, CLC-STIG and CLC-HAT were 50.25%, 50.49% and 56.08%, respectively. Consequently, the HAT cycle was the best power production cycle. [49]
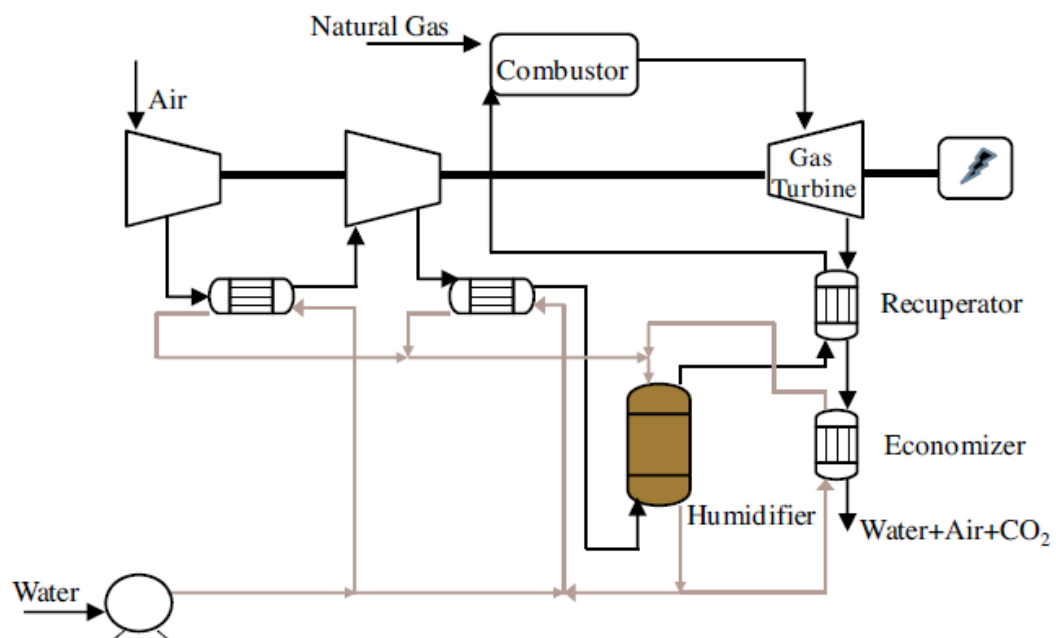
Fig. 2.14 HAT cycle [49]

2.5. Aspen plus program

The advanced system for process engineering (ASPEN) program was the powerful tool and extensive usability for the virtual chemical processes. This program has arisen by the cooperation of Massachusetts Institute of Technology (MIT) and US Department of Energy since 1981. The aspen plus program has been used to simulate the whole process at steady state. [53] This software consists of the various thermodynamic properties which is suitable for a specific process. The used

components in the process are customized. Therefore, it could be used for various reactants and products. The most advantage is process optimization with high accuracy. The optimum operation condition of the process could provide high material and energy utilization.

The guideline for simulation by aspen plus is as followed. Firstly, the problem of a case study for simulation was determined. Then, the given conditions of the simulation case such as components, compositions, and thermodynamic properties were specified. After that, each unit operation was selected and connected with each other to represent the simulated process. Eventually, the connected unit operations were simulated until the result was validated or the simulation was completed, as shown in Fig. 2.15.
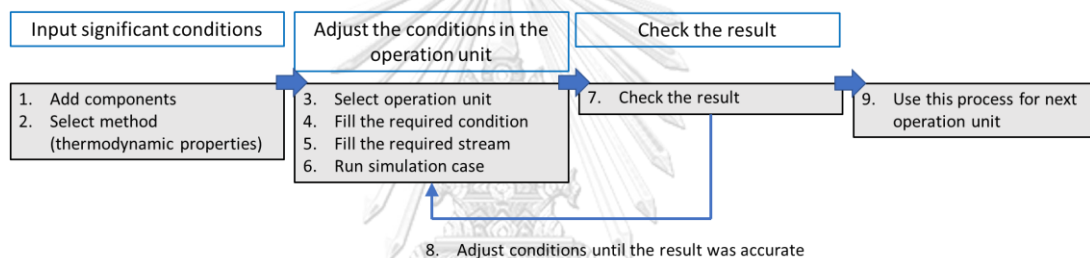
Fig. 2.15 The process to achieve the ASPEN plus simulation [54]

2.6. The computational fluid dynamic.

Computational fluid dynamics (CFD) is used to investigate the fluid flow behavior by the numerical analysis. [55] CFD simulation is an efficient tool to explore the detailed local data and multiscale flow structures in a fluidized bed reactor. [56] CFD simulation is a suitably engineering tool that could build the understanding of the complex behavior of gas-solid flow within the CLC reactor. [57] The gas-solid flow model is divided into 2 methods;

2.6.1. Eulerian-Eulerian method

- Gas and solid phases (carrier phase) are determined as the continuous phase.
- The advantage of this method is that it uses lower computational resource because the effects of particle size distribution is neglected.

2.6.2. Eulerian-Lagrangian method

- Gas phase is determined as the continuous phase. Solid phase is determined as particle by particle.

- The advantage of this method is the detailed data of particle behavior.

The guideline for implementing CFD simulation is shown in Fig. 2.16. The first step, the problem is identified. The second step, the geometry of equipment or object that will be investigated to fluid behavior is created and set up the solver with suitable conditions. The third step, the simulation case is calculated with numerical method until it converges. The final step, the result is interpreted. When the result is not reasonable, the model will be adjusted until it is validated with the experimental data. Ansys fluent is the commercial simulation program that is the most powerful tool, well-validated physical model and high accuracy result. [58]
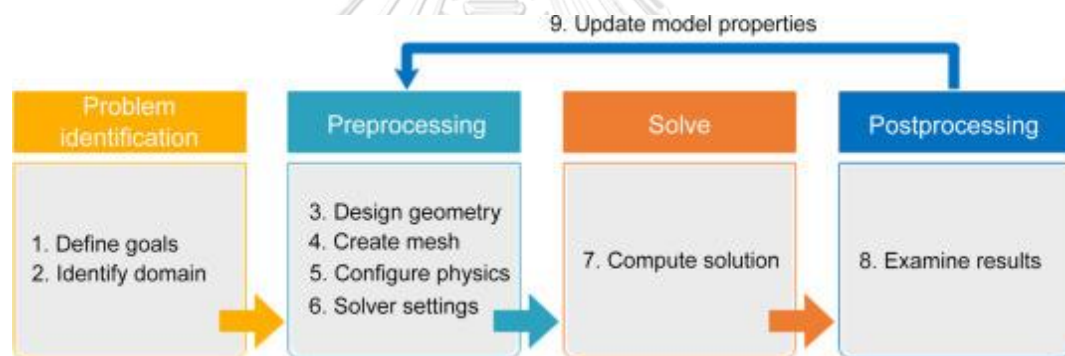
Fig. 2.16 The process to achieve the CFD simulation [58]

2.7. Economic analysis

The outcome of economic analysis indicated the investment cost, operation cost and the project benefit. [59] It was also used for the best-case comparison in decision making.

The step for economic analysis in this study was followed. [60, 61] Firstly, the problem description of a case study for economic analysis was specified. Then, equipment cost, fix capital cost (FCI), total capital cost (TCI), cost of manufacturing without depreciation (COM_d) depreciation, sale price, total annual income and expenses and indicators of economics were calculated respectively, as shown in Fig. 2.17.
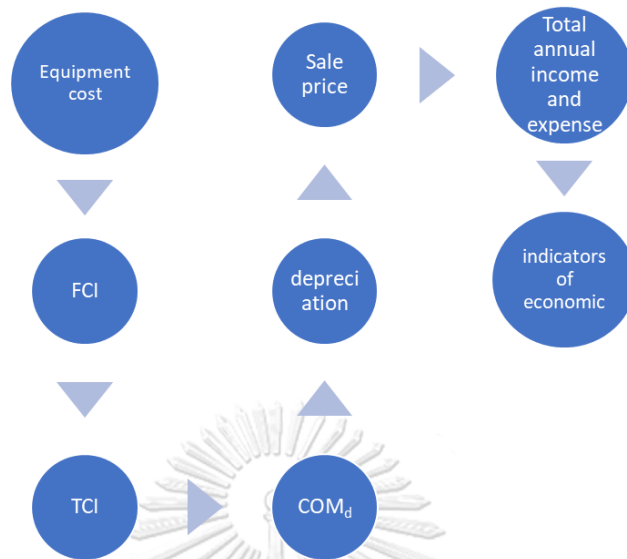
Fig. 2.17 The process to achieve the economic analysis [60, 61]

2.7.1. Equipment cost

The equipment cost was obtained from the economic analysis data provided by aspen plus program or the cost estimation from the plant design and economics for chemical engineer's book. [60]

2.7.2. Fixed capital investment cost, FCI

FCI consists of direct cost and indirect cost. The main part of the direct cost includes purchased equipment and service facilities costs. The main part of the indirect cost was contingency. FCI was relied on the Table 17 of plant design and economics for chemical engineer's book which represented the details of the FCI composition and the ratio factors for estimating capital-investment items which based on delivered equipment cost for solid and fluid processes. [60] In this study, the details of the FCI composition for the solid and fluid processes after normalized is shown in Table 2.1.

Table 2.1 The components of FCI

Component	%FCI
Direct cost	
Purchased equipment	22.35
Purchased-equipment installation	8.72
Instrumentation and controls (installed)	2.68
Piping (installed)	6.93
Electrical system (installed)	2.23
Buildings (including services)	6.48
Yard improvements	2.23
Service facilities (installed)	12.29
Land	1.34
Indirect cost	
Engineering and supervision	7.15
Construction expense	7.60
Contractor's fee (about 5% of direct and indirect plant cost)	5.00
Contingency (about 10% of direct and indirect plant cost)	15.00

2.7.3. Total capital investment cost, TCI

The total capital investment cost (TCI) is composed of fixed capital cost (FCI) and working capital cost (WC). The 85% of TCI is FCI and 15% of TCI is WC, as shown in Fig. 2.18. The total capital cost is the annual cost at the beginning of the plant operation.
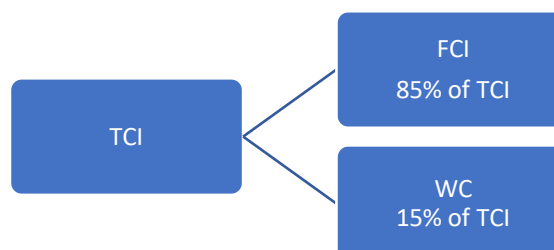
Fig. 2.18 The component of TCI.

2.7.4. The operation and maintenance costs [61]

$$COM_d = 0.180FCI + 2.735C_{OL} + 1.235(C_U + C_{WT} + C_{RM}) \tag{2.14}$$

COM_d = cost of manufacturing without depreciation

COL = cost of administrative, supervisory or laboratory

CU = cost of utility

CWT = cost of waste material

CRM = cost of raw material

2.7.5. The cost of administration, supervisor or laboratory

The calculation of this cost is based on the number of operators and the unit operations that involved with particulate handling.

N_{NP} = Total unit of compressor, tower, heat exchanger and reactor

N_{OL} = Number of operators per shift = $(6.29 + 31.7P^2 + 0.23N_{NP})^{0.5}$ (2.15)

P = Number of solid process

Total number of labors (persons) = Shifts per day x N_{OL}

Total labor cost = Cost of operating labor cost x Total number of labors

2.7.6. Depreciation cost

The depreciation cost is the decrease of asset cost. There are several types of depreciation calculation; straight-line, double declining, units of production and sum of years digits.

2.7.7. The significant indicator for economic analysis

2.7.7.1. Net present value (NPV)

NPV indicates the total annual cash flow at the present viewpoint. NPV is calculated by using Eq. 2.16.

$$NPV = \sum_{n=0}^{M} \frac{CF_n}{(1+I)^n} \tag{2.16}$$

When   CF = cash flow

n = each period

M = the end of plant operation

I = discount rate

2.7.7.2. Internal rate of return (IRR)

IRR indicates the return rate when NPV is zero. IRR is calculated by using Eq. 2.17.

$$\sum_{n=0}^{M} \frac{CF_n}{(1+IRR)^n} = NPV = 0 \tag{2.17}$$

2.7.7.3. Breakeven point

Breakeven point indicates the point that the accumulated present value is equal to zero.

2.7.7.4. Payback period

Payback period indicates the period that the accumulated present value equal zero.

2.8. Sustainability evaluation

The sustainability evaluation has been proposed by Odum [62] which it is emergy analysis. The emergy is "the available energy of one kind previously used up directly and indirectly to make a product or service". Every material, energy, monetary, and manpower are counted in this analysis which it will transform into the same unit. The analysis combines ecology concepts into energy calculations to measure the direct and indirect inputs along with the transformation processes. This

evaluation procedure covers all the energy-related to the system, including the material, energy, monetary, and manpower, and then converts them all into solar energy. In an energy view, 1 joule of electricity is equal to 1 joule of thermal energy. However, in terms of emergy analysis, 1 joule of electricity represents 8.05E+04 solar equivalent joules (sej), whereas 1 joule of thermal energy can represent different sej values depending on the fuel used. For example, 1 joule of thermal energy obtained from coal, methane, or wood would be 1.69E+05 sej/J, 1.70E+05 sej/J, or 6.72E+04 sej/J [62], respectively. The solar energy that was used to produce 1 joule of energy was the UEV. The UEV was calculated from the total solar energy utilized by the process to produce the product divided by the energy of the product. However, the accuracy of the emergy analysis depended on the assumption and the database of the UEV. The distinct advantage of emergy analysis was the consideration of types of resources and the sources of resources that are different from other analyses. The summary of emergy analysis is the analysis that converts of material, energy, cost, and all data that involve the process into a solar energy form. When the procedure was based on solar energy, it represented all solar energy that was used to perform the resource. Accordingly, this analysis expresses the genuine value of the resource. With the procedure of emergy analysis, the result reveals the self-sufficiency which other methods could not explain. This analysis result would reveal both economic and environmental impact by significant emergy indicator which included of 1) unit emergy value (UEV), 2) environmental loading ratio (ELR), 3) emergy yield ratio (EYR), and 4) emergy sustainability index (ESI).

2.8.1. Unit emergy values, UEV

UEV is a transform factor which it was calculated from the ratio between the total emergy and energy flow product and service as shown in Eq. 2.18. In good case, UEV is low. The low UEV indicate the low total emergy flow for product one unit of product. [62] This transformity make different between economic and emergy analysis. Economic take everything into account by price which it is indicated by the human need. However, the emergy flow is indicated by all the solar energy that used to produce the products, energy or service. Accordingly, the emergy analysis will

represent more reasonable result than economic. In addition, the UEV is used to transform all of energy stream into one form of solar energy (sej), as well.

$$UEVs = \frac{Total\ Emergy\ flow}{Energy\ flow,\ Products\ flow,\ Service} \qquad (2.18)$$

2.8.2. Environmental loading ratio, ELR

ELR is the environmental loading ratio which it represents the loading of the process to the environment as shown in Eq. 2.19. In good case, ELR should low. When ELR is close to 2, it is low environmental loading. When ELR between 3-10, it is moderate level of environmental loading. Finally, when ELR is more than 10, the environmental loading is high level. [63]

$$ELR = \frac{N+F}{R} \qquad (2.19)$$

N = local non- renewable resource; natural gas.

R= local renewable resource; water, air.

F = expense cost, external goods, Ni, Na_2CO_3, Al_2O_3, equipment, labor cost.

2.8.3. Emergy yield ratio, EYR

EYR is emergy yield ratio which it indicates competitive ability in economic and the stability of process. EYR is calculated from the total emergy flow which divided by the emergy of expense goods (F), as shown in Eq. 2.20. In good case, EYR is high. The reason of high EYR is low F. It represents that the process is hardly relied on external resource. When the process relies on internal resource, the process will high stability which it is highly competitive ability in economic, as well. In good case, EYR is high but, in worst case, EYR is equal to 1. Moreover, when EYR is lower than 2, it indicates that the process is not suitable to be an energy source by the study of Ulgiati and Brown. [29]

$$EYR = \frac{Total\ emergy}{External\ resources} = \frac{R+N+F}{F+L} \qquad (2.20)$$

2.8.4. Emergy sustainability index, ESI

ESI is emergy sustainability index which it indicates the sustainability of the process. It is calculated from the ratio of EYR to ELR, as shown in Eq. 2.21. It is the ratio of profit to the loading of the environment. When ESI is lower than 1, the process is not long-term sustainability. When ESI is 1-5, the process is medium sustainability. Finally, when ESI is higher than 5, the process is long term sustainability.

$$ESI = \frac{EYR}{ELR} \qquad (2.21)$$

2.9. The literature reviews

2.9.1. The investigation of the operation conditions

There were many researches that studied the operating conditions to improve the system efficiency. The thermal efficiency of the CLC was higher than the conventional combustion with CO_2 capture process because it was not only heat generator unit but also inherent CO_2 separator unit. [34, 64, 65] The countercurrent gas–solid flow pattern, low moisture content of feeding biomass, temperature of fuel reactor (>600 $^\circ$C), low pressure (<40 atm) in the fuel reactor increased the conversion of oxygen carrier. [4] The five parameters for operating the reactors were studied; temperature inlet of air and fuel, temperature of reactors, temperature inlet to turbine, temperature outlet from reactors and pressure of reactor. [28] The high temperature and pressure led to high efficiency of the system. Olaleye and Wang [66] studied a CLC with HAT cycle for power production which reached 57% thermal efficiency. They investigated four effects including 1) effect of humidified air to fuel ratio on concentration products, 2) effect of fuel flow on NiO conversion, 3) effect on temperature inlet of fuel to thermal efficiency, and 4) effect of inlet and outlet temperature of air reactor on thermal efficiency. The use of supercritical steam for power production also increased the net efficiency of natural gas [67] to 43.11% because this steam boiler was operated in high pressure operating condition (240 bar). [67] The change of compression ratios showed that there was an optimum point for the operation. Beyond that point the efficiency would decrease. [27] Furthermore, there were other groups of research works focusing on modification the system to improve the system efficiency. The modified power generation system called CLSA, which

had a multistage of compressors increased the thermal efficiency to 55.1% [68]. Ibrahim studied types of the CLC and types of oxygen carriers for power generation [49]. The results indicated that the thermal efficiency of the CLC with HAT cycle by using Ni as an oxygen carrier was 56.08% The CLC with HAT cycle for power production was investigated. Olaleye and Wang [69] studied the effect of fuel inlet temperature, inlet and outlet temperature of air reactor, effect of humid air and Ni flow rate, and effect of air to oxygen carrier ratio on thermal efficiency. Nevertheless, it could not explain the interaction between each effect. In fact, all variables affected to each other and could not be separately investigated. The 2^k factorial would be the methodology to explain all of the main and interaction effects on the system. Fun et al. [70, 71] studied a CLC operated with combined cooling, heating and power production (CCHP-CLC). The obtained thermal efficiency of the process was 58.20% in summer and 60.34% in winter. This process was suitable for some countries that had enough different temperatures by season change. Other combination process, the CLC with solid oxide fuel cells (SOFCs) gained very high thermal efficiency that was 63-70 % [34] because chemical energy from fuel was directly converted to electricity. SOEC was solid oxide electrolysis that had high efficiency for H_2 production. [72] The combination of the SOEC and CLC obtained 56% efficiency [9]. Power and H_2 were produced from this process at the same time. However, the result was based on the operation in a lab scale equipment only.

2.9.2. The investigation of the hydrodynamics.

There were many researches that studied the operating conditions to improve the hydrodynamics. For the latest investigation of a fluidized bed reactor for the CLC process, the study of cold flow models which the reactions were not included in calculation was highly investigated. The solid circulation rate (SCR) was examined in a cold flow model by the CFD-DEM (dynamics-discrete element) in the study of Peng et al. [73] The result of Peng et. al. demonstrated that SCR was strong impacted to the conversion of oxygen carrier, the size of reactor and the heat transfer between air and fuel reactor which it was transferred by the oxygen carrier. Yin et al. researched the bubbling regime in fuel reactor which the fluidized bed reactor was used for their study. [74] The result of Yin et. al. demonstrated that the high CO_2

concentration was obtained when the pressure in the fuel reactor was increased. In addition, the fuel feeding position was studied. Yin et. al. suggested that the better hydrodynamic behavior was achieved when fuel was introduced at the lower feeding position. The CLC reactor in pilot scale at 1 MW_{th} was investigated in the three dimensional system by May et al. [75] The simulation was validated with the experimental data. The result demonstrated that the temperature result from the simulation and the experimental data was insignificant different. The deviation of temperature might be the result of the assumption in the simulation. The result of Merrett and Whitty demonstrated that the carbon conversion was significantly increased in the chemical looping with oxygen uncoupling process (CLOU) because of temperature. [76] In this study, the DCFBR was performed in simulation investigation.

The suitable operation condition provided the high conversion in reactor. Furthermore, the configuration of reactor was the important part for enhancing the conversion reaction, as well. Chen et al. investigated the hydrodynamics within the dual circulating fluidized bed reactor (DCFBR) . The DCFBR enhanced the conversion of the fuel reactor. [57] The height of fuel reactor was higher than air reactor. Therefore, the residence time and conversion within fuel reactor was increased when DCFBR was selected as the reactor. The loop seal was the critical part of the DCFBR. The loop seal was the connecting part between downer and riser. It was contained with solid return from the cyclone and prevented the reverse flow of gas to the downer section.

2.9.3. The investigation of Emergy.

The development of power production is also important for the industrial and commercial sectors. Hence, it is crucial to evaluate the environmental impact of any power production processes before deciding on constructing a new power plant. The life cycle assessment (LCA) is the most widely used tool for environmental assessment. [77, 78] A previous LCA study of a CLC indicated that the CLC produces a lower environmental impact than a conventional power production process. [79] The limitation of the LCA is that the method cannot ascertain the economics and long term sustainability of the process [80], nor can it quantify the social cost and the impact of

the environment [81]. Several issues related to conventional analysis tools include: (i) that the mixing units, such as the weight, heat capacity, volume, power, and cost, cannot be exactly compared; and (ii) the resources, products, and processes, that cannot be evaluated in a price form, are not quantified. [82]

The emergy analysis was used to assess the performance of the process in various fields such as agricultural system, energy production, city development, etc. The evaluation from the emergy analysis represented the deep information which deserved for further development. [83] The best-case study exhibited the net benefit to society and low environmental loading. In the study of Yazdani et. al., the emergy analysis was used to evaluate the 2 power plants which used the different fuel types; natural gas (NG) and municipal solid waste (MSW). The result indicated that the ESI of the MSW cases was higher because the percent of renewability (PR) of MSW case was higher. [84] Sha and Hurme investigated the cogeneration process for heat and power production, the study indicated that the emergy analysis could be applied for evaluating efficiently the power plants in a sustainable viewpoint. The sustainability index of biomass based was higher than coal based in 1.5 times. [85] The cogeneration was a 20-35% reduction of the emergy in the production process when compared to the individual production process. In the study of Zhang et. al., the emergy analysis was used to evaluate the waste heat power generation process. [86] The waste heat utilization was the one approach to increase the efficiency of the system. The power was generated by the organic Rankine cycle (ORC). The result indicated that the ESI of ORC power was lower than wind, hydro and geothermal power plant. However, the ESI of ORC power plant was higher than fossil fuel power plant. The EYR of ORC was the highest of the six-power plants (wind, geothermal, hydroelectric, methane-fired power plant, oil-fired plant and coal-fired power plant) because the purchase from the ORC case was the lowest. In the study of Wang et. al., the process for power production was evaluated by emergy analysis. [87] The 3 processes were included of 1) pulverized coal-fire with combined heat and power plant, 2) coal-fired and pressurized fluidized bed combustion with combined cycle, and 3) coal-fired with integrated gasification combined cycle. The result indicated that EYR of case 3 and case 2 were higher than case 1. With this reason, ESI of case 3 was the highest. In the study of Ulgiati et. al., the process for power production was

evaluated by emergy analysis, especially the cycle for power production. [88] The steam cycle and the combined cycle were compared. The emergy analysis indicated that the electrical transformity of combine cycle (1.905E+05 seJ/J) was lower than steam cycle (3.15E+05 seJ/J). It represented that the combined cycle required the lower total resources. When the main product was changed from only electricity to heat and electricity, the transformity of 2 cases was highly reduced. The co-generated product transformity of combine cycle and steam cycle were 1.56E+05 and 1.73E+05 seJ/J, respectively. The result indicated that the co-products production and the optimal resources were the key to obtain the sustainable development.

Chapter 3
The methodology of this research

The research was divided into three sections: (1) The process efficiency improvement for the power production using a CLC as the key thermal engine had been explored. (2) The hydrodynamics of the CLC was investigated. (3) The sustainability of the process was evaluated.

The operation conditions of a CLC process with the HAT cycle for power production was systematically investigated by 3^k factorial experimental design, in chapter 4. The four input parameters and the four responses provided the optimum operation condition that reached the highest thermal efficiency.

The hydrodynamic behavior of the CLC reactor was investigated in chapter 5. The dual circulating fluidized bed reactor was selected to be studied. The suitable hydrodynamic behavior would provide high performance of the CLC process. In this section, there were two types of fuel; solid fuel and gaseous fuel. For gaseous fuel, the operation conditions from chapter 4 were used to prove whether the operation condition was suitable. The outcomes of this section were the operation condition and the reactor size.

In chapter 6, there were three types of analysis including 1) thermal efficiency, 2) economic analysis and 3) the sustainability analysis, for selecting the best-case study. The effects of combustion types, CO_2 capture efficiency, carbon tax and HAT cycle were included in this section which provided six case studies. The equipment and operation costs from chapter 4 were used in economic and sustainability analyses. In addition, the CLC reactor size was calculated from chapter 5, as shown in Fig. 3.1. The outcomes of this section were the viewpoint of different analyses on the process and the suggestion for the CLC process improvement.
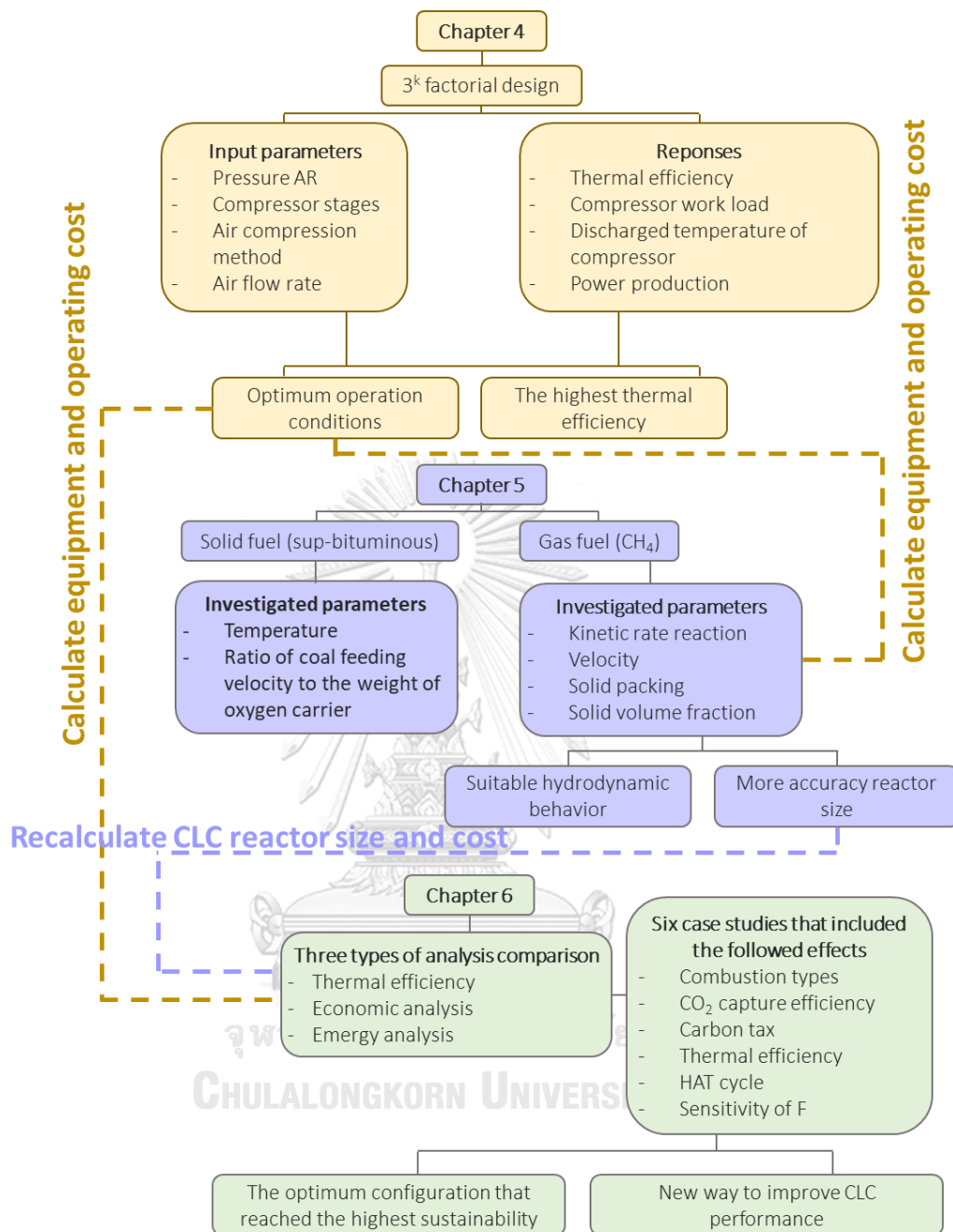
Fig. 3.1.1 The flow diagram that represents the relationship among chapter 4, 5 and 6

3.1 The methodology of chapter 4; the investigation of operating parameters of a CLC with HAT cycle process for power production

   3.1.1 The research gaps

   The limitations of previous studies of the CLC study are the individual investigation of each parameter. However, all parameters in the system have interacted with each other and they could not be studied separately. In this study, the 3^k factorial design was used for examining the effects of these parameters systematically and identify their effects and interaction with the minimum treatment number. For this part, four independent input variables are the pressure of the air reactor, the number of stages of air compressors, methods of air compression operation and airflow rate. Four responses of the process consist of thermal efficiency, power production from air reactor, work of air compressors and air compressor discharge temperature. It is the first time that the operating parameters of the HAT cycle and those of a CLC process were systematically investigated. The HAT cycle is composed of the multi-stage compressors, heat exchangers for intercooler between compressors and a turbine. Accordingly, the operation of the HAT cycle is directly relating to compressors and turbine workloads, which affect on power production of the system. The 3^k factorial result could reveal the main factors, the interaction and curvature interaction among operation parameters on the thermal efficiency of the system.

   3.1.2 Objective

   To study the effects of operating conditions on the power production of the chemical looping combustion process with the HAT cycle.

3.1.3 Methodology

3.1.3.1 Process description
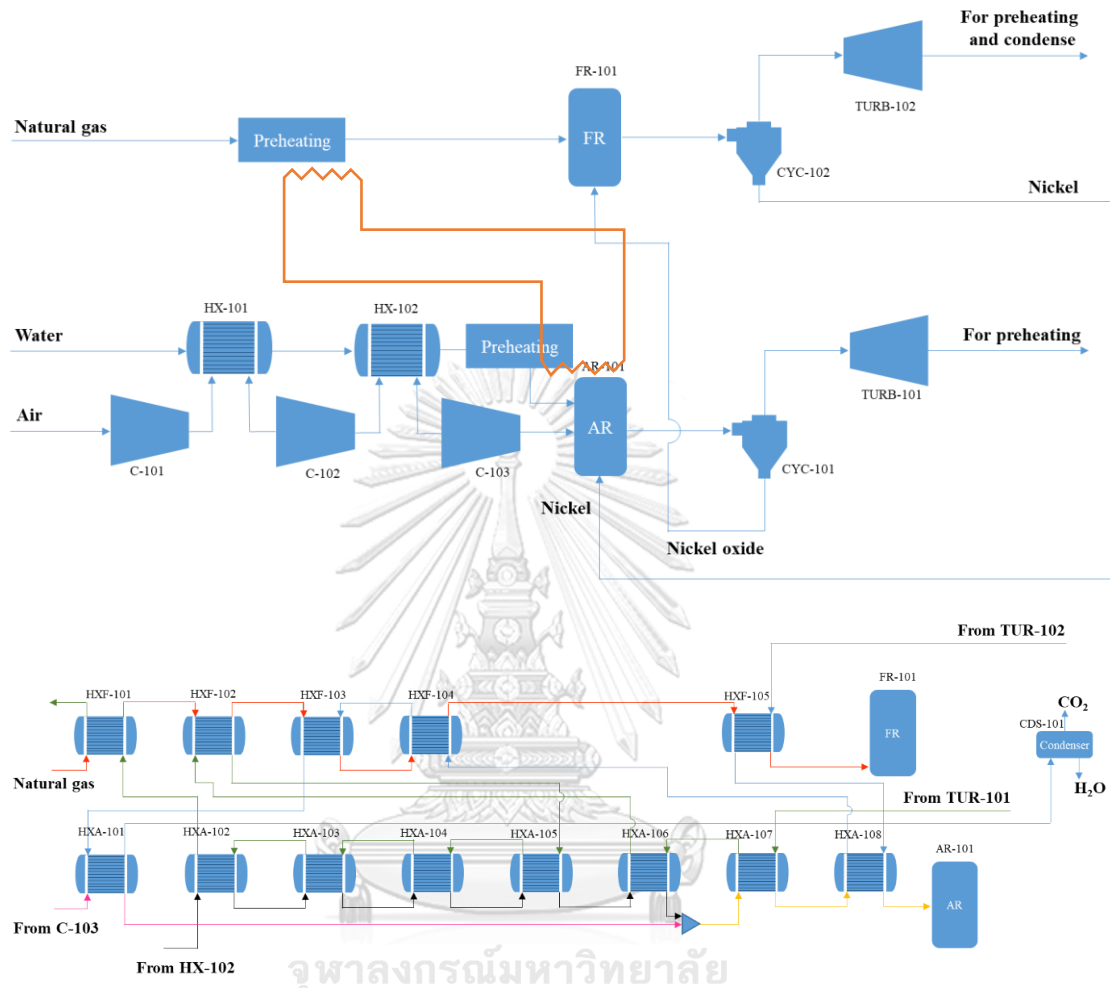
Fig. 3.1.2 The flowchart of CLC for power production system and flow chart of preheating section

The CLC process with the HAT cycle was simulated for evaluating the system efficiency by Aspen plus simulator. In this study, it was the gas and solid system because natural gas was used as a fuel and NiO on Al_2O_3 was used as the oxygen carrier. The Peng-Robinson-Boston-Mathias (PR-BM) was the thermodynamics properties suitable for simulating the solid and fluid process. The PR-BM was the modified equation of state with a high explicit prediction for multiphase system [89] and the solid-gas process. [49] The CLC process with the HAT cycle was complete by Petriz-Prieto [49] and the thermal efficiency of their system was 55.88%. This developed process was including of a CLC process for heat production and the HAT

cycle for power production. There were two reactors in the CLC section, air reactor (AR-101) and fuel reactor (FR-101), which was operated as a cycle as shown in Fig. 3.1.2. The multi-stages compressor was a part of the HAT cycle for decreasing the workload of the compressors. The heat exchangers were installed between the compressor stages. The cooling water was fed into a heat exchanger for releasing heat in the compressed air. Then the compressed air was sent to the next compressor stage. Its workload was reduced. For the three-stage compressors, air would be compressed at C-101; it was cooled down at HX-101. The compressed air was sent to the next compressor, C-102, and next heat exchanger, HX-102. Finally, the compressed air would be transferred to the last stage compressor, C-103. For other number stages of compressors, air would be alternately introduced into compressors and heat exchangers until the last stage of the compressor. The compressed air and cooling water were fed into the HAT cycle; after that, it was preheated at the preheating section. Water was preheated until it was vaporized. The stream was combined with compressed air. Then the humid air was fed into the air reactor. The Ni metal and Al_2O_3 supporter were fed into the air reactor (AR-101) for reacting with the compressed air and producing oxygen carrier: NiO. The ratio of Ni to Al_2O_3 was 0.25/0.75 by a mole at 1350ºC. The NiO was separated from excess air by a cyclone (CYC-101). The excess air with high temperature and high pressure was introduced to a turbine (TURB-101) for power production. The natural gas was preheated at the preheating section. After that, it was introduced into a fuel reactor (FR-101) for reacting with NiO. The spent metal oxide was separated from gas products by a cyclone (CYC-102). The gas outlet from the fuel reactor (FR-101) was sent to a turbine (TUR-102) for power production. The gas products from the fuel reactor consisted of water and CO_2, which water was condensed from flue gas by a condenser, CSR-101. The solid product from the fuel reactor was Ni, which was sent to the air reactor (AR-101) for regeneration. The metal in the system was recycled in the CLC process. The outflow from the cyclone was introduced to the preheating section for heat recovery. Air and water were preheated by the high temperature streams from TUR-101 by HXA-107, HXA-106, HXF-102, HXA-105, HXA-104, HXA-103, HXA-102 and HXF-101, respectively. The high temperature stream from

TUR-102 by HXF-105, HXA-108, HXF-104, HXF-103 and HXA-101, respectively, preheated natural gas.

3.1.3.2 Experimental design

The CLC with the HAT cycle process was investigated to improve thermal efficiency when using natural gas. The condition of natural was shown in Table 3.1.1.

Table 3.1.1 Aspen Plus models and operating parameters

Thermodynamics properties		PR-BM
Ni/Al_2O_3	Flow rate (kmol/hr)	48658.04
	Mass fraction (-) [47]	0.16/0.84
	Temperature (^oC)	1350
	Pressure (atm)	1
Water	Mass fraction in humid air by weight	0.14-0.18
Natural gas	Flow rate (kg/s)	14.2
	Temperature (^oC)	25
	Pressure (atm)	20
Composition of natural gas	Nitrogen	0.28
	Carbon dioxide	0.70
	Methane	89.51
	Ethane	5.92
	Propane	2.36
	n-Butane	0.40
	i-Butane	0.56
	n-Pentane	0.08
	i-Pentane	0.13
	Hexane	0.06

The factorial experimental design was selected to investigate the effects of all parameters on the process performance with the minimum case studies. [90] The 3^k factorial experimental design was implemented to identify the operating parameters that led to optimum thermal efficiency. Since pressure significantly affected the efficiency system [49, 91, 92], it was included as a parameter to be evaluated. In this study, there were four parameters: the pressure of the air reactor, the number of air compressor stages, the Method of air compression and airflow rate. The four responses to be observed are: thermal efficiency consists of thermal efficiency, power production from air reactor, work of air compressors and air compressor discharge

temperature. In summary, there were 81 cases in total to be simulated and evaluated the outputs. The values of these four input variables which were used in the study were shown in Table 3.1.2.

Table 3.1.2 The values of four parameters that was conducted in 3^k factorial experiment.

Variable	Name	Units	Low value	Middle value	High value
A	The pressure of air reactor	atm	5	10	15
B	Number of compressors	Number	3	5	7
C	Air compression method	-	Method 1	Method 2	Method 3
D	Air flow rate	kmol/hr	58000	59500	61000

3.1.3.3 Thermal efficiency

Thermal efficiency indicated the efficiency of the fuel used to produce electricity in the system. It can be expressed as the ratio of net power production to the thermal energy of the fuel, as shown in Eq. 3.1. The net power production was calculated from the power production from air and fuel reactors which was subtracted by the power consumption from compressors and pump. The thermal energy of the fuel was calculated from the lower heating value of natural gas.

$$Thermal\ efficiency\ (\%) = \frac{P_{AR} + P_{FR} - P_C - P_P}{LHV_{NG}} \times 100 \qquad (3.1)$$

Note that;

P_{AR} = power production from air reactor (kW)

P_{FR} = power production from fuel reactor (kW)

P_C = power consumption from air compressors (kW)

P_P = power consumption from pump (kW)

LHV =lower heating value (kW)

NG = natural gas

3.1.3.4 Method of air compression

The operation of multi-stage compressors with a different compression ratio of each compressor has never been studied before. In a previous study, the compression ratio of multi-stage compressors was fixed to be equal in every stage [93, 94]. The significance of this operation and the effect on four responses were assessed in this study. Because the HAT cycle uses many compressors, the compression ratio became a significant parameter of the system. The compression ratio is the ratio of the outlet stream pressure to the input stream pressure, as shown in Eq. 3.2.

$$Compression\ ratio = \frac{Pressure\ outlet}{Pressure\ inlet} \qquad (3.2)$$

The compression ratio directly affects its compressor workload, discharge temperature, and the temperature of the air reactor. When a high compression ratio was used, the pressure and temperature outlet of the compressor would be high, and the workload of the compressor would also be high. Thus, the compression ratio would be kept less than 3 to avoid too much workload and too high temperature outlet [95, 96]. Some compression ratio of the compressor in this study was higher than three and the temperature of the outlet stream is high. The heat of the outlet stream would be used in the preheat section. Typically, the high compression ratio consumes higher work in multi-stage compressors. There were many alternatives for setting up

operation methods. In this study, three operational methods were being studied their effects on the four responses.

Method 1: The outlet pressure of the first stage compressor is 65% of the total pressure of the air reactor. The rest of the compressors has an equal compression ratio by sharing of 35% of total pressure.

Method 2: All compressors in the system use an equal compression ratio.

Method 3: The outlet pressure of the last stage compressor is 65% of the total pressure of the air reactor. The rest of the compressors has an equal compression ratio by sharing of 35% of total pressure.

The compression operation for 5 compressors and 10 atm was shown in Table 3.1.3

Table 3.1.3 The compression ratio of all method of compression.

	Compression ratios				
	stage 1	stage 2	stage 3	stage 4	stage 5
Method 1	6.5	1.1	1.1	1.1	1.1
Method 2	1.6	1.6	1.6	1.6	1.6
Method 3	1.1	1.1	1.1	1.1	6.5

3.2. The methodology of chapter 5; hydrodynamic behavior of chemical looping combustion

3.2.1 The research gaps

Chemical looping combustion could be used for solid fuel or gaseous fuel. The challenge of fuel types was different. The solid fuel for CLC is coal or biomass. The significant problem of solid fuel is the unburnt char because of the slow gasification step. For the gaseous fuel system, mostly, it is complete combustion. Nonetheless, the improper operation condition was also the reason for incomplete combustion as well. The consequence of incomplete combustion was the CO_2 emission from the air reactor. Accordingly, the operation conditions were also crucial factors for suitable hydrodynamic behavior in the CLC reactors.

3.2.2 The objectives

The dimension of the dual circulating fluidized bed reactor was selected from the study of Su et al. [97]. However, the fuel and oxygen carriers from this study were coal and iron oxide, respectively. Therefore, the system of coal and iron oxide was first investigated to obtain the proper hydrodynamics in the reactor. After that, the system of methane and nickel oxide was investigated in the second part, as shown in Fig. 3.2.1.

For the first section, the operating conditions of the reactors were systematically investigated for suitable hydrodynamic behavior. The fuel and oxygen carriers for this section were coal and iron oxide (Fe_2O_3/Fe_3O_4).

For the second section, the operating condition which obtained the highest thermal efficiency from chapter 4 was investigated for suitable hydrodynamic behavior, conversion and temperature achievement. The fuel and oxygen carrier for this section was CH_4 and nickel oxide (NiO/Ni).
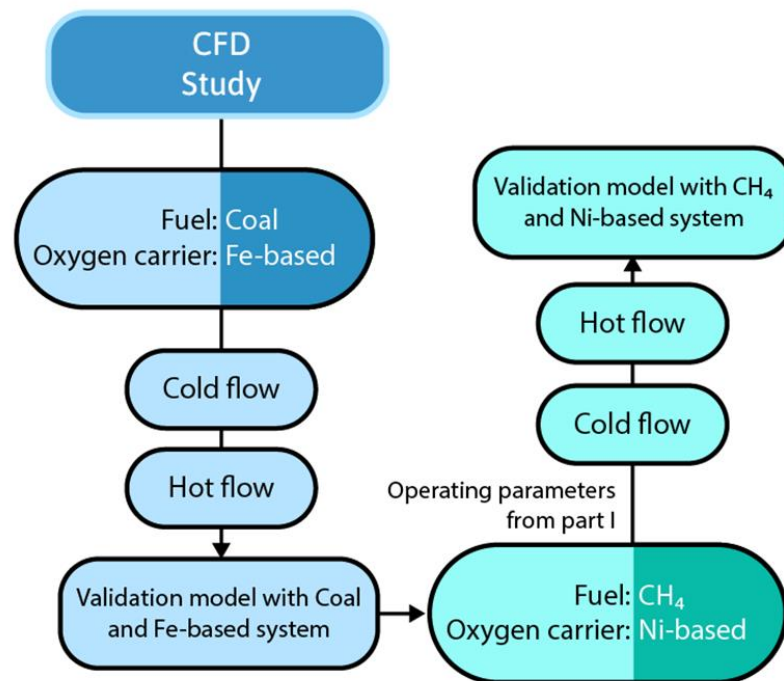
Fig. 3.2.1 The methodology of hydrodynamic behavior of CLC reactor investigation

3.2.3 Model description

The hydrodynamic behavior in a two-dimensional CLC system was investigated. The dual circulating fluidized bed reactor (DCFBR) was selected in this investigation. This reactor consisted of an air reactor and fuel reactor, as shown in Fig. 3.2.2. The reactor configuration was modified from Su et al.'s study. [97] In this study, the downer and air reactor were larger than those compared with Su's study. Accordingly, the solid in the system was more than Su's work. Besides, there was much solid retention in the downer and loop seal. The loop seal was the section that connected the downer and the riser. It was a key point for preventing the reverse flow at the loop seal. The air reactor (AR) was the inner reactor and the fuel reactor (FR) was the outer reactor. Fuel was oxidized by an oxygen carrier at the riser of the fuel reactor. Its products were CO_2, H_2O, and spent oxygen carrier. CO_2 and H_2O were discharged at a cyclone of the fuel reactor. The air was used to regenerate the spent oxygen carrier at the air reactor. There were two types of fuel in the section; coal and natural gas.
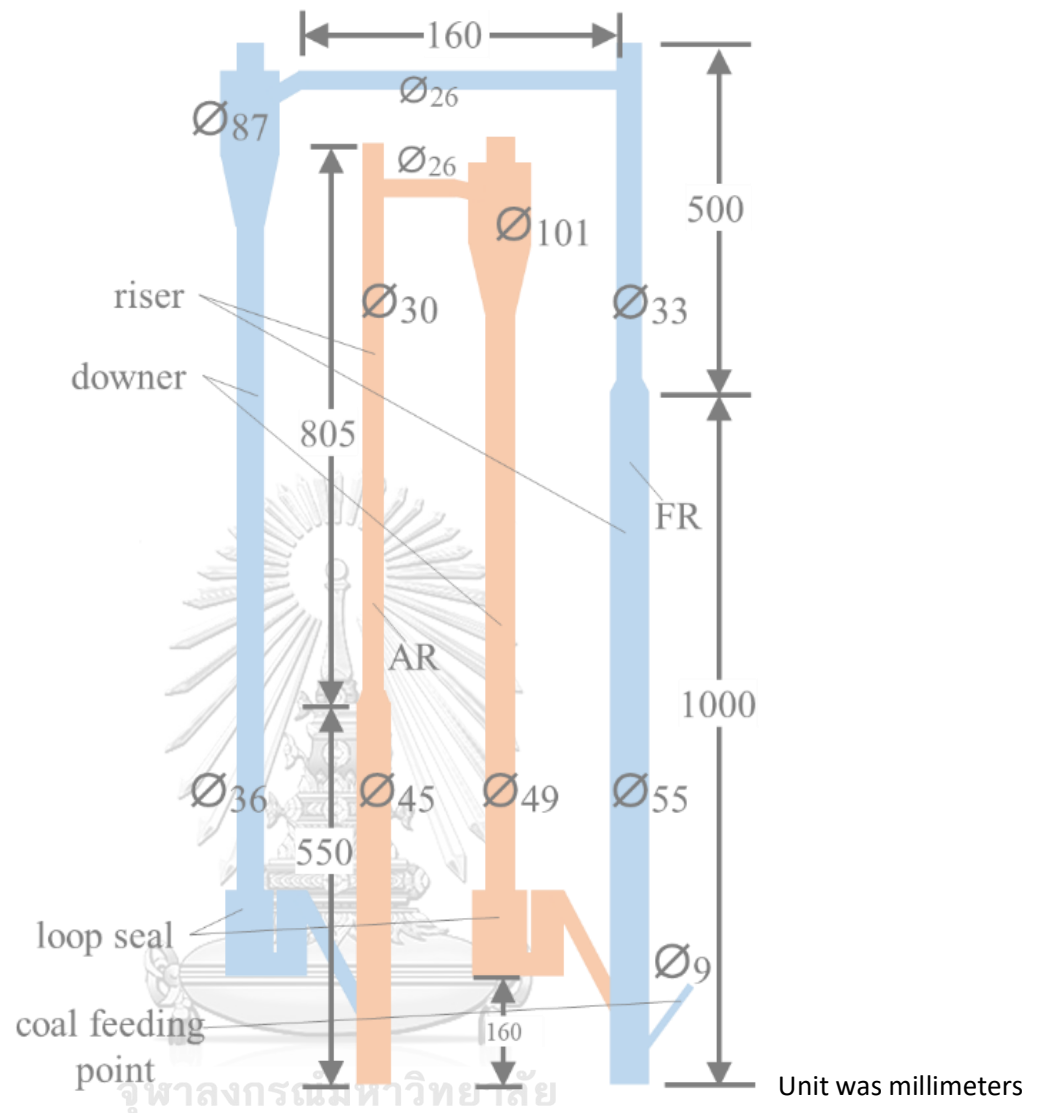
Fig. 3.2.2 The dimension of DCFBR. [97]

3.2.4 The first section

In this section, coal was used as the fuel and Fe_2O_3/Fe_3O_4 was used as the oxygen carrier.

3.2.4.1 Methodology for the first part

There were three phases (Eulerian-Eulerian); gases, coal, and a solid sorbent in the model. In this hydrodynamic model, the drag model was Gidaspow; The heat transfer coefficient model was Gunn and the viscous model was k-epsilon. The oxygen carrier was Fe_2O_3/Fe_3O_4. In the fuel reactor riser, coal was gasified to char and gas species by CO_2. Fe_2O_3 oxidized char and gas species. Subsequently, Fe_2O_3 was transformed to be Fe_3O_4. In the air reactor or the riser, the spent metal oxide, Fe_3O_4, was regenerated to Fe_2O_3 by air. The boundary and initial conditions for this section were shown in Table 3.2.1.

The investigation of the operation condition was systematically designed by using a 3^k factorial experimental design. There were two operation parameters: 1) the system temperature and 2) the ratio between the coal feeding velocity to the weight of the oxygen carrier. The responses of this analysis were % combustible gas species from the FR and % CO_2 from the AR. The total case studies were nine. The three levels of temperature were 1173, 1373, 1573 K. In the study of Petriz-Prieto, the temperature in the range of 1373-1623 K was investigated. However, the study has not revealed the effect of temperature on the hydrodynamic behavior of the reactor. [49] The total Fe_2O_3/Fe_3O_4 in the system was 400 kg. The three levels of gas velocity were 0.1, 0.5, and 1.0 m/s. Accordingly, the three levels of the ratio between coal feeding velocity to the weight of the oxygen carrier were 0.00025, 0.00125 and 0.0025 (m/s)/kg, as shown in Table 3.2.2.

Table 3.2.1 Boundary and initial conditions for the first section.

Boundary conditions	
Right of FR loop seal velocity (m/s)	0
Left of FR loop seal velocity (m/s)	0.00353
Right of AR loop seal velocity (m/s)	0
Left of AR loop seal velocity (m/s)	0.0027
CO_2 velocity inlet at FR riser (m/s)	1.2
CO_2 velocity inlet at coal feeding (m/s)	4
Air velocity inlet at AR riser (m/s)	1.6
Outlet pressure of AR cyclone (pa)	2000
Initial conditions	
Fe_2O_3 mass fraction at AR downer	1
Fe_2O_3 volume fraction at AR downer	0.6
Bed height of AR downer (m)	1.28
Fe_3O_4 mass fraction at FR downer	1
Fe_3O_4 volume fraction at FR downer	0.6
Bed height of FR downer (m)	1.42

Table 3.2.2 The total case studies from 3^k factorial experimental design and the results.

Case	Temperature (K)	V_{coal} to weight of OC (m/s)/(kg)
1	1173	0.00025
2	1373	0.00025
3	1573	0.00025
4	1173	0.00125
5	1373	0.00125
6	1573	0.00125
7	1173	0.0025
8	1373	0.0025
9	1573	0.0025

3.2.4.2. The equations for CFD simulation included of this followed. [98]

3.2.4.2.1. Governing equation

a) Conversion of mass

i.   Gas phase

$$\frac{\partial}{\partial t}\left(\varepsilon_g\rho_g\right) + \nabla \cdot \left(\varepsilon_g\rho_g v_g\right) = 0 \tag{3.2.1}$$

ii.   Solid phase

$$\frac{\partial}{\partial t}\left(\varepsilon_s\rho_s\right) + \nabla \cdot \left(\varepsilon_s\rho_s v_s\right) = 0 \tag{3.2.2}$$

b) Conversion of momentum

i.   Gas phase

$$\frac{\partial}{\partial t}\left(\varepsilon_g\rho_g v_g\right) + \nabla \cdot \left(\varepsilon_g\rho_g v_g v_g\right) = -\varepsilon_g\nabla P + \nabla \cdot \tau_g + \varepsilon_g\rho_g g + \beta_{gs}\left(v_g - v_s\right) \tag{3.2.3}$$

ii. Solid phase

$$\frac{\partial}{\partial t}(\varepsilon_s\rho_s v_s) + \nabla \cdot (\varepsilon_s\rho_s v_s v_s) = -\varepsilon_s\nabla P + \nabla \cdot \tau_s - \nabla P_s + \varepsilon_s\rho_s g +$$
$$\beta_{gs}\left(v_g - v_s\right) \tag{3.2.4}$$

c) Conversion of solid phase fluctuating energy

$$\frac{3}{2}\left[\frac{\partial}{\partial t}\varepsilon_s\rho_s\theta + \nabla \cdot (\varepsilon_s\rho_s\theta)v_s\right] = (-\nabla p_s\bar{I} + \tau_s){:}\nabla v_s + \nabla \cdot (\kappa_s\nabla\theta) - \gamma_s + \emptyset_s \tag{3.2.5}$$

3.2.4.2.2. Constitutive equations

a) Gas phase stress

$$\tau_g = \varepsilon_g\mu_g\left[\nabla v_g + \left(\nabla v_g\right)^T\right] - \frac{2}{3}\varepsilon_g\mu_g(\nabla \cdot v_g)I \tag{3.2.6}$$

b) Solid phase stress

$$\tau_s = \varepsilon_s\mu_s[\nabla v_s + (\nabla v_s)^T] + \varepsilon_s\left(\xi_s - \frac{2}{3}\mu_s\right)\nabla \cdot v_sI \tag{3.2.7}$$

c) Collisional dissipation of solid fluctuating energy

$$\gamma_s = 3(1 - e^2)\varepsilon_s^2\rho_s g_0\,\theta\left(\frac{4}{d}\sqrt{\frac{\theta}{\pi}}\right) \tag{3.2.8}$$

d) Radial distribution function

$$g_0 = \left[1 - \left(\frac{\varepsilon_s}{\varepsilon_{s,max}}\right)^{1/3}\right]^{-1} \tag{3.2.9}$$

e) Solid phase pressure

$$p_s = \varepsilon_s \rho_s \theta [1 + 2g_0 \varepsilon_s (1 - e)] \tag{3.2.10}$$

f) Solid phase shear viscosity

$$\mu_s = \tfrac{4}{5} \varepsilon_s p_s d g_0 (1 + e) \sqrt{\tfrac{\theta}{\pi}} + \tfrac{10 \rho_s d \sqrt{\pi \theta}}{96(1+e)g_0 \varepsilon_s} \left[1 + \tfrac{4}{5} g_0 \varepsilon_s (1 + e)\right]^2 \tag{3.2.11}$$

g) Solid phase bulk viscosity

$$\xi_s = \tfrac{4}{3} \varepsilon_s p_s d g_0 (1 + e) \sqrt{\tfrac{\theta}{\pi}} \tag{3.2.12}$$

h) Exchange of the fluctuating energy between gas and solid

$$\emptyset_s = -3\beta_{gs}\theta \tag{3.2.13}$$

i) Gas–solid phase interphase exchange coefficient

Gidaspow model

when $\varepsilon_g > 0.80$; $\beta_{gs} = \tfrac{3}{4} \tfrac{(1-\varepsilon_g)\varepsilon_g}{d} \rho_g |v_g - v_s| C_{D0} \varepsilon_g^{-2.65}$ $\quad$ (3.2.14)

when $\varepsilon_g \leq 0.80$; $\beta_{gs} = 150 \tfrac{(1-\varepsilon_g)^2 \mu_g}{\varepsilon_g d^2} + 1.75 \tfrac{(1-\varepsilon_g)\rho_g |v_g - v_s|}{d}$ $\quad$ (3.2.15)

with

$Re_k < 1000$; $\quad C_{D0} = \tfrac{24}{Re_k}(1 + 0.15 Re_k^{0.687})$; $Re_k = \tfrac{\rho_g \varepsilon_g |v_g - v_s| d}{\mu_g}$

$Re_k \geq 1000$; $\qquad C_{D0} = 0.44$

when $0.74 \leq \varepsilon_g \leq 0.82$; $\quad \omega(\varepsilon) = -0.5760 + \tfrac{0.0214}{4(\varepsilon_g - 0.7463)^2 + 0.0044}$

when $0.82 < \varepsilon_g \leq 0.97$; $\quad \omega(\varepsilon) = -0.0101 + \tfrac{0.0038}{4(\varepsilon_g - 0.7789)^2 + 0.0040}$

when $\varepsilon_g > 0.97$; $\qquad \omega(\varepsilon) = -31.8295 + 32.8295\varepsilon_g$

3.2.4.2.3 The reactions for the coal reduction and the iron oxide oxidation

Coal pyrolysis reaction [97, 99]

$$Coal + 0.0666CO_2 \rightarrow 0.4663Char + 0.05192CH_4 + 0.00554C_2H_6 +$$
$$0.1672CO + 0.0604H_2 + 0.0269H_2O + 0.01007ASH \tag{3.2.16}$$
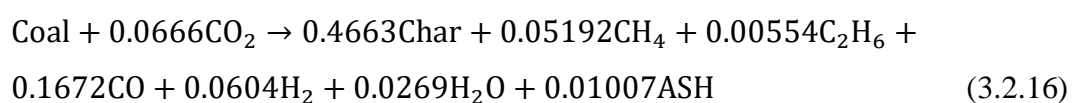
The reaction rate of pyrolysis was followed;

$$r_{pyrolysis} = (1 \times 10^{-3})\big(0.3(2 \times 10^5)exp(-104.6/RT) + (1.3 \times$$

$$10^7)exp(-167.4/RT)\big)C_{coal} \qquad (3.2.17)$$

Char gasification reaction [100]

$$\text{Char} + CO_2 \rightarrow 2CO \qquad (3.2.18)$$

The reaction rate of char gasification was followed;

$$r_{char} = \frac{(8.83 \times 10^4)\rho_{char}\varepsilon_{char}r_g(1-x_{char})^{2/3}}{MW_{char}} \qquad (3.2.19)$$

r_{char} (kmol/m³/s) was char gasification rate, ρ_{char} (kg/m³) was char density, ε_{char} was char volume fraction, x_{char} was char conversion, and MW_{char} was char molecular weight.

Methane reduction reaction [101, 102]

$$CH_4 + 12Fe_2O_3 \rightarrow 8Fe_3O_4 + 2H_2O + CO_2 \qquad (3.2.20)$$
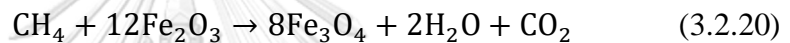
The reaction rate of methane reduction was followed;

$$r_{CH_4} = \frac{(0.30085)k_{CH_4}(x)\rho_{Fe_2O_3}(m_{ox})Y_{CH_4}}{0.2(MW_{O_2})} \qquad (3.2.21)$$

Where;

$$x = \frac{m\_ox}{m\_ox - m\_red2}$$

$$m\_ox = Y_{Fe_2O_3} + Y_{Fe_3O_4}\frac{12MW_{Fe_2O_3}}{8MW_{Fe_3O_4}} \qquad (3.2.22)$$

$$m_{red2} = Y_{Fe_2O_3}\frac{8MW_{Fe_3O_4}}{12MW_{Fe_2O_3}} + Y_{Fe_2O_3} \qquad (3.2.23)$$

$$k_{CH_4} = 3.37598exp(-49/RT)C_{CH_4}^{1.3} \qquad (3.2.24)$$

Ethane reduction reaction [101, 102]

$$C_2H_6 + 21Fe_2O_3 \rightarrow 14Fe_3O_4 + 3H_2O + 2CO_2 \qquad (3.2.25)$$
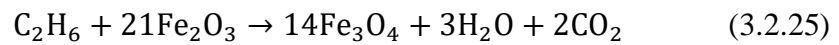
The reaction rate of ethane and methane reduction were equal.

$$r_{C_2H_6} = r_{CH_4}(R\ 4.4) \qquad (3.2.26)$$

Carbon monoxide reduction

$$CO + 3Fe_2O_3 \rightarrow 2Fe_3O_4 + CO_2 \qquad (3.2.27)$$
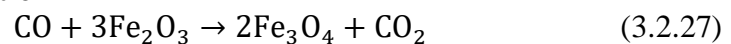
The reaction rate of carbon monoxide reduction was followed;

$$r_{H_2} = \frac{(2)(0.30085)k_{CO}(\rho_{Fe_2O_3})(m\_ox)(1-x)^{2/3}}{MW_{O_2}} \qquad (3.2.28)$$

Where; $\qquad k_{CO} = 0.65410exp(-20/RT)C_{CO} \qquad (3.2.29)$

Hydrogen reduction [101, 102]

$$H_2 + 3Fe_2O_3 \rightarrow 2Fe_3O_4 + H_2O\ (4.6) \qquad (3.2.30)$$
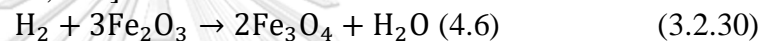
The reaction rate of hydrogen reduction was followed;

$$r_{H_2} = \frac{(2)(0.30085)k_{H_2}(\rho_{Fe_2O_3})(m\_ox)(1-x)^{2/3}}{MW_{O_2}} \qquad (3.2.31)$$

Where;

$$k_{H_2} = 2.42648exp(-24/RT)C_{H_2}^{0.8} \qquad (3.2.32)$$

Water gas shift reaction [103]

$$CO + H_2O \rightarrow CO_2 + H_2 \qquad (3.2.33)$$

The reaction rate of water gas shift was followed;

$$r_{CO} = -2.17 \times 10^7 exp(-192/RT)\left(C_{H_2}^{0.5}C_{CO_2} - \frac{C_{H_2O}C_{CO}}{exp(-4.33+(4577.8/T))}\right)$$

$$(3.2.34)$$

Iron oxide oxidation [101, 102]

$$4Fe_3O_4 + O_2 \rightarrow 6Fe_2O_3 \qquad (3.2.35)$$
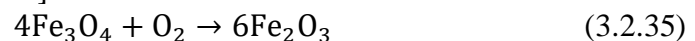
The reaction rate of carbon monoxide reduction was followed;

$$r_{H_2} = \frac{(2)(0.30085)k_{O_2}(\rho_{Fe_2O_3})(m\_ox)(1-x)^{2/3}}{MW_{O_2}} \qquad (3.2.36)$$

Where;

$$k_{O_2} = 0.63669exp(-20/RT)C_{O_2} \qquad (3.2.37)$$

3.2.5 The second section

In this section, methane (CH_4) was used as the fuel and NiO/Ni was used as the oxygen carrier.

3.2.5.1 Methodology for the second section

In this model, the drag model was Gidaspow, the heat transfer coefficient model was Gunn, and the viscous model was k-epsilon, as the same in the first part. The difference from the first part would be mentioned as followed. There were two phases (Eulerian-Eulerian); gases and solid sorbent. The oxygen carrier was NiO/Ni. In the fuel reactor riser, CH_4 was mixed with CO_2. The mixture was introduced into the riser of the fuel reactor. NiO oxidized the CH4. The gas products were CO_2 and H_2O. The solid product was Ni. In the air reactor riser, the spent metal oxide, Ni, was regenerated to NiO by air. The boundary and initial conditions for this section were shown in Table 3.2.3. At the initials, the solid was patched in the reactor downer. The gas mixture was patched in the reactor riser to reduce the temperature deviation from the gas density changing.

Table 3.2.3 Boundary and initial conditions for the second section.

Boundary conditions	
Right of FR loop seal velocity (m/s)	0
Left of FR loop seal velocity (m/s)	0.00353
Right of AR loop seal velocity (m/s)	0
Left of AR loop seal velocity (m/s)	0.0027
CO_2 velocity inlet at FR riser (m/s)	1.2
Air velocity inlet at AR riser (m/s)	1.6
Outlet pressure of AR cyclone (pa)	2000
Initial conditions	
Reactor temperature and the inlet stream (K)	873
Ni mass fraction at AR downer	0.277
Al_2O_3 mass fraction at AR downer	0.723
Solid volume fraction at AR downer	0.35/0.45
Bed height of AR downer (m)	1.28
NiO mass fraction at FR downer	0.277
Al_2O_3 mass fraction at FR downer	0.723
Solid volume fraction at FR downer	0.35/0.45
Bed height of AR downer (m)	1.42
CH_4 mass fraction at FR riser	0.3
CO_2 mass fraction at FR riser	0.7
Bed height of FR riser (m)	1.50
O_2 mass fraction at AR riser	0.168
N_2 mass fraction at AR riser	0.2
H_2O mass fraction at AR riser	0.632
Bed height of AR riser (m)	1.35

The crucial point for the model in this system was the properties of the mixture, such as density, the heat of formation, heat capacity. The properties must be checked in the mixture section of the Ansys fluent programs. The properties of the mixture were acquired from Perry's chemical engineers' handbook. [104] The accurate properties data led to the accuracy of the results.

The aim of this section was the using operation conditions from the chapter 4. The rate reaction, initial solid volume fraction, velocity and CH_4 mass fraction in feed were investigated to obtain the suitable hydrodynamic behavior. The pre-exponential

factor of reaction rate was adjusted at 1, 1E+3 and 1E+5. The initial solid volume fraction was adjusted at 0.35 and 0.45. The velocity was adjusted from the previous section at 1 and 1.5 times. The CH_4 mass fraction in feed was adjusted at, 0.05, 0.15 and 0.30, as shown in Table 3.2.4. The total cases were 10 cases. After that, the simulation data was validated with the temperature, CH_4 conversion and MW thermal of the experimental data.

Table 3.2.4 The adjusted parameters

Cases	Rate constant	Volume fraction of solid phase	Velocity when compare with base case	Mass fraction of CH_4 at feed
1	1	0.35	1	0.3
2	1	0.45	1	0.3
3	1.00E+03	0.35	1	0.3
4	1.00E+03	0.45	1	0.3
5	1.00E+05	0.35	1	0.3
6	1.00E+05	0.45	1	0.3
8	1.00E+05	0.45	1	0.15
7	1.00E+05	0.45	1	0.05
9	1.00E+05	0.35	1.5	0.3
10	1.00E+05	0.45	1.5	0.3

3.3 Methodology for chapter 6; the sustainability assessment of chemical looping combustion for power production

3.3.1. The research gaps

In a previous CLC study, the best case of the CLC process was investigated only thermal efficiency and economic analysis. However, the study did not investigate whether those implementations would enhance the sustainability of the improved CLC processes. The significance of thermal efficiency to the sustainability of the CLC process had not been reported. The approach for CLC process improvement by sustainability analysis was reported, as well. There were 6 case studies in which different operation conditions and configurations were investigated. The best case of 3 viewpoints (thermal efficiency, economic analysis, and sustainability analysis) was proposed. The comparison among the 3-analysis types has not been performed before. Besides, this study revealed the results, comparing combustion types between conventional combustion (CC) and CLC, the effect of the CO_2 capture efficiency of the CC, and the effect of thermal efficiency on sustainability analysis. The interesting point was the approach of the operation condition or configuration of the case study that obtained high sustainability was suggested in this study.

3.3.2. Objective

Perform emergy analysis for sustainability assessment

3.3.3. Methodology

The main objectives of this section were the sustainability assessment of the CLC process. In addition, there was an investigation of the impact of combustion types and the impact of system configuration to the 3 points of view, thermal efficiency analysis, economic analysis and sustainability analysis. The CLC process was the combustion unit that almost captures CO_2 in flue gas with a simple process. The other process that had to compare with the CLC process was the combustion process that included the CO_2 capture also. This comparison would express the impact of combustion types on sustainability. Accordingly, the conventional combustion (CC) with solid adsorption and the CLC process were selected to compare. The CLC

process for power production was achieved high thermal efficiency. The high thermal efficiency indicated the efficiency of fuel usage in power production. There was not an investigation of the significance of thermal efficiency to sustainability. Accordingly, the significance of efficiency improvement of the CLC process was the one topic in the sustainability assessment of the CLC process. The benefit of this section would be the first time that represents the sustainability assessment of the CLC process. It could be a new proposal for the CLC process improvement in the future, as shown in Fig. 3.3.1
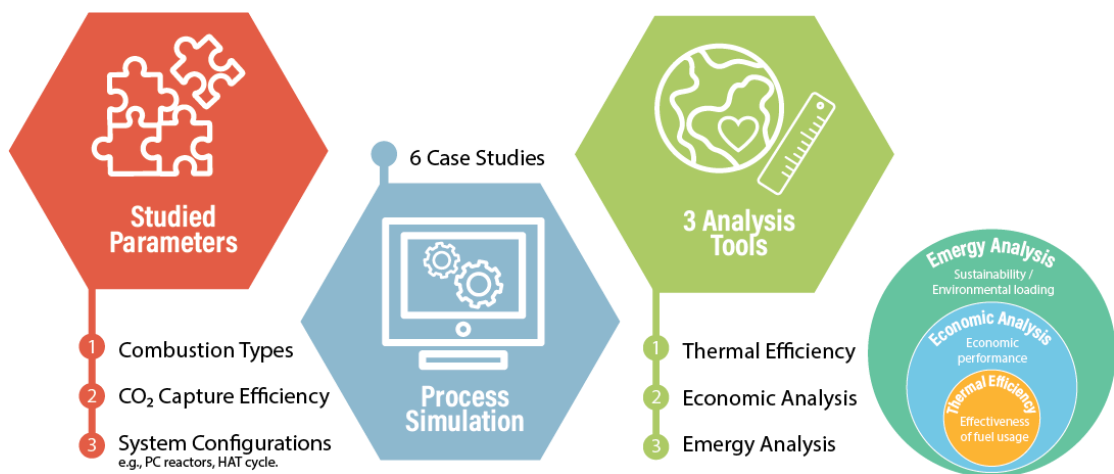
Fig. 3.3.1 The graphical abstract of the sustainability of CLC process investigation

The comparison of combustion types for decision-making in a sustainability viewpoint between the CC with solid adsorption and the CLC process was developed and investigated. The total cases for this investigation were 6 cases. Cases 1-3 were CC cases and cases 4-6 were CLC cases. The brief operation of all case study was shown in Fig. 3.3.2.
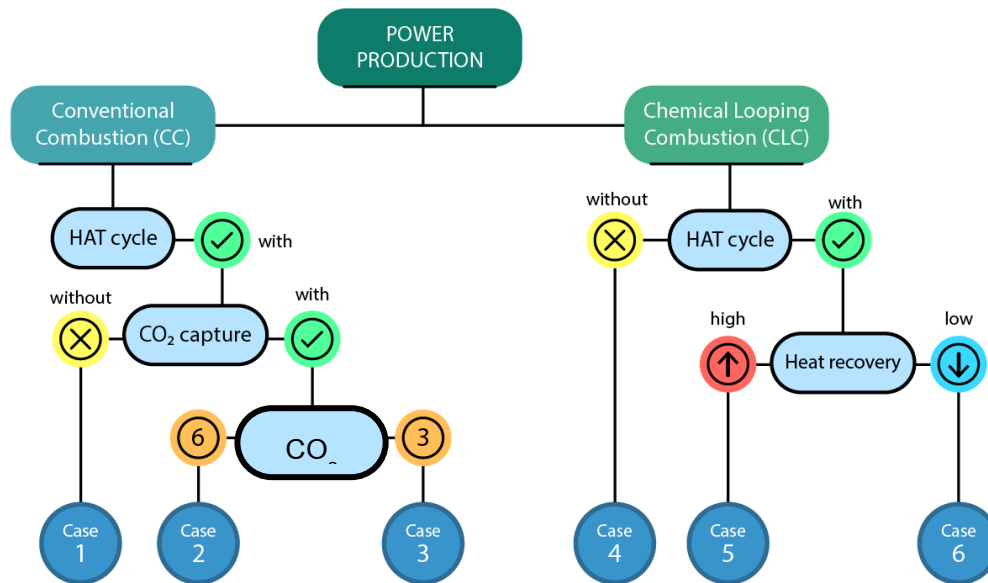
Fig. 3.3.2 The system configurations of all case studies

The significant section for power production was the HAT cycle. HAT cycle was the power production unit that obtained high thermal efficiency. It consisted of a multi-stage compressor which it had an intercooler between the compressor stage. This cycle increased the thermal efficiency of the power plant by decrease the work consumption of the compression process. The decrease in compressed air temperature was the reason for the work consumption of compression reduction. The operation of compression in this case study was method 3 because of its increased temperature of the combustion reactor and power production. The compression operation of case 6 was method 2 because the work consumption of compression from method 2 was the lowest. In other multi-stage compressor studies, its compression ratio of every stage was equal, which was corresponding to method 2 in case 6. [93] The compression ratio affected power production and thermal efficiency, as well. In the compression operation of all case studies except case 6, the compression ratio was 1.115, 1.38 and 9.75, for stages 1, 2 and 3, respectively. In the last stage compressor, it was 65% of total pressure change. Accordingly, this operation increased the temperature of the compressed air before it was introduced to the combustion section. In this compression operation, the work consumption of compression was the highest workload. However, the power production and thermal efficiency of this operation

were the highest obtaining. The compression operation of case 6 was different from others. The compression ratio of all stages was 2.466.

In the CC case, there were three major sections; 1) combustion section, 2) HAT cycle for power production (Fig.3.3.1), and 3) solid adsorption for CO_2 capture. Case 1 was the CC case that was not employed solid adsorption. There were only a combustion section and the HAT cycle. The analysis from cases would be to express the impact of the process without CO_2 capture. Cases 2 and 3 were the CC case that employed three major sections, which stated above. The difference between cases 2 and 3 was the CO_2 capture efficiency in the CO_2 capture section, 96.22% and 77.66% in case 2 and case 3, respectively. Accordingly, the effect of the CO_2 capture efficiency would be investigated from 3 points of view. In the CO_2 capture section, the operation conditions were followed Boonprasop study. [105-107] The multi-stage CO_2 capture reactor was the main section of the CO_2 capture section. The solid sorbent in CC cases was Na_2CO_3. [16]

In CLC cases, there were 3 major sections; 1) CLC process for combustion and CO_2 separation and 2) HAT cycle. Case 3 was the CLC case that was not employed the HAT cycle. Case 3 was the only CLC process without a multi-stage compressor from the HAT cycle. HAT cycle was the power production that reduced the work consumption of compression. Since the HAT cycle was not employed in case 4, therefore the thermal efficiency of case 4 would be the lowest of all case studies. Moreover, the equipment cost of case 4 would be the lowest of all, as well. The effect of low thermal efficiency and low equipment cost on the 3 points of view would be analyzed. Cases 5 and 6 were the CLC case that employed 2 major sections, which stated above. The operation conditions of case 4 led to the highest thermal efficiency obtaining. The heat recovery and the type of compression operation of case 4 were the cause of high equipment cost. The operation condition of case 6 was adjusted; low heat recovery and type of compression operation. Accordingly, the thermal efficiency of case 6 was slightly lower than case 5.

For all six case studies, the power plants were operated at a 50 MW capacity using natural gas as the feedstock. The case studies were developed with the ASPEN PLUS process simulation software using Peng-Robinson-Boston-Mathias for thermodynamics properties [49]. This simulation was considered as the adiabatic

process for obtain the highest efficiency of the system. The solid metal inventory in the process was 700 kg/MW$_{th}$ for all case studies [108]. The RGibbs reactor was used for air and fuel reactor. The RYield was used for CO_2 capture reactor. RYield is suitable to determine the conversion of each stage to consistent with experimental data. [105-107] The minimum temperature approach of heat exchanger was 10°C. The isentropic efficiency of compressor and turbine was 90% . The parameters related to the case studies are presented in Table 1 for cases 1-3, and in Table 2 for cases 4–6. The parameters in CC cases and CLC cases were shown in Table 3.3.1 and Table 3.3.2, respectively. The process description of case studies would be explained in the following section.

Table 3.3.1 Conditions of cases 1-3.

	Case 1	Case 2	Case 3
CLC	no	no	no
HAT cycle	yes	yes	yes
Compression ratio in HAT cycles of all stages	2.466	2.466	2.466
Solid in system	no	Na_2CO_3/ Al_2O_3	Na_2CO_3/ Al_2O_3
Pressure of combustor (atm) [69]	15	15	15
Pressure of CO_2 capturing reactor (atm) [105]	-	2	2
Temperature of CO_2 capturing reactor (°C) [105]	-	60	60
Pressure of regeneration reactor (atm) [105]	-	0.2	0.2
Temperature of regeneration reactor (°C) [105]	-	60	60
Temperature of Na_2CO_3 fed into reactor (°C) [105]	-	60	60
Natural gas (kg/h)	7176.02	7929.79	7496.78
Air (kg/h)	292461.10	323181.09	305533.80
Isentropic efficiency of compressor (%)	85	85	85
Isentropic efficiency of turbine (%)	90	90	90
Water in inter cooling (kg/h)	13964	13964	13971
Na_2CO_3 loading on Al_2O_3 (%wt) [105]	-	17	17
Na_2CO_3 (kg/h)	-	599137.40	566421.60
Al_2O_3 (kg/h)	-	2925200.52	2765470.68
CO_2 removal (%)	0	96.27	77.76
The mass fraction of flue gas (%)			
H_2O	8.77	1.47	4.84
N_2	71.98	83.27	79.34
O_2	12.92	14.98	14.26
CO_2	6.33	0.28	1.55

Table 3.3.2 Conditions of cases 4–6.

	Case 4	Case 5	Case 6
CLC	yes	yes	yes
HAT cycle	no	yes	yes
Compression ratio in HAT cycles of the 1st, 2nd, 3th stages	-	1.115, 1.38, 9.75	2.466, 2.466, 2.466
Solid in system	NiO/Al_2O_3	NiO/Al_2O_3	NiO/Al_2O_3
Pressure of fuel reactor (atm) [69]	15	15	15
Pressure of air reactor (atm) [69]	20	20	20
Temperature of NiO fed into reactor (ºC)	1350	1350	1350
Natural gas (kg/h)	7903	6742	7061
Air (kg/h)	349985	232100	243635
Isentropic efficiency of compressor (%)	85	85	85
Isentropic efficiency of turbine (%)	90	90	90
Water in inter cooling (kg/h)	no	36333	24762
NiO loading on Al_2O_3 (%mol)	25	25	40
Ni (kg/h)	110362	94157	98603
Al_2O_3 (kg/h)	575190	490731	256952
Conversion in fuel reactor (%) [109]	100	100	100
CO_2 removal (%)	100	100	100
The mass fraction of flue gas (%)			
H_2O	0.00	14.96	10.28
N_2	84.03	73.22	77.48
O_2	15.97	11.57	12.24
CO_2	0.00	0.00	0.00

จุฬาลงกรณ์มหาวิทยาลัย

CHULALONGKORN UNIVERSITY

3.3.3.1. Process descriptions

HAT Cycle

In HAT cycle, air was compressed by the multi-stage compressor and was reduced temperature by the intercooler which was between compressors. Therefore, the fresh air was introduced into C-101, HX-101, C-102, HX-102, and C-103, respectively, as shown in Fig. 3.3.3. Water gained the heat from the compressed air and HX-101 and HX-102, respectively. Water and compressed air were preheated and generated to be the humid air, before introduced to air reactor.
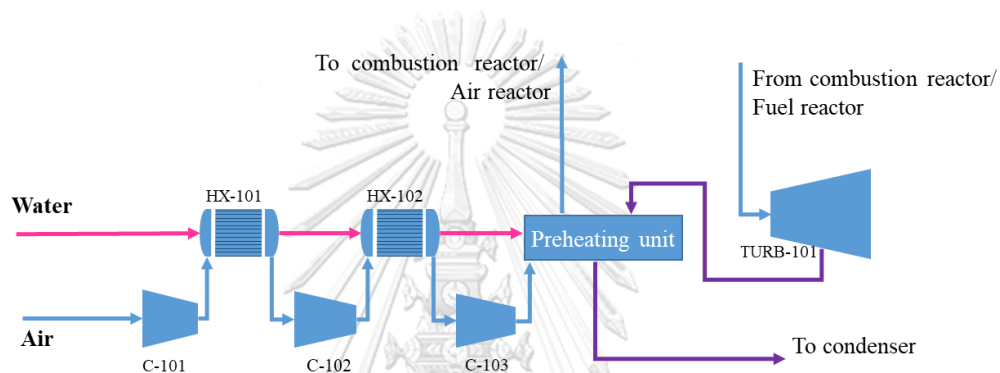
Fig. 3.3.3 Flowchart of a HAT cycle

Case 1: CC and HAT cycle without CO_2 capture

Case 1 was the CC and HAT cycle. The CO_2 capture process was not employed in this case. The flow diagram of case 1 was shown in Fig. 3.3.4. The 3 major sections of this case were the natural gas preheating section, combustion chamber (CB-101), and HAT cycle section. After that, the compressed air and water were introduced to the preheating section. The discharged from turbine (TRUB-101) was the heat source which was used to preheat natural gas, water, and air. Natural gas was preheated before it was introduced into CB-101 for combustion. The flow chart of natural gas preheating was shown in Fig. 3.3.5. Natural gas was preheated by high temperature turbine discharge at HXF-101 and HXF-102, and water was preheated at HX-201. Compressed air was preheated at HX-202. Water and compressed air were preheated by the discharged turbine, as well. The analysis of this case will reveal the power plant performance that was not employed CO_2 capture section in 3 points of view.
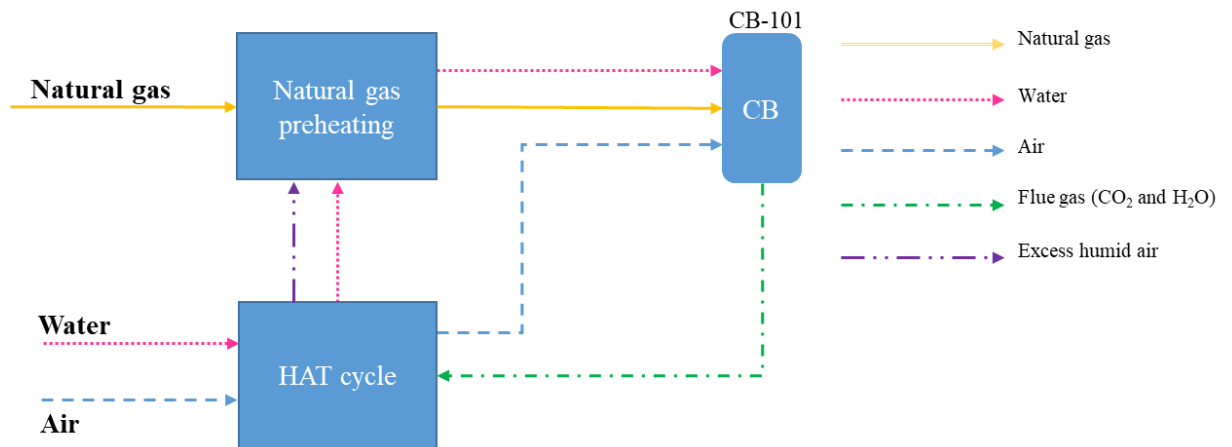
Fig. 3.3.4 Flow process of CB with a HAT cycle and CO_2 capture process (case 1)
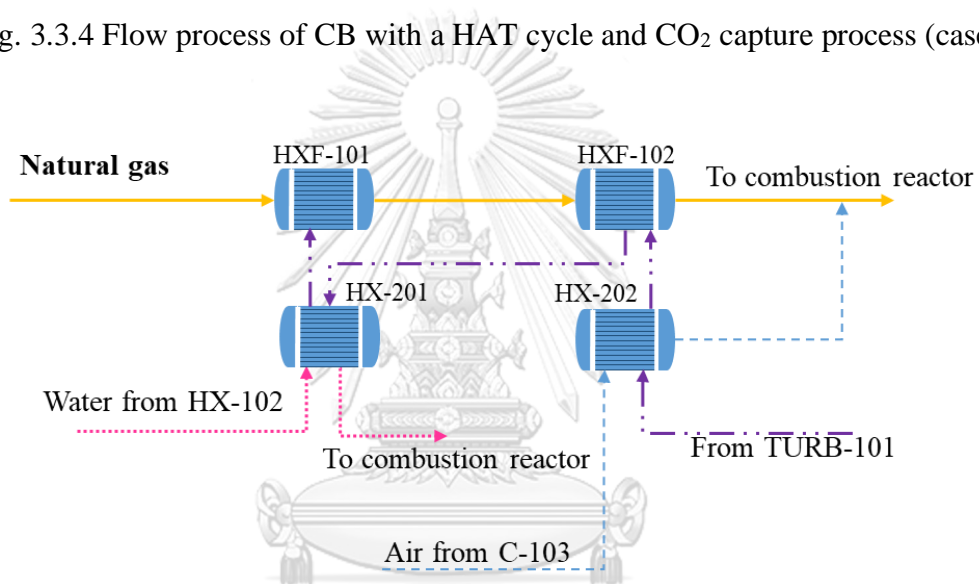
Fig. 3.3.5 Flow chart of natural gas preheating for case 1

Case 2: CC and HAT cycle with 96.22% CO_2 capture and Case 3: CC and HAT cycle with 77.76% CO_2 capture.

Case 2 and case 3 were the CC with the CO_2 capture section. The flow chart of cases 2 and 3 were shown in Fig. 3.3.6. There were 5 sections in these cases; natural gas preheating, combustion (CC), HAT cycle, CO2 capture process, and condenser (CDS). Water and air were introduced into the HAT cycle. Water was used as coolant media in the intercooler. Air was compressed at the multi-stage compressor. They were combined with being humid air and were introduced into the combustion chamber (CC-101). The flue gas from CC-101 was used to preheat other sections. The preheating section was shown in Fig. 3.3.7. Natural gas was preheated at HXF-101

and HXF-102. Water was preheated at HX-201. Compressed air was preheated at HXA-103. Natural gas, water and air were preheated by the discharged turbine (TURB-101). The CO_2 capture efficiency process in case 2 was higher than case 3 because of the higher CO_2 capture reactors. There were six reactors of CO_2 capture in case 2, but 3 reactors for case 3. The CO_2 conversion of each reactor was to follow Boonprsop's study. [105-107] The CO_2 capture and solid regeneration of case 2 and case 3 were shown in Fig. 3.3.8. (a) and Fig. 3.3.8. (b), respectively. The discharged from the turbine after the preheating section was introduced into CO_2 capture reactors. The flue gas, after treated by Na_2CO_3, was sent to CYC-101 for separated the spent solid sorbent and treated flue gas. The solid sorbent was preheated by turbine discharge before being regenerated. The regeneration condition was followed by Boonprasop's study, which was shown in Table 3.3.1. The CO_2 and water would be separated from sorbent and they were sent to a condenser (CDS-101) for obtained higher purity of CO_2. The regenerated sorbent was further used to captured CO_2. In between CO_2 capture reactors, there was a heat exchanger for temperature reduction. This approach increased CO_2 capture efficiency, as well. Case 2 had 6 reactors; CP-101, CP-102, CP-103, CP-104, CP-105 and CP-106 and 3 heat exchangers; HXC-101, HXC-102, HXC-103. Case 3 had 3 reactors; CP-101, CP-102 and CP-103, and 1 heat exchangers; HXC-101.
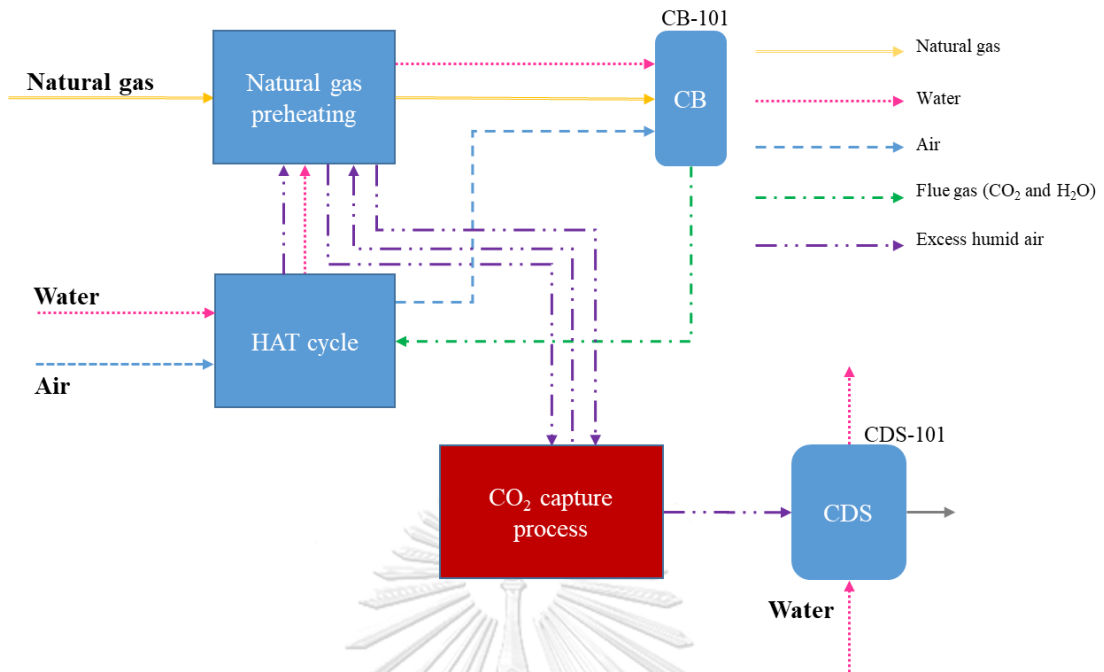
Fig. 3.3.6 Flow process of conventional combustion with a HAT cycle and CO_2 capture process (cases 2 and 3)
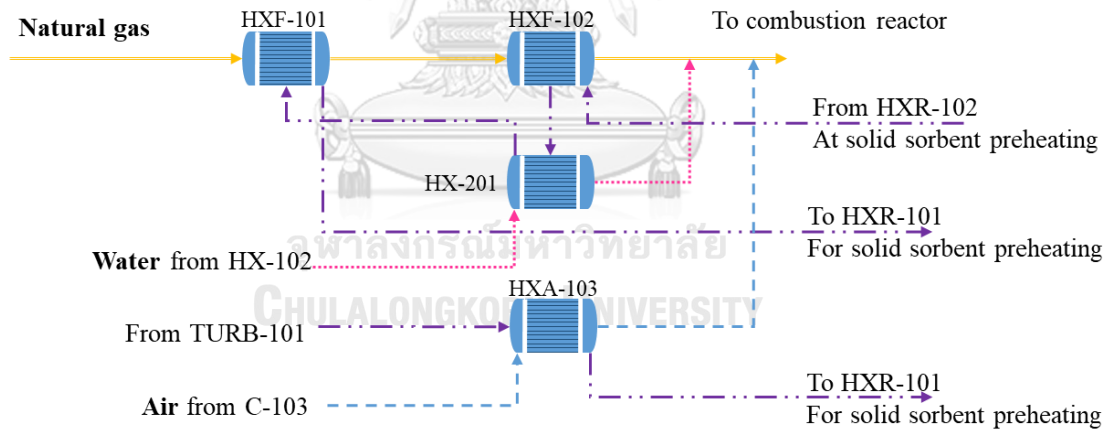
Fig. 3.3.7 Flow chart of natural gas preheating for cases 2 and 3

(a)

(b)
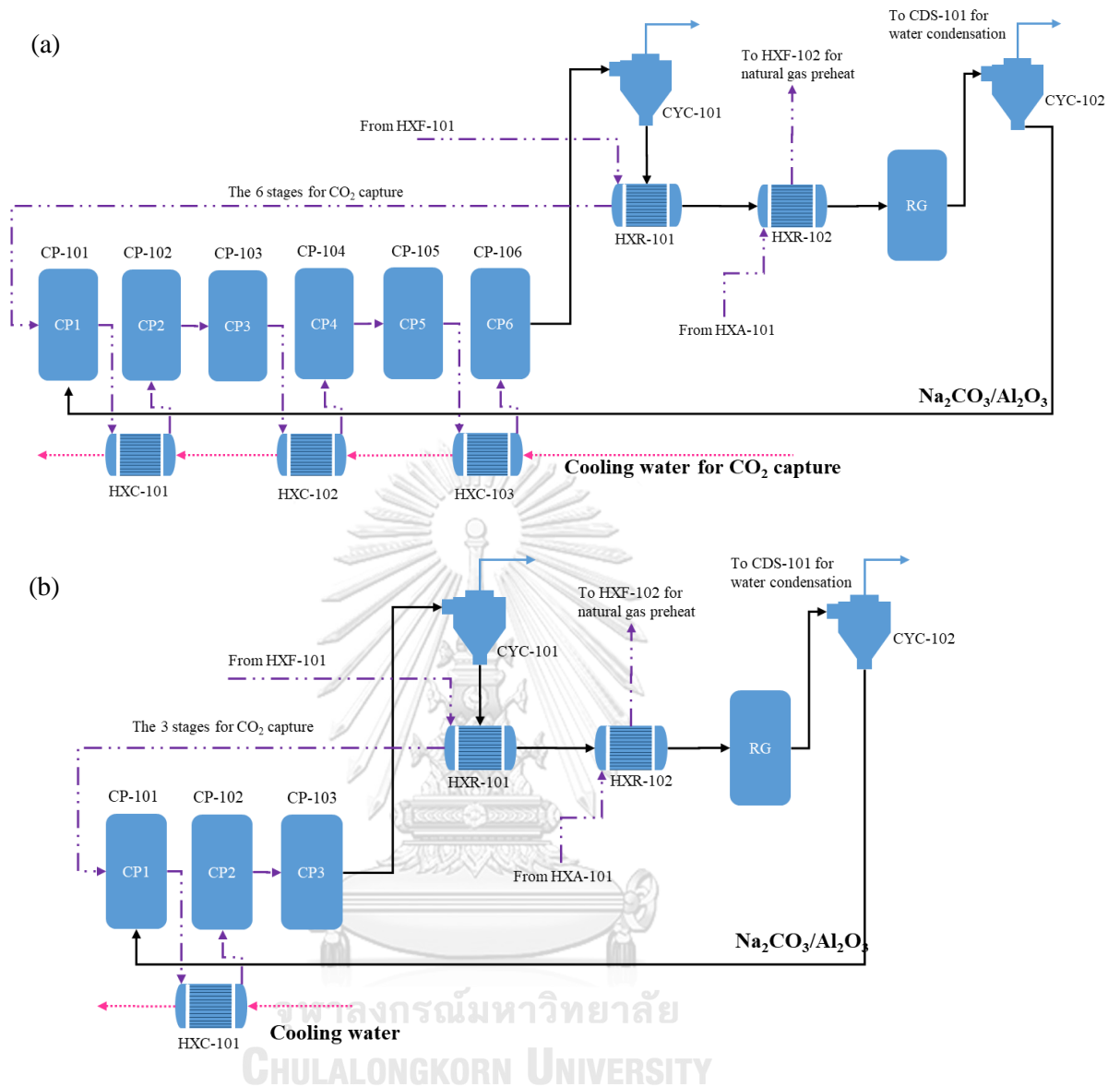
Fig. 3.3.8 Flow chart of CO_2 capture and regeneration process for (a) case 2 and (b) case 3

Case 4: CLC without HAT

Case 4 was the only CLC process without a HAT cycle, as shown in Fig. 3.3.9. There were 4 main sections for this case; natural gas and compressed air preheating, CLC, turbine (TURB-101), and condenser (CDS-101). Natural gas was preheated by the turbine discharge. Then it was introduced into CLC. Air was compressed and it was introduced into CLC. After combustion, the flue gas and the excess air were used to preheat in the preheating section. After that, CO_2 was separated from water by CDS. The flow chart of the CLC process was shown in Fig. 3.3.10.

The compressed air from HXA-103 was used to oxidized Ni in the air reactor (AR-101), as shown in 3.3.1. The outlet from the air reactor was sent to a cyclone (CYC-101). The excess air was sent to the turbine (TURB-102) for power production. Natural gas was introduced into the fuel reactor (FR-101). Natural gas was oxidized by NiO, as shown in 3.3.2. Then the outlet from FR-101 was sent to a cyclone (CYC-102). The flue gas was used for power production at the turbine (TURB-101). The discharges from 2 turbines were used in the preheating section.

Reaction in air reactor: $Ni + 0.5\,O_2 \rightarrow NiO + Heat$ (3.3.1)

Reaction in fuel reactor: $CH_4 + 4\,NiO + Heat \rightarrow 4\,Ni + CO_2 + 2H_2O$ (3.3.2)
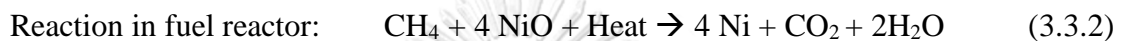
The flowchart of the preheating section was shown in Fig. 3.3.11. Natural gas was preheated at HXF-101, HXF-102, HXF-103, HXF-104, and HXF-105. Air was compressed at C-101; after that, the compressed air was preheated at HXA-101, HXA-102, and HXA-103. The discharge from TURB-101 was used to preheat at HXF-105, HXA-103, HXF-104, HXF-103, and HXA-101, respectively. Then it would be introduced to CDS-101. The discharge from TURB-102 was used to preheat at HXA-102, HXF-102, and HXF-101, respectively. This case was not employed in the HAT cycle in the process. The thermal efficiency of this case would low, but the equipment cost of this case was low. The economic and sustainability analysis of the low thermal efficiency case would be illustrated in the economic and sustainability analysis part.
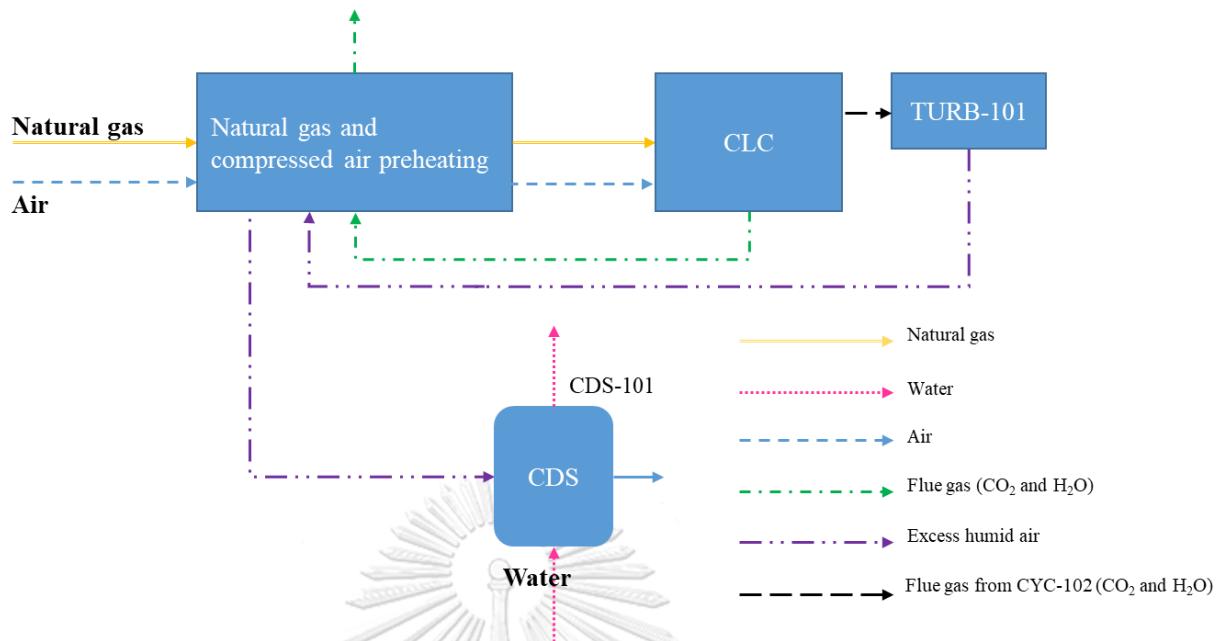
Fig. 3.3.9 Flow process of CLC without a HAT cycle for case 4
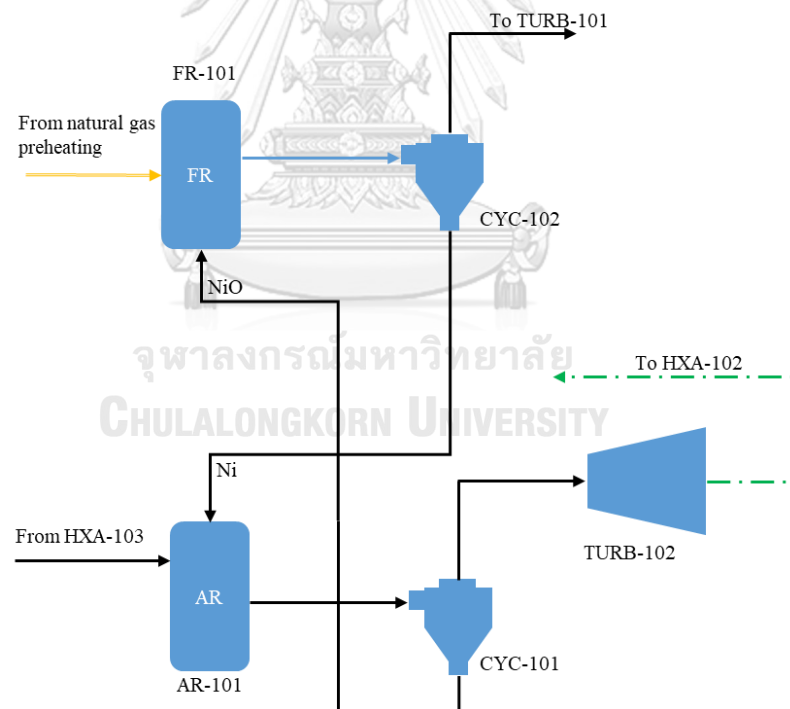
Fig. 3.3.10 Flow chart of the CLC process (a) without a HAT cycle for case 4

and (b) for cases 4, 5, and 6
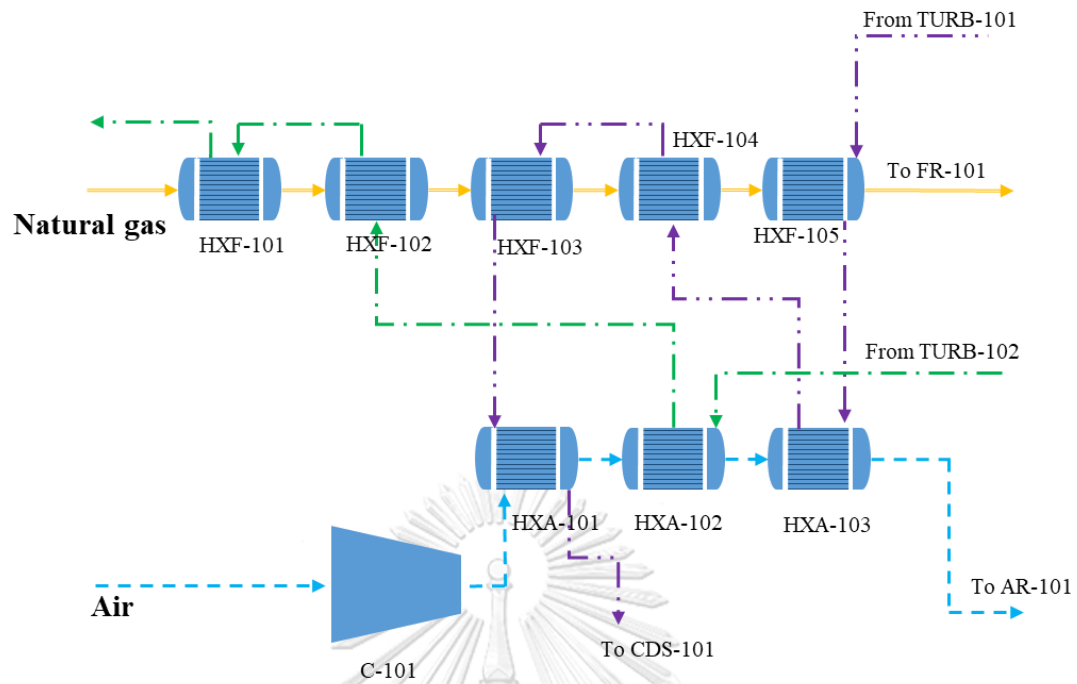
Fig. 3.3.11 Flow chart of natural gas and compressed air preheating for case 4

Case 5: CLC with HAT cycle and high heat recovery

Case 5 was the CLC process with the HAT cycle, which was high heat recovery. The flow chart of case 5 was shown in Fig. 3.3.12. There were four major sections; preheating, CLC, HAT cycle, and CDS. Natural gas was preheated, then it was introduced to CLC for heat production and CO_2 separation. Water and air were introduced into the HAT cycle. Then they were preheated and were introduced into CLC, as well. The CO_2 in the flue gas was separated at CDS. CLC process was the heat production unit that inherent separated CO_2. Accordingly, the thermal efficiency of CLC would higher than CC with the CO_2 capture section. Besides, the operation conditions of this case led to obtaining high thermal efficiency. The compression operation of this case increased power production. This case was high heat recovery. Accordingly, the heat exchanger unit in the preheating section of this case was higher than the others. The flow chart of the preheating section was shown in Fig. 3.3.13. Natural gas was preheated at HXF-101, HXF-102, HXF-103, and HXF-104. Then natural gas was introduced to the fuel reactor (FR-101). The compressed air was preheated at HXA-101. Water was preheated at HXA-102, HXA-103, HXA-104,

HXA-105, and HXA-106 After that, water was dissolved in dry air which it became humid air at mixer. The humid air was preheated at HXA-107, and HXA-108. Humid air was introduced to air reactor (AR-101). The discharged from TURB-101 was used to preheated at HXF-105, HXA-108, HXF-104 HXF-103, and HXA-101. The discharged from TUR-102 was used to preheated at HXA-107, HXA-106, HXF-102, HXA-105, HXA-104, HXA-103, HXA-102, and HXF-101. This case was designed to obtain the highest thermal efficiency. The economic and sustainability analysis of this cases was explained in other section.
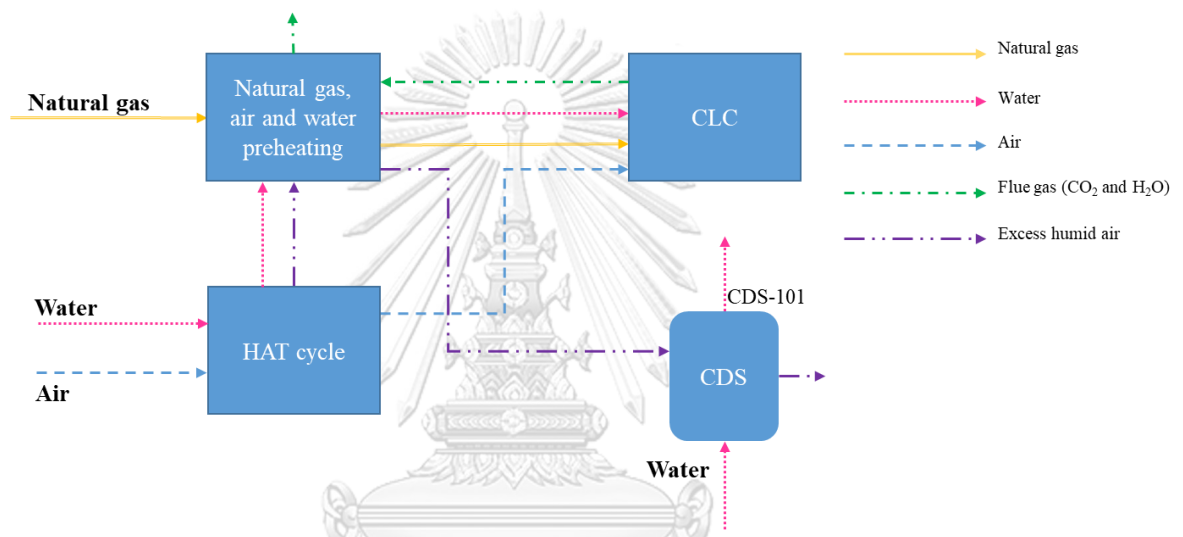
Fig. 3.3.12 Flow chart of CLC with HAT for cases 5 and 6
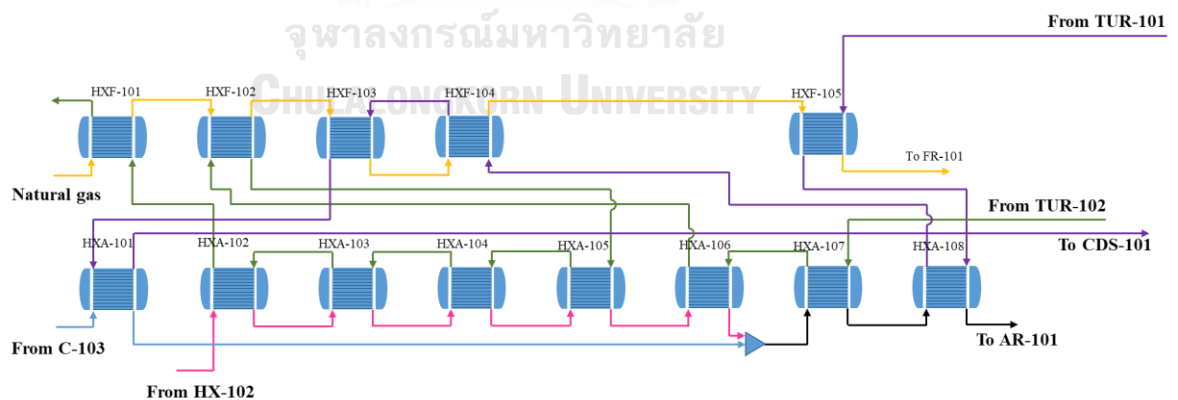
Fig. 3.3.13 Flow chart of natural gas, air and water preheating for case 5

Case 6: CLC with HAT cycle and low heat recovery

Case 6 was the CLC process with the HAT cycle, which was low heat recovery. The flow chart of this was shown in Fig. 3.3.12. There were four major sections, like case 5, preheating, CLC, HAT cycle, and CDS. The differences between this case and case 5 were the compression operation and the configuration in the preheating unit. The pressure ratio of all stages of this case was equal. The compressor ratio of this case was lower than others, which led to the smaller size of compressors. The preheating section of this case was shown in Fig. 3.3.14. Natural gas was preheated at HXF-101, HXF-102- HXF-103, and HXF-104. The compressed air was preheated at HXA-101. Water was preheated at HXA-102 and HXA-103. After that, the humid air was preheated at HXA-104 and HXA-105. The discharged from turbines were used to preheated in the preheating section. The discharged from TUR-101 were used to preheated at HXF-104, HXA-105, HXF-103 and HXA-101, respectively. The discharged from TUR-102 was used to preheated at HXA-104, HXF-102, HXA-102, and HXF-101.

The heat exchanger units of case 6 were lower than case 5. Therefore, the equipment and total capital cost of case 6 were lower than case 5. The other difference between case 5 and case 6 was the Ni loading in the system. The loadings were 16% and 28%, respectively. The ratio between natural gas and Ni was equal. This increase in Ni loading affected the mass flow rate of Al_2O_3 only. When high Ni loading, the mass flow rate of Al_2O_3 was low; on the other hand, the Al_2O_3 in case 6 was lower than case 5 and the total solid mass flow rate of case 6 was lower than case 5, as well. Solid in the process was utilized in oxygen carrier duty and heat source duty. When the low solid mass flow rate co, the temperature of the fuel reactor was too low, which it deserved the external heat when the low solid mass flow rate. The external heat was the reason for the low thermal efficiency. However, the suitable solid mass flow rate led to adequate heat for the fuel reactor. The lower solid mass flow rate of case 6 led to the high temperature of the air reactor and fuel reactor. This operation would affect thermal efficiency, economy and sustainability, as well.
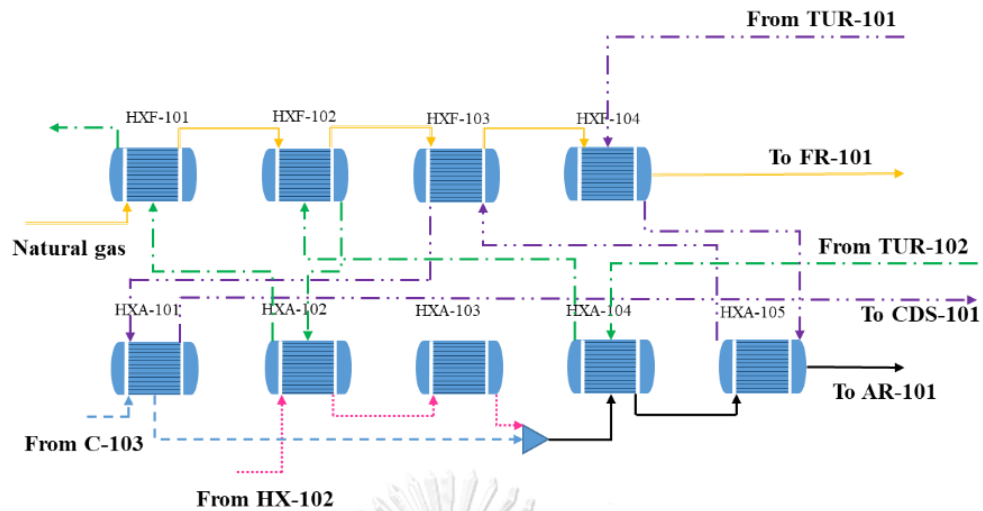
Fig. 3.3.14 Flow chart of natural gas, air and water preheating for case 6

3.3.4. Analysis tools

3.3.4.1. Thermal efficiency analysis

Thermal efficiency is calculated from the ratio of net power production divided by the lower heating value of fuel. The net power production was the total power production which subtracted by the power consumption of compression. High efficiency leads to the fuel utilization with efficiency.

$$Thermal\ efficiency\ (\%) = \frac{P_{AR}+P_{FR}-P_C-P_P}{LHV_{NG}} \times 100 \qquad (3.3.1)$$

Note that;

P_{AR} = power production from air reactor (kW)

P_{FR} = power production from fuel reactor (kW)

P_C = power consumption from air compressors (kW)

P_P = power consumption from pump (kW)

LHV = lower heating value (kW)

NG = natural gas

3.3.4.2. Economic analysis

The economic analysis indicated the profit of the case study and the competition in economic. The comparison types of CLC work in the previous study were only thermal efficiency and economic analysis. Therefore, it was convenient for

comparing the result of other CLC work with this analysis. The economic result was a preliminary result for deciding on investment by considering the IRR and payback period. Many studies investigated the economic analysis of the CLC process. The chemical looping with the air separation process for oxy-fuel combustion was conducted in the economic analysis by Shi et al. [110]. It was 500 MW power production capacity. However, the 50 MW (thermal) power production was investigated by Olaleye and Wang. [69]

In this study, the total capital investment and operating costs were estimated based on these following assumptions.

1) The power plant capacity was 50 MW.

2) Lifetime of the plant was 30 years.

3) Tax rate was 20%.

4) Plant salvage value was estimated from 20% of fixed capital investment (FCI).

5) The plant was operated at full capacity (8760 hrs./year). 6) The chemical engineering plant index (CEPCI) was 558.5 (January, 2017). [111]

Aspen Plus software and manufacturing cost would be estimated the equipment cost. The other unit operation that was not estimated by Aspen plus software was estimated as followed Turton et al. [96]. Fixed capital investment (FCI) composes of direct cost and indirect cost. The summation of FCI and working capital (WC) is total capital investment (TCI) as shown in Eq. 5.2. Working capital (WC) was 15% of FCI.

$$TCI = FCI + WC \qquad\qquad (3.3.2)$$

The payback period is the time (years) that the investment reaches the breakeven point. The point that total income equal to total cost is the breakeven point.

The other indicator in economic analysis for comparison is the internal rate of return (IRR). The IRR is the rate that is calculated when the net present value (NPV) was zero value, as shown in Eq. 5.3. It is the return of investment, which was calculated from the beginning to the last year of the plant operation. The high profit of the project led to high IRR, which is more competitive for investment, as well.

$$\sum_{n=0}^{M} \frac{CF_n}{(1+IRR)^n} = NPV = 0 \qquad (3.3.3)$$

Note that

CF = cash flow

n = each period

M = the end of plant operation

IRR = internal rate of return

NPV = net present value

3.3.4.3. Carbon tax calculation [112]

The cost of CO_2 emission was included with the cost of the expenses. This cost would be counted in analysis for environmental impact. The carbon tax must be paid when CO_2 was released to the environment, as shown in Eq. 5.4.

The cost of CO_2 emission (\$) = mass flow rate of CO_2 (metric ton/y) x 49 (\$/metric ton) [112] (3.3.4)

3.4.4.4. Sustainability evaluation

The sustainability evaluation has been proposed by Odum [62], which is an emergy analysis. The emergy is "the available energy of one kind previously used up directly and indirectly to make a product or service." Every material, energy, monetary, and manpower are counted in this analysis, which will transform into the same unit. The transformity or unit emergy value (UEV) was used to convert all stream into emergy flow (sej/Y). This analysis result would reveal both economic and environmental impact. The emergy indices including of; unit emergy value (UEV), environmental loading ratio (ELR), emergy yield ratio (EYR), and emergy sustainability index (ESI).

3.3.4.4.1. UEV, Unit emergy values

$$UEVs = \frac{Total\ Emergy\ flow}{Energy\ flow,\ Products\ flow,\ Service} \qquad (3.3.5)$$

UEV is a transforming factor calculated from the ratio between the total emergy and energy flow product and service, as shown in Eq. 3.3.5. In a good case, UEV is low. The low UEV indicates the low total emergy flow for producing one unit of product. [62] This transformity makes the difference between economic and emergy analysis. Economics takes everything into account by the price, which is indicated by the human need. However, the emergy flow indicates all the solar energy used to produce the products, energy or service. Accordingly, the emergy analysis will represent a more reasonable result than economic. In addition, the UEV is used to transform all of the energy streams into one form of solar energy (sej).

3.3.4.4.2. ELR, Environmental loading ratio

ELR is the environmental loading ratio, representing the loading of the process to the environment, as shown in Eq. 3.3.6. In a good case, ELR should low. When ELR is close to 2, it is low environmental loading. When ELR between 3-10, it is a moderate level of environmental loading. Finally, when ELR is more than 10, the environmental loading is high level [63].

$$ELR = \frac{N+F}{R}$$
(3.3.6)

Note that

N = local non- renewable resource; natural gas.

R= local renewable resource; water, air.

F = expense cost, external goods, Ni, Na_2CO_3, Al_2O_3, equipment, labor cost.

3.3.4.4.3. EYR, Emergy yield ratio

EYR is emergy yield ratio which it indicates competitive ability in the economic and the stability of the process. EYR is calculated from the total emergy flow divided by the emergy of expense goods (F), as shown in Eq. 3.3.7. In the good case, EYR is high. The reason for high EYR is low F. It represents that the process hardly relies on external resources. When the process relies on the internal resource, the process will provide high stability, which is a highly competitive ability in the economy. In the good case, EYR is high, but, in the worst case, EYR is equal to 1.

Moreover, when EYR is lower than 2, it indicates that the process is not suitable to be an energy source by the study of Ulgiati and Brown. [29]

$$EYR = \frac{Total\ emergy}{External\ resources} = \frac{R+N+F}{F+L} \qquad (3.3.7)$$

3.3.4.4.4. ESI, Emergy sustainability index

ESI is emergy sustainability index that indicates the sustainability of the process. It is calculated from the ratio of EYR to ELR, as shown in Eq. 3.3.8. It is the ratio of profit to the loading of the environment. When ESI is lower than 1, the process is not long-term sustainability. When ESI is lower than 1, the process is not long-term sustainable. When ESI is 1-5, the process is medium sustainability. Finally, when ESI is higher than 5, the process is long-term sustainable

$$ESI = \frac{EYR}{ELR} \qquad (5.8)$$

จุฬาลงกรณ์มหาวิทยาลัย

CHULALONGKORN UNIVERSITY

Chapter 4
Investigation of parameters of the HAT cycle in CLC for power production.

4.1 Research gaps

The limitation of previous studies of the CLC study is the investigation of each parameter individually. However, the synergistic effects among parameters in the system were not considered. In this study, the 3^k factorial design is used for solving this problem and systematically indicating their interaction. In this study, four independent input variables, which were the pressure of air reactor, number stages of air compressors, methods of air compression, and airflow rate on the lower heating value (LHV) efficiency or thermal efficiency, were studied. There are also four responses to be observed, which consist of thermal efficiency, power production from air reactor, work of air compressors, and air compressor discharge temperature. The HAT cycle included the multi-stage compressor, heat exchanger for intercooler between compressors and turbines. Accordingly, the operation of the HAT cycle is directly relating to the work consumed by all compressors and the work produced by the turbines. The 3^k factorial experimental result can reveal the effects and the curvature interactions of operating parameters, which leads to high thermal efficiency. The advantages of this study are obtaining the operating condition for the highest thermal efficiency of CLC with the HAT cycle process.

4.2 Objective

To study the effects of HAT operation conditions on power production with the chemical looping combustion process.

4.3 Results and discussion

This investigation aimed to identify the operating condition that reaches the highest thermal efficiency of CLC with the HAT cycle system. The 3^k factorial experimental design was selected for investigation. There were 81 cases in total to be simulated and evaluated the outputs. The values of these four input variables which were used in the study were shown in Table 4.1. Furthermore, the detail of each case study was shown in Table 4.2.

Table 4.1 The values of four parameters conducted in 3^k factorial experiment.

Variable	Name	Units	Low value	Middle value	High value
A	Pressure of air reactor	atm	5	10	15
B	Number of compressors	Number	3	5	7
C	Air compression method	-	Method 1	Method 2	Method 3
D	Air flow rate	kmol/hr	58000	59500	61000

Table 4.2 Results of 3^k factorial design

Case	A	B	C	D	Efficiency	Power production from air reactor	Work of compressors	Temperature discharge of air compressor
No.	atm	Number	Ratio	kmol/hr	%	MW	MW	°C
1	5	3	Method 1	58000	48.188	347.113	92.700	136.34
2	10	3	Method 1	58000	52.726	433.031	147.807	207.45
3	15	3	Method 1	58000	52.512	467.154	183.376	207.46
4	5	5	Method 1	58000	48.219	347.073	92.449	136.08
5	10	5	Method 1	58000	52.754	432.978	147.560	207.45
6	15	5	Method 1	58000	52.621	467.149	182.636	207.44
7	5	7	Method 1	58000	48.226	347.067	92.399	136.03
8	10	7	Method 1	58000	52.758	432.957	147.511	207.45
9	15	7	Method 1	58000	52.642	467.149	182.491	207.45
10	5	3	Method 2	58000	48.747	349.223	91.018	161.52
11	10	3	Method 2	58000	53.962	436.384	142.763	247.62
12	15	3	Method 2	58000	55.225	479.925	177.726	306.47
13	5	5	Method 2	58000	48.695	347.893	90.041	147.05
14	10	5	Method 2	58000	53.866	433.817	140.852	226.67
15	15	5	Method 2	58000	55.142	476.607	174.975	279.14
16	5	7	Method 2	58000	48.672	347.324	89.626	140.85
17	10	7	Method 2	58000	53.822	432.712	140.046	217.62
18	15	7	Method 2	58000	55.324	475.840	172.972	252.64
19	5	3	Method 3	58000	48.930	353.106	93.659	204.24
20	10	3	Method 3	58000	54.305	445.207	149.263	320.25
21	15	3	Method 3	58000	55.655	492.339	187.228	397.18
22	5	5	Method 3	58000	48.962	353.063	93.398	203.92
23	10	5	Method 3	58000	54.335	445.151	148.999	319.89
24	15	5	Method 3	58000	55.684	492.270	186.957	396.80
25	5	7	Method 3	58000	48.968	353.053	93.346	203.86

	Variables				Responses			
Case	A	B	C	D	Efficiency	Power production from air reactor	Work of compressors	Temperature discharge of air compressor
No.	atm	Number	Ratio	kmol/hr	%	MW	MW	ºC
26	10	7	Method 3	58000	54.341	445.137	148.947	319.82
27	15	7	Method 3	58000	55.690	492.258	186.905	396.73
28	5	3	Method 1	59500	48.526	351.919	95.214	138.54
29	10	3	Method 1	59500	52.814	437.663	151.839	207.44
30	15	3	Method 1	59500	51.703	466.391	188.107	207.46
31	5	5	Method 1	59500	48.557	351.884	94.965	138.29
32	10	5	Method 1	59500	52.850	437.664	151.596	207.45
33	15	5	Method 1	59500	51.814	466.385	187.348	207.44
34	5	7	Method 1	59500	48.564	351.878	94.914	138.24
35	10	7	Method 1	59500	52.861	437.660	151.515	207.46
36	15	7	Method 1	59500	51.835	466.383	187.199	207.45
37	5	3	Method 2	59500	49.114	354.238	93.541	163.09
38	10	3	Method 2	59500	54.207	442.242	146.961	250.92
39	15	3	Method 2	59500	45.388	424.686	190.374	344.93
40	5	5	Method 2	59500	49.055	352.874	92.575	148.94
41	10	5	Method 2	59500	54.140	439.912	145.081	230.47
42	15	5	Method 2	59500	54.944	480.521	180.229	279.15
43	5	7	Method 2	59500	49.029	352.288	92.165	142.88
44	10	7	Method 2	59500	54.081	438.735	144.304	221.72
45	15	7	Method 2	59500	54.360	475.216	178.889	252.64
46	5	3	Method 3	59500	49.312	358.207	96.164	204.81
47	10	3	Method 3	59500	54.598	451.246	153.307	321.08
48	15	3	Method 3	59500	55.766	498.220	192.349	398.26
49	5	5	Method 3	59500	49.344	358.164	95.905	204.50
50	10	5	Method 3	59500	54.628	451.185	153.045	320.72
51	15	5	Method 3	59500	55.792	498.133	192.085	397.89
52	5	7	Method 3	59500	49.350	358.154	95.853	204.43
53	10	7	Method 3	59500	54.634	451.172	152.993	320.65
54	15	7	Method 3	59500	55.798	498.112	192.029	397.81
55	5	3	Method 1	61000	48.798	356.302	97.745	140.94
56	10	3	Method 1	61000	52.040	436.634	156.060	207.44
57	15	3	Method 1	61000	50.899	465.667	192.838	207.46
58	5	5	Method 1	61000	48.829	356.265	97.498	140.69
59	10	5	Method 1	61000	52.094	436.630	155.692	207.45
60	15	5	Method 1	61000	51.013	465.660	192.059	207.44
61	5	7	Method 1	61000	48.833	356.239	97.448	140.65

	Variables				Responses			
Case	A	B	C	D	Efficiency	Power production from air reactor	Work of compressors	Temperature discharge of air compressor
No.	atm	Number	Ratio	kmol/hr	%	MW	MW	ºC
62	10	7	Method 1	61000	52.108	436.632	155.597	207.46
63	15	7	Method 1	61000	51.036	465.663	191.907	207.45
64	5	3	Method 2	61000	49.318	358.200	96.114	165.02
65	10	3	Method 2	61000	54.070	445.741	151.388	255.53
66	15	3	Method 2	61000	54.763	488.189	189.129	318.66
67	5	5	Method 2	61000	49.276	356.961	95.161	151.20
68	10	5	Method 2	61000	53.809	442.315	149.730	236.75
69	15	5	Method 2	61000	54.029	480.001	185.925	279.15
70	5	7	Method 2	61000	49.255	356.415	94.756	145.27
71	10	7	Method 2	61000	53.677	440.742	149.057	228.74
72	15	7	Method 2	61000	53.375	474.615	184.974	252.63
73	5	3	Method 3	61000	49.478	361.870	98.701	205.55
74	10	3	Method 3	61000	54.824	456.845	157.371	321.96
75	15	3	Method 3	61000	55.843	503.882	197.490	399.36
76	5	5	Method 3	61000	49.508	361.822	98.445	205.24
77	10	5	Method 3	61000	54.851	456.775	157.116	321.62
78	15	5	Method 3	61000	55.869	503.803	197.233	399.01
79	5	7	Method 3	61000	49.515	361.814	98.393	205.18
80	10	7	Method 3	61000	54.860	456.780	157.064	321.55
81	15	7	Method 3	61000	55.875	503.791	197.179	398.93

In this study, the four individual input parameters have investigated the effect on the four responses. The four parameters were the pressure of the air reactor, the number of air compressor stages, method of air compression, and airflow rate. The four responses were thermal efficiency consist of thermal efficiency, power production from air reactor, work of air compressors, and air compressor discharge temperature. All of the parameters were systematically conducted to express the relation of all operations in the system. In Table 4.2, the highest thermal efficiency was case 81, which obtained 55.87% of thermal efficiency and 503.88 MW of power production. Case 16 had a minimum of compressor workload, but there was only 48.67% thermal efficiency.

Furthermore, the operation to achieve the low-temperature air compressor outlet led to low compressor work, but there was 48.23% thermal efficiency. The analysis from this study would express the relation of operation that represents a good understanding of CLC with the HAT cycle system, which it was not straightforward to choose the operating conditions. The effect of the parameters on the responses which was expressed in the next section.

4.3.1 The effect of operating parameters on the thermal efficiency

The high thermal efficiency indicated the high worthiness of the fuel used for power production. The result of variance analysis (ANOVA) indicated that A, C, and AC had affected thermal efficiency since their p-values were lower than 0.05, as shown in Table 4.3. The pressure of air compressor (A), compression method (C) and the interaction between the pressure of air compressor and compression method (AC) had an impact on thermal efficiency. The simulation showed that the pressure of air compressor (A) and compression method (C) significantly affected thermal efficiency shown by the high slope, as shown in Fig. 4.1. Nevertheless, the number of compressors (B) and airflow rate (D) had less impact on thermal efficiency in this range, as shown in Table 4.1. Case 81 achieved the maximum thermal efficiency of 55.875% at 15 atm, 7 stages, method 3, and 61000 kmol/hr. Case 39 obtained the minimum thermal efficiency of 45.388% at 15 atm, 3 stages, method 2, and 59,500 kg/hr. The case studies that obtained thermal efficiency higher than 55% were case numbers 21, 24, 27, 48, 51, 54, 75, 78 and 81. These cases operated at 15 atm of pressure and compression method 3, but the number of compressors and airflow rates differed.

Case 75 shows an interesting result. Its thermal efficiency was slightly lower than case 81, with a value of 55.84%. The difference between case 75 and case 81 was the number of air compressor stages in which there were 3 and 7 stages, respectively. The increase of the stage of air compressor led to the increased unit of an intercooler between compressor stages. However, the increase up to 7 stages to gain 0.03% higher in thermal efficiency was not worthwhile for investment. The operation condition of the cases 75 and 81 were 15 atm of air reactor pressure, method 3 of air compression, and 61,000 kmol/hr of airflow.

Table 4.3 The ANOVA for the thermal efficiency

Variables & Interaction	Sum of Squares	df	Mean Square	F Value	p-value Prob > F	
A-Pressure of air reactor	411.15	2	205.57	177.25	< 0.0001	significant
B-Number of compressors	1.76	2	0.88	0.76	0.4741	
C-Compression method	68.91	2	34.45	29.71	< 0.0001	significant
D-Air flow rate	1.17	2	0.59	0.51	0.6059	
AB	3.87	4	0.97	0.83	0.5103	
AC	25.01	4	6.25	5.39	0.0011	significant
AD	10.38	4	2.59	2.24	0.0788	
BC	2.53	4	0.63	0.54	0.7038	
BD	4.92	4	1.23	1.06	0.3859	
CD	6.32	4	1.58	1.36	0.2607	
Residual	55.67	48	1.16			
Cor Total	591.68	80				

The thermal efficiency was calculated from the net power production divided by the lower heating efficiency of fuel. In this case, the natural gas was the fuel, as shown in Eq. 4.1.

$$\text{Thermal efficiency } (\%) = \frac{\text{Power production from AR and FR}(kW) - \text{Work of compressor }(kW) - \text{Work of water pump }(kW)}{\text{Lower heating value of fuel }(kW)} \times 100 \tag{4.1}$$

The effect of air reactor pressure and compression method for air compressors on thermal efficiency is shown in Fig. 4.2. Method 3 reached the highest thermal efficiency, followed by method 2 and method 1, respectively. In method 3, the compression ratio of the last compressor stage was higher than the others. It led to the highest temperature of the outlet stream. After this stream was preheated, it was introduced to the air reactor, which led to increased air reactor temperature. The outlet of the air reactor would be finally sent to produce power at the turbine. Accordingly, the increase in air compressor pressure would be why the increase in power production and thermal efficiency, as shown in Table 4.4. On the other hand, the

compression ratio at the last stage in method 1 was the lowest. The temperature of compressor discharge would be the lowest. It was the reason for low power production and low thermal efficiency. The compression ratio of method 2 was lower than method 3 but higher than method 1. Accordingly, method 3 requires the highest work, method 2 require the least work and method 1 is in the middle of the two methods. For method 2 and method 3, the increase of air reactor pressure from 5 to 15 atm increased thermal efficiency. In method 1, the increased pressure from 5 to 10 atm would increase thermal efficiency, but thermal efficiency decreased when pressure was increased to 15 atm. Simultaneously, the increase in temperature discharge would increase the water flow rate into the system. However, the increase of pressure led to a decrease in water flow rate. Method 3 brought about the highest temperature discharge of the air compressor. Subsequently, the water was fed into the system more than other methods. At the same method, the increase of pressure was higher thermal efficiency than the increase in temperature. The pressure discharge of the turbine was 1 atm. When the pressure inlet increase, the temperature discharge from the turbine would decrease. Because the outlet stream from the turbine was used to preheat other streams, the decrease in temperature discharge from the turbine would decrease the total heat recovery. Water would be fed lower into the system, as shown in Table 4.4. Thereby, the increase in pressure would decrease the water flow rate of the system.

Table 4.4 The temperature discharge of air compressor, water flow rate and temperature discharge of air turbine.

Case	Pressure (atm)	Method of air compressor	Temperature discharge of air compressor (^{o}C)	Water flow rate (kg/hr)	Temperature discharge of air turbine (^{o}C)
61	5	Method 1	140.65	348,850.44	971.06
62	10	Method 1	207.46	247,829.04	805.16
63	15	Method 1	207.45	185,210.46	715.38
70	5	Method 2	145.27	349,489.62	971.10
71	10	Method 2	228.74	258,838.56	806.16
72	15	Method 2	252.63	206,281.26	717.66
79	5	Method 3	205.18	369,025.38	972.35
80	10	Method 3	321.55	301,811.22	809.92
81	15	Method 3	398.93	275,018.58	724.50
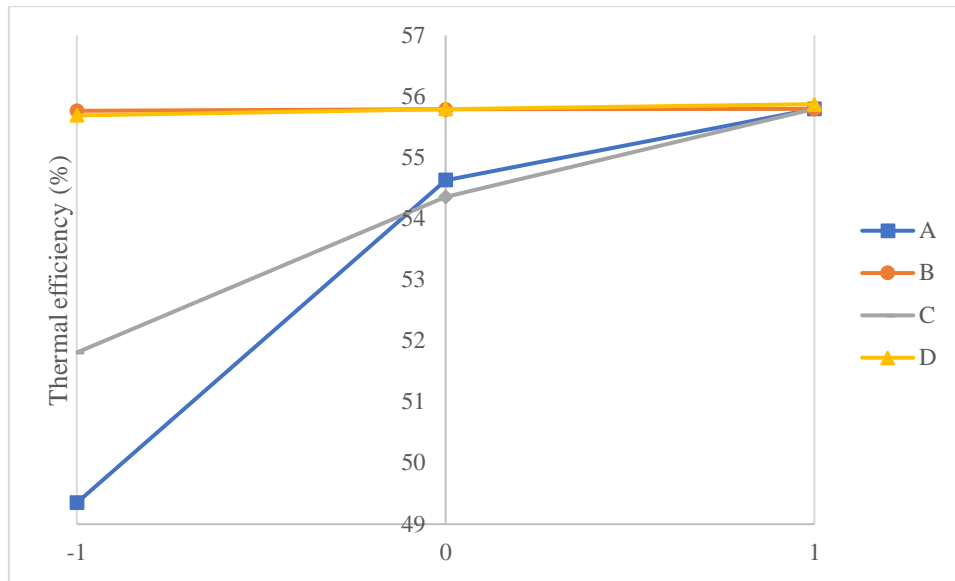
Fig. 4.1 The effect of main operating parameters on thermal efficiency.
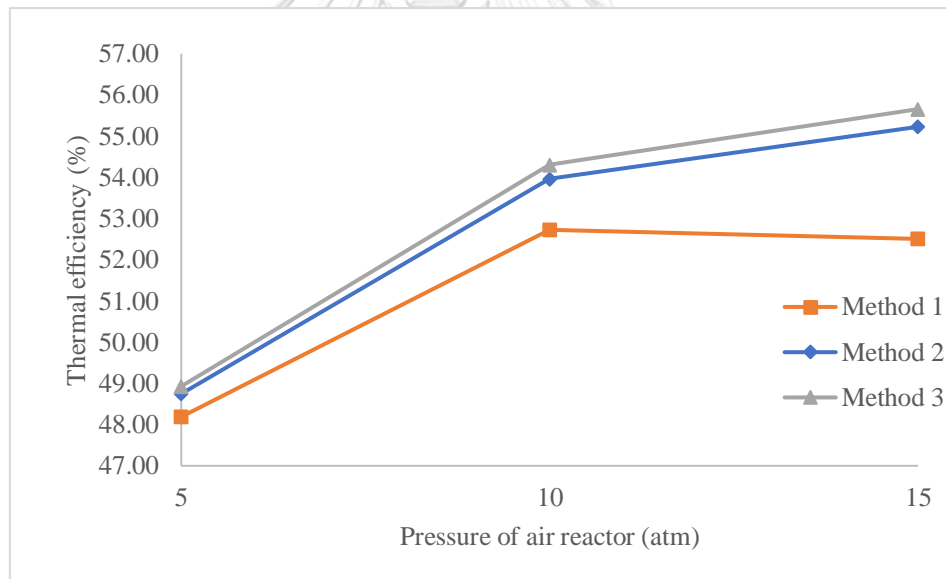
Fig. 4.2 The effect of pressure of air reactor and air compression method on thermal efficiency.

4.3.2 The effect of operating parameters on the power production from air reactor

The increase in power production would increase thermal efficiency, as shown in the thermal efficiency equation. In this study, the air reactor's power production

was focused because it produced high power production than the fuel reactor's power production. The power production from the air reactor was 503.88 – 347.07 MW, but that from the fuel reactor was 77.8 MW. In this study, the power production from the air reactor was selected as a response. The four input parameters were exactly affected by power production from the air reactor. The power production from the fuel reactor was not significantly affected, as shown in table 4.2.

The variance analysis in Table 4.5 indicated that pressure of air reactor (A), compression method (C), airflow rate (D), and the interaction between the pressure of air reactor and compression method (AC) affected the response parameter since their p-values were lower than 0.005. Case 75 achieved the maximum power production at 15 atm, 3 stages, method 3, and 61,000 kmol/hr. On the other hand, case 7 achieved the minimum power production at 5 atm, 7 stages, method 1, and 58,000 kmol/hr. Even though case 75 was the maximum power production, it was not the highest thermal efficiency. However, case 75 reached the 2nd highest thermal efficiency, which inferior to case 81. The increase of air reactor pressure highly affected power production because the slope was higher than the other, as shown in Fig. 4.3. The increase in airflow rate increased power production. Method 3 produced power more than the other methods, as shown in Fig. 4.4.

Table 4.5 The ANOVA for the power production from the air reactor

Variables & Interaction	Sum of Squares	df	Mean Square	F Value	p-value Prob > F	
A-Pressure of air reactor	222623.11	2	111311.55	2562.26	< 0.0001	significant
B-Number of compressors	18.24	2	9.12	0.21	0.8114	
C-Compression method	4684.68	2	2342.34	53.92	< 0.0001	significant
D-Air flow rate	728.32	2	364.16	8.38	0.0008	significant
AB	109.03	4	27.26	0.63	0.6453	
AC	1705.31	4	426.33	9.81	< 0.0001	significant
AD	269.65	4	67.41	1.55	0.2024	
BC	39.02	4	9.75	0.22	0.9234	
BD	187.98	4	46.99	1.08	0.3761	
CD	267.14	4	66.79	1.54	0.2064	
Residual	2085.25	48	43.44			
Cor Total	232717.72	80				
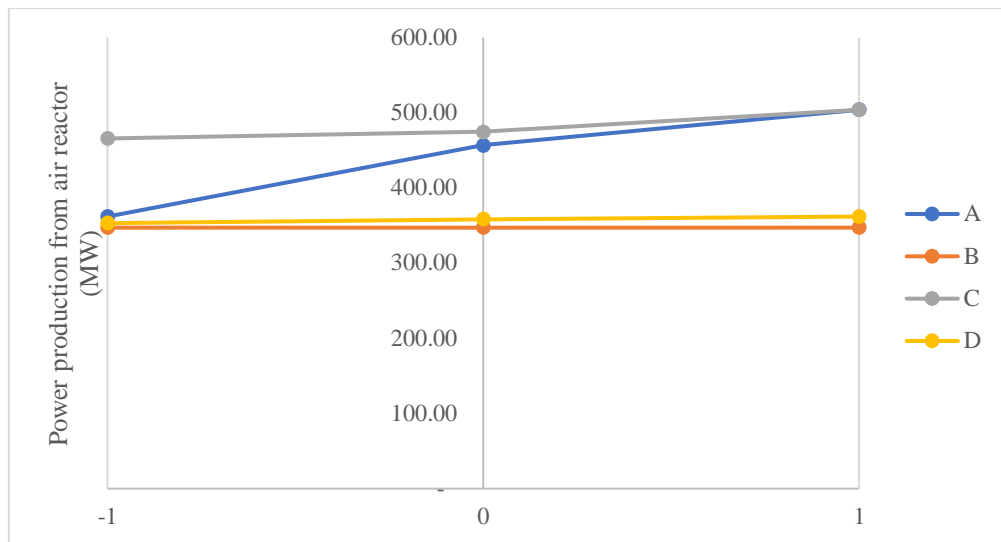
Fig. 4.3 The effect of main operating parameters on power production from the air reactor.
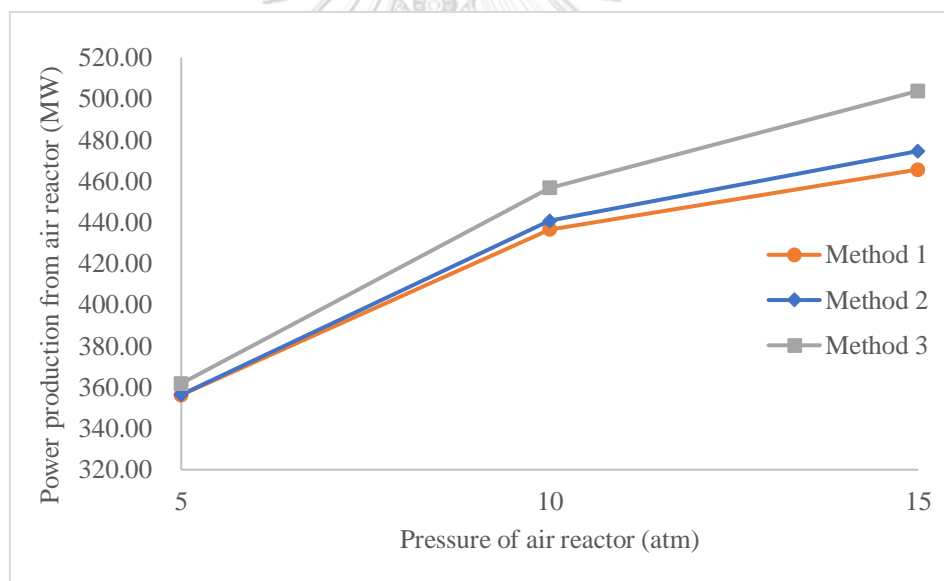
Fig. 4.4 The effect of pressure of air reactor and air compression method on the power production from air reactor.
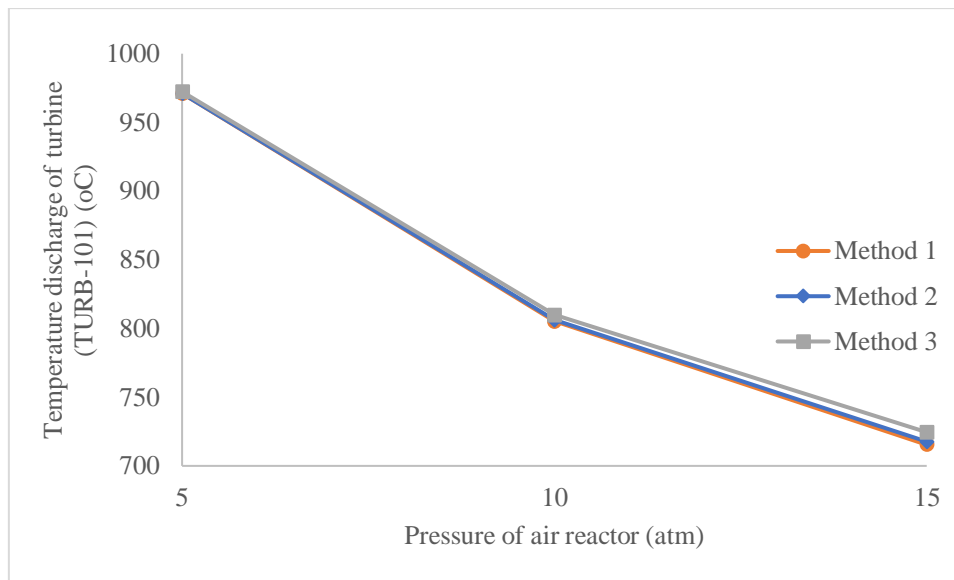
Fig. 4.5 The effect of pressure of air reactor and air compression method on temperature discharge of turbine (TURB-101).

For all air compression methods, the air reactor's pressure was increased the power production from the air reactor. Especially for the combination of the method of air compression and the pressure level, the combination between method 3 and the high-pressure level provided the highest power production of all combinations, as shown in Fig. 4.4. Besides, this combination brought about the highest temperature discharge from the turbine (TUR-101), as shown in Fig. 4.5. The operation of method 3 was the reason for the highest temperature of air compressor discharge obtained.

The sequence of compression ratio was different in each method of air compression operation. Table 4.6 shows the compression ratio in each stage for all compression methods. The high compression ratio led to the high temperature and pressure discharge of the compressor, which provided the high work consumption of the air compressor. There was an intercooler for transfer heat from the compressed air to the cooling water. The compression ratio of method 1 was highest in the first stage. Therefore, the majority of heat in the air compression process was released into the cooling water. While the compression ratio of method 3 was highest at the last stage, the discharge temperature of method 3 was higher than case 1. This reason provided the air reactor's higher temperature, which led to high power production when method 3 was selected for operation.

Table 4.6 The compression ratio for 5 stages at the highest level (20 atm)

	Stage 1	Stage 2	Stage 3	Stage 4	Stage 5
Method 1	13.00	1.114	1.114	1.114	1.114
Method 2	1.821	1.821	1.821	1.821	1.821
Method 3	1.114	1.114	1.114	1.114	13.000
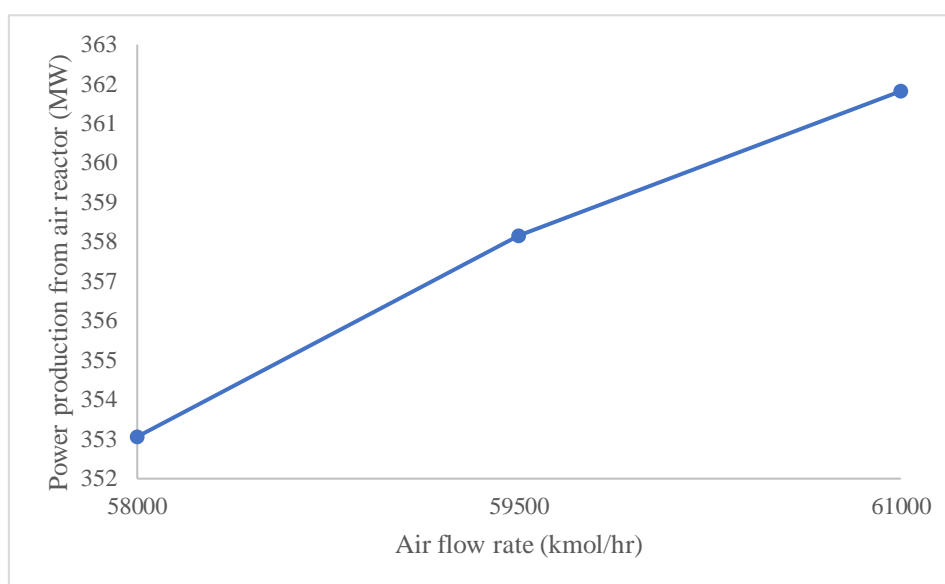
Fig. 4.6 The effect of air flow rate on the power production from the air reactor.

The high temperature discharge from the air compressor would increase the air reactor's temperature and increase power production from the air reactor. Accordingly, the synergistic effect from the high-pressure level and the suitable compression method was the reason for the high-power production. The increase of the air flow rate into the system increased power production from the air reactor because it increased working fluid into the turbine, as shown in Fig. 4.6. The turbine's power production was affected by the pressure and temperature of the introduced stream to the turbine. The increase in power production resulted from the high pressure, high temperature, and high mass flow rate of the introduced stream to the turbine.

On the other hand, the combination of Method 1 and the lowest level of air reactor pressure provided the low power production from the turbine. The suitable

operation of pressure level, compression method, and the airflow rate caused the high mass flow rate of water. Water would be introduced into the system as much as the fuel reactor's temperature was not lower than 1,350ºC, as shown in Table 4. 4. Accordingly, the suitable condition led to an increase in the working fluid of the turbine in which air and water were the working fluid in this system.

The decrease in water flow rate would directly affect power production, as shown in Table 4.7. For dissection, there were 4 additional cases simulated. The water flow rate of those cases was decreased to 90%, 80% and 70% from case 81. The 30 MW of power production decreased when the water flow rate was decreased. The thermal efficiency also decreased from 55.875% to 51.036% as well. Nevertheless, the compressor's work slightly increased because the water was used in cooling down the compressed air. The decrease in water flow rate led to increased compressed air temperature and the workload of the compressor.

Table 4.7 The effect of water fed to air reactor and turbine on the power production and efficiency of the system

% Water flow rate of case 81	Water flow rate (kg/hr)	Power production from air reactor (MW)	Thermal efficiency (%)	Work of compressor (MW)
100%	275,252	503.79	55.875	197.18
90%	247,726	493.33	54.29	197.67
80%	220,201	482.71	52.673	198.2
70%	192,676	472.01	51.036	198.79

4.3.3 The effect of operating parameters on the work consumption of compressors

The decrease in compressor's work would increase thermal efficiency. The HAT cycle was applied to the system to decrease the work consumption of the compressors. All of the parameters that were investigated in this study completely affected to workload of the compressor. The work of compressor highly consumed power which was about 25.8 - 44.8% of total power production, as shown in Table 4.6. Accordingly, studied the effect of compressor's work was significant for investigation. The variance analysis in Table 4.8 indicated that pressure of air reactor (A), a number of the compressors (B), compression method (C), the air flow rate (D),

the interaction between the pressure of air reactor and compression method (AC), the interaction between pressure of air reactor and the air flow rate (AD) , and the interaction between a number of the compressors and compression method (BC) had impacts on the compressor's work, since their p-values were lower than 0.005.

Table 4.8 The ANOVA for the work of the compressor

Variables & Interaction	Sum of Squares	Df	Mean Square	F Value	p-value Prob > F	
A-Pressure of air reactor	117138.38	2	58569.19	65440.75	< 0.0001	significant
B-Number of compressors	32.15	2	16.07	17.96	< 0.0001	significant
C-Compression method	702.13	2	351.07	392.25	< 0.0001	significant
D-Air flow rate	852.21	2	426.10	476.10	< 0.0001	significant
AB	11.56	4	2.89	3.23	0.02	
AC	131.79	4	32.95	36.81	< 0.0001	significant
AD	67.30	4	16.82	18.80	< 0.0001	significant
BC	32.60	4	8.15	9.11	< 0.0001	significant
BD	2.57	4	0.64	0.72	0.5836	
CD	3.90	4	0.97	1.09	0.3729	
Residual	42.96	48	0.89			
Cor Total	119017.55	80				

The increase in air reactor pressure highly increased the compressor's work, as shown by the high slope of response curves in Fig. 4.7. The increase in the airflow rate increased the work of the compressor. Method 2 of compression operation brought about the lowest compressor's work, but Method 1 and Method 3 reached the higher work consumption of air compressors. The heat releasing from compressed air in method 2 was better than other methods because the heat was evenly released from each compressor. The heat releasing from compressed air by other methods was lower than method 2. The reduction of compressed air temperature within multi-stage compressors decreased their work, which method 2 provided this suitable operation for the compressor. In case 16, method 2 was operated and achieved the minimum work requirement, as shown in Fig. 4.8. The lowest workload of the compressor was achieved from the minimum airflow rate, but it led to lower power production and low system efficiency.

Method 3 operated with the highest compressor work, as shown in Fig. 4. 8 – 4. 9. The highest workload of the compressor brought about the

high temperature outlet from the air compressor. Then, the high temperature stream was introduced into the air reactor and increased the air reactor's temperature, power production, and thermal efficiency.

The increase in the number of compressors decreased the work of compressors, as shown in Fig. 4.9. The 7 stages of compressor obtained the lowest compressors' work while the 3 stages of compressor obtained the highest compressors' work. Accordingly, the increase of stages of the compressor decreased the work of the compressor. The increase in compression stages highly affected only method 2, as shown in Fig. 4.9. Even the increase of the compression stage did not highly affect the power of the compressor; the single-stage compressor consumed the highest work, as shown in Fig. 4.10. The increase of compressor stages highly affected the power of the compressor at a high-pressure level. The increase of the air flow rate and pressure of the air reactor would increase the work of compressors. The high air flow rate and the air reactor's high pressure would increase the work of the compressor. On the other hand, the low air flow rate and the air reactor's low pressure decreased the work of compressors, as shown in Fig. 4.11. The best case for operating the compressor would likely be with a lower power requirement. Case 16 showed the minimum compressor work, 89.636 MW, operated at 5 atm, 7 stages, method 2, and 58,000 kmol/hr. Case 75 showed the maximum compressor work, 197.490 MW, operated at 15 atm, 3 stages, method 3, and 61,000 kmol/hr. The thermal efficiency of case 16 was 48.672%, but that of case 75 was 55.843%. The work of compressor and thermal efficiency in case 81 was 197.179 MW, and 55.875%. The compressor work in case 81 and case 75 were 2 times higher than case 16. Thus, the operating conditions which low compression consumption did not enough to achieve the high system efficiency.
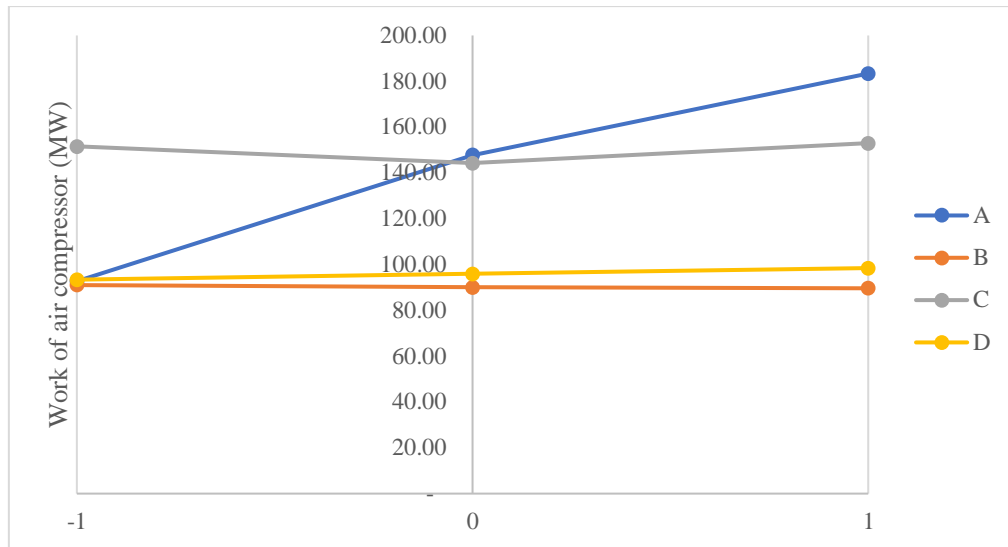
Fig. 4.7 The effect on main operating parameters on compressor work.
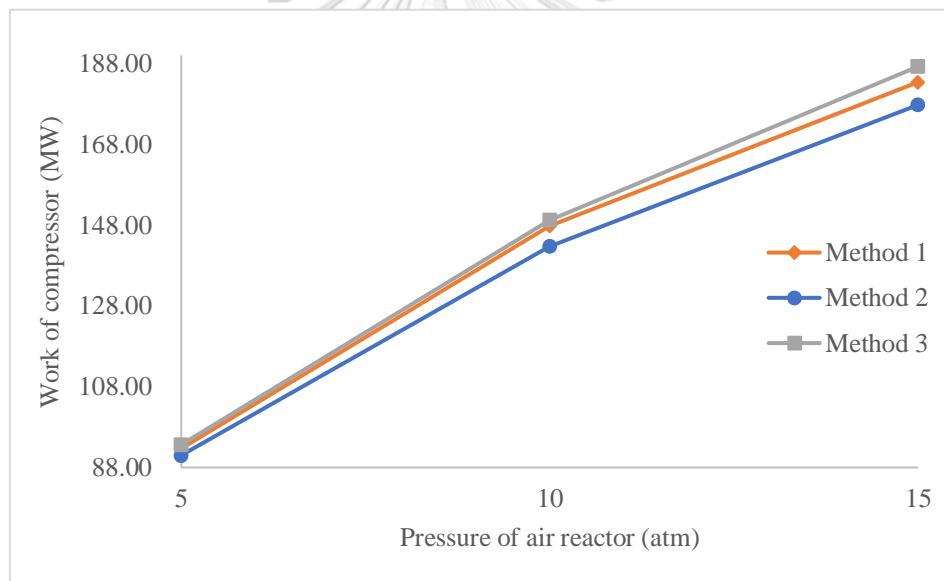
Fig. 4.8 The effect of the air reactor pressure and air compression method on compressor work.
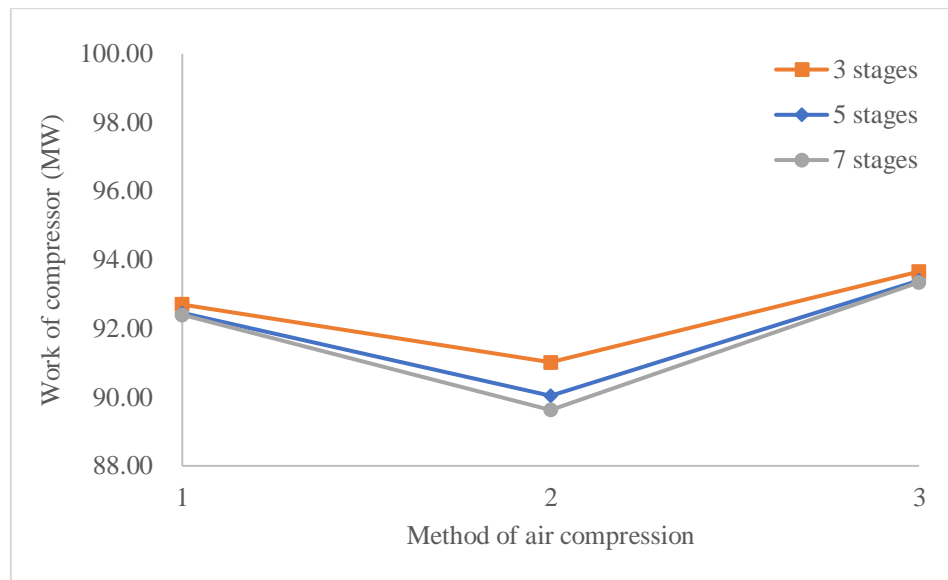
Fig. 4.9 The effect of the number of compressors and air compression method on the compressor work.
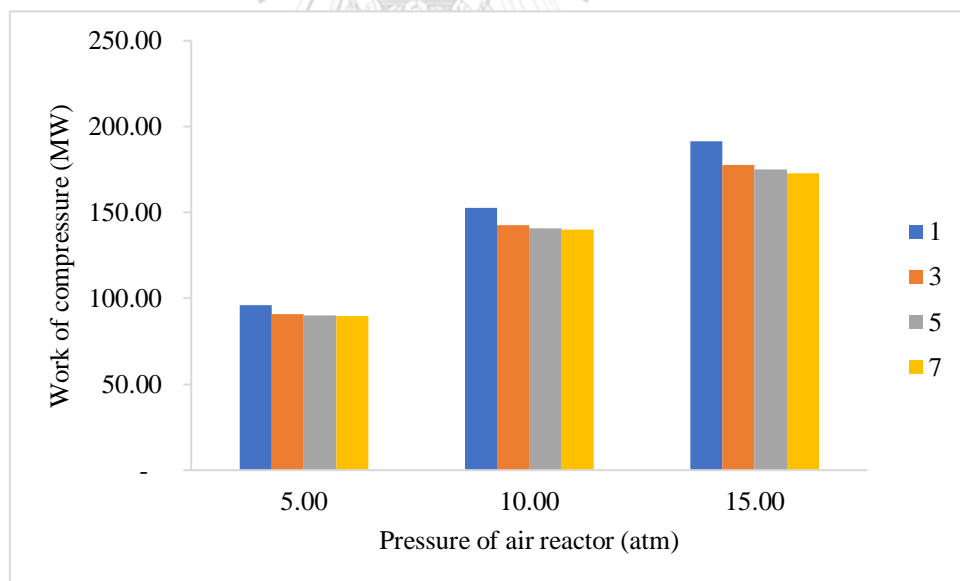
Fig. 4.10 The effect on air reactor pressure and the number of compressors on the compressor work.
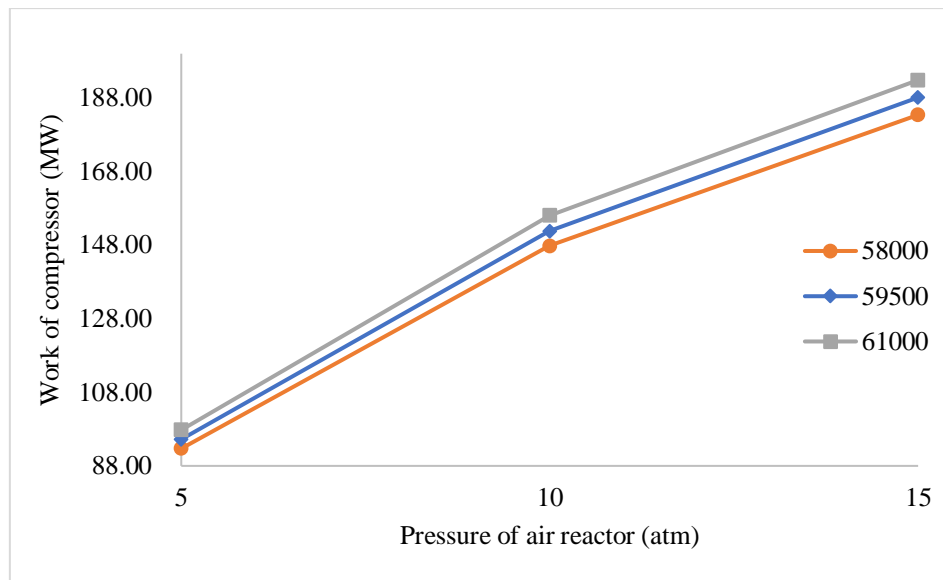
Fig. 4.11 The effect of air reactor pressure and air flow rates on the compressor work.

4.3.4 The effect of operating parameters on the discharge temperature of air compressor

The effect of temperature discharge of air compressors on power production was barely investigated in the CLC system. This parameter directly affected power production and thermal efficiency, as well. The high discharge temperature of the air compressor increased the air reactor temperature. The outlet stream from the air reactor would be sent into the turbine for power production after it was preheated. The high temperature inlet to the turbine would increase the power production and thermal efficiency of the system. Accordingly, this parameter was a significant parameter to achieve high thermal efficiency. The variance analysis in Table 4.9 indicated that the parameters affected the discharge temperature of the air compressor. These parameters were air reactor pressure (A), the number of compressors (B), compression method (C), the interaction between air reactor pressure and the number of the compressors (AB), the interaction between air reactor pressure and compression method (AC), and the interaction between the number of compressors and compression method (BC).

Table 4.9 The ANOVA for the discharge temperature of the air compressors

Source	Sum of Squares	Df	Mean Square	F Value	p-value Prob > F	
A-Pressure of air reactor	244847.52	2	122423.76	2787.98	< 0.0001	significant
B-Number of compressors	2526.75	2	1263.37	28.77	< 0.0001	significant
C-Compression method	214353.74	2	107176.87	2440.76	< 0.0001	significant
D-Air flow rate	146.45	2	73.23	1.67	0.1994	
AB	735.77	4	183.94	4.19	0.0055	significant
AC	35894.44	4	8973.61	204.36	< 0.0001	significant
AD	66.41	4	16.60	0.38	0.8232	
BC	4856.17	4	1214.04	27.65	< 0.0001	significant
BD	56.83	4	14.21	0.32	0.8608	
CD	96.25	4	24.06	0.55	0.7013	
Residual	2107.74	48	43.91			
Cor Total	505688.07	80				
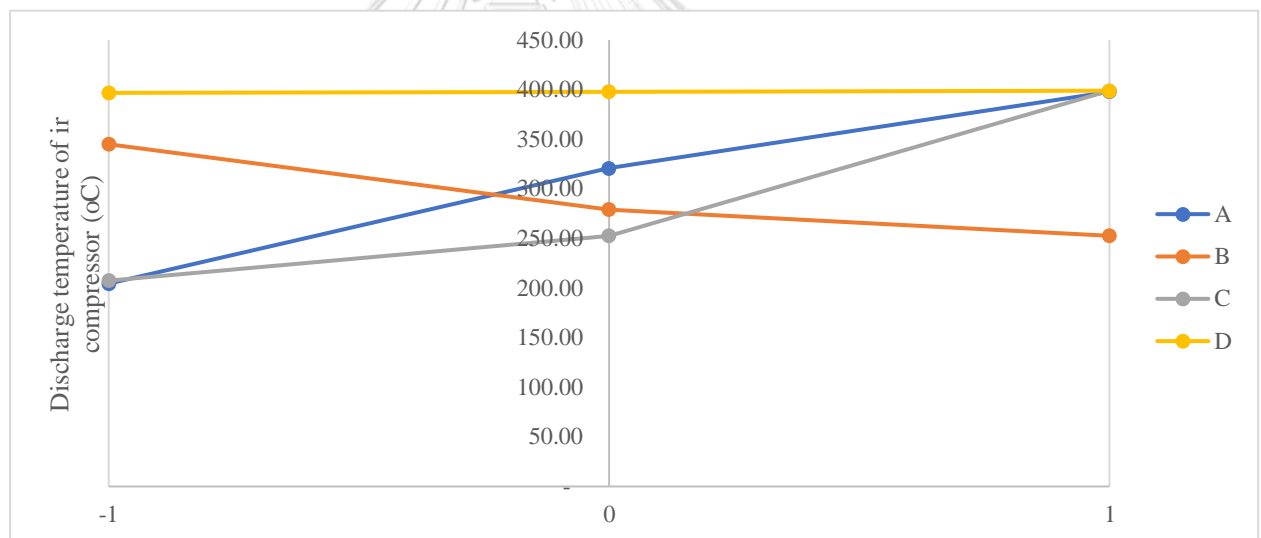
Fig. 4.12 The effect of the main operating parameters on the discharge temperature of
the air compressor.

The increase of air reactor pressure extremely increased the air compressor's discharge temperature, as shown in Fig. 4. 12. The decrease in the number of compressors highly decreased the air compressor's discharge temperature because it was high slope also. The increase of the number of air compressors would increase the units of inter-cooler that were installed between stages of compressors. The high

units of inter-cooler led to high heat releasing from the compressed air. The discharge temperature would be decreased. The effect of the number of compressors on temperature discharge from air compressors highly affected method 2 of compression operation, as shown in Fig. 4.13. Method 3 was the best compression operation to reach the highest discharge temperature, as shown in Fig. 4.13. The increase in the number of air compressors in method 1 and method 3 did not affect discharge temperature. The high heat source in method 1 and method 2 were the first and the last compressors. Accordingly, the heat in the system operated with method 1 and method 3 was not well transfer. The increase in the number of compressors highly affects at a high-pressure level, as shown in Fig. 4.14. The compressor operation highly affected the air compressor's discharge temperature, as shown in Fig. 4.12. Furthermore, the compression method in method 3 at high pressure achieved the highest temperature discharge, as shown in Fig. 4.15. The combination of method 1 for compression operation with low-pressure level obtained the lowest temperature discharge.

Case 75 obtained the highest discharge temperature of air compressor, 399.36°C at 15 atm, 3 stages, method 3, and 61,000 kmol/hr. On the other hand, case 7 obtained the lowest discharge temperature of air compressor, 136.03°C at 5 atm, 7 stages, method 1, and 61,000 kmol/hr. For these two cases, there was a trend of discharge temperature and power production. In case 75, the highest discharge temperature led to the highest power production. On the other hand, the lowest discharge temperature, case 7, led to the lowest power production case. From this analysis, the operation condition for obtaining the high temperature discharge was also selected for high power production achievement.
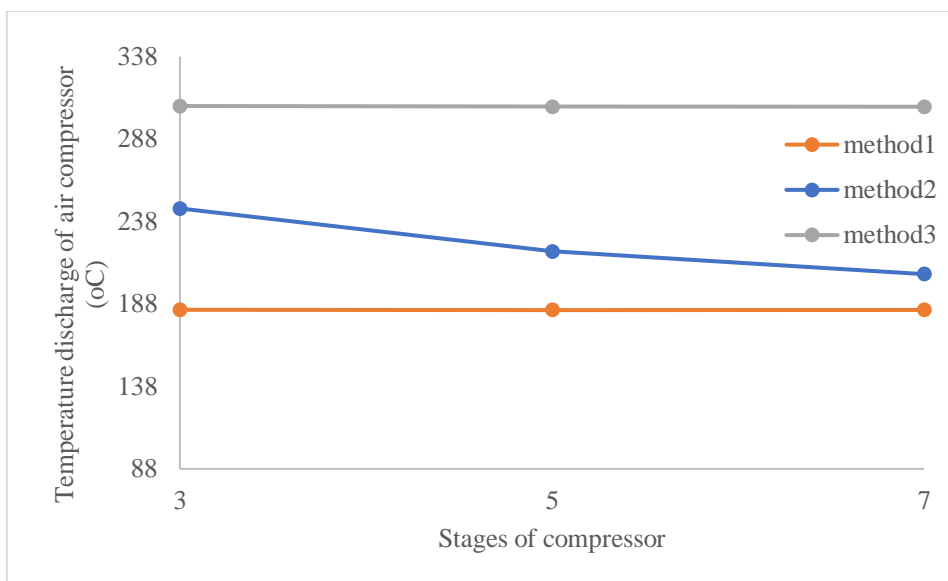
Fig. 4.13 The effect of the number of compressors and compression ratio method on
the discharge temperature of the air compressor.
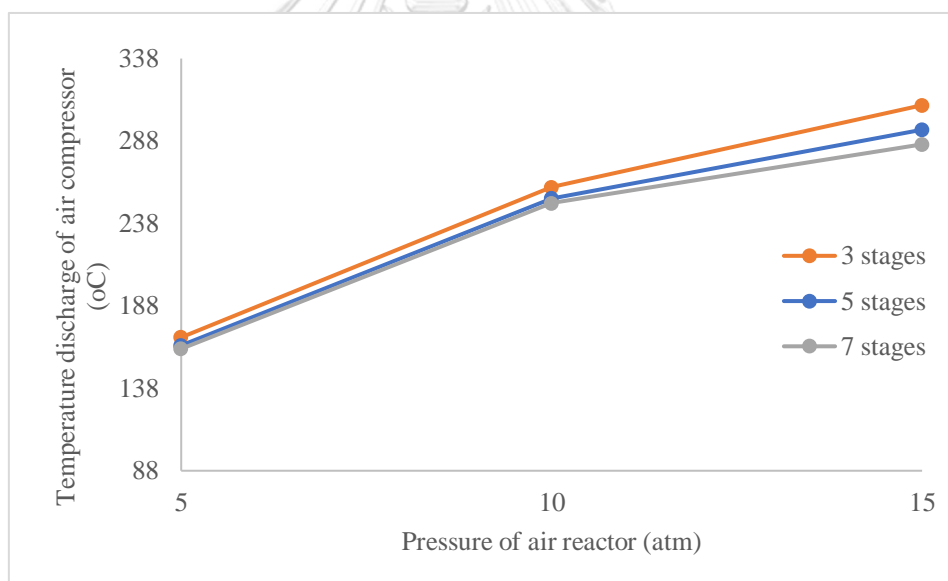
Fig. 4.14 The effect of air reactor pressure and the number of compressors on the
discharge temperature of the air compressor
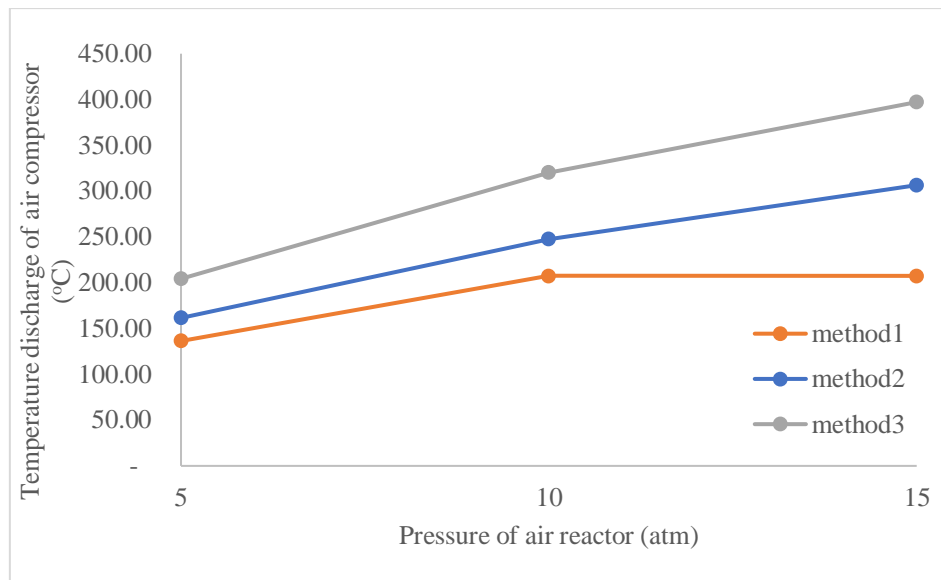
Fig. 4.15 The effect of air reactor pressure and compression ratio method on the discharge temperature of the air compressor.

4.4 Further efficiency improvement

The proportion of Ni loading was investigated because it affected the temperature of the air reactor which influenced to the power production from the air reactor and thermal efficiency, in the end. The loading of Ni on the Al_2O_3 supporter was investigated in various studies. As the study of Huijun et al., the reason for the high conversion of carbon was the increase of $\%$ Ni loading [113]. In the study of Huijun et al. and Ishida et al., the high NiO loading on Al_2O_3 achieved the maximum conversion of carbon and syngas in the biomass combustion process [113, 114]. The 50% of NiO loading on Al_2O_3 reached the highest conversion in the biomass combustion process. However, the increase of Ni loading had not been considered the effect on power production and thermal efficiency of the system. Accordingly, the effect of Ni loading on thermal efficiency was investigated. The investigated range of Ni loading was 10-60% by mole or 6-46% by weight (wt). The highest thermal efficiency case as case 81 was selected for the investigation. In the previous section, the Ni loading of case studies was 16. The increase of Ni loading was conducted by fix the total mass flow of Ni, 908,649 kg/hr. The Ni mass flow rate was kept constant to provide complete combustion with natural gas. Therefore, the adjustment of Ni loading was the changing of Al_2O_3 only. Typically, Al_2O_3 had two functions. First, it

was the supporter of Ni or NiO for improving the mechanical properties of the oxygen carrier. Since, the reaction in the air reactor was exothermic and the reaction in the fuel reactor was endothermic. The temperature of air reactor was higher than fuel reactor. Consequently, the generated heat in air reactor was the heat source for the fuel reactor. Second, Al_2O_3 could carry heat from the air reactor to the fuel reactor.

The increase of Ni loading provided the low Al_2O_3 and the total mass of the solid. When the total mass of solid was low, the temperature of the air reactor was increased, followed by the calculation of enthalpy ($Q = mC_p\Delta T$). Accordingly, the increase of Ni loading from 6% to 46%wt provided the increased temperature of the air reactor from 1,375°C to 1,625°C, as shown in Fig. 4.15.

The increase of air reactor temperature would be a cause of the high-power production of air reactor, as shown in Fig. 4.16. The increase of Ni loading from 6% to 28%wt led to the increase of power production from the air reactor because the temperature inlet to the turbine was increased.

Since the CLC process was operated with the HAT cycle which humid air was generated. The humid air was introduced to the air reactor which provided the high mass flow rate to the turbine and high-power production. When water flow rate had been decreased, the power production from the air reactor was decreased. Therefore, when the Ni loading was increased higher than 28%wt, the power production from the air reactor was decreased because the water flowrate was decreased, as shown in Fig. 4.17. In addition, the high-water flow rate provided the high-power production from the air reactor, but the temperature of the air reactor was decreased. At the high proportion of Ni loading, the solid from the air reactor was sent to fuel reactor with low mass flow rate. Therefore, the solid from the air reactor should be sent at high temperature for remain total heat supplied to the fuel reactor.

The increase of Ni load led to the increase of work consumption of compression, as shown in Fig. 4.18. Since the water flow rate was decreased. The water was introduced to the HAT cycle for 2 reasons; 1) humid air generation and 2) work consumption of air compression reduction. Water was the coolant at the intercooler. Water was received heat from the compressed air between the multi-stage compressor. The low temperature inlet to the compressor provided the low work

consumption of air compression. According, when the water flow rate of the process was decreased, the work consumption of air compression was increased.

Eventually, the thermal efficiency was increased when Ni loading was increased from 6% to 28%wt because of the increase of temperature and power production from the air reactor, as shown in Fig. 4.19. When Ni loading was higher than 28%wt, the thermal efficiency was decreased because of the increase of work consumption of air compression and the decrease of water flowrate. The suitable Ni loading could carry the fuel reactor's heat needed without external energy supplies. It would lead to optimum air reactor temperature, optimum solid temperature, optimum water mass flow rate, and high efficiency. For this process, the suitable Ni loading was 28%wt, which achieved the highest thermal efficiency of the CLC process with the HAT cycle, 57.67% at 15 atm, 7 stages, and method 3.
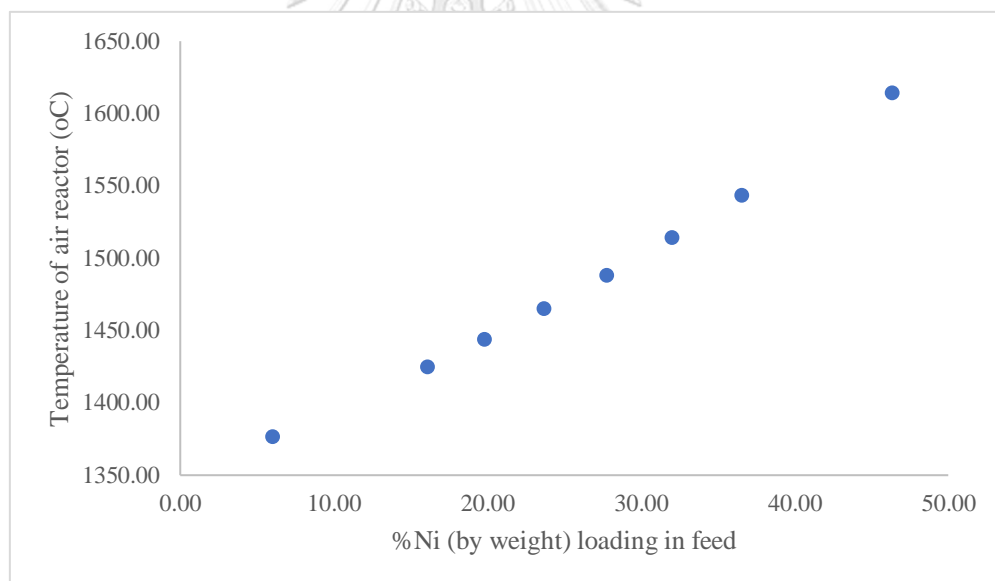
Fig. 4.16 The effect of % Ni loading on the temperature of the air reactor.
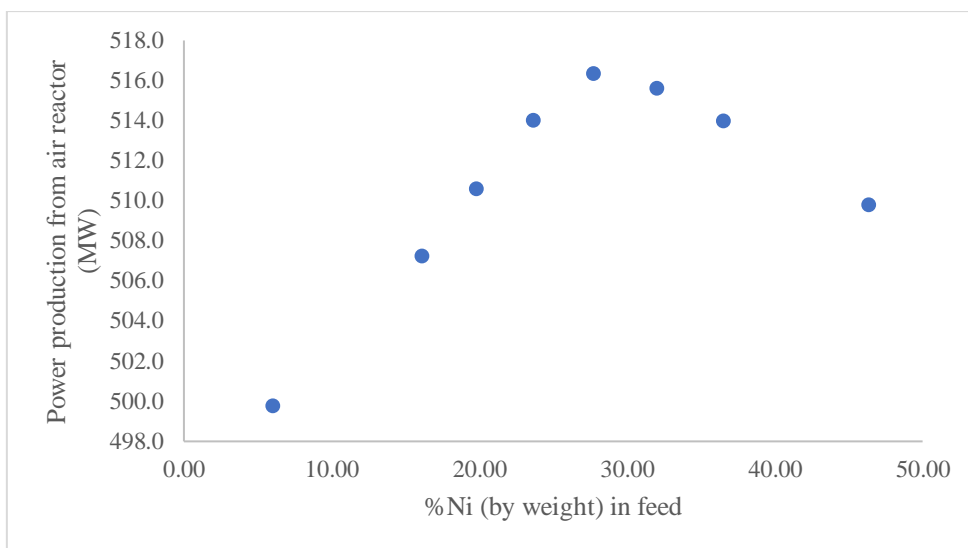
Fig. 4.17 The effect of %Ni loading on power production from the air reactor.
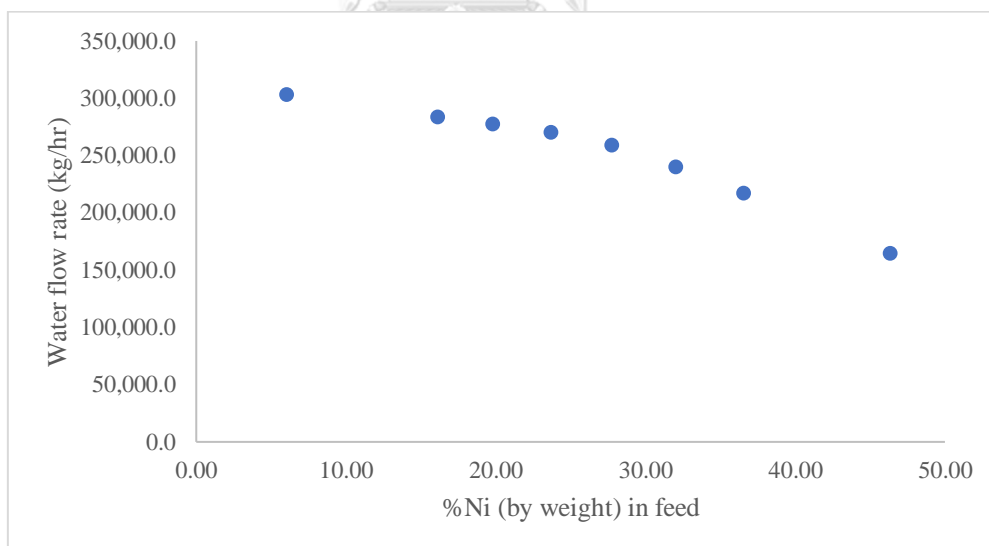
Fig. 4.18 The effect of %Ni loading on water flow rate in the system.
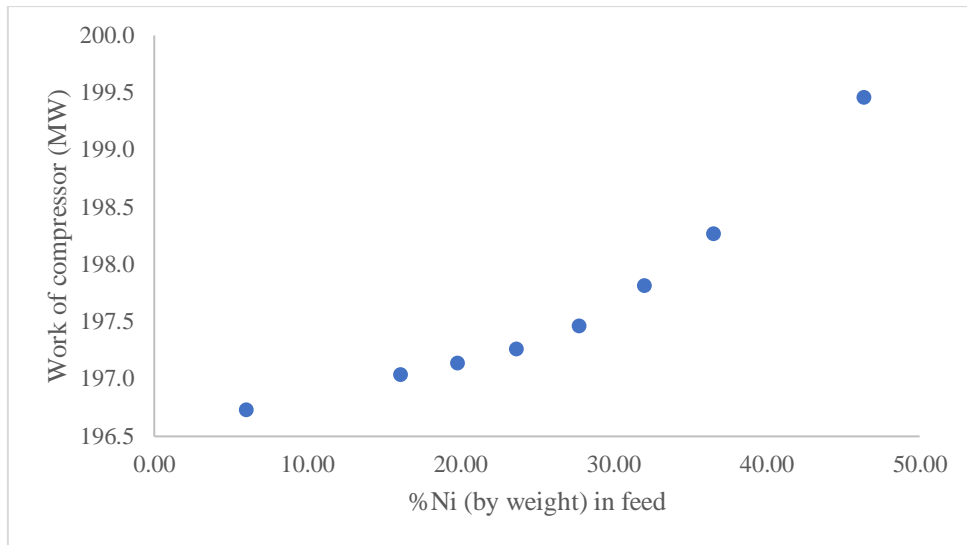
Fig. 4.19 The effect of %Ni loading on work of air compressor.
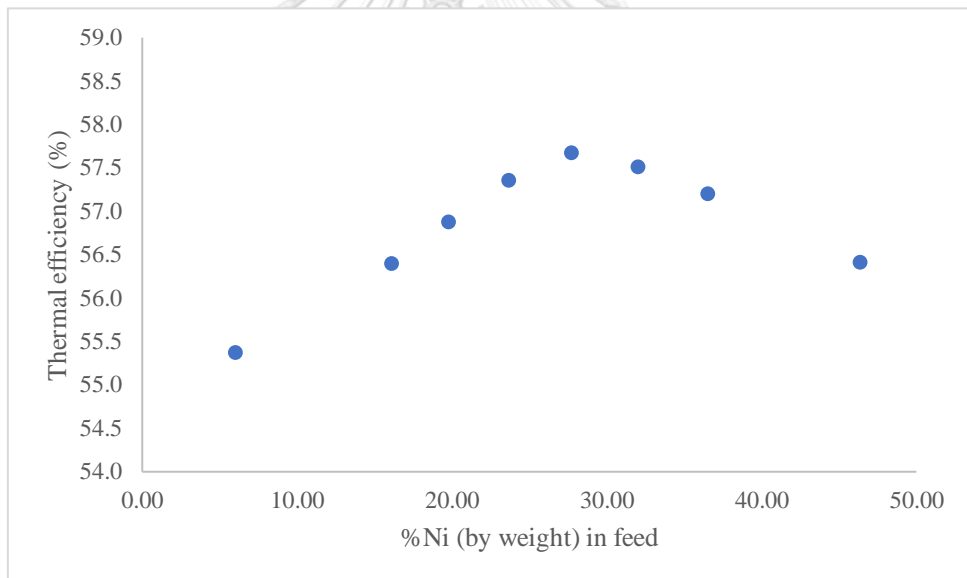
Fig. 4.20 The effect of % Ni loading on thermal efficiency.

4.5 Conclusion

This study objective is to systematically investigate the operating variables that have effects on the efficiency of the CLC combined with HAT unit to produce electricity. Both system configurations and operating conditions were simultaneously investigated. The high thermal efficiency represented the worthiness of the using of fuel. Four operating variables; pressure of the air reactor, number of air compressor

stages, methods of air compression and air flow rate were investigated their effects on four responses; the thermal efficiency, power production from air reactor, work of air compressor and air compressor discharge temperature. In this study, the maximum thermal efficiency of the CLC process with the HAT cycle was 57.67%, while that of Petriz-Prieto et al. study was 56.08% [49]. However, the result did not aim for comparison. It was used to be the preliminary data in operation for reach the high efficiency in power production and making decision for the practical operation.

For more understanding of the system, four input parameters, which were the pressure of the air reactor, the number of compressors, the compression method and the air flow rate, were investigated their effects on the four responses: the thermal efficiency, the power production from air reactor, the work of air compressor, and the discharge temperature from the air compressor. The 3^k factorial design was used for investigation. Case 81 gave the maximum thermal efficiency, 55.87% , with the operation at 15 atm, 7 stages, method 3, and 61,000 kmol/hr. However, case 75 operated the same operating condition as case 81, but used only 3 stages of compression, had a thermal efficiency of 55.84% . In this case, case 75 could be a better solution since the investment cost would be lower than case 81, while the thermal efficiencies were quite the same. Thus, case 75 was selected as the base case for the CLC process with the HAT cycle.

The result showed that the increase in air reactor pressure, the number of compressors, and the air flow rate would increase the thermal efficiency. Method 3 of the compression operation led to high thermal efficiency. It was also found that air reactor pressure and compression operation methods highly affected thermal efficiency. Method 3 for compression operation reached high thermal efficiency because it brought about the highest discharge temperature for the turbine. The high discharge temperature was the reason for the high air reactor temperature, high power production from the turbine, and high thermal efficiency. The high discharge temperature was the reason for the high-water flow rate introduced into the HAT cycle. Water absorbed the heat in compressed air, causing the reduction of compression work. Therefore, a high-water flow rate was fed into the system when method 3 was operated. The increase of compression stages would increase the inter-coolers to release heat of compressed air. The operation for obtaining the high-power

production and high temperature discharge should be selected to operate more than low power consumption of air compression. At last, the amount of Ni loading in the system was studied. Since the Ni mass flow rate was constant, the increase of Ni loading was carried out by decreasing Al_2O_3. The Al_2O_3 acted as a heat source for the fuel reactor. It was found that the system with 28%wt of Ni loading gave the highest thermal efficiency of 57.67%.

Chapter 5
Hydrodynamic behavior of chemical looping combustion

5.1 Research gaps

Chemical looping combustion could be used with solid fuel and gaseous fuel. The solid fuel would be coal and biomass, while the gaseous fuel could be natural gas. The challenges to operate the process with these fuels were different. The major challenge of solid fuel is the unburnt char because of the slow gasification rate. However, for the gaseous fuel system, the combustion was mostly complete.

Nonetheless, improper operating conditions could also lead to incomplete combustion. Its consequence is the CO_2 emission from the air reactor. Therefore, the operating conditions are a crucial factor in achieving suitable hydrodynamics and obtaining high thermal and CO_2 capture efficiencies.

5.2 The objectives

For the first section, the operating conditions were systematic investigation for suitably hydrodynamic behavior. The fuel and oxygen carriers for this section were coal and iron oxide (Fe_2O_3/Fe_3O_4).

For the second section, the operating conditions which obtained the high thermal efficiency from chapter 3 were investigated for suitably hydrodynamic behavior under chemical reactions. The fuel and oxygen carrier for this section was methane (CH_4) and nickel oxide (NiO/Ni). Then, the conversion and temperature achievements would be determined.

5.3 Results and discussion of the first part

5.3.1 Model validation

When the system reached the steady-state condition, the mass fraction outlet of the reactor would fluctuate around the constant value. The result of the simulation model was collected and interpreted. The model without reaction or cold flow model was validated with the experimental data. After that, the model will include the reaction model and simulate when reactions occur.

The model was validated by running the cold flow model under isothermal at 1173 K and the coal feeding velocity at 1 m/s. The obtained solid volume fraction (VOF) contour from the simulation was compared with the experimental data studied

by Su et al. [97]. The solids in their system, including iron oxide and coal. The contours of the solid volume fraction of the model simulation and experimental data were consistent, as shown in Fig. 5.1. It represented that the VOF was dense in the downers and the VOF was well dispersed in the risers. In the hot flow model, the mass fraction outlet from the reactor was compared with the experimental data, which was studied by Su et al. [97]. The result of fuel and air reactors are shown in Fig. 5.2 and 5.3, respectively. The mass fraction outlet results between the simulation data and the experimental data were consistent. When the simulation data and the experimental data were consistent in cold and hot flow models, the model was used for further investigation because this model could represent the reasonable result of the dual circulating fluidized bed reactor (DCFBR) for the CLC process.

The interested point of this model was CO_2 in the outlet of the air reactor. It occurred from the unburnt coal in the fuel reactor. In theory, the air reactor's gas composition should not consist of CO_2 because the air reactor's total outlet would be directly released to the environment. CO_2 contamination was the cause of the environmental crisis and it was the indicator of unsuitable operation. Consequently, the investigation of the operating condition was crucial for process improvement.
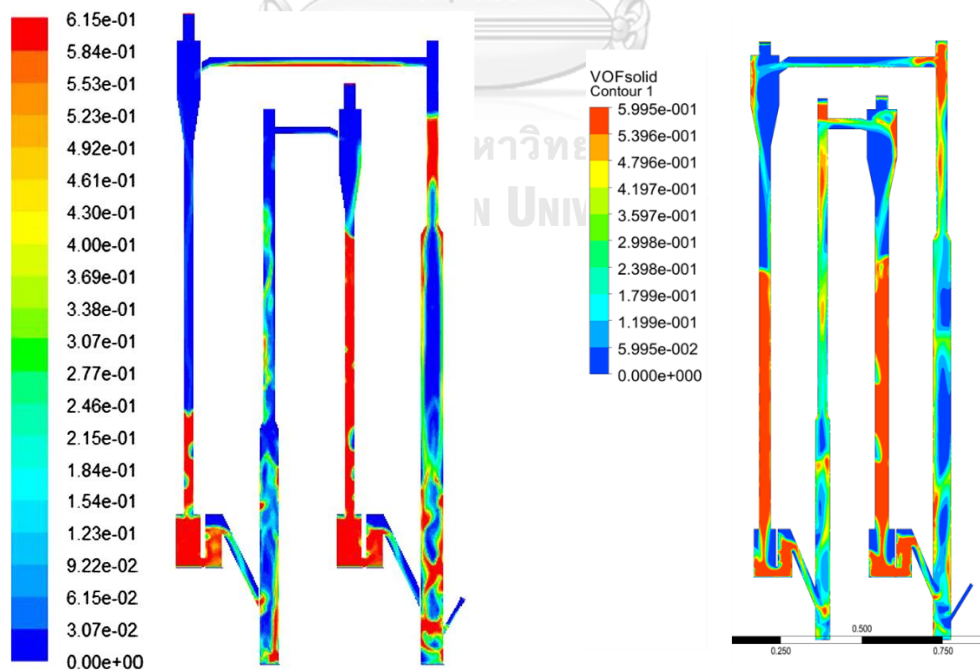
Fig. 5.1 The flow direction of total solid volume fraction (Left) from Su's study and (Right) from simulation
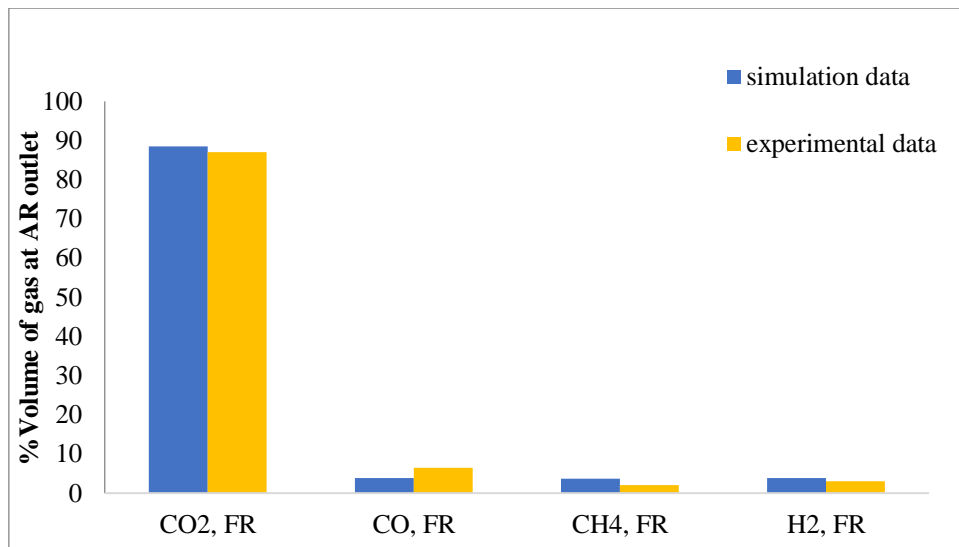
Fig. 5.2 The mass fraction of gas outlet from the fuel reactor
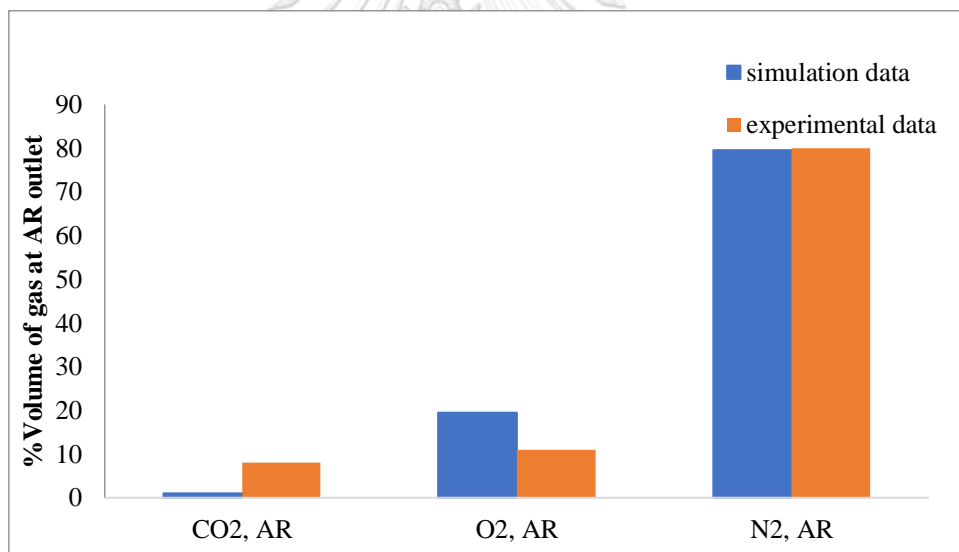
Fig. 5.3 The mass fraction of gas outlet from the air reactor

5.3.2 ANOVA result

The ANOVA analysis could indicate the significant parameters and the interaction of parameters on the system responses. The two input parameters consisted of the reactor's temperature (parameter A) and the ratio of coal feeding velocity to the oxygen carrier's weight (parameter B). Three levels of parameter A were 1173, 1373, 1583 K and the three levels of parameter B were 0.1/400, 0.5/400, 1.0/400 (m/s)/kg. The two responses consisted of the combustible gas percentage from the fuel reactor

and the CO_2 percentage from the air reactor. The result of ANOVA analysis is shown in Table 5.1 and 5.2. The two models were significant because the p-value was lower than 0.05.

Table 5.1 The effect on the combustible gas percentage from the fuel reactor

Source	Sum of Squares	DF	Mean Square	F Value	Prob > F	
Model	1826.70	4	456.68	11.88	0.0171	significant
A	748.53	2	374.26	9.74	0.0290	
B	1078.18	2	539.09	14.02	0.0156	
Residual	153.77	4	38.44			
Cor Total	1980.47	8				

Table 5.2 The effect on the CO_2 percentage from the air reactor

Source	Sum of Squares	DF	Mean Square	F Value	Prob > F	
Model	2141.13	6	356.85	104.10	0.0095	significant
B	2128.43	2	1064.21	310.44	0.0032	
AB	12.70	4	3.17	0.93	0.5783	
Residual	6.86	2	3.43			
Cor Total	2147.98	8				

5.3.3 The effect on combustible gas percentage from the fuel reactor

The combustible gas percentage from the fuel reactor was calculated from the molar flow rate of CH_4, C_2H_6, H_2, and CO from the fuel reactor's outlet divided by the total molar flow rate of the fuel reactor. The high percentage indicated low performance. The ANOVA result in Table 5.1 represented that the temperature (A) and the ratio of coal velocity to the oxygen carrier's weight (B) affected the combustible gas percentage from the fuel gas since the p-value was lower than 0.05. The increase of A and B caused an increase in the combustible gas species, as shown in Fig. 5.4.

The reaction in the fuel reactor was endothermic. [76, 115] The increasing temperature provided a higher rate of gasification reaction. Accordingly, the products of gasification were increased. The combustible gas, which included CH_4, CO, and H_2, were increased. [76] The increase in temperature would push the reaction forward. When the combustible gas was highly increased, the gas conversion in the fuel reactor's riser was decreased because the total solid was constant. Nonetheless, the result showed that the increase in temperature increased the combustible gas. The

increase of temperature was not only pushed the reaction forward but also increased the gas velocity in the riser. The high gas velocity decreased the residence time of the reactants in the riser and decrease the reaction between the oxygen carrier and gas reactants.

The increase of this ratio provided the high amount of coal in the reactor. This was because the oxygen carrier's weight was fixed while the coal amount was varied. When coal was introduced into the reactor, coal was gasified by the gasifier medium (CO_2). The gas species were the products of coal gasification. After that, the gas species was reacted with the oxygen carrier. The coal then excessed. Eventually, the increase of this ratio would increase gas species in the fuel reactor because the gasification rate was increased when the temperature was increased. [76]

The best case was case 1, with the lowest value of the combustible gas. In case 1, the temperature and the ratio of coal velocity to the oxygen carrier's weight were at the lowest values of 1173 K and 0.00025, respectively. In contrast, the worst case was case 9, with the highest value of the combustible gas. In case 9, the temperature and the ratio of coal velocity to the oxygen carrier's weight were at the highest values of at 1573 k and 0.00250, respectively.
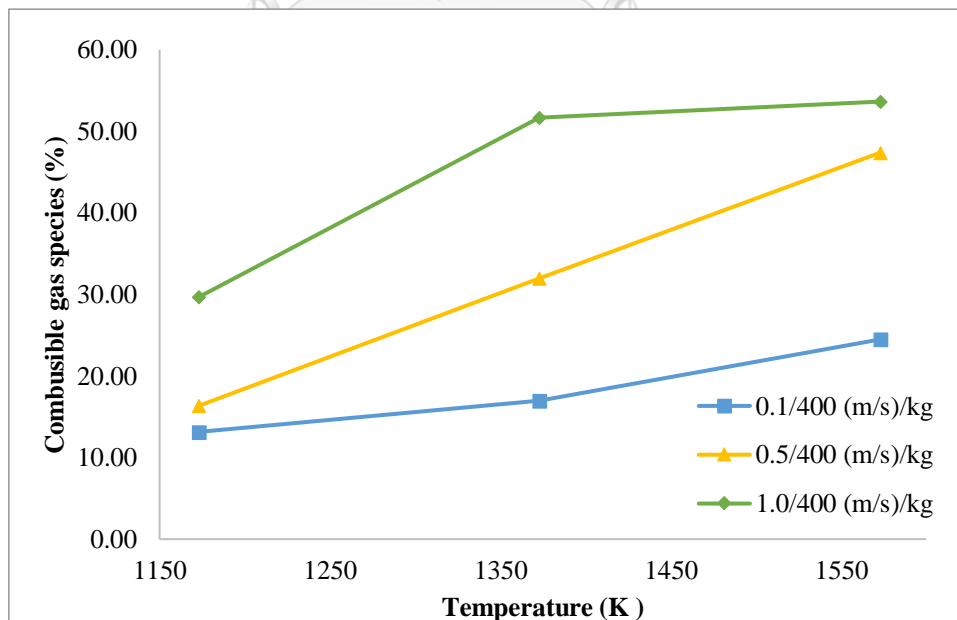
Fig. 5.4 The effect on the combustible gas from the fuel reactor

5.3.4 CO_2 percentage from the air reactor

The CO_2 percentage from the air reactor was calculated from the molar flow rate of CO_2 from the air reactor's outlet divided by the total molar flow rate from the air reactor. The high percentage indicated low performance. The ANOVA result in Table 5.2 indicated that the ratio of coal velocity to the weight of the oxygen carrier (B) and the relationship of temperature and the ratio of coal velocity to the weight of the oxygen carrier (AB) affected CO_2 percentage from the air reactor since their p-value was lower than 0.05. The increase of B and AB caused the increase of the CO_2 from the air reactor, as shown in Fig. 5.5.

After coal was gasified, the process produced gas products and char. The unburnt char from the fuel reactor was transfer to the air reactor. At the air reactor, the air was oxidized with the metal to produce an oxygen carrier. When the unburnt char was transferred to the air reactor, the char was oxidized by O_2 in the air. CO_2 was produced and contaminated in the excess air, which was directly released into the environment. The high ratio of coal velocity to the oxygen carrier's weight led to high introduced coal in the reactor, which increased the unburnt char in the fuel reactor, as shown in Fig. 5.5.

When the reactor was operated at high temperature and high ratio of coal velocity to the oxygen carrier's weight, the gas velocity and coal were high, which led to the high unburnt char in the fuel reactor.

The increase in temperature provided the rate of gasification reaction. Accordingly, the products of gasification were increased. The gasification products, CH_4, CO, H_2, CO_2, and char were increased. [76] The excess gasification products, especially the unburnt char in the fuel reactor, were sent to the air reactor. Eventually, it led to the high CO_2 at the air reactor.

The best case was cases 1- 3 with the lowest values of the CO_2 from the air reactor. In these cases, the ratio of coal velocity to the oxygen carrier's weight was the lowest at 0.0025. In contrast, the worst case was cases 7-9 with the highest values of the CO_2 from the air reactor. The ratio of coal velocity to the oxygen carrier's weight was at the highest value of 0.00250.
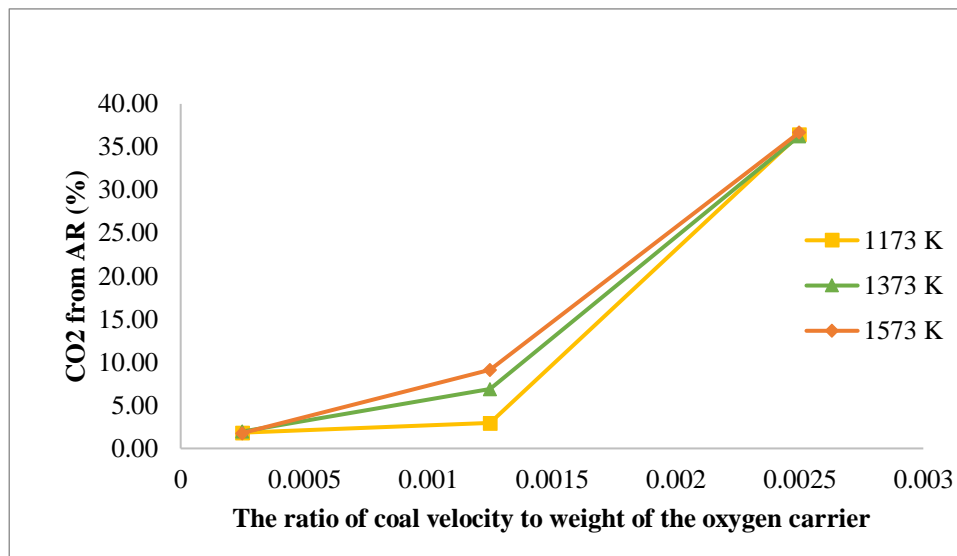
Fig. 5.5 The effect on the CO_2 combustible gas from air reactor

5.3.5 Conclusion of the first section

The high performance of the CLC process was provided by suitable hydrodynamic behavior. The high performance of the CLC process led to good CO_2 capture efficiency. In this section, the hydrodynamic behavior of DCFBR was systematically investigated by the 2^k factorial experimental design. There were two input parameters; the temperature of the reactor and the ratio of coal velocity to the oxygen carrier's weight. This systematic investigation would include the curvature behavior of the result to obtain the optimum operating condition. There were two responses; the combustible gas percentage from the fuel reactor and the CO_2 from the air reactor, which directly indicated this reactor performance. The result showed that the low temperature (1,173 K) and the low ratio of coal velocity to the weight of oxygen carriers (0.00025) provided the best performance of this system.

5.4 The results and discussion of the second section

In this section, methane (CH4) was used as the fuel and NiO/Ni was used as the oxygen carrier.

5.4.1 The hydrodynamics of cold flow

After model validation from the last section, the model was further used to investigate the CLC process, but the fuel and oxygen carriers were changed. The CH4 was used as the fuel and NiO/Ni with Al_2O_3 was used as the oxygen carrier. In the

first step, the cold flow model was performed for suitable hydrodynamics behavior achievement.

At the inlet of the fuel reactor riser, CH_4 and CO_2 were introduced into the riser. CO_2 was introduced to keeping suitable hydrodynamic behavior and reduce the total amount of CH_4 using in the system. At the inlet of the air reactor riser, the humid air was introduced into the riser. The humid air was used to follow the operating condition from the chapter 4 result. NiO/Ni and Al_2O_3 were used as the active metal and the support followed the chapter 4 result. The optimum Ni loading on Al_2O_3 was 40%mol, which convert into %mass

There were 2 values of the initial solid volume fraction; 0.35 and 0.45, which were studied. The simulation data indicated that the flow direction was correct. The solid volume fraction was dense in the downers. The solid was well dispersed in the riser. The increase of the initial solid volume fraction would increase the solid volume fraction in the downers. The contour of the solid volume fraction is shown in Fig. 5.6. It was not found the reverse flow from the riser inlet to the loop-seal. The solid was dense at the loop-seal. Therefore, it would block the inlet gas, which flowed through the downer. The reverse flow led to the low performance of the reactor and low CO_2 capture efficiency. In the cold model, the initial temperature was 873 K. The temperature contour was slightly different because the density of the mixture was changed. The temperature contour of the initial solid volume fraction at 0.35 and 0.45, as shown in Fig. 5.7 and Fig. 5.8, respectively. The gas temperature profile was slightly higher than the solid temperature. The mixture of gas density directly affected the temperature because the mixture of gas was calculated by the volume-weighted-mixing-law method. With this method, the high change of gas composition would be the reason for gas density and gas temperature. The composition of the solid phase was not highly changed. Therefore, the change of solid temperature was low.
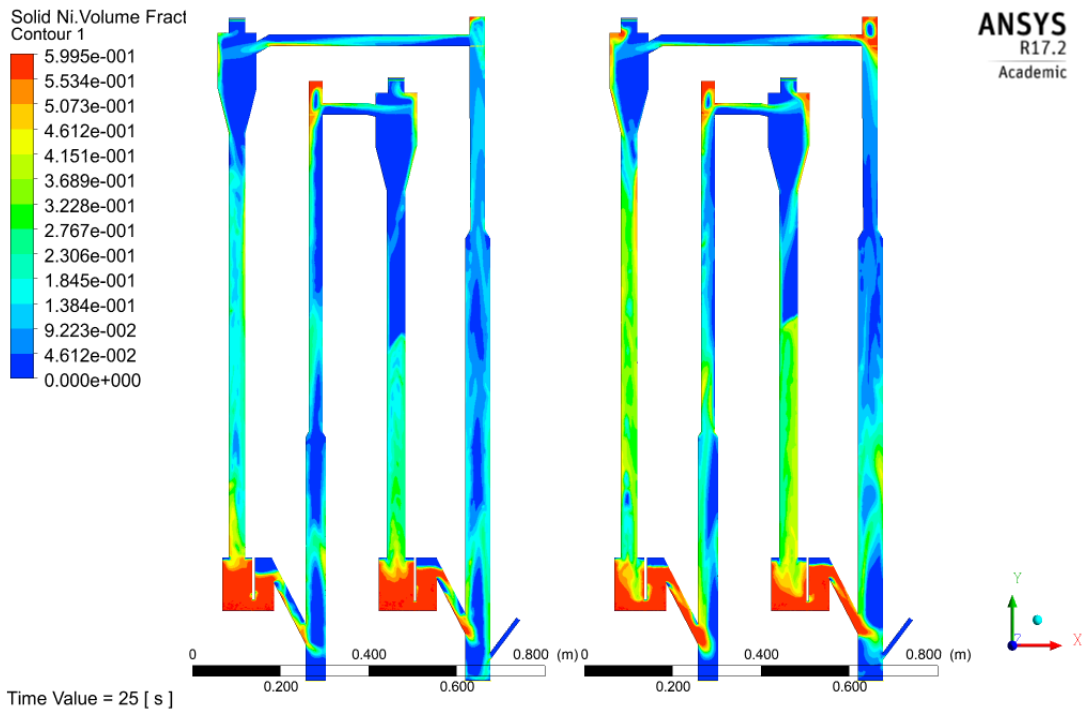
Fig. 5.6 The solid volume fraction contour when the initial was 0.35 (left) and 0.45 (right)
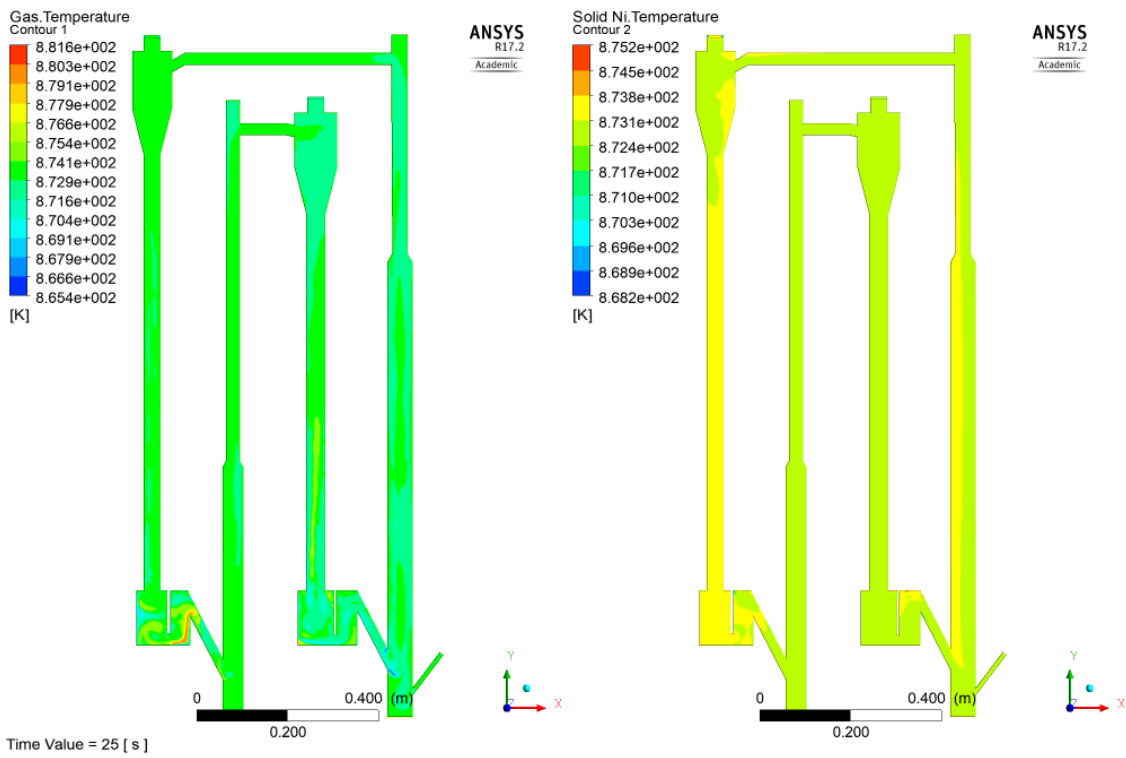
Fig. 5.7 The temperature contour of the gas phase (left) and solid phase (right) at initial VOF 0.35
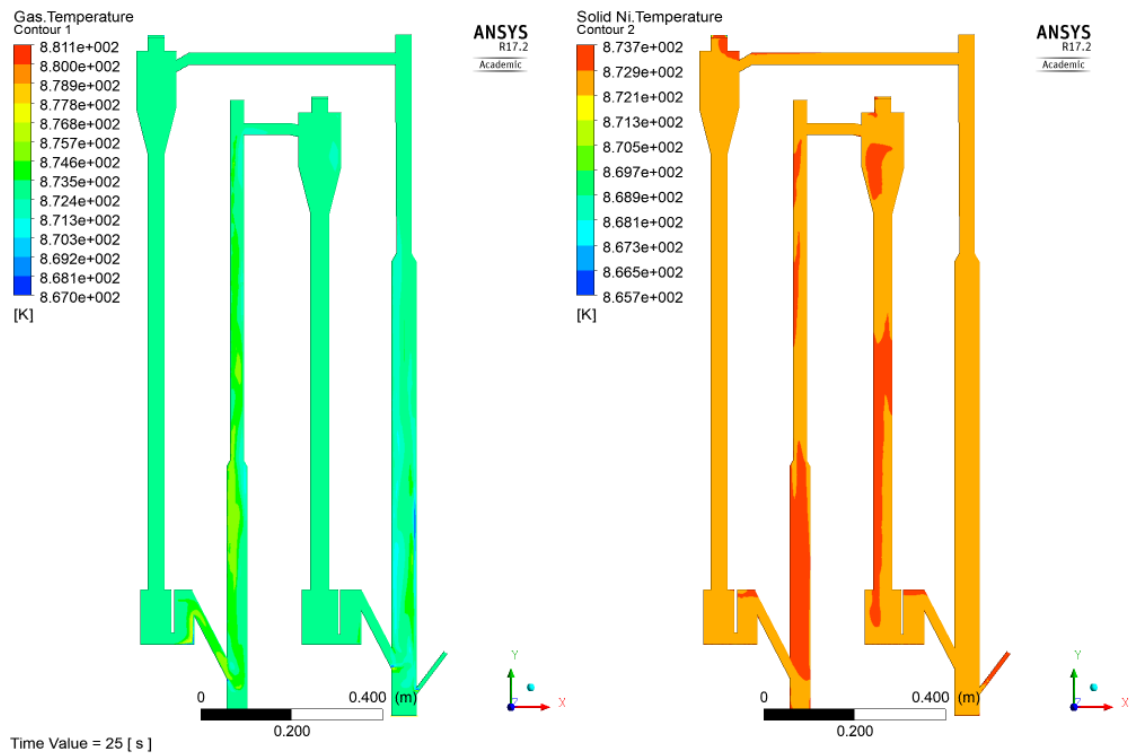
Fig. 5.8 The temperature contour of the gas phase (left) and solid phase (right) at initial VOF 0.45

5.1.1. The hydrodynamics of hot flow

After the cold flow model was completely investigated, the model was proven that the boundary and the setup of significant input data were satisfied for suitable hydrodynamic behavior of the cold flow. The data of the cold flow model at the 20 seconds was used to perform in the hot flow model. For the hot flow model, the reaction of Ni and O_2 in the air reactor and the reaction of CH_4 and NiO in the fuel reactor were included, as shown in Eqs. 5.1 and 5.2, respectively.

$$2Ni + O_2 \rightarrow 2NiO \tag{5.1}$$
$$CH_4 + NiO \rightarrow CO_2 + H_2O + 4Ni \tag{5.2}$$
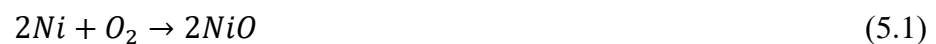
The activation energies of these equations from the study of Abad et al. were adjusted to 7 kJ/mol for all reactions. [102] There were four investigated parameters; rate reaction, initial solid volume fraction, velocity, and CH_4 mass fraction in the feed. The parameters were adjusted to obtain a suitable conversion and temperature, as

shown in Table 5.3. The simulation data was validated with the temperature, CH_4 conversion, and MW thermal from the experimental data. The caution for the hot flow model is the properties of the material in the system. The heat of heterogeneous reaction is the heat source of the system. The heat of the heterogeneous reaction in the air reactor (reaction 5.1) should be a positive value because it was the exothermic reaction. The heat of the heterogeneous reaction in the fuel reactor (reaction 5.2) should be a positive value because it was the endothermic reaction. When the heat of heterogeneous reaction was incorrect, the heat of formation of the material was checked. Besides, the rate exponent of the reaction was checked to obtain the responses' accuracy (temperature conversion).

Table 5.3 The total cases study from 3^k factorial experimental design and the results.

Case	Temperature (K)	V_{coal} to weight of OC (m/s)/(kg)	% Combustible gas species from FR	%CO_2 from AR
1	1173	0.00025	13.15	1.84
2	1373	0.00025	16.94	1.97
3	1573	0.00025	24.48	1.80
4	1173	0.00125	16.34	2.97
5	1373	0.00125	31.96	6.93
6	1573	0.00125	47.38	9.12
7	1173	0.0025	29.68	36.47
8	1373	0.0025	51.68	36.30
9	1573	0.0025	53.64	36.71

5.1.1. The validation with experimental data

The results of the hot flow model are shown in Table 5.4 and Table 5.5. The conditions of all case studies were compared with the other studies investigating the hydrodynamics of the CLC reactor. The fuel reactor temperature validated with experimental data included cases 1-10, as shown in Fig. 5.9. The air reactor temperature validated with experimental data included cases 5-10, as shown in Fig. 5.9. The CH_4 conversion validated with experimental data included case 7, as shown

in Fig. 5.10. The thermal energy that was produced by the reactor at 1.5 m was 0.225 MW thermal. [97] The thermal energy that was produced from this study were 0.27-0.97. The thermal energy that was validated with experimental data included cases 1-10. The conditions of case 7 were 1E+5 of pre-exponential factor, 0.45 of the initial VOF, 1 time of velocity compared with the base case, and 0.05 of CH_4 mass fraction. Accordingly, the results were confirmed that the operating conditions were realistic with the experiment. In the next section, the effect on temperature and conversion were represented.

Table 5.4 The output conditions from the adjusted parameters

Cases	Average Temp Solid AR (K)	Average Temp Gas AR (K)	Average Temp Solid FR (K)	Average Temp Gas FR (K)
1	874.51	874.50	874.51	874.19
2	876.66	876.66	876.66	874.78
3	1014.31	1014.12	1014.31	782.10
4	986.43	986.42	986.43	918.41
5	1236.78	1236.56	1236.78	1165.45
6	1280.99	1280.98	1280.99	1200.03
8	1258.15	1258.17	1258.15	1209.40
7	1320.94	1320.91	1320.94	1186.18
9	1146.72	1146.00	1146.72	1015.32
10	1149.18	1148.96	1149.22	1040.89

Table 5.5 The temperature, conversion and MW thermal of other studies.

		Ref
FR temperature (K)	873-1273	[116-118]
AR temperature (K)	1123-1273	[116-118]
CH4 conversion (%)	95-100	[116]
MW thermal	0.225	[97]
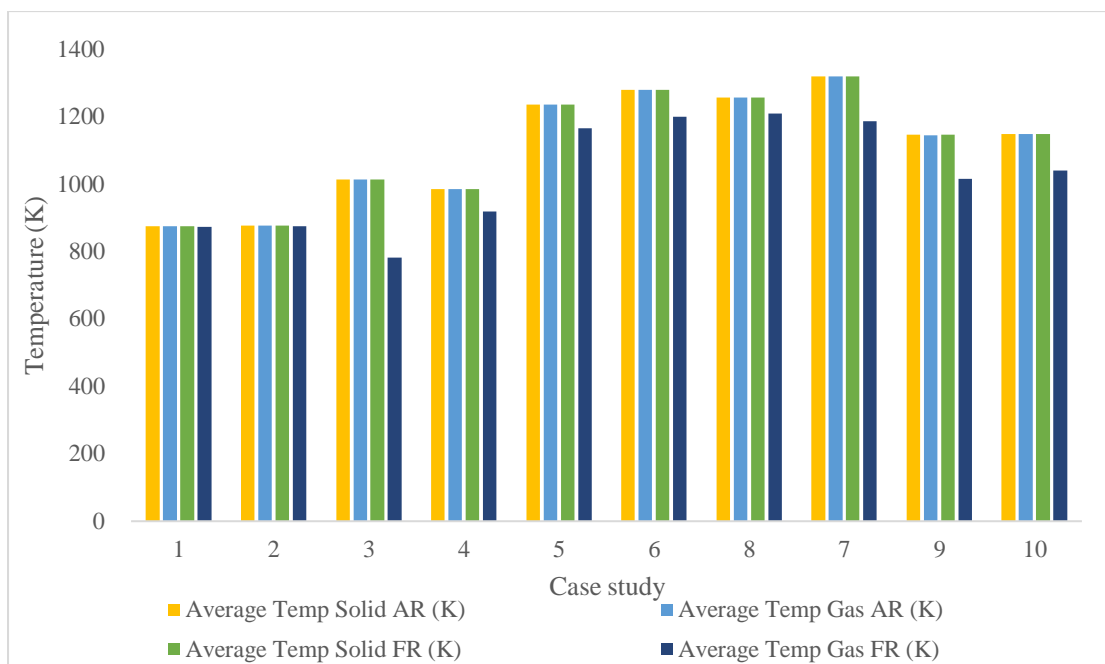
Fig. 5.9 The temperatures of air and fuel reactor of all case studies
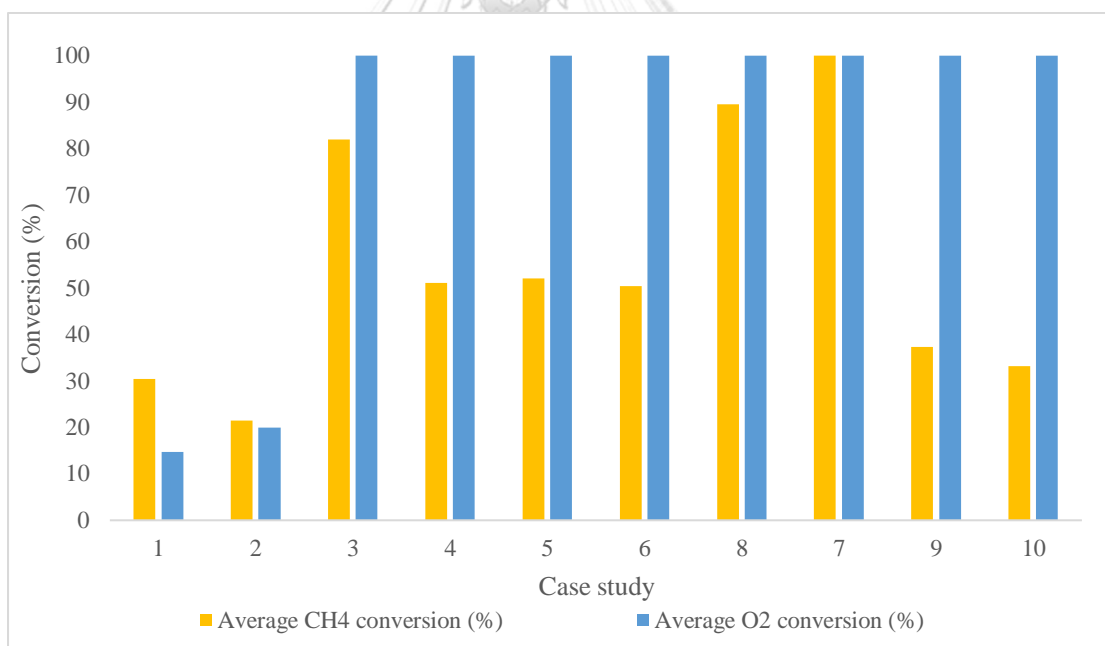
Fig. 5.10 The CH$_4$ and O$_2$ conversion of all case studies.

5.4.2 The effect of rate reaction

The pre-exponential reaction rate factor was the constant (A) in the Arrhenius equation, as shown in Eq. 5.3. The increase in this factor led to an increase in rate reaction.

$$k = Ae^{Ea/RT} \tag{5.3}$$

When the initial solid volume fraction was adjusted to 0.35, the pre-exponential factors in Eqs 4.1 and 4.2, were adjusted to 1, 1E+3, and 1E+5. The increase of the pre-exponential factor was why the higher conversion of CH_4 and O_2 obtained, as shown in Fig. 5.11. When the pre-exponential factor was increased from 1 to 1E+5, the conversion of O_2 was almost completely converted. The O_2 conversion was increased when the pre-exponential factor was increased. The O_2 conversion was the highest at the pre-exponential factor of 1E+3.

The result of the temperature in the air reactor and fuel reactor was shown in Fig. 5.12. When the pre-exponential factor was 1, the temperature of air and fuel reactors was not highly changed from the beginning condition. At the beginning condition, the temperature of all materials in the reactor and feed was 800 K. The high conversion led to high temperature in the air reactor and low temperature of fuel reactor because the reactions were exothermic and endothermic in air and fuel reactors, respectively. Therefore, the temperature in the air reactor was increased. At the pre-exponential factor of 1E+3, the fuel reactor's temperature was the lowest because the CH_4 conversion was the highest. At the pre-exponential factor of 1E+5, the fuel reactor's temperature was high because the temperature of the air reactor was high. In the CLC reactor, the heat was carried by the oxygen carrier from the air reactor to the fuel reactor. Accordingly, the air reactor's high temperature led to high temperatures in the fuel reactor.
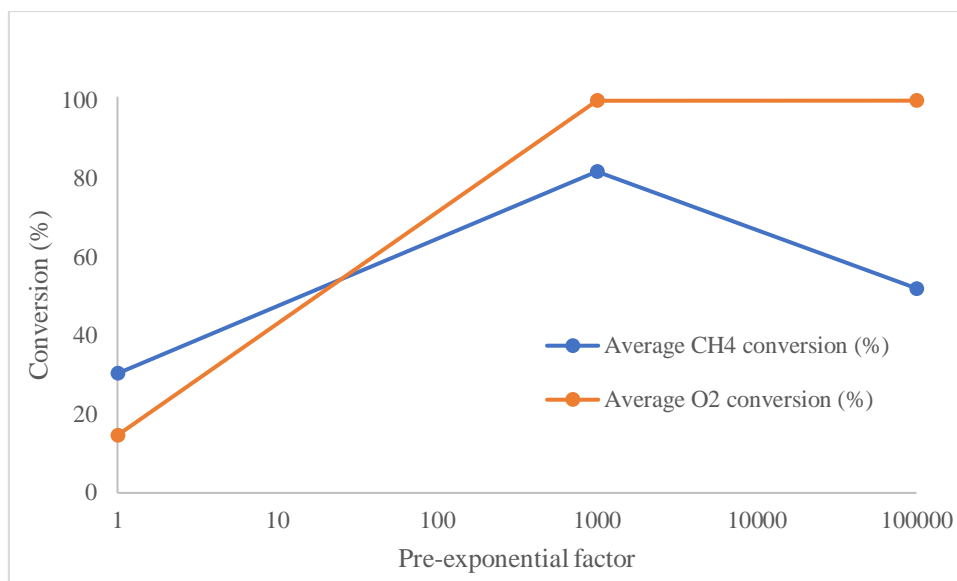
Fig. 5.11 The conversion of CH_4 and O_2 when the initial VOF was 0.35
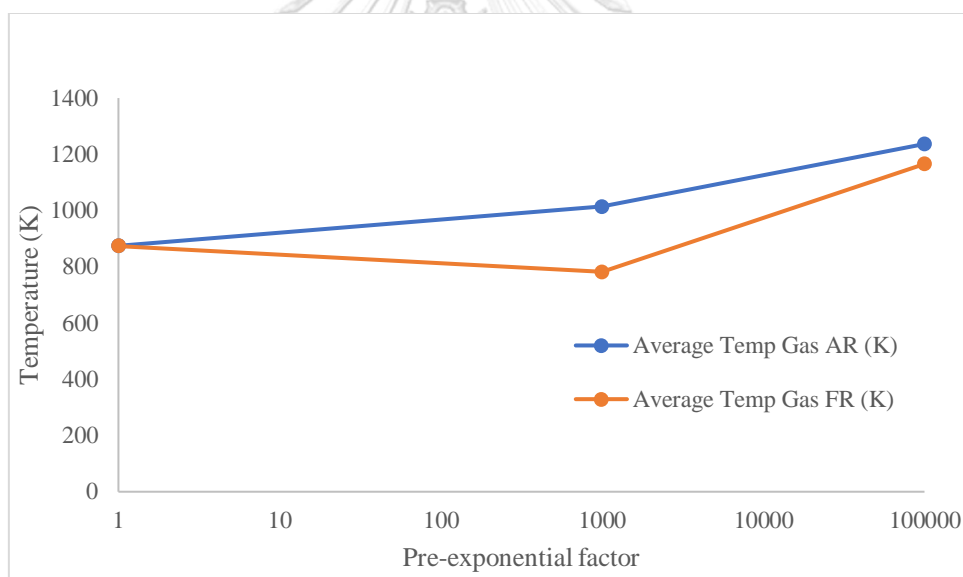
Fig. 5.12 The temperature of the air reactor and fuel reactor when the initial VOF was 0.35

When the initial solid volume fraction was changed to 0.45, the increase of the pre-exponential factor was why the higher conversion of CH_4 and O_2 obtained, as shown in Fig. 5.13. When the pre-exponential factor was increased from 1 to 1E+5, the O_2 and CH_4 conversion were increased. The high conversion led to a high temperature of rectors, as shown in Fig. 5.14.
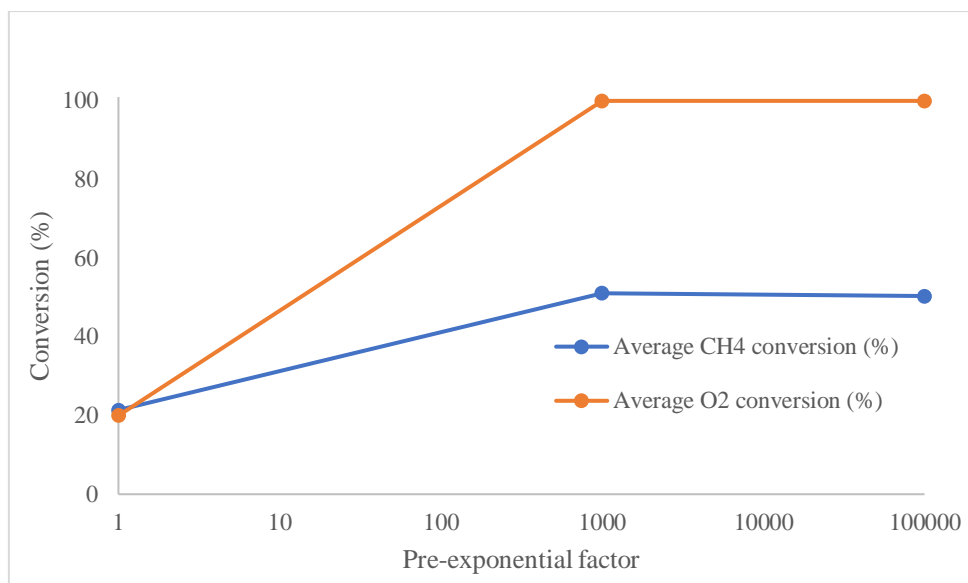
Fig. 5.13 The conversion of CH_4 and O_2 when the initial VOF was 0.45
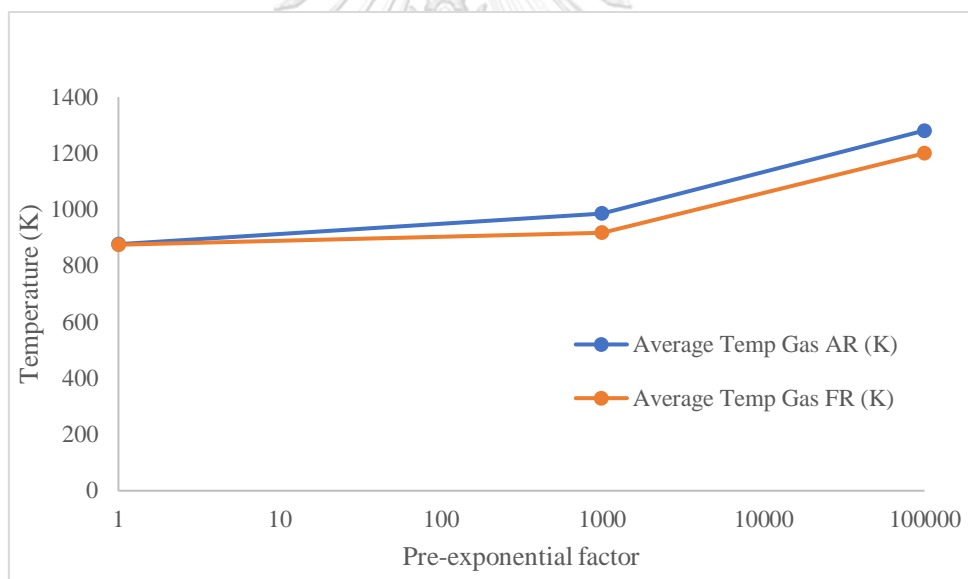
Fig. 5.14 The temperature of air reactor and fuel reactor when the initial VOF was 0.45

5.4.3 The effect of the initial solid volume fraction

The initial solid volume fraction (VOF) was used at 0.35 and 0.45. The high initial solid volume fraction indicated the high total solids in the system. The total amount of solid, when initial VOFs were at 0.35 and 0.45, were 39.03 kg and 50.18 kg, respectively. The high amount of solid would be the reason for high conversion, but too much solid would fall into the bottom of the downer, as shown in Fig. 5.15.

Accordingly, too much solid in the system led to low conversion. The higher cluster was found in the riser when the initial VOF was 0.45. Accordingly, the mixing when the initial VOF was 0.35 was better.
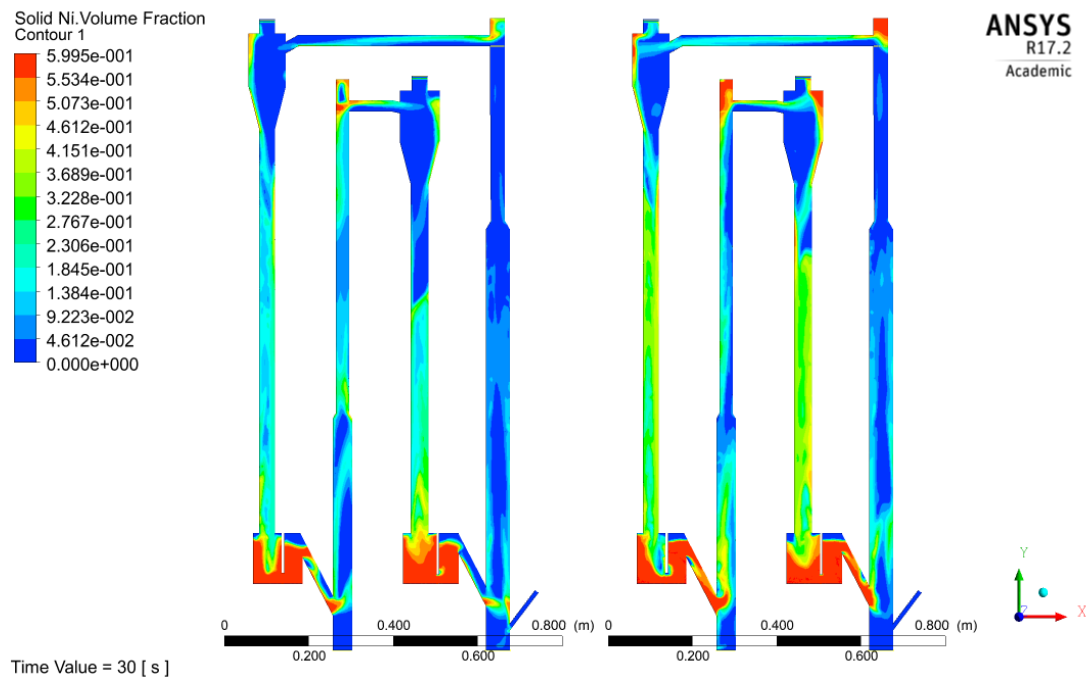
Fig. 5.15 The volume fraction contour of the initial VOF 0.35 (left), and the initial VOF was 0.45 (right)

The conversion of O_2 when the initial VOF at 0.35 and 0.45 was almost complete combustion. The increase of the initial VOF from 0.35 to 0.40 led to a decrease of CH_4 conversion, as shown in Fig. 5.16. The high conversion of O_2 provided the air reactor's high temperature, and the high conversion of CH_4 provided the low temperature of the fuel reactor, as shown in Fig. 5.17.
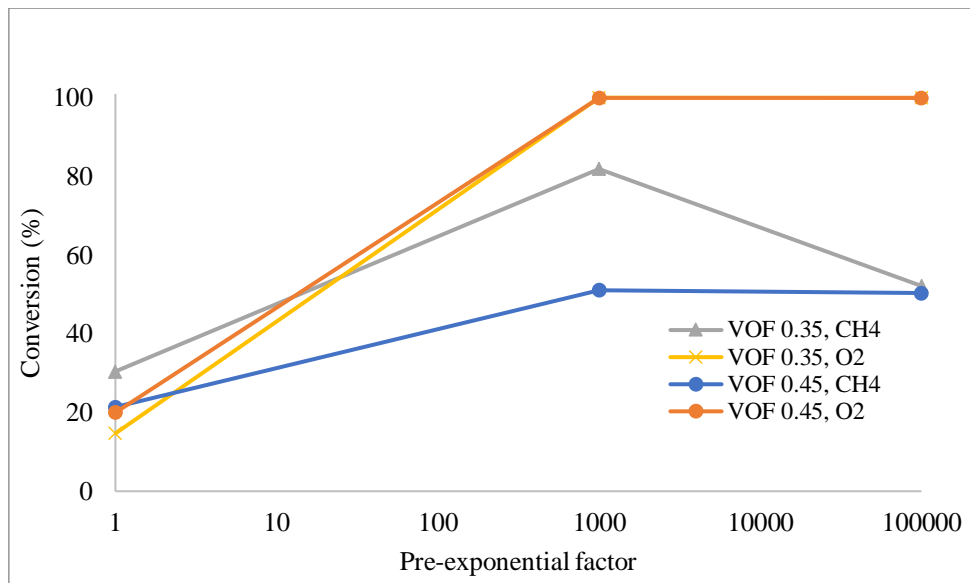
Fig. 5.16 The conversion of CH_4 and O_2 when the velocity was adjusted
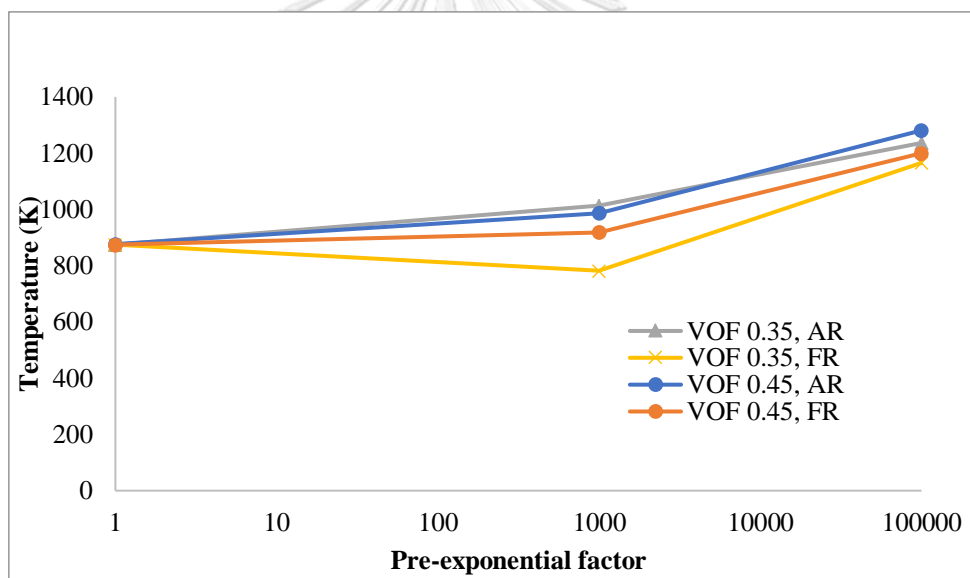
Fig. 5.17 The temperature of the air reactor and fuel reactor when the velocity was adjusted

5.4.4. The effect of velocity

The increase of velocity increased the homogeneity of the mixture, which increased the conversion in the reactors. In Shen's study, their result indicated that the low gas velocity led to high residence time. [119] However, too high velocity was the reason for residence time reduction, which decrease the conversion in the reactors. The velocity was adjusted from the base case at 1 and 1.5 times. For the base case, the

velocities at the risers of air and fuel reactors were 1.6 and 1.2 m/s, respectively. For the adjusted velocity case by 1.5 times, the velocity at the risers of air and fuel reactors were 2.4 and 1.8 m/s, respectively. The increase of velocity provided the decrease of CH_4 conversion in air and fuel reactor. On the other hand, it was not affected by O_2 conversion in air and fuel reactor. It indicated the air flow rate of this condition could be increased, which would increase the CH_4 conversion, as well. In addition, the increased velocity led to the decrease of conversion when the initial VOF was 0.35 and 0.45, as shown in Fig. 5.18. However, the increase in velocity was a significant reason for the temperature decrease, as shown in Fig. 5.19. The temperature of air and fuel were decreased when the velocity increase. The air and fuel were introduced into the reactors at 873 K, lower than the reactor temperature. The high velocity led to a high amount of mass that lower temperature, which decreased the reactor temperature.
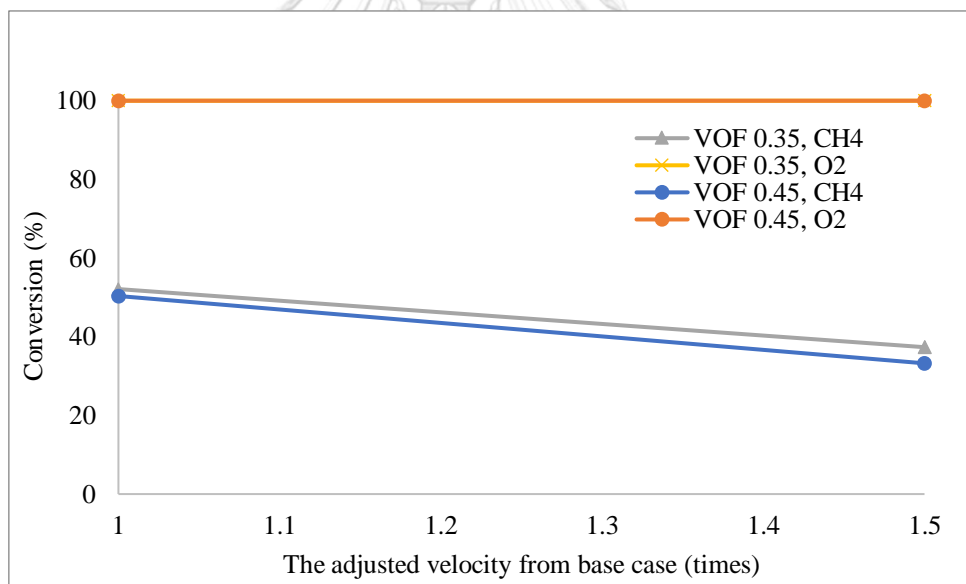
Fig. 5.18 The temperature of air reactor and fuel reactor when velocity was adjusted
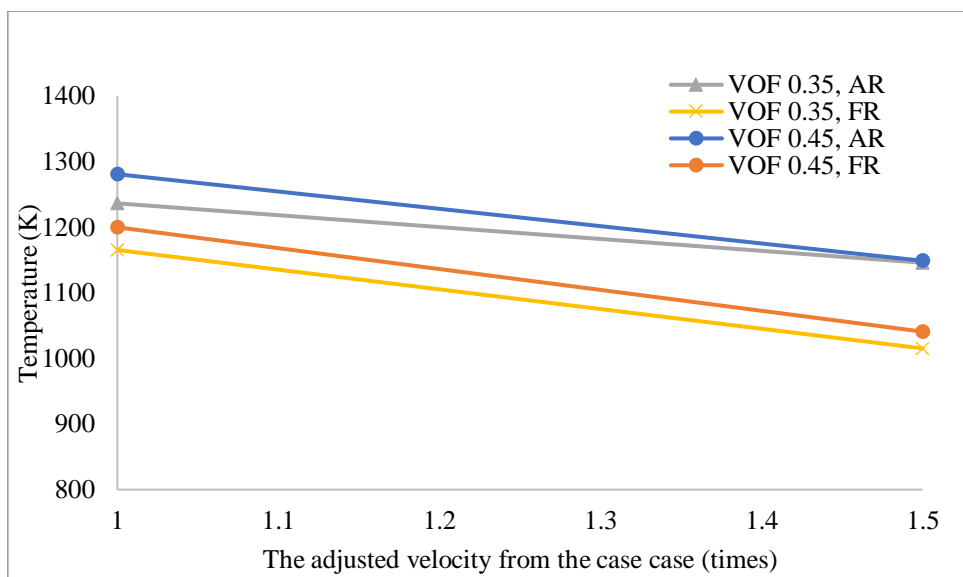
Fig. 5.19 The temperature of the air reactor and fuel reactor when velocity was adjusted

The better mixing was occurred when the initial VOF was 0.35, as shown in Fig. 5.20 and Fig. 5.21. Accordingly, the methane conversion when the initial VOF was 0.35 was higher than the methane conversion when the initial VOF was 0.45, as shown in Fig. 5.18.
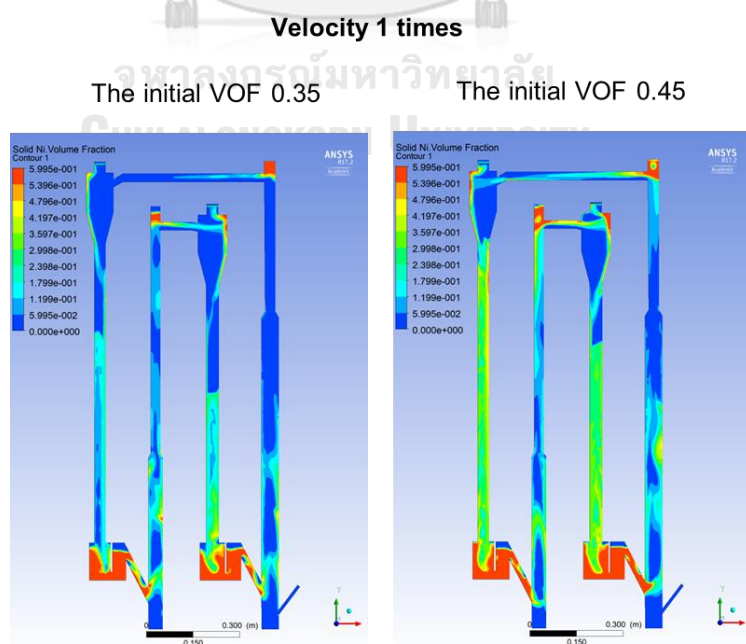
Fig. 5.20 The solid volume fraction when the velocity was 1 time

Velocity 1.5 times

The initial VOF 0.35   The initial VOF 0.45
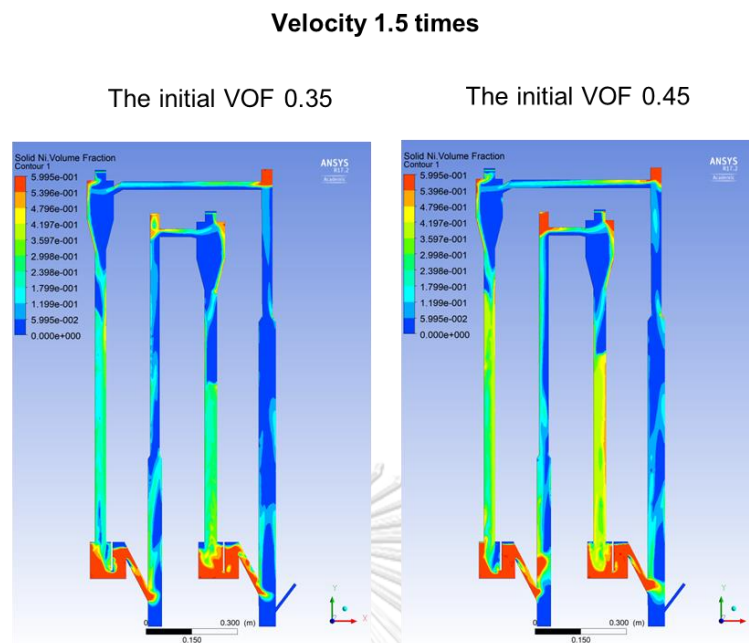
Fig. 5.21 The solid volume fraction when the velocity was 1.5 times

5.4.5 The effect of CH_4 mass fraction in the feed

The composition in feed at the riser of the fuel reactor included CH_4 and CO_2. The CH_4 mass fraction of the base case was 0.3. Then the mass fraction in feed was adjusted to 0.05, 0.15, and 0.30. The high CH_4 mass fraction led to a low CO_2 mass fraction in the fuel reactor. The adjustment of CH_4 mass fraction would not interrupt the velocity of the fuel reactor riser. Therefore, the hydrodynamic of the fuel reactor was not affected. The decrease of CH_4 mass fraction from 0.3 to 0.05 would increase CH_4 conversion, but the O_2 conversion was not affected by this condition, as shown in Fig. 5.22. At the lowest of CH_4 mass fraction, the CH_4 conversion was almost complete. The fuel reactor temperature at the lowest of CH_4 mass fraction was the lowest, and the air reactor temperature was the highest. When the CH_4 conversion was high, the oxygen carrier was highly used in the CH_4 reaction. Therefore, the spent oxygen carrier from the fuel reactor was highly oxidized by O_2 in the air reactor. The temperature of the air reactor was the highest. The high CH_4 conversion led to a low temperature of the fuel reactor, as shown in Fig. 5.23. The reaction in the fuel reactor was endothermic. [76, 115] Accordingly, the high conversion of CH_4 in the fuel reactor provided the low temperature in the fuel reactor.
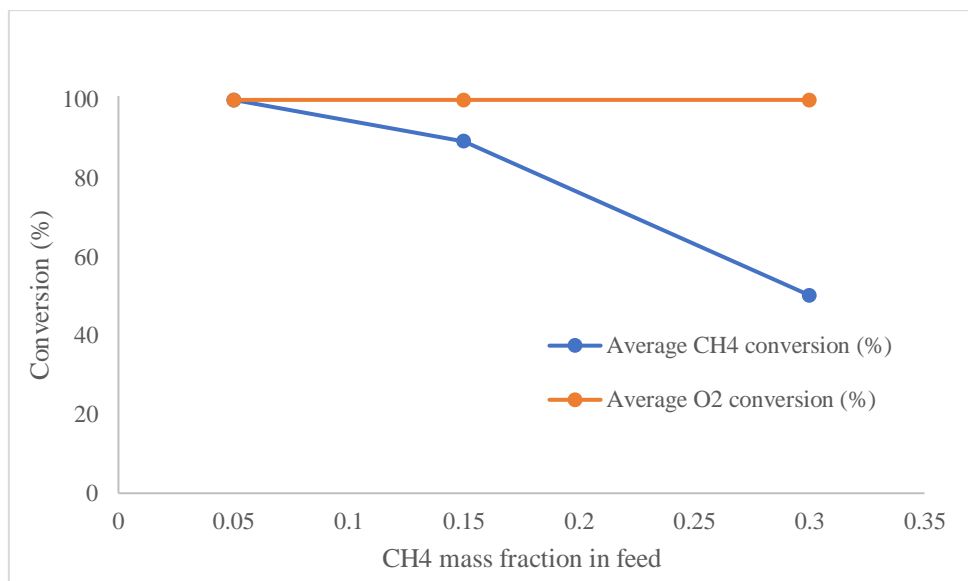
Fig. 5.22 The temperature of the air reactor and fuel reactor when CH$_4$ mass fraction in feed was adjusted
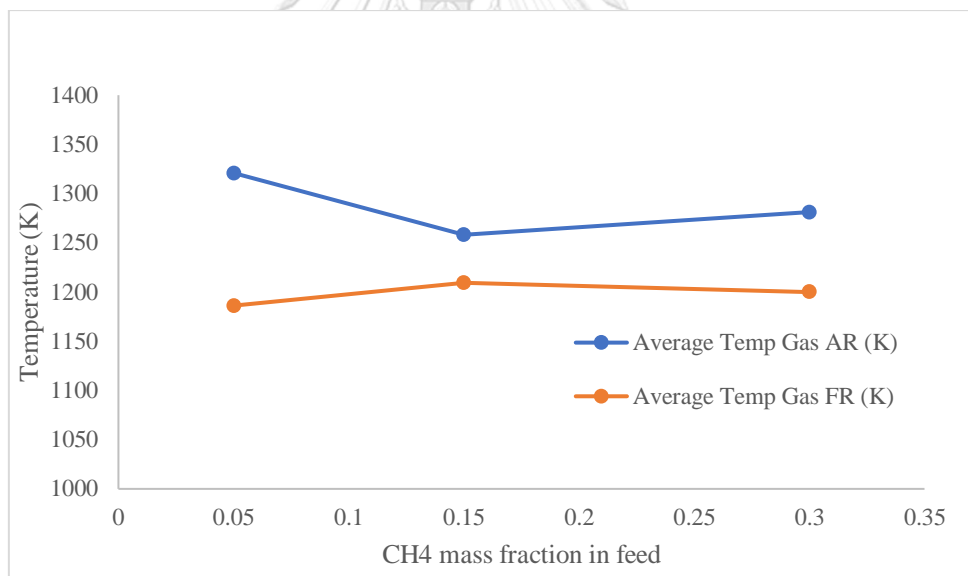
Fig. 5.23 The temperature of the air reactor and fuel reactor when CH$_4$ mass fraction in feed was adjusted

5.4.6 The size of the reactor

The result from the hydrodynamic investigation could be further calculated the reactor size, which it was useful in the next chapter. (Economic and emergy analysis) In calculating reactor size from the hydrodynamic investigation, the thermal energy was calculated from the converted CH$_4$, as shown in Eq. 5.4. The electrical energy

was calculated from the multiplication of the thermal efficiency and the thermal energy, as shown in Eq. 5.5. The thermal efficiency was set as 55%, which was obtained from chapter 4. Finally, the reactor size was calculated from the interpolation to 50 MW electrical, which was the power production capacity of chapter 6, as shown in Eq. 5.6. The result of the reactor size was shown in Table 5.6. It indicated that the high converted CH_4 provided high thermal energy, high electrical energy, small reactor size, and low reactor cost.

$$Thermal\ energy\ (MW\ thermal) = The\ converted\ CH_4 \left(\frac{mol}{s}\right) \times Heating\ value\ of\ CH_4 \left(\frac{MJ}{mol}\right)$$

(5.4)

$$Electrical\ energy\ (MW\ electrical) = \frac{Thermal\ efficiency\ (\%) \times Thermal\ energy\ (MW\ thermal)}{100}$$

(5.5)

$$Reactor\ size\ (m^3) = \frac{50\ (MW electrical) \times Volume\ of\ reactor\ from\ CFD\ simulation\ (m^3)}{Electrical\ energy\ (MW\ electrical)}$$

(5.6)

Table 5.6 The thermal energy, electrical energy, reactor size and the reactor cost

Case	Thermal energy (MW)	Electrical energy (MW)	Reactor size (m3)	Reactor cost ($)
1	0.359	0.198	70.45	1,587,419.73
2	0.253	0.139	100.22	1,961,339.07
3	0.967	0.532	26.18	876,596.77
4	0.603	0.332	41.98	1,163,628.82
5	0.615	0.338	41.16	1,149,855.58
6	0.594	0.327	42.60	1,173,857.22
8	0.634	0.349	39.92	1,128,999.15
7	0.273	0.150	92.80	1,872,871.93
9	0.661	0.364	38.29	1,101,167.55
10	0.588	0.324	43.024	1,180,866.646

5.4.7 Conclusion for the second part

The operating condition from chapter 4, pressure and Ni loading were used in this section. After that, the rate reaction, initial VOF, velocity and CH_4 mass fraction in feed were investigated to obtain suitable hydrodynamic behavior. This range of investigation, the high pre-exponential factor, low initial VOF, low velocity, and low CH_4 mass fraction in feed increased temperature and conversion. The result was validated with the experimental data. Accordingly, the operating condition from chapter 4 was reasonable. After that, the reactor size was calculated, which provided the reactor cost, as well. The cost of the reactor will be used in Chapter 6 for economic and emergy analysis

Chapter 6
The sustainability assessment of chemical looping combustion for power production

6.1 Research gaps

In a previous CLC study, the analysis of the best case of the CLC process was investigated only thermal efficiency and economic analysis. However, the study did not investigate whether those implementations would enhance the sustainability of the improved CLC processes. The significance of thermal efficiency to the sustainability of the CLC process had not been reported. In this study, the approach for CLC process improvement from the viewpoint of sustainability analysis was reported. There were 6 case studies in which different operation conditions and configurations were investigated. The best case of 3 viewpoints (thermal efficiency, economic analysis, and sustainability analysis) was investigated. The comparison among the 3-analysis types has not been performed before. Besides, this study revealed the results, comparing combustion types between CC and CLC, the effect of the CO_2 capture efficiency of the CC, and the effect of thermal efficiency on sustainability analysis. The interesting point was that which approach of the operating condition or process configuration of these case studies could provide high sustainability.

6.2 Objective

To perform an emergy analysis for sustainability assessment of the CLC process.

6.3 Results and discussion

6.3.1 Thermal efficiency result

The thermal efficiency indicates the efficient fuel usage for power production, as shown in Table 6.1. The high thermal efficiencies of case studies indicated that the used resources were effectively employed. Case 1, case 2, and case 3 were the power production unit from the natural gas combustion with post-combustion. The combustion section was the conventional combustion (CC). As mentioned earlier,

even though amine scrubbing was the mature process for CO_2 capture, the solid sorbent system was selected in this study because of its low cost and high efficiency for CO_2 capture. For case 1, it represents a typical power plant where there was no CO_2 capture section to treat the flue gas. Thus, the total produced power was the output of the plant. Consequently, the thermal efficiency of case 1 was the highest at 52.47%, and the result was comparable with the study of Kanniche et al. Their thermal efficiency of natural gas powerplant without a CO_2 capture system was 60%. The thermal efficiencies of case 2 and case 3 were lower than case 1, and their efficiencies were 47.48% and 50.22%, respectively. These results also coincided with Kanniche's work, which reported the thermal efficiency to be at 50% for the system with a CO_2 capture system. [7] In cases 2 and 3, the different CO_2 capture systems for post-combustion were set up. There were 6 and 3 stages for CO_2 capture adsorbers in case 2 and case 3, respectively. The CO_2 was not completely captured by the CC cases. However, the CO_2 was completely separated in the CLC cases. The CLC without a HAT cycle was performed in case 4. The thermal efficiency of case 4 was 39.58 %. Even though the thermal efficiency of case 4 was the lowest of all case studies, it was completely captured CO_2 from flue gas. Cases 5 and 6 were the CLC process with a HAT cycle, and they both had higher thermal efficiencies than case 4.

The HAT cycle improved the performance of the process by reducing the required work of the compressors and increasing the power production of the turbines. This study revealed that the HAT cycle could improve the thermal efficiency up to 13–16%, with the highest thermal efficiency (55.84%) in case 5 (Table 3). The heat exchangers in the HAT cycle for each multistage compressor reduced the workload of each compressor. At the same time, the cooling water was used in the HAT cycle to remove the heat from the compressed air and to produce steam, which was then used to increase the mass of the working fluid in the turbine. The operation of the air compressors in case 6 was different from those of other cases by employing the same compression ratio in all stages of the compressors.

On the contrary, the compression ratio of the last-stage compressor in cases 1, 2, 3, and 5 employed the highest ratio, which led to obtaining a high thermal efficiency system. The other difference in the operating conditions of case 5 and case 6 was the

amount of NiO loading. The higher loading of NiO on the Al_2O_3 in case 6 also led to obtaining higher thermal efficiency. In addition, case 6 had lower heat recovery units when comparing to case 5. The thermal efficiency of case 6 was slightly lower than case 5. In general, from the thermal efficiency result, case 5 would be the candidate process for implementation. From the early case of the CLC study with the HAT cycle, the thermal efficiency was 56.08%, which was higher than case 5. [49] The reason for lower thermal efficiency might come from the different heat recovery processes. The thermal efficiency of the CLC process with multistage turbine 55.9% in Brandvoll and Bolland study. [120] The thermal efficiency of the CLC process with STIG was 55.1% in Ishida and Jin. [68] Eventually, the rank of these case studies from the thermal efficiency viewpoint was 5, 6, 1, 3, 2, and 4, respectively.

Table 6.1 The thermal efficiencies for each case study.

Case	Description	Thermal efficiency (%)
1	CC and HAT without CO_2 capture	52.47
2	CC with HAT and 96.27% CO_2 capture	47.48
3	CC with HAT and 77.76% CO_2 capture	50.22
4	CLC without HAT	39.58
5	CLC with HAT high heat recovery	55.84
6	CLC with HAT low heat recovery	53.31

6.3.2 Economics analysis results

The economic analysis, which exhibited the profit of each case study, was shown in Table 6.2. Case 1 was the CC case without CO_2 capture. The payback period of case 1 was 6.82 y, and IRR was 13.51%. Case 2 and case 3 were operated to achieve 96.27% and 77.76% CO_2 removal, respectively. The payback period and IRR were 15.63 y with 4.42% for case 2 and 8.94 y with 9.86% for case 3. For case 1, the equipment and total capital costs were the lowest among all CC cases because there was no CO_2 capture section included. Therefore, the payback period was the shortest and the IRR was the highest. The profit of case 2 was lower than case 3 because the number of operation units in case 2 (25 units) was higher than case 3 (18 units), which were required to achieve the higher CO_2 capture efficiency. With this analysis, case 1

should be select for investment more than cases 2 and 3. On the other hand, this result would support the CO_2 emission to the environment without CO_2 treatment and increase the environmental loading. Accordingly, the carbon tax should be included in economic analysis for including the environmental impact.

However, if the carbon tax were included in the expenses, the payback period and IRR would be 11.44 y and 7.21% for case 1, 16.02 y, and 4.17 % for case 2 and 15.11 y and 4.77 % for case 3, respectively. It can be noted that the profit of CC cases was decreased, the payback period was extended, and IRR was decreased when the carbon tax was included. The profit of case 1 was significantly decreased because the untreated CO_2 from flue gas was taxed. The cost of electricity in this study was higher than in Hu's study. [121] Hu reported that the cost of electricity produced by natural gas combined cycle without CO_2 capture at 552.82 MW was 59.21 $/MWh while that with post-combustion CO2 capture at 467.25 MW was 87.51 $/MWh. In this study, the cost of electricity of case 1 (CC case without CO_2 capture) was 94.49 $/MWh. Those of case 2 (CC case with 96.27% CO_2 capture) and case 3 (CC case with 77.76% CO_2 capture) were 101.69 $/MWh and 99.53 $/MWh, respectively. The reason that the cost of the electricity in this study was higher than the cost of Hu's could be because the power plant capacity in this study was 10 times less than that in the case of Hu's.

The CLCs of natural gas were operated in cases 4–6. These cases were not taxed because it was assumed that no CO_2 was released to the environment when natural gas was employed in the CLC [122]. Besides, the fuel conversion was completely combusted when methane was used as a fuel. [48] However, when coal was used as fuel, CO_2 was found from the air reactor due to the incomplete combustion [97]. In CLC cases, the payback period and IRR were 5.73 y with 16.35 % for case 4, 6.16 y with 15.11% for case 5, and 4.60 y with 20.69 % for case 6, respectively. Case 6 showed the fastest payback period and the highest IRR among all case studies. The payback period and IRR of case 4 were slightly better than case 5 because the capital cost and operating cost of case 4 was lower than case 5, even though the thermal efficiency of case 5 was higher than case 4. Case 4 was the only case study that was not applied the HAT cycle and its thermal efficiency was low. Thus, the size of unit

operations in case 4 was increased for obtaining the same net power output at 50 MW. The IRR of case 4 was slightly higher than case 5. Case 5 had a high number of heat recovery units, which increased the heat recovery from the gas outlet of the turbine. The high number of unit operations in case 5 led to the high investment costs and low profit. Besides, the compression operation of cases 1, 2, 3, and 5 led to the large size and high investment cost of compressors. The equipment cost of other cases was higher than case 6. Thus, case 6 achieved the highest IRR and the shortest payback period among all case studies. Nevertheless, the economic analysis of CLC cases in this study was better than that previously reported for the CLC using Ni as an O_2 carrier in a 100 MW power production [108]. Their study concluded that the payback period and IRR of the process were 10.3 y and 16.71%, respectively [108]. The profit of cases 6 was higher because the HAT cycle was installed in this study.

From the economic perspective, case 6 was the best choice because it obtained the shortest payback period and the highest IRR, and case 1 was the second-best choice when the carbon tax was not included in the analysis. However, the inclusion of carbon tax in the plant expenses reduced the economic performance of the plant. The profit of case 1 was significantly reduced because the CO_2 emission, in this case, was the highest due to no installation of the carbon capture process. The installation of the CO_2 capture process of the CC cases was the reason for the decrease of IRR and the extension of the payback period. The CO_2 emission from case 2 and case 3 were 3.73% and 22.24%, respectively, while the CO_2 emission of CLC cases (case 4, case 5, and case 6) was almost none. Since the environmental burden should be considered in all cases, the economic analysis must include the cost of environmental damage or a carbon tax. Thus, the carbon tax would be included in both the economic and emergy analyses to allow a fair comparison between processes with different CO_2 removal capabilities. The rank of all cases from an economic viewpoint, for both carbon tax and no carbon tax considerations, was the same at 6, 4, 5, 1, 3, and 2, respectively.

Table 6.2 Economic analysis of all cases.

Case		Not include the carbon tax		Include carbon tax		Cost of electricity ($/MWh)
		Payback period (y)	IRR (%)	Payback period (y)	IRR (%)	
1	CC and HAT without CO_2 capture	6.82	13.51	11.44	7.21	94.49
2	CC with HAT and 96.27% CO_2 capture	15.63	4.42	16.02	4.17	101.69
3	CC with HAT and 77.76% CO_2 capture	8.94	9.86	15.11	4.77	99.53
4	CLC without HAT	5.73	16.35	5.73	16.35	69.83
5	CLC with HAT high heat recovery	6.16	15.11	6.16	15.11	71.37
6	CLC with HAT low heat recovery	4.60	20.69	4.60	20.69	61.94

6.3.3 The emergy analysis results

All of the resources were included in the calculation. It was classified into 3 parameters; F, N and R. The 3 parameters were the local nonrenewable resource (N), the local renewable resource (R), and the external goods or the expense cost (F). The three parameters were exhibited in Table 6.3. The parameters would be calculated to be emergy indicators, unit emergy values (UEV), environmental loading ratio (ELR), emergy yield ratio (EYR), and emergy sustainability index (ESI), as shown in Table 6.4.

Table 6.3 The F, L, and R of each case study.

Case	Process description	F (sej/Y)	R (sej/Y)	N (sej/Y)	Total
1	CC and HAT without CO_2 capture	6.01E+19	3.08E+19	4.21E+20	5.12E+20
2	CC with HAT and 96.27% CO_2 capture	6.46E+19	3.43E+19	4.65E+20	5.64E+20
3	CC with HAT and 77.76% CO_2 capture	6.33E+19	3.23E+19	4.40E+20	5.35E+20
4	CLC without HAT	4.40E+19	3.47E+19	5.58E+20	6.37E+20
5	CLC with HAT high heat recovery	4.52E+19	2.46E+19	3.95E+20	4.65E+20
6	CLC with HAT low heat recovery	3.91E+19	2.58E+19	4.14E+20	4.79E+20

Where F = Purchase resource, R = Local renewable resources, and N = Local nonrenewable resources

Table 6.4 Emergy indicators of each case study.

Case	Process description	UEVs	EYR	ELR	ESI
1	CC and HAT without CO_2 capture	3.24E+05	8.513	15.615	0.545
2	CC with HAT and 96.27% CO_2 capture	3.58E+05	8.724	15.433	0.565
3	CC with HAT and 77.76% CO_2 capture	3.39E+05	8.454	15.569	0.543
4	CLC without HAT	4.04E+05	14.490	17.363	0.835
5	CLC with HAT high heat recovery	2.95E+05	10.280	17.933	0.573
6	CLC with HAT low heat recovery	3.04E+05	12.236	17.577	0.696

6.3.3.1 Case 1: CC with HAT and without CO_2 capture

Case 1 was the CC with a HAT cycle and without the CO_2 capture process. When CO_2 capture was not applied, the CO_2 capture efficiency was 0% . The investment cost, manufacturing, and service cost were the lowest of the CC case. The carbon tax of this case was the highest among the CC cases because of untreated CO_2. The purchase resource, F, was the lowest of the CC cases, as shown in Table. 6.3. Even though the carbon tax was the highest, the investment and manufacturing cost of this case was lower than cases 2 and 3, as shown in Table 6.5. Natural gas was counted in nonrenewable resources, N. N of case 1 was low because of its high thermal efficiency. O_2 consumption in the air was also low, followed the natural gas for complete combustion. Water consumption was also low because it was not supplied to the CO_2 capture section. O_2 and water were counted as local renewable resources, R. R of case 1 was the lowest of the CC cases. The total emergy flow of case 1 was the lowest among the CC cases. Accordingly, UEV of this case was the lowest of the CC cases, which indicated that it consumed low solar energy for producing 1 J of electricity, as shown in Table 6.4. However, the high F led to the low EYR and the high ELR of CC cases.

6.3.3.2 Cases 2 and 3: CC with HAT and a CO_2 capture of 96.27% (case 2) and 77.76% (case 3)

Cases 2 and 3 were the CC with HAT and CO_2 capture systems. CO_2 in the flue gas was removed at 96.27% and 77.76% for cases 2 and 3, respectively. The solid adsorber was used in the CO_2 capture process. The emergy flows of solid metal in cases 2 and 3 was not high because it had a low cost, as shown in Tables 6.6 and 6.7. The CO_2 capture section of cases 2 and 3 led to high investment, manufacturing, and service costs, in which these costs were higher than case 1. Especially, the cost of case 2 was the highest of all case studies. The purchase resources, F, of cases 2 and 3, was high. The F was the highest in case 2, as shown in Table. 6.3. Natural gas was supplied to case 2 higher than case 3 because the thermal efficiency of case 2 was lower than case 3. Thus, the local nonrenewable resources, N, of case 2 was also higher than case 3 and were the highest of the CC cases, as well. O_2 consumption was higher in case 2 and it was higher than case 3 for complete combustion with natural

gas. Subsequently, water was also higher used in case 2 than in case 3 because the amount of flue gas in case 2 was higher than that in case 3. Since O_2 and water were local resources, they were counted as R. Therefore, the R of case 2 was higher than case 3. The total emergy flow of case 2 was the highest of all case studies. As shown in Table 6.4, the UEV of case 2 was also the highest among the CC cases due to the highest investment and manufacturing cost. The highest R led to the highest EYR and lowest ELR of case 2. Finally, the ESI of case 2 was the highest of all the CC cases. This result supported that power plants with CO_2 capture process provided higher sustainability than those without CO_2 capture process. Also, the high CO_2 capture efficiency increased the sustainability of the process.

6.3.3.3 Case 4 CLC without HAT cycle

Case 4 was a CLC process without a HAT cycle. CO_2 produced by natural gas combustion in the CLC process was completely captured and separated [122]. The carbon tax of the CLC was zero. The investment, manufacturing, and service costs were high, as shown in Table 6.8. In case 4, the costs of oxygen carrier and metal oxide support were the highest among the CLC cases and it was also the highest cost of solid materials in all case studies. It led to a high F even though the HAT cycle was not applied. The demand for natural gas was the highest among all case studies. Thus, N of this case was also the highest, as shown in Table 6.3. The water usage in the condensation section was the highest because of the high mass flow rate of flue gas. The process also consumed the highest O_2 for the complete combustion.

Consequently, the R of this case was the highest. This case study required all resources to produce equal power capacity to other cases because it was the lowest thermal efficiency. Because of the highest required resources, the total emergy flow and the UEV of this case were the highest, as shown in Table 6.4. The highest R led to the highest EYR and the highest of ESI among the CLC cases. From the sustainability aspect, this case was the best case among the CLC processes.

6.3.3.4 Case 5 CLC with HAT and high heat recovery

Case 5 was the CLC process with a HAT cycle and a high heat recovery system. The investment, manufacturing, and service costs were the highest of all CLC

cases because of the high number of unit operations, leading to the highest F of all CLC cases, as shown in Table 6.3. This case utilized the lowest oxygen carrier and metal oxide support because less natural gas was consumed since the process had high thermal efficiency. Therefore, N of this case was the lowest. O_2 in air consumed in the process was also the lowest among all case studies, as shown in Table 6.9.

Consequently, the R of this case was the lowest. The total emergy flow was the lowest; thereby, the UEV was the lowest, as shown in Table 6.4. It indicated that this case used the lowest solar energy for producing electricity. However, the highest F and the lowest R of this CLC case led to the lowest EYR and the highest ELR of the CLC cases, representing the low sustainability of the process and high environmental loading. Consequently, the ESI of this case was the lowest of the CLC cases.

6.3.3.5 Case 6 CLC with HAT and low heat recovery

Case 6 was the CLC process with a HAT cycle and a low heat recovery system. The oxygen carrier was slightly higher than case 5, but the metal oxide supporter was extremely lower than case 5 because the Ni loading of case 6 was higher than case 5, as shown in Tables 6.9 and 6.10. The investment, manufacturing, and service costs were the lowest of all case studies because of the different compression operation methods. Accordingly, F of case 6 was the lowest of all case studies, as shown in Table 6.3. The natural gas consumption was slightly higher than case 5 because of its lower thermal efficiency. N of this case was higher than case 5 but was lower than case 4. More O_2 in the air was consumed to complete the combustion with natural gas. Therefore, O_2 in air and R of this case would be higher than case 5 but lower than case 4. The low investment, manufacturing, and service costs led to lower total emergy flow. The UEV of this case was low and was slightly higher than case 5, because of the lower purchased resources, as shown in Table 6.4.

6.3.3.6 The conclusion on emergy analysis

The UEVs of all six case studies were higher than those previously reported for a geothermal power plant, 2.18E+05 (sej/J), coal power plant, 1.63E+05 (sej/J), wind power plant, 1.74E+04 (sej/J), and hydropower plant, 5.04E+04 (sej/J) [123]. For the CC cases, the UEV of case 1 (3.24E+05 sej/J) was the lowest even though the

carbon tax was included. The UEV of case 2 (3.58E+05 sej/J) was slightly higher than case 3 (3.39E+05 sej/J), which reflects the higher solid sorbent, support, investment, and operating costs of case 2, but the carbon tax of case 3 (3.40E+18 sej/y) was some 5.5 times higher than case 2. Eventually, the total emergy of case 2 was still higher than case 3 for producing the same amount of electricity. For the CLC cases, the UEV of case 5 was the best because the thermal efficiency of case 5 (2.95E+05 sej/J) was the highest. The UEV of the CLC was lower than CC cases because the carbon tax effect was included in the CC cases, except case 4 (4.04E+05 sej/J). The UEV of case 4 was higher than CC cases because the demand for natural gas of case 4 was the highest among all case studies. The UEV of case 6 (3.04E+05 sej/J) was slightly higher than case 5 because the demand for natural gas of case 6 was higher than case 5.

For EYR, ELR and ESI comparison, N, F, and R of CC cases were higher than CLC cases. The low value of F in CLC cases was the reason for obtaining high EYR, which indicated the high stability of the process. Accordingly, the stability of CLC cases was higher than in CC cases. The emergy flow of oxygen carrier (NiO) in CLC cases was higher than solid sorbent (Na_2CO_3). The emergy flow of solid was included in F. Therefore, the %F was high and %R was low in CLC cases. The high value of %R in CC cases was the reason for obtaining low ELR, which indicated the low loading to the environment. The analysis showed that the environmental loading in the case of CLC cases was higher than those of CC cases. Eventually, the sustainability of the process has to consider both the process yield and the environmental loading and the ESI is an indicator which is the ratio between EYR and ELR. It was found that the ESI of the CLC cases were higher than those of CC cases. It shows that the CLC cases were more sustainable than the CC cases. The rank of the ESI of all case studies was 4, 6, 5, 2, 1, and 3, respectively.

Table 6.5 Case 1 (CC and HAT without CO_2 capture)

Note	Amount	Unit	UEVs (sej/unit)	Emergy flow (sej/y)	% Emergy
Purchase Resources (F)					
Na_2CO_3	0.00E+00	$/y	1.73E+12	0.00E+00	0.00
Al_2O_3	0.00E+00	$/y	1.73E+12	0.00E+00	0.00
Investment cost	4.56E+06	$/y	1.73E+12	7.89E+18	1.54
Manufacturing and service cost	2.17E+07	$/y	1.73E+12	3.76E+19	7.35
Carbon tax	8.46E+06	$/y	1.73E+12	1.46E+19	2.86
Local Renewable Resources (R)					
Water	5.08E+06	kg/y	6.64E+08	3.37E+15	0.00
O_2 in air	5.97E+08	kg/y	5.16E+10	3.08E+19	6.02
Local Nonrenewable Resources (N)					
Natural gas	3.01E+15	J/y	1.40E+05	4.21E+20	82.23
			Total emergy	**5.12E+20**	
Product					
Electricity	1.58E+15	J/y	**3.24E+05**		

1) Natural gas (J/y) = Mass flow rate (7,176.02 kg/h) x Heat value (47.81 x 10^6 J/kg) x (8,760 h/y) = 3.01 x 10^{15} (J/y)

2) N_{NP} = Total unit of compressor, tower, heat exchanger and reactor = 9 (unit)

   N_{OL} = Number of operators per shift = $(6.29 + 31.7P^2 + 0.23N_{NP})^{0.5}$ = 6.33 (persons/shift)

   P = Number of solid process = 1

   3.5 shifts/d

   Total number of labors (persons) = Shifts per day x N_{OL} = 3.5 x 45.18 (persons/shift) = 23 (persons)

   Cost of operating labor cost ($/person/y) = 12,775 ($/person/y)

   Total labor cost = Cost of operating labor cost x Total number of labors = 12,775 ($/person/y) x 23 = 293,825.00 ($/y)

3) Manufacturing and service cost ($/y) = 0.18(Fixed capital investment cost) + 2.735(Labor cost) = 0.18 x (116,230,649.11 $/y) + 2.735 x (293,825.00 $/y) = 21,725,128.21 $

   Fixed capital investment cost = Equipment cost /0.2235 = 25,973,329.41/0.2235 = 116,230,649.11 $

4) Investment cost ($/y) = Total equipment cost (136,741,940.13 $)/Plant lifetime (30 y)

   Carbon tax ($/y) = 49 ($/ton CO_2 emission) x 172,656.12 (ton/y)

5) Mass flow of water (kg/y) = Total mass flow rate/y + Make up water/y = 5,075,994.77 (kg/y)

   Make up water (kg/y) = 20% of Total mass flow rate

6) Global EMR = 1.73 x 10^{12} sej/$ [16]

7) UEV of water and O_2 in air.[85]

8) UEV of natural gas.[124]

Table 6.6 Case 2 (CC with HAT and 96.27% CO_2 capture)

Note	Amount	Unit	UEVs (sej/unit)	Emergy flow (sej/y)	% Emergy
Purchase Resources (F)					
Na_2CO_3	4.31E+04	$/y	1.73E+12	7.46E+16	0.01
Al_2O_3	3.51E+05	$/y	1.73E+12	6.07E+17	0.11
Investment cost	5.56E+06	$/y	1.73E+12	9.61E+18	1.70
Manufacturing and service cost	3.11E+07	$/y	1.73E+12	5.37E+19	9.53
Carbon tax	3.53E+05	$/y	1.73E+12	6.11E+17	0.11
Local Renewable Resources (R)					
Water	4.37E+08	kg/y	6.64E+08	2.90E+17	0.05
O_2 in air	6.59E+08	kg/y	5.16E+10	3.40E+19	6.03
Local Nonrenewable Resources (N)					
Natural gas	3.32E+15	J/y	1.40E+05	4.65E+20	82.45
			Total emergy	**5.64E+20**	
Product					
Electricity	1.58E+15	J/y	**3.58E+05**		

1) Natural gas (J/y) = Mass flow rate (7,929.79 kg/h) x Heat value (47.81 x 10^6 J/kg) x (8,760 h/y) = 3.32 x 10^{15} (J/y)

2) N_{NP} = Total unit of compressor, tower, heat exchanger and reactor = 25 (unit)
   N_{OL} = Number of operators per shift = $(6.29 + 31.7P^2 + 0.23N_{NP})^{0.5}$ = 45.18 (persons/shift)
   P = Number of solid process = 8
   3.5 shifts/d
   Total number of labors (persons) = Shifts per day x N_{OL} = 3.5 x 45.18 (persons/shift) = 159 (persons)
   Cost of operating labor cost ($/person/y) = 12,775 ($/person/y)
   Total labor cost = Cost of operating labor cost x Total number of labors = 12,775 ($/person/y) x 159 = 2,031,225.00 ($/y)

3) Manufacturing and service cost ($/y) = 0.18(Fixed capital investment cost) + 2.735(Labor cost) = 0.18 x (141,680,024.44 $/y) + 2.735 x (2,031,225.00 $/y) = 31,057,804.77 $
   Fixed capital investment cost = Equipment cost /0.2235 = 31,660,340.66/0.2235 = 141,680,024.44 $

4) Investment cost ($/y) = Total equipment cost (166,682,381.69 $)/Plant lifetime (30 y)
   Carbon tax ($/y) = 49 ($/ton CO_2 emission) x 7,212.04 (ton/y)

5) Mass of Na_2CO_3 (kg) = (Solid metal inventory 700 kg/y/MW thermal) [108] x (MW thermal of case study) x Batch of solid = 700 kg/y x 105.32 MW thermal x 1.95 = 143,755.41 kg/y
   MW thermal of case study = 50 MW power/thermal efficiency (%) x 100 = 50 MW power / 47.48 x 100 = 105.32 MW thermal
   Lifetime of solid particles 4,500 h
   Batch of solid = 8750 h/ Lifetime of solid particle (4500 h) = 1.95

6) Mass flow rate of Al_2O_3 (kg/y) = Mass flow rate of Na_2CO_3 / (%Mass loading of Na_2CO_3) x (100 - %Mass loading of Na_2CO_3) = (143,755.41 kg/y) / (17) x (100 - 17) x 100 = 701,864.65 kg/y
   % Mass loading of Na_2CO_3 = 17%

7) Mass flow of water (kg/y) = Total mass flow rate/y + Make up water/y = 436,632,711.17 (kg/y)
   Make up water (kg/y) = 20% of Total mass flow rate

8) Cost of Na_2CO_3 = 0.3 $/kg

9) Cost of Al_2O_3 = 0.5 $/kg

Table 6.7 Case 3 (CC with HAT and 77.76% CO_2 capture)

Note	Amount	Unit	UEVs (sej/unit)	Emergy flow (sej/y)	% Emergy
Purchase Resources (F)					
Na_2CO_3	4.08E+04	$/y	1.73E+12	7.05E+16	0.01
Al_2O_3	3.32E+05	$/y	1.73E+12	5.74E+17	0.11
Investment cost	5.50E+06	$/y	1.73E+12	9.52E+18	1.78
Manufacturing and service cost	2.88E+07	$/y	1.73E+12	4.97E+19	9.29
Carbon tax	1.97E+06	$/y	1.73E+12	3.40E+18	0.64
Local Renewable Resources (R)					
Water	1.98E+08	kg/y	6.64E+08	1.32E+17	0.02
O_2 in air	6.23E+08	kg/y	5.16E+10	3.22E+19	6.01
Local Nonrenewable Resources (N)					
Natural gas	3.14E+15	J/y	1.40E+05	4.40E+20	82.14
			Total emergy	**5.35E+20**	
Product					
Electricity	1.58E+15	J/y	**3.39E+05**		

1) Natural gas (J/y) = Mass flow rate (7,496.76 kg/hr) x Heat value (47.81 x 10^6 J/kg) x (8,760 hr/y) = 3.14 x 10^{15} (J/y)

2) N_{NP} = Total unit of compressor, tower, heat exchanger and reactor = 18 (unit)
   N_{OL} = Number of operators per shift = $(6.29 + 31.7P^2 + 0.23N_{NP})^{0.5}$ = 28.34 (persons/shift)
   P = Number of solid process = 5
   3.5 shifts/d
   Total number of labors (persons) = Shifts per day x N_{OL} = 3.5 x 11.75 (persons/shift) = 100 (persons)
   Cost of operating labor cost ($/person/y) = 12,775 ($/person/y)
   Total labor cost = Cost of operating labor x Total number of labors = 12,775 ($/person/y) x 18 = 1,277,500.00 ($/y)

3) Manufacturing and service cost ($/y) = 0.18(Fixed capital investment cost) + 2.735(Labor cost) = 0.18 x (140,316,307.71 $/y) + 2.735 x (1,277,500.00 $/y) = 28,750,897.89 $
   Fixed capital investment cost = Equipment cost /0.2235 = 31,355,599.49/0.2235 = 140,316,307.71 $

4) Investment cost ($/y) = Total equipment cost (165,078,009.07 $)/Plant lifetime (30 y)
   Carbon tax ($/y) = 49 ($/ton CO_2 emission) x 40,115.23 (ton/y)

5) Mass of Na_2CO_3 (kg) = (Solid metal inventory 700 kg/y/MW thermal) [108] x (MW thermal of case study) x Batch of solid = 700 kg/y x 99.57 MW thermal x 1.95 = 135,914.03 kg/y
   MW thermal of case study = 50 MW power/thermal efficiency (%) x 100 = 50 MW power / 50.22 x 100 = 99.57 MW thermal
   Lifetime of solid particles 4,500 h
   Batch of solid = 8750 h/Lifetime of solid particle (4500 h) = 1.95

6) Mass flow rate of Al_2O_3 (kg/y) = Mass flow rate of Na_2CO_3 / (%Mass loading of Na_2CO_3) x (100 - %Mass loading of Na_2CO_3) = (135,914.03 kg/y) / (17) x (100 - 17) x 100 = 663,580.24 kg/y
   %Mass loading of Na_2CO_3 = 17%

7) Mass flow of water (kg/y) = Total mass flow rate/y + Make up water/y = 198,081,277.44 (kg/y)
   Make up water (kg/y) = 20% of Total mass flow rate

8) Cost of Na_2CO_3 = 0.3 $/kg

9) Cost of Al_2O_3 = 0.5 $/kg

Table 6.8 Case 4 (CLC without HAT)

Note	Amount	Unit	UEVs (sej/unit)	Emergy flow (sej/y)	% Emergy
Purchase Resources (F)					
Ni	2.28E+06	$/y	1.73E+12	3.94E+18	0.62
Al_2O_3	4.53E+05	$/y	1.73E+12	7.83E+17	0.12
Investment cost	3.80E+06	$/y	1.73E+12	6.58E+18	1.03
Manufacturing and service cost	1.89E+07	$/y	1.73E+12	3.27E+19	5.13
Carbon tax	0.00E+00	$/y	1.73E+12	0.00E+00	0.00
Local Renewable Resources (R)					
Water	2.64E+08	kg/y	6.64E+08	1.75E+17	0.03
O_2 in air	6.69E+08	kg/y	5.16E+10	3.45E+19	5.42
Local Nonrenewable Resources (N)					5.45
Natural gas	3.99E+15	J/y	1.40E+05	5.58E+20	87.65
			Total emergy	**6.37E+20**	
Product					
Electricity	1.58E+15	J/y	**4.04E+05**		

1) Natural gas (J/y) = Mass flow rate (9,521.18 kg/h) x Heat value (47.81 x 10^6 J/kg) x (8,760 hr/y) = 3.99E+15 (J/y)

2) N_{NP} = Total unit of compressor, tower, heat exchanger and reactor = 13 (unit)

   N_{OL} = Number of operators per shift = $(6.29 + 31.7P^2 + 0.23N_{NP})^{0.5}$ = 11.67 (persons/shift)

   P = Number of solid process = 2

   3.5 shifts/d

   Total number of labors (persons) = Shifts per day x N_{OL} = 3.5 x 11.71 (persons/shift) = 41 (persons)

   Cost of operating labor cost ($/person/year) = 12,775 ($/person/y)

   Total labor cost = Cost of operating labor cost x Total number of labors = 12,775 ($/person/y) x 41 = 523,775.00 ($/y)

3) Manufacturing and service cost ($/y) = 0.18(Fixed capital investment cost) + 2.735(Labor cost) = 0.18 x (96,915,222.38 $/y) + 2.735 x (523,775.00 $/y) = 18,877,264.65 $

   Fixed capital investment cost = Equipment cost /0.2235 = 21,657,032.93/0.2235 = 96,915,222.38 $

4) Investment cost ($/y) = Total equipment cost (114,017,908.69 $)/Plant lifetime (30 y)

5) Mass of Ni (kg) = (Solid metal inventory 700 kg/y/MW thermal) [108] x (MW thermal of case study) x Batch of solid = 700 kg/y x 126.34 MW thermal x 1.95 = 172,449.53 kg/y

   MW thermal of case study = 50 MW power/thermal efficiency (%) x 100 = 50 MW power / 39.58 x 100 = 126.34 MW thermal

   Lifetime of solid particles 4,500 h

   Batch of solid = 8750 h/ Lifetime of solid particle (4500 h) = 1.95

6) Mass flow rate of Al_2O_3 (kg/y) = Mass flow rate of Ni / (%Mass loading of Ni) x (100 - %Mass loading of Ni) = (172,449.53 kg/y) / (16) x (100 - 16) x 100 = 905,360.03 kg/y

   %Mass loading of Ni = 16%

7) Mass flow of water (kg/y) = Total mass flow rate/y + Make up water/y = 263,979,886.59 (kg/y)

   Make up water (kg/y) = 20% of Total mass flow rate

8) Cost of Ni = 13.2 $/kg

9) Cost of Al_2O_3 = 0.5 $/kg

Table 6.9 Case 5 (CLC with HAT high heat recovery)

Note	Amount	Unit	UEVs (sej/unit)	Emergy flow (sej/y)	% Emergy
Purchase Resources (F)					
Ni	1.61E+06	$/y	1.73E+12	2.79E+18	0.60
Al_2O_3	3.21E+05	$/y	1.73E+12	5.55E+17	0.12
Investment cost	4.07E+06	$/y	1.73E+12	7.04E+18	1.51
Manufacturing and service cost	2.02E+07	$/y	1.73E+12	3.49E+19	7.49
Carbon tax	0.00E+00	$/y	1.73E+12	0.00E+00	0.00
Local Renewable Resources (R)					
Water	1.98E+08	kg/y	6.64E+08	1.32E+17	0.03
O_2 in air	4.74E+08	kg/y	5.16E+10	2.44E+19	5.25
Local Nonrenewable Resources (N)					
Natural gas	2.82E+15	J/y	1.40E+05	3.95E+20	84.99
			Total emergy	**4.65E+20**	
Product					
Electricity	1.58E+15	J/y	**2.95E+05**		

1) Natural gas (J/y) = Mass flow rate (6,742.20 kg/h) x Heat value (47.81 x 10^6 J/kg) x (8,760 h/y) = 2.82 x 10^{15} (J/y)

2) N_{NP} = Total unit of compressor, tower, heat exchanger and reactor = 22 (unit)
   N_{OL} = Number of operators per shift = $(6.29 + 31.7P^2 + 0.23N_{NP})^{0.5}$ = 11.75 (persons/shift)
   P = Number of solid process = 2
   3.5 shifts/d
   Total number of labors (persons) = Shifts/d x N_{OL} = 3.5 x 11.75 (persons/shift) = 42 (persons)
   Cost of operating labor cost ($/person/y) = 12,775 ($/person/y)
   Total labor cost = Cost of operating labor cost x Total number of labors = 12,775 ($/person/y) x 42 = 536,550.00 ($/y)

3) Manufacturing and service cost ($/y) = 0.18(Fixed capital investment cost) + 2.735(Labor cost) = 0.18 x (103,794,020.84 $/y) + 2.735 x (536,550.00 $/y) = 20,150,388.00 $
   Fixed capital investment cost = Equipment cost /0.2235 = 23,194,194.60/0.2235 = 103,794,020.84 $

4) Investment cost ($/y) = Total equipment cost (122,110,612.75 $)/Plant lifetime (30 y)

5) Mass of Ni (kg) = (Solid metal inventory 700 kg/y/MW thermal) [108] x (MW thermal of case study) x Batch of solid = 700 kg/y x 89.55 MW thermal x 1.95 = 122,234.08 kg/y
   MW thermal of case study = 50 MW power/thermal efficiency (%) x 100 = 50 MW power / 55.84 x 100 = 89.55 MW thermal
   Lifetime of solid particles 4,500 h
   Batch of solid = 8750 h/ Lifetime of solid particle (4500 h) = 1.95

6) Mass flow rate of Al_2O_3 (kg/y) = Mass flow rate of Ni / (%Mass loading of Ni) x (100 - %Mass loading of Ni) = (122,234.08 kg/y) / (16) x (100 - 16) x 100 = 641,728.91 kg/y
   %Mass loading of Ni = 16%

7) Mass flow of water (kg/y) = Total mass flow rate/y + Make up water/y = 198,272,179.10 (kg/y)
   Make up water (kg/y) = 20% of Total mass flow rate

8) Cost of Ni = 13.2 $/kg

9) Cost of Al_2O_3 = 0.5 $/kg

Table 6.10 Case 6 (CLC with HAT low heat recovery)

Note	Amount	Unit	UEVs (sej/unit)	Emergy flow (sej/y)	% Emergy
Purchase Resources (F)					
Ni	1.69E+06	$/y	1.73E+12	2.92E+18	0.61
Al_2O_3	1.67E+05	$/y	1.73E+12	2.89E+17	0.06
Investment cost	3.45E+06	$/y	1.73E+12	5.97E+18	1.25
Manufacturing and service cost	1.73E+07	$/y	1.73E+12	3.00E+19	6.25
Carbon tax	0.00E+00	$/y	1.73E+12	0.00E+00	0.00
Local Renewable Resources (R)					
Water	1.92E+08	kg/y	6.64E+08	1.28E+17	0.03
O_2 in air	4.97E+08	kg/y	5.16E+10	2.57E+19	5.36
Local Nonrenewable Resources (N)					
Natural gas	2.96E+15	J/y	1.40E+05	4.14E+20	86.44
			Total emergy	**4.79E+20**	
Product					
Electricity	1.58E+15	J/y	**3.04E+05**		

1) Natural gas (J/y) = Mass flow rate (7,060.57 kg/h) x Heat value (47.81 x 10^6 J/kg) x (8,760 h/y) = 2.96 x 10^{15} (J/y)

2) N_{NP} = Total unit of compressor, tower, heat exchanger and reactor = 18 (unit)
   N_{OL} = Number of operators per shift = $(6.29 + 31.7P^2 + 0.23N_{NP})^{0.5}$ = 11.71 (persons/shift)
   P = Number of solid process = 2
   3.5 shifts/d
   Total number of labors (persons) = Shifts/d x N_{OL} = 3.5 x 11.71 (persons/shift) = 42 (persons)
   Cost of operating labor cost ($/person/y) = 12,775 ($/person/y)
   Total labor cost = Cost of operating labor cost x Total number of labors = 12,775 ($/person/y) x 42 = 536,550.00 ($/y)

3) Manufacturing and service cost ($/y) = 0.18(Fixed capital investment cost) + 2.735(Labor cost) = 0.18 x (88,040,626.92 $/y) + 2.735 x (536,550.00 $/y) = 17,314,777.10 $
   Fixed capital investment cost = Equipment cost /0.2235 = 19,673,883.11/0.2235 = 88,040,626.92 $

4) Investment cost ($/y) = Total equipment cost (103,577,208.14 $)/Plant lifetime (30 y)

5) Mass of Ni (kg) = (Solid metal inventory 700 kg/y/MW thermal) [108] x (MW thermal of case study) x Batch of solid = 700 kg/y x 93.78 MW thermal x 1.95 = 128,006.92 kg/y
   MW thermal of case study = 50 MW power/thermal efficiency (%) x 100 = 50 MW power / 53.32 x 100 = 93.78 MW thermal
   Lifetime of solid particles 4,500 h
   Batch of solid = 8750 h/Lifetime of solid particle (4500 h) = 1.95

6) Mass flow rate of Al_2O_3 (kg/y) = Mass flow rate of Ni / (%Mass loading of Ni) x (100 - %Mass loading of Ni) = (128,006.92 kg/y) / (27.7) x (100 – 27.7) x 100 = 334,111.93 kg/y
   %Mass loading of Ni = 27.7%

7) Mass flow of water (kg/y) = Total mass flow rate/y + Make up water/y = 192,294,365.62 (kg/y)
   Make up water (kg/y) = 20% of Total mass flow rate

8) Cost of Ni = 13.2 $/kg

9) Cost of Al_2O_3 = 0.5 $/kg
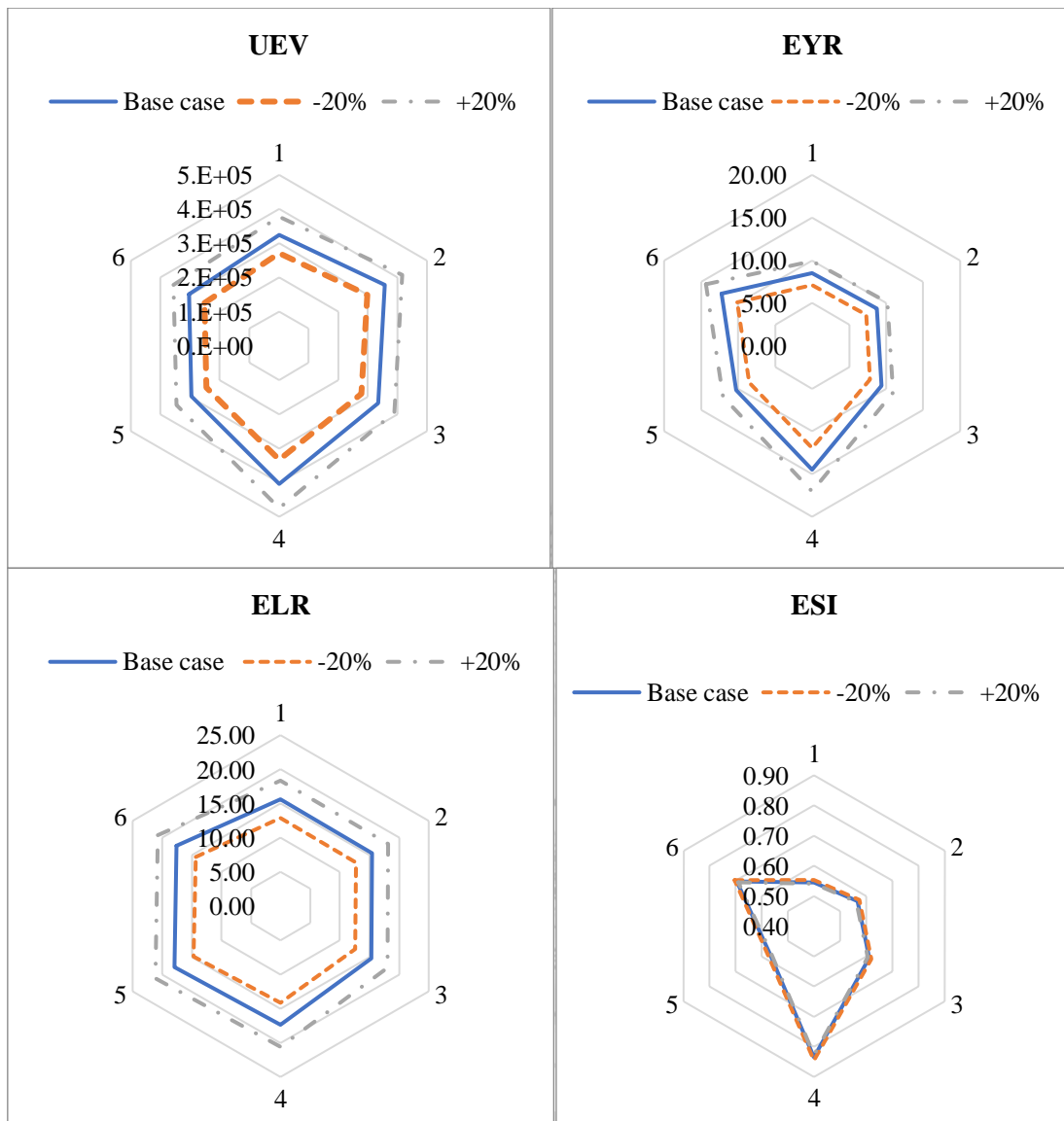
Fig. 6.1 The sensitivity of natural gas to EYR, ELR, ESI and UEV.

6.3.3.7 The sensitivity of emergy analysis.

The high value of ESI could be obtained by decreasing the ELR or increasing the EYR. From Tables 6.5 to 6.10 the emergy of natural gas was the largest fraction of the total emergy in all cases. Subsequently, the variation of natural gas emergy would highly affect the sustainability assessment of these processes. Natural gas was the only component of N. The increase of natural gas would reduce the ESI since it increased the ELR higher than the EYR. The UEV was another significant parameter of the emergy analysis that was used for comparing process performance. The UEVs in Fig. 12 were calculated from the total emergy flow divided by the emergy of power

production. The increase of natural gas's emergy would increase total emergy, which was the cause of increasing UEV of power production. On the other hand, the decrease in natural gas emergy would decrease the UEV. The 20% variation of natural gas emergy gave the UEV in the range of 2.51E+05 and 4.75E+05 sej/J, which was close to the UEV of power production in other studies ($8.05E+04$ sej/J) [125]. Subsequently, ESI for each case study was in the range of 0.55 and 0.84. The 20% variation of natural gas emergy value did not change the rank of sustainability of all the case studies when compared with the base case. This sensitivity confirmed that the result from the emergy analysis was reliable comparing to other studies [123, 126-128].

From the result of the reactor cost calculation in chapter 5, the cost of the reactor which calculated from the hydrodynamics investigation was increased from \$ 1.0eE+5 – 4.2E+5 to be \$ 8.7E+5 – 2.0E+6 with different considered reactors. However, the equipment cost and the manufacturing cost was accounted for only 10% of the total emergy. The reactor cost calculated based on data from chapter 5 was not highly affected the sustainability of the process. Besides, the increased equipment cost affected the F fraction. The trend from the increase in equipment cost would give the result similar to the sensitivity investigation.

6.3.3.8 Another scenario: natural gas as an imported resource

This investigation is to explore the significance of domestic or foreign resources on system sustainability. In the previous section, natural gas was considered a nonrenewable local resource. Thus, its contribution was included in the N. However, in this section, natural gas was considered as an imported resource. Therefore, its contribution would be included in the F. When natural gas was an imported resource, it does not change the values of UEV and ELR. However, it led to the decreased EYR because the numerator decreased. The results of the analysis are summarized in Tables 6.11 and 6.12. The sustainability of the process, ESI, decreased when resources of the process highly depended on the external resources. It was also noted that the EYR decreased drastically and the ESI of CC cases was slightly higher than CLC cases, which contradicted the former scenario. The ESIs of all cases were much lower than those of domestic natural gas cases. However, the CC case with the CO_2

capture process, case 2, provided slightly better ESI than the other cases. Comparing these two scenarios, the ESI of the former scenario was much higher than the latter. That is, if natural gas were a domestic resource, the system would be more self-sufficient. The analysis also shows not only process technology but also the sources of the major raw materials that determine the sustainability of power production.

Table 6.11 The F, L, R and N fractions of each case study when natural gas was included in the F fraction.

Case	Process description	F (sej/Y)	R (sej/Y)	N (sej/Y)
1	CC and HAT without CO_2 capture	4.81E+20	3.08E+19	0
2	CC with HAT and 96.27% CO_2 capture	5.30E+20	3.43E+19	0
3	CC with HAT and 77.76% CO_2 capture	5.03E+20	3.23E+19	0
4	CLC without HAT	6.02E+20	3.47E+19	0
5	CLC with HAT high heat recovery	4.41E+20	2.46E+19	0
6	CLC with HAT low heat recovery	4.53E+20	2.58E+19	0

Table 6.12 Emergy indicators of each case study when natural gas was included in F
fraction.

Case	Process description	UEV	EYR	ELR	ESI
1	CC and HAT without CO_2 capture	3.24E+05	1.064	15.615	0.0681
2	CC with HAT and 96.27% CO_2 capture	3.58E+05	1.065	15.433	0.0690
3	CC with HAT and 77.76% CO_2 capture	3.39E+05	1.064	15.569	0.0684
4	CLC without HAT	4.04E+05	1.058	17.363	0.0609
5	CLC with HAT high heat recovery	2.95E+05	1.056	17.933	0.0589
6	CLC with HAT low heat recovery	3.04E+05	1.057	17.577	0.0601

6.4 The three analysis tools comparison

From the evaluation, it was found that the best case was depended on the types
of analysis. In this study, three types of analysis for decision making were considered
based on thermal efficiency, economic performance, and emergy evaluation. The
thermal efficiency indicated the effectiveness of fuel usage. Case 5 was the best
solution since it gave the highest efficiency (55.84%). The ranking of thermal
efficiency was 5, 6, 1, 3, 2, 4. This analysis should not be selected because the process
without CO_2 management (case 1) would be selected before the process CO_2
management (case 2, 3 and 4). The economic analysis indicated the profit for
investment. Case 6 was best solution which it had 20.69 % IRR and 4.60 y of the
payback period. When the environmental impact was included in economic analysis
by include carbon tax, the ranking of economic performance was not changed.
However, the emergy analysis also gave a different conclusion from the former
analyses. The emergy analysis showed that case 4 was the best case because it had the
highest ESI (0.835). The high ESI indicated the high sustainability. In emergy
analysis, UEV indicated the usage of global resource, EYR indicated the economic

performance, ELR indicated the environmental loading, and ESI indicated the sustainability. Accordingly, the perspective of thermal efficiency and economic analysis were included in the emergy analysis. Case 5 was the best case in only the effectiveness of resources usage but low economic performance. Case 6 was the best case in economic performance, but the sustainability of case 6 was lower than case 4. Even though, the thermal efficiency of case 6 was low, but it was the highest sustainability. Accordingly, the resource usage, the economic performance and the environmental impact of case 4 was the best in the long period which could be operated with stability.

6.5 Conclusion

The main objective of this study was to evaluate technologies and their operations for decision making on power production. The effects of combustion types (CC and CLC), the CO2 capture efficiency, and the process configuration and operation were investigated. Since the emergy index is a holistic parameter that takes many factors into account, which were resource management, economics, environment, and sustainability, ESI. Accordingly, emergy analysis could be the better decision-making indicator. From the above analysis, case 4 could be the solution to this power production since it had high sustainability index and relatively high economic performance. The result also indicated that thermal efficiency alone was not adequate for the conclusion of technology selection since it considered only the efficient use of energy while ignoring other operating factors. The economic analysis had included all costs of the built plant, but it did not consider the environmental burden. Thus, the carbon tax or environmental tax could improve the economic model to satisfy both economic and environmental issues. However, some natural resources or environmental capitals were also not included in the current economic model. On the contrary, the emergy analysis was the tool that incorporates various factors from several dimensions, such as natural resources, human workforce, economics, environment, and others, into the analysis so that the evaluation could give a better holistic view of the solution than the former analyses.

Chapter 7
Conclusion and suggestion

Conclusion of the study

This study investigated the chemical looping combustion (CLC) process improvement for power production from energy management, system hydrodynamics, and a sustainability perspective.

In the first part, energy management was investigated to achieve the highest thermal efficiency of the CLC process with the HAT cycle for power production. The limitation of previous studies of the CLC study has individually investigated the effect of each parameter. However, the synergistic of the parameters in the system may influence each other. In this study, the 3^k factorial design was used for exploring these parametric effects and indicating their interaction with the systematic treatment. The power production from the air reactor is 2-5 times higher than the power production from the fuel reactor. Therefore, the parameters that might affect the power production from AR were selected, which including of 1) pressure of air reactor, 2) the number of air compressors, 3) compression ratio and 4) air flow rate. All of the case studies were simulated by Aspen plus program. The result indicated the pressure of the air reactor and compression method highly affected the thermal efficiency. The high pressure and method 3 provided high thermal efficiency. Method 3 provided high thermal efficiency because it led to the highest temperature discharged from the compression, which contributed to high power production from the air reactor and high thermal efficiency. With the systematic investigation, the thermal efficiency of the CLC process with the HAT cycle had higher than the previous study (57.7%). The optimum operating condition from this section would be used in the second and last parts.

In the second part, CLC could be used with solid and gaseous fuels. The challenge of solid fuel operation is incomplete combustion because of the slow gasification rate. The challenge of gaseous fuel operation is the improper operating condition, which provides the CO_2 emission to the environment. Accordingly, the operating conditions are crucial for suitable hydrodynamics achievement and the CO_2 capture efficiency of the system. The dual circulating fluidized bed reactor (DCFBR) was selected for the CLC system and investigated its operation by

2-D computational fluid dynamics (CFD) simulation. The CFD simulation was conducted by solving three conservative equations; continuity, momentum and energy of the considered system. The Eulerian method and the kinetic theory of granular flow were also used in this study. In this section, there were 2 objectives. First, it is to specify the suitable hydrodynamics' operating condition in the full-loop DCFBR for the CLC process. Second, hydrodynamic investigation of operating condition which achieved high thermal efficiency. The result for the solid fuel, the system hydrodynamics had validated with the experimental data before the model was further used in the study. The result of the operating conditions indicated that the low temperature and the low ratio of coal velocity to the oxygen carrier's weight provided the best performance of this system. For the gaseous fuel, the obtained operating conditions from the former investigation were used in this part. The result indicated high pre-exponential factor, low initial solid volume fraction (VOF), low velocity, and low CH_4 mass fraction in feed increased temperature and conversion. After that, the reactor size was estimated to provide the reactor cost. It will be used for economic and emergy analyses. Suitable hydrodynamic behavior provides good mixing and correct flow direction. From the simulation, it suggested keeping low velocity and low solid in the reactor. For the actual operation, the pressure balance at the loop seal was a crucial point to operate to obtain good hydrodynamic behavior, which provides the high performance of the CLC reactor.

In previous CLC study, the improvement of CLC had been developed only the efficiency and economic analysis viewpoints. However, the CLC process in sustainability improvement had not been investigated. In the last part of the study, three analyses, which were energy performance, economics, and sustainability, were evaluated to identify the best case of the CLC process by aiming to enhance the process sustainability. The emergy analysis investigated the sustainability of the process. Besides, six case studies were investigated to identify the effects of the combustion types (conventional combustion (CC) and CLC) and the system configuration (CO_2 capture stages and operating conditions). The case studies included 1) CC without CO_2 capture, 2) CC with HAT at 96.22% CO_2 capture, 3) CC with HAT at 77.76% CO_2 capture, 4) CLC without HAT, 5) CLC with HAT with high heat recovery, and 6) CLC with HAT with low heat recovery. The result indicated the

best-case study depending on the analysis, which obtained a different viewpoint. However, the emergy analysis expressed the holistic perspective, including the resource, the competition of investment, environmental loading, and sustainability. The sustainability of CLC was higher than in CC cases. The configuration and operating conditions affected the sustainability of the process. Case 4 was the best-case study because it obtained the highest sustainability since its local resource fraction was the highest. It reflected the self-sufficiency of this case was higher than others. The result indicated that the further improvement of the CLC process to achieve high sustainability was the increase of local resource dependence, especially the renewable local resource. On the other hand, when considering the process from the global viewpoint, case 5 will be the best since its UEV was the lowest. It implies the least natural resource consumption of the considered process.

Suggestion for the further study

The improvement of the CLC process in the perspective of sustainability was a novel investigation. From the emergy analysis, there are various potential factors to improve the CLC process's sustainability. First, by increasing the local renewable resources, the sustainability of process will be increased. O_2 in air and water are counted as the local renewable resources. The uses of O_2 in air and water in the system should be systematically investigated against the optimal sustainability index. The fuel for the fuel reactor could be changed to local renewable fuel, such as biomasses. Second, the type and life of an oxygen carrier should be considered since the oxygen carrier's transformity was high. Therefore, oxygen carrier materials with the same performance, but lower transformity should be investigated. The life expectancy of the oxygen carrier should also be considered since it will reduce its annual consumption. However, the materials' reactivity will also affect reactor hydrodynamics. Changing the oxygen carrier could need the reactor hydrodynamic investigation.

Index

The information for hydrodynamic investigation in chapter 5.

The heat capacity of all species in the mixtures was provided for consistent with Eq. I.1, as shown in Fig. I.1. The input data was shown in Table I.1. The heat of formation of mixtures was shown in Table I.2.

$$C_P = C_1 + C_2 T + C_3 T^2 + C_4 T^3 + C_5 T^4 + C_6 T^5 \tag{I.1}$$

Fig. I.1. The form of heat capacity in Ansys fluent programs

Table I.1 The input data for the heat capacity of the mixtures

Species	C1	C2	C3	C4	C5	C6
Ni	4.983E-01	6.451E-05				
NiO	6.330E-01	1.204E-04				
Al_2O_3	4.515E-01	1.500E-03	-9.000E-07	2.000E-10		
CH_4	2.200E+03	-2.620E+00	1.230E-02	-1.000E-05	3.000E-09	
O_2	9.303E+02	-3.829E-01	1.600E-03	-2.000E-06	8.000E-10	-1.000E-13
N_2	1.040E+03	2.260E-02	-4.000E-04	1.000E-06	-1.000E-09	3.000E-13
H_2O	1.874E+03	-4.006E-01	1.500E-03	-9.000E-07	2.000E-10	2.000E-15
CO_2	6.420E+02	-4.260E-02	4.000E-03	-7.000E-06	5.000E-09	-1.000E-12

Table I.2 The heat of formation of the mixtures.

Species	Standard state enthalpy (J/kmol)
Ni	0
NiO	-2.44E+08
Al_2O_3	-1.67E+09
CH_4	-7.45E+07
O_2	0
N_2	0
H_2O	-2.42E+08
CO_2	-3.94E+08
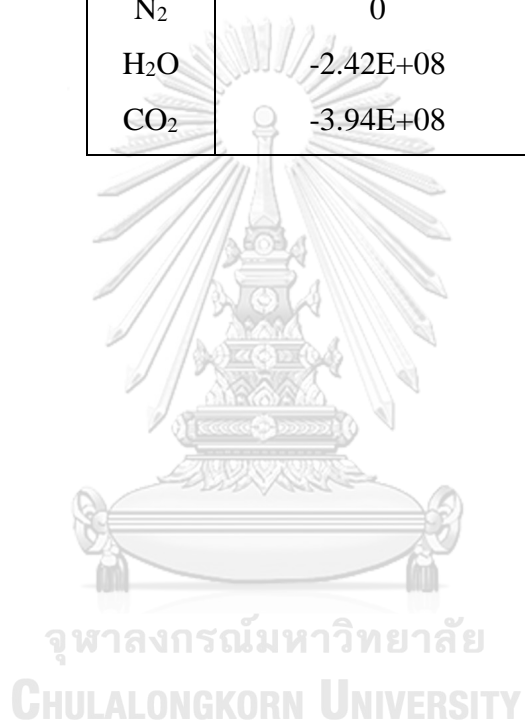
จุฬาลงกรณ์มหาวิทยาลัย

CHULALONGKORN UNIVERSITY

REFERENCES

[1]   IEA.   "Electricity   Information   2019."   IEA.
        https://www.iea.org/reports/electricity-information-2019 (accessed 16 April
        2020, 2020).

[2]   U. S. E. P. A. EPA. Overview of Greenhouse Gases [Online] Available:
        https://www.epa.gov/ghgemissions/overview-greenhouse-gases

[3]   T. u. s. e. p. IEA. Explore energy data by category, indicator, country or region
        [Online]   Available: https://www.iea.org/data-and-
        statistics?country=WORLD&fuel=CO2%20emissions&indicator=CO2%20em
        issions%20by%20energy%20source

[4]   F. Li, L. Zeng, and L.-S. Fan, "Biomass direct chemical looping process:
        Process simulation," *Fuel,* vol. 89, no. 12, pp. 3773-3784, 2010/12/01/ 2010,
        doi: https://doi.org/10.1016/j.fuel.2010.07.018.

[5]   F. Zerobin and T. Pröll, "Potential and limitations of power generation via
        chemical looping combustion of gaseous fuels," *International Journal of
        Greenhouse Gas Control,* vol. 64, pp. 174-182, 2017/09/01/ 2017, doi:
        https://doi.org/10.1016/j.ijggc.2017.07.011.

[6]   L. Han and G. M. Bollas, "Dynamic optimization of fixed bed chemical-
        looping combustion processes," *Energy,* vol. 112, pp. 1107-1119, 2016/10/01/
        2016, doi: https://doi.org/10.1016/j.energy.2016.07.031.

[7]   M. Kanniche, R. Gros-Bonnivard, P. Jaud, J. Valle-Marcos, J.-M. Amann, and
        C. Bouallou, "Pre-combustion, post-combustion and oxy-combustion in
        thermal power plant for CO_2 capture," *Applied Thermal Engineering,* vol. 30,
        no.   1,   pp.   53-62,   2010/01/01/   2010,   doi:
        https://doi.org/10.1016/j.applthermaleng.2009.05.005.

[8]   J. D. Figueroa, T. Fout, S. Plasynski, H. McIlvried, and R. D. Srivastava,
        "Advances in CO_2 capture technology—The U.S. Department of Energy's
        Carbon Sequestration Program," *International Journal of Greenhouse Gas
        Control,* vol. 2, no. 1, pp. 9-20, 2008/01/01/ 2008, doi:
        https://doi.org/10.1016/S1750-5836(07)00094-1.

[9]   M. W. Ajiwibowo, A. Darmawan, and M. Aziz, "A conceptual chemical
        looping combustion power system design in a power-to-gas energy storage
        scenario," *International Journal of Hydrogen Energy,* vol. 44, no. 19, pp.

9636-9642, 2019/04/12/ 2019, doi: https://doi.org/10.1016/j.ijhydene.2018.11.177.

[10] P. Wang *et al.*, "Structurally improved, urea-templated, K_2CO_3-based sorbent pellets for CO2 capture," *Chemical Engineering Journal,* vol. 374, pp. 20-28, 2019/10/15/ 2019, doi: https://doi.org/10.1016/j.cej.2019.05.091.

[11] C. Zhao *et al.*, "Capturing CO2 in flue gas from fossil fuel-fired power plants using dry regenerable alkali metal-based sorbent," *Progress in Energy and Combustion Science,* vol. 39, no. 6, pp. 515-534, 2013/12/01/ 2013, doi: https://doi.org/10.1016/j.pecs.2013.05.001.

[12] D. Fu and J. Xie, "Absorption capacity and viscosity for CO_2 capture process using [N1111][Gly] promoted K_2CO_3 aqueous solution," *The Journal of Chemical Thermodynamics,* vol. 102, pp. 310-315, 2016/11/01/ 2016, doi: https://doi.org/10.1016/j.jct.2016.07.026.

[13] E. E. Ünveren, B. Ö. Monkul, Ş. Sarıoğlan, N. Karademir, and E. Alper, "Solid amine sorbents for CO_2 capture by chemical adsorption: A review," *Petroleum,* vol. 3, no. 1, pp. 37-50, 2017/03/01/ 2017, doi: https://doi.org/10.1016/j.petlm.2016.11.001.

[14] S. C. Lee and J. C. Kim, "Dry Potassium-Based Sorbents for CO_2 Capture," *Catalysis Surveys from Asia,* vol. 11, no. 4, pp. 171-185, 2007/12/01 2007, doi: 10.1007/s10563-007-9035-z.

[15] A. Jayakumar, A. Gomez, and N. Mahinpey, "Post-combustion CO_2 capture using solid K_2CO_3: Discovering the carbonation reaction mechanism," *Applied Energy,* vol. 179, pp. 531-543, 2016/10/01/ 2016, doi: https://doi.org/10.1016/j.apenergy.2016.06.149.

[16] P. Nimmanterdwong, B. Chalermsinsuwan, and P. Piumsomboon, "Emergy analysis of three alternative carbon dioxide capture processes," *Energy,* vol. 128, pp. 101-108, 2017/06/01/ 2017, doi: https://doi.org/10.1016/j.energy.2017.03.154.

[17] M. Wang, A. S. Joel, C. Ramshaw, D. Eimer, and N. M. Musa, "Process intensification for post-combustion CO_2 capture with chemical absorption: A critical review," *Applied Energy,* vol. 158, pp. 275-291, 2015/11/15/ 2015, doi: https://doi.org/10.1016/j.apenergy.2015.08.083.

[18]   M. K. Mondal, H. K. Balsora, and P. Varshney, "Progress and trends in CO_2 capture/separation technologies: A review," *Energy,* vol. 46, no. 1, pp. 431-441, 2012/10/01/ 2012, doi: https://doi.org/10.1016/j.energy.2012.08.006.

[19]   A. Mukherjee, J. A. Okolie, A. Abdelrasoul, C. Niu, and A. K. Dalai, "Review of post-combustion carbon dioxide capture technologies using activated carbon," *Journal of Environmental Sciences,* vol. 83, pp. 46-63, 2019/09/01/ 2019, doi: https://doi.org/10.1016/j.jes.2019.03.014.

[20]   R. Soltani, M. A. Rosen, and I. Dincer, "Assessment of CO2 capture options from various points in steam methane reforming for hydrogen production," *International Journal of Hydrogen Energy,* vol. 39, no. 35, pp. 20266-20275, 2014/12/03/ 2014, doi: https://doi.org/10.1016/j.ijhydene.2014.09.161.

[21]   H. B. Carminati, J. L. de Medeiros, G. T. Moure, L. C. Barbosa, and O. d. Q. F. Araújo, "Low-emission pre-combustion gas-to-wire via ionic-liquid [Bmim][NTf2] absorption with high-pressure stripping," *Renewable and Sustainable Energy Reviews,* vol. 131, p. 109995, 2020/10/01/ 2020, doi: https://doi.org/10.1016/j.rser.2020.109995.

[22]   A. I. Escudero *et al.*, "Minimization of CO_2 capture energy penalty in second generation oxy-fuel power plants," *Applied Thermal Engineering,* vol. 103, pp. 274-281, 2016/06/25/ 2016, doi: https://doi.org/10.1016/j.applthermaleng.2016.04.116.

[23]   B. G. Miller, "13 - Carbon Dioxide Emissions Reduction and Storage," in *Clean Coal Engineering Technology (Second Edition)*, B. G. Miller Ed.: Butterworth-Heinemann, 2017, pp. 609-668.

[24]   M. Ishida and H. Jin, "CO_2 recovery in a power plant with chemical looping combustion," *Energy Conversion and Management,* vol. 38, pp. S187-S192, 1997/01/01/ 1997, doi: https://doi.org/10.1016/S0196-8904(96)00267-1.

[25]   H. Jin and M. Ishida, "A novel gas turbine cycle with hydrogen-fueled chemical-looping combustion," *International Journal of Hydrogen Energy,* vol. 25, no. 12, pp. 1209-1215, 2000/12/01/ 2000, doi: https://doi.org/10.1016/S0360-3199(00)00032-X.

[26]   R. Naqvi and O. Bolland, "Multi-stage chemical looping combustion (CLC) for combined cycles with CO_2 capture," *International Journal of Greenhouse*

Gas Control, vol. 1, no. 1, pp. 19-30, 2007/04/01/ 2007, doi: https://doi.org/10.1016/S1750-5836(07)00012-6.

[27] T. Ibrahim and P. D. M. M. Rahman, *Effective Parameters on Performance of Multipressure Combined Cycle Power Plants*. 2015, pp. 781503-781503.

[28] O. Brandvoll and O. Bolland, "Inherent CO_2 Capture Using Chemical Looping Combustion in a Natural Gas Fired Power Cycle," *Journal of Engineering for Gas Turbines and Power,* vol. 126, no. 2, pp. 316-321, 2004, doi: 10.1115/1.1615251.

[29] S. Ulgiati and M. T. Brown, "Quantifying the environmental support for dilution and abatement of process emissions: The case of electricity production," *Journal of Cleaner Production,* vol. 10, no. 4, pp. 335-348, 2002/08/01/ 2002, doi: https://doi.org/10.1016/S0959-6526(01)00044-0.

[30] M. Rajabi, M. Mehrpooya, Z. Haibo, and Z. Huang, "Chemical looping technology in CHP (combined heat and power) and CCHP (combined cooling heating and power) systems: A critical review," *Applied Energy,* vol. 253, p. 113544, 2019/11/01/ 2019, doi: https://doi.org/10.1016/j.apenergy.2019.113544.

[31] S. Chen, Q. Shi, Z. Xue, X. Sun, and W. Xiang, "Experimental investigation of chemical-looping hydrogen generation using Al2O3 or TiO2-supported iron oxides in a batch fluidized bed," *International Journal of Hydrogen Energy,* vol. 36, no. 15, pp. 8915-8926, 2011/07/01/ 2011, doi: https://doi.org/10.1016/j.ijhydene.2011.04.204.

[32] L.-S. Fan, *Chemical looping systems for fossil energy conversions*. John Wiley & Sons, 2011.

[33] S. Chen, J. Hu, and W. Xiang, "Process integration of coal fueled chemical looping hydrogen generation with SOFC for power production and CO_2 capture," *International Journal of Hydrogen Energy,* vol. 42, no. 48, pp. 28732-28746, 2017/11/30/ 2017, doi: https://doi.org/10.1016/j.ijhydene.2017.09.156.

[34] V. Spallina, P. Nocerino, M. C. Romano, M. van Sint Annaland, S. Campanari, and F. Gallucci, "Integration of solid oxide fuel cell (SOFC) and chemical looping combustion (CLC) for ultra-high efficiency power

generation and CO2 production," *International Journal of Greenhouse Gas Control,* vol. 71, pp. 9-19, 2018/04/01/ 2018, doi: https://doi.org/10.1016/j.ijggc.2018.02.005.

[35] M. Pérez-Fortes *et al.*, "Design of a Pilot SOFC System for the Combined Production of Hydrogen and Electricity under Refueling Station Requirements," *Fuel Cells,* vol. 19, no. 4, pp. 389-407, 2019, doi: 10.1002/fuce.201800200.

[36] P. Vairakannu and G. Kumari, "CO2-Oxy underground coal gasification integrated proton exchange membrane fuel cell operating in a chemical looping mode of reforming," *International Journal of Hydrogen Energy,* vol. 41, no. 44, pp. 20063-20077, 2016/11/26/ 2016, doi: https://doi.org/10.1016/j.ijhydene.2016.09.022.

[37] N. H. Behling, "Chapter 2 - Fuel Cells and the Challenges Ahead," in *Fuel Cells*, N. H. Behling Ed.: Elsevier, 2013, pp. 7-36.

[38] R. Napoli, M. Gandiglio, A. Lanzini, and M. Santarelli, "Techno-economic analysis of PEMFC and SOFC micro-CHP fuel cell systems for the residential sector," *Energy and Buildings,* vol. 103, pp. 131-146, 2015/09/15/ 2015, doi: https://doi.org/10.1016/j.enbuild.2015.06.052.

[39] L. F. de Diego, M. Ortiz, J. Adánez, F. García-Labiano, A. Abad, and P. Gayán, "Synthesis gas generation by chemical-looping reforming in a batch fluidized bed reactor using Ni-based oxygen carriers," *Chemical Engineering Journal,* vol. 144, no. 2, pp. 289-298, 2008/10/15/ 2008, doi: https://doi.org/10.1016/j.cej.2008.06.004.

[40] F. He, Y. Wei, H. Li, and H. Wang, "Synthesis gas generation by chemical-looping reforming using Ce-based oxygen carriers modified with Fe, Cu, and Mn oxides," *Energy & Fuels,* vol. 23, no. 4, pp. 2095-2102, 2009.

[41] Q. Zafar, T. Mattisson, and B. Gevert, "Integrated hydrogen and power production with CO_2 capture using chemical-looping reforming redox reactivity of particles of CuO, Mn_2O_3, NiO, and Fe_2O_3 using SiO_2 as a support," *Industrial & engineering chemistry research,* vol. 44, no. 10, pp. 3485-3496, 2005.

[42]   M. Rydén, A. Lyngfelt, and T. Mattisson, "Chemical-Looping Combustion and Chemical-Looping Reforming in a Circulating Fluidized-Bed Reactor Using Ni-Based Oxygen Carriers," *Energy & Fuels,* vol. 22, no. 4, pp. 2585-2597, 2008/07/01 2008, doi: 10.1021/ef800065m.

[43]   C. Zhou, K. Shah, and B. Moghtaderi, "Techno-Economic Assessment of Integrated Chemical Looping Air Separation for Oxy-Fuel Combustion: An Australian Case Study," *Energy & Fuels,* vol. 29, no. 4, pp. 2074-2088, 2015/04/16 2015, doi: 10.1021/ef5022076.

[44]   K. Shah, B. Moghtaderi, and T. Wall, "Selection of Suitable Oxygen Carriers for Chemical Looping Air Separation: A Thermodynamic Approach," *Energy & Fuels,* vol. 26, no. 4, pp. 2038-2045, 2012/04/19 2012, doi: 10.1021/ef300132c.

[45]   C. Zhou, K. Shah, H. Song, J. Zanganeh, E. Doroodchi, and B. Moghtaderi, "Integration Options and Economic Analysis of an Integrated Chemical Looping Air Separation Process for Oxy-fuel Combustion," *Energy & Fuels,* vol. 30, no. 3, pp. 1741-1755, 2016/03/17 2016, doi: 10.1021/acs.energyfuels.5b02209.

[46]   C.-C. Cormos, "Chemical Looping with Oxygen Uncoupling (CLOU) concepts for high energy efficient power generation with near total fuel decarbonisation," *Applied Thermal Engineering,* vol. 112, pp. 924-931, 2017/02/05/ 2017, doi: https://doi.org/10.1016/j.applthermaleng.2016.10.156.

[47]   A. H. Sahir, J. K. Dansie, A. L. Cadore, and J. S. Lighty, "A comparative process study of chemical-looping combustion (CLC) and chemical-looping with oxygen uncoupling (CLOU) for solid fuels," *International Journal of Greenhouse Gas Control,* vol. 22, pp. 237-243, 2014.

[48]   S. Ebrahimian and D. Iranshahi, "An investigative study on replacing the conventional furnaces of naphtha reforming with chemical looping combustion for clean hydrogen production," *International Journal of Hydrogen Energy,* vol. 45, no. 38, pp. 19405-19419, 2020/07/31/ 2020, doi: https://doi.org/10.1016/j.ijhydene.2019.10.092.

[49]   M. A. Petriz-Prieto, V. Rico-Ramirez, G. Gonzalez-Alatorre, F. I. Gómez-Castro, and U. M. Diwekar, "A comparative simulation study of power

generation plants involving chemical looping combustion systems," *Computers & Chemical Engineering,* vol. 84, pp. 434-445, 2016/01/04/ 2016, doi: https://doi.org/10.1016/j.compchemeng.2015.10.002.

[50] H. K. Kayadelen and Y. Ust, "Thermodynamic, environmental and economic performance optimization of simple, regenerative, STIG and RSTIG gas turbine cycles," *Energy,* vol. 121, pp. 751-771, 2017/02/15/ 2017, doi: https://doi.org/10.1016/j.energy.2017.01.060.

[51] G. Brighenti, P. Orts-Gonzalez, L. Sánchez de León, and P. K. Zachos, "Design point performance and optimization of humid air turbine power plants," *Applied Sciences (Switzerland),* vol. 7, 04/20 2017, doi: 10.3390/app7040413.

[52] A. A. Sullerey R, "Performance improvement of gas turbine cycles," *International Journal of Turbo Jet Engines,* vol. 25, pp. 209-210, 2008, doi: 10.1515/TJJ.2008.25.3.209.

[53] E. Sarath Yadav, T. Indiran, D. Nayak, C. Aditya Kumar, and M. Selvakumar, "Simulation study of distillation column using Aspen plus," *Materials Today: Proceedings,* 2020/09/04/ 2020, doi: https://doi.org/10.1016/j.matpr.2020.07.609.

[54] C. o. E. a. M. s. university. "ASPEN Tutorial." https://www.chems.msu.edu/resources/tutorials/ASPEN (accessed 29 2020).

[55] S. N. P. Vegendla, G. J. Heynderickx, and G. B. Marin, "Comparison of Eulerian–Lagrangian and Eulerian–Eulerian method for dilute gas–solid flow with side inlet," *Computers & Chemical Engineering,* vol. 35, no. 7, pp. 1192-1199, 2011/07/11/ 2011, doi: https://doi.org/10.1016/j.compchemeng.2010.09.001.

[56] S. Belošević, I. Tomanović, N. Crnomarković, and A. Milićević, "Full-scale CFD investigation of gas-particle flow, interactions and combustion in tangentially fired pulverized coal furnace," *Energy,* Article vol. 179, pp. 1036-1053, 2019, doi: 10.1016/j.energy.2019.05.066.

[57] X. Chen, J. Ma, X. Tian, J. Wan, and H. Zhao, "CPFD simulation and optimization of a 50 kWth dual circulating fluidized bed reactor for chemical looping combustion of coal," *International Journal of Greenhouse Gas*

Control, vol. 90, p. 102800, 2019/11/01/ 2019, doi: https://doi.org/10.1016/j.ijggc.2019.102800.

[58]   V. B. R. E. Silva and J. Cardoso, "Chapter 1 - Introduction and overview of using computational fluid dynamics tools," in *Computational Fluid Dynamics Applied to Waste-to-Energy Processes*, V. B. R. E. Silva and J. Cardoso Eds.: Butterworth-Heinemann, 2020, pp. 3-28.

[59]   N. Edomah, "Economics of Energy Supply☆," in *Reference Module in Earth Systems and Environmental Sciences*: Elsevier, 2018.

[60]   M. S. Peters, K. D. Timmerhaus, and R. E. West, *Plant design and economics for chemical engineers*, 5th ed. ed. (McGraw-Hill chemical engineering series). McGraw-Hill, 2003.

[61]   W. B. Bequette, *Process control : modeling, design, and simulation* (Prentice-Hall international series in the physical and chemical engineering sciences). Prentice Hall PTR, 2003.

[62]   H. T. Odum, *Environmental accounting : EMERGY and environment decision making*. New York : John Wiley, c1996., 1996.

[63]   K. Cao and X. Feng, "Distribution of emergy indices and its application," *Energy & fuels,* vol. 21, no. 3, pp. 1717-1723, 2007.

[64]   M. Ishida, D. Zheng, and T. Akehata, "Evaluation of a chemical-looping-combustion power-generation system by graphic exergy analysis," *Energy,* Article vol. 12, no. 2, pp. 147-154, 1987, doi: 10.1016/0360-5442(87)90119-8.

[65]   Ø. Brandvoll and O. Bolland, "Inherent CO_2 Capture Using Chemical Looping Combustion in a Natural Gas Fired Power Cycle," *Journal of Engineering for Gas Turbines and Power,* vol. 126, no. 2, pp. 316-321, 2004, doi: 10.1115/1.1615251.

[66]   A. Olaleye and M. Wang, "Technical and Economic Analysis of Chemical Looping Combustion with Humid Air Turbine Power Cycle," in *Computer Aided Chemical Engineering*, vol. 33, J. J. Klemeš, P. S. Varbanov, and P. Y. Liew Eds.: Elsevier, 2014, pp. 1123-1128.

[67]   R. J. Basavaraja and S. Jayanti, "Viability of fuel switching of a gas-fired power plant operating in chemical looping combustion mode," *Energy,* vol.

81, pp. 213-221, 2015/03/01/ 2015, doi: https://doi.org/10.1016/j.energy.2014.12.027.

[68]   M. Ishida and H. Jin, "A new advanced power-generation system using chemical-looping combustion," *Energy,* vol. 19, no. 4, pp. 415-422, 1994/04/01/ 1994, doi: https://doi.org/10.1016/0360-5442(94)90120-1.

[69]   A. K. Olaleye and M. Wang, "Techno-economic analysis of chemical looping combustion with humid air turbine power cycle," *Fuel,* vol. 124, pp. 221-231, 2014/05/15/ 2014, doi: https://doi.org/10.1016/j.fuel.2014.02.002.

[70]   J. Fan, H. Hong, L. Zhu, Z. Wang, and H. Jin, "Thermodynamic evaluation of chemical looping combustion for combined cooling heating and power production driven by coal," *Energy Conversion and Management,* vol. 135, pp. 200-211, 2017/03/01/ 2017, doi: https://doi.org/10.1016/j.enconman.2016.12.022.

[71]   J. Fan, H. Hong, L. Zhu, Q. Jiang, and H. Jin, "Thermodynamic and environmental evaluation of biomass and coal co-fuelled gasification chemical looping combustion with CO_2 capture for combined cooling, heating and power production," *Applied Energy,* vol. 195, pp. 861-876, 2017/06/01/ 2017, doi: https://doi.org/10.1016/j.apenergy.2017.03.093.

[72]   S. H. Jensen, X. Sun, S. D. Ebbesen, R. Knibbe, and M. Mogensen, "Hydrogen and synthetic fuel production using pressurized solid oxide electrolysis cells," *International Journal of Hydrogen Energy,* vol. 35, no. 18, pp. 9544-9549, 2010/09/01/ 2010, doi: https://doi.org/10.1016/j.ijhydene.2010.06.065.

[73]   Z. Peng, E. Doroodchi, Y. A. Alghamdi, K. Shah, C. Luo, and B. Moghtaderi, "CFD–DEM simulation of solid circulation rate in the cold flow model of chemical looping systems," *Chemical Engineering Research and Design,* vol. 95, pp. 262-280, 2015/03/01/ 2015, doi: https://doi.org/10.1016/j.cherd.2014.11.005.

[74]   W. Yin, S. Wang, K. Zhang, and Y. He, "Numerical investigation of in situ gasification chemical looping combustion of biomass in a fluidized bed reactor," *Renewable Energy,* vol. 151, pp. 216-225, 2020/05/01/ 2020, doi: https://doi.org/10.1016/j.renene.2019.11.016.

[75] J. May, F. Alobaid, P. Ohlemüller, A. Stroh, J. Ströhle, and B. Epple, "Reactive two–fluid model for chemical–looping combustion – Simulation of fuel and air reactors," *International Journal of Greenhouse Gas Control,* vol. 76, pp. 175-192, 2018/09/01/ 2018, doi: https://doi.org/10.1016/j.ijggc.2018.06.023.

[76] K. M. Merrett and K. J. Whitty, "Evaluation of coal conversion pathways in fluidized bed chemical looping combustion with oxygen uncoupling (CLOU)," *Fuel,* vol. 258, p. 116157, 2019/12/15/ 2019, doi: https://doi.org/10.1016/j.fuel.2019.116157.

[77] P. Yu, Z. Luo, Q. Wang, and M. Fang, "Life cycle assessment of transformation from a sub-critical power plant into a polygeneration plant," *Energy Conversion and Management,* vol. 198, p. 111801, 2019/10/15/ 2019, doi: https://doi.org/10.1016/j.enconman.2019.111801.

[78] B. B. Kanbur, L. Xiang, S. Dubey, F. H. Choo, and F. Duan, "Life cycle integrated thermoeconomic assessment method for energy conversion systems," *Energy Conversion and Management,* vol. 148, pp. 1409-1425, 2017/09/15/ 2017, doi: https://doi.org/10.1016/j.enconman.2017.06.079.

[79] R. J. Thorne *et al.*, "Environmental impacts of a chemical looping combustion power plant," *International Journal of Greenhouse Gas Control,* vol. 86, pp. 101-111, 2019/07/01/ 2019, doi: https://doi.org/10.1016/j.ijggc.2019.04.011.

[80] J. Yang and B. Chen, "Emergy-based sustainability evaluation of wind power generation systems," *Applied Energy,* vol. 177, pp. 239-246, 2016/09/01/ 2016, doi: https://doi.org/10.1016/j.apenergy.2016.05.126.

[81] R. A. Herendeen, "Energy analysis and EMERGY analysis—a comparison," *Ecological Modelling,* vol. 178, no. 1, pp. 227-237, 2004/10/15/ 2004, doi: https://doi.org/10.1016/j.ecolmodel.2003.12.017.

[82] M. Brown, M. Wackernagel, and C. A. S. Hall, "Chapter 25 - Comparative Estimates of Sustainability: Economic, Resource Base, Ecological Footprint, and Emergy," in *Quantifying Sustainable Development*, C. A. S. Hall, C. L. Perez, and G. Leclerc Eds. San Diego: Academic Press, 2000, pp. 695-714.

[83] L. Lugaric and S. Krajcar, "Transforming cities towards sustainable low-carbon energy systems using emergy synthesis for support in decision

making," *Energy Policy,* vol. 98, pp. 471-482, 2016/11/01/ 2016, doi: https://doi.org/10.1016/j.enpol.2016.09.028.

[84] S. Yazdani, E. Salimipour, and M. S. Moghaddam, "A comparison between a natural gas power plant and a municipal solid waste incineration power plant based on an emergy analysis," *Journal of Cleaner Production,* vol. 274, p. 123158, 2020/11/20/ 2020, doi: https://doi.org/10.1016/j.jclepro.2020.123158.

[85] S. Sha and M. Hurme, "Emergy evaluation of combined heat and power plant processes," *Applied Thermal Engineering,* vol. 43, pp. 67-74, 2012/10/01/ 2012, doi: https://doi.org/10.1016/j.applthermaleng.2011.11.063.

[86] H. Zhang, X. Guan, Y. Ding, and C. Liu, "Emergy analysis of Organic Rankine Cycle (ORC) for waste heat power generation," *Journal of Cleaner Production,* vol. 183, pp. 1207-1215, 2018/05/10/ 2018, doi: https://doi.org/10.1016/j.jclepro.2018.02.170.

[87] L. Wang, W. Ni, and Z. Li, "Emergy evaluation of combined heat and power plant eco-industrial park (CHP plant EIP)," *Resources, Conservation and Recycling,* vol. 48, no. 1, pp. 56-70, 2006/07/01/ 2006, doi: https://doi.org/10.1016/j.resconrec.2005.12.012.

[88] S. Ulgiati, S. Bargigli, and M. Raugei, "An emergy evaluation of complexity, information and technology, towards maximum power and zero emissions," *Journal of Cleaner Production,* vol. 15, no. 13, pp. 1359-1372, 2007/09/01/ 2007, doi: https://doi.org/10.1016/j.jclepro.2006.07.008.

[89] E. Neau, O. Hernández-Garduza, J. Escandell, C. Nicolas, and I. Raspo, *The Soave, Twu and Boston–Mathias alpha functions in cubic equations of state: Part I. Theoretical analysis of their variations according to temperature.* 2009, pp. 87–93.

[90] D. C. Montgomery, *Design and analysis of experiments*, 5th ed. ed. New York: John Wiley, 2001.

[91] H. P. Hamers, F. Gallucci, P. D. Cobden, E. Kimball, and M. van Sint Annaland, "CLC in packed beds using syngas and CuO/Al_2O_3: Model description and experimental validation," *Applied Energy,* vol. 119, pp. 163-172, 2014/04/15/ 2014, doi: https://doi.org/10.1016/j.apenergy.2013.12.053.

[92]   R. Porrazzo, G. White, and R. Ocone, "Fuel reactor modelling for chemical looping combustion: From micro-scale to macro-scale," *Fuel,* vol. 175, pp. 87-98, 2016/07/01/ 2016, doi: https://doi.org/10.1016/j.fuel.2016.01.041.

[93]   Q. He, G. Li, C. Lu, D. Du, and W. Liu, "A compressed air energy storage system with variable pressure ratio and its operation control," *Energy,* vol. 169, pp. 881-894, 2019/02/15/ 2019, doi: https://doi.org/10.1016/j.energy.2018.12.108.

[94]   W. L. Luyben, "Compressor Heuristics for Conceptual Process Design," *Industrial & Engineering Chemistry Research,* vol. 50, no. 24, pp. 13984-13989, 2011/12/21 2011, doi: 10.1021/ie202027h.

[95]   W. Seider, J. Seader, D. Lewin, and S. Widagdo, "Product and Process Design Principles: Synthesis, Analysis, and Design, Section 9.3," ed: Wiley, 2008.

[96]   R. Turton, R. C. Bailie, W. B. Whiting, and J. A. Shaeiwitz, *Analysis, synthesis and design of chemical processes*. Pearson Education, 2008.

[97]   M. Su, H. Zhao, and J. Ma, "Computational fluid dynamics simulation for chemical looping combustion of coal in a dual circulation fluidized bed," *Energy Conversion and Management,* vol. 105, pp. 1-12, 2015/11/15/ 2015, doi: https://doi.org/10.1016/j.enconman.2015.07.042.

[98]   B. Chalermsinsuwan, P. Kuchonthara, and P. Piumsomboon, "Effect of circulating fluidized bed reactor riser geometries on chemical reaction rates by using CFD simulations," *Chemical Engineering and Processing: Process Intensification,* vol. 48, no. 1, pp. 165-177, 2009/01/01/ 2009, doi: https://doi.org/10.1016/j.cep.2008.03.008.

[99]   D. Smoot, L and P. Smith, J, *Coal combustion and gasification*. Springer Science & Business Media, 2013.

[100]   R. C. Everson, H. W. J. P. Neomagus, H. Kasaini, and D. Njapha, "Reaction kinetics of pulverized coal-chars derived from inertinite-rich coal discards: Characterisation and combustion," *Fuel,* vol. 85, no. 7, pp. 1067-1075, 2006/05/01/ 2006, doi: https://doi.org/10.1016/j.fuel.2005.10.025.

[101]   K. Mahalatkar, J. Kuhlman, E. D. Huckaby, and T. O'Brien, "Computational fluid dynamic simulations of chemical looping fuel reactors utilizing gaseous

fuels," *Chemical Engineering Science,* vol. 66, no. 3, pp. 469-479, 2011/02/01/ 2011, doi: https://doi.org/10.1016/j.ces.2010.11.003.

[102] A. Abad, J. Adánez, F. García-Labiano, L. F. de Diego, P. Gayán, and J. Celaya, "Mapping of the range of operational conditions for Cu-, Fe-, and Ni-based oxygen carriers in chemical-looping combustion," *Chemical Engineering Science,* vol. 62, no. 1, pp. 533-549, 2007/01/01/ 2007, doi: https://doi.org/10.1016/j.ces.2006.09.019.

[103] F. Bustamante *et al.*, "High-temperature kinetics of the homogeneous reverse water–gas shift reaction," *AIChE Journal,* vol. 50, no. 5, pp. 1028-1041, 2004/05/01 2004, doi: 10.1002/aic.10099.

[104] W. G. Don and H. P. Robert, *Perry's Chemical Engineers' Handbook, Eighth Edition*, 8th ed. / ed. New York: McGraw-Hill Education (in en), 2008.

[105] S. Boonprasop, B. Chalermsinsuwan, and P. Piumsomboon, "CO_2 sorption and sorbent depressurized regeneration in circulating-turbulent fluidized bed regime," *Journal of Environmental Chemical Engineering,* vol. 7, no. 1, p. 102928, 2019/02/01/ 2019, doi: https://doi.org/10.1016/j.jece.2019.102928.

[106] S. Boonprasop, D. Gidaspow, B. Chalermsinsuwan, and P. Piumsomboon, "CO_2 capture in a multistage CFB: Part I: Number of stages," *AIChE Journal,* vol. 63, no. 12, pp. 5267-5279, 2017/12/01 2017, doi: 10.1002/aic.15776.

[107] S. Boonprasop, D. Gidaspow, B. Chalermsinsuwan, and P. Piumsomboon, "CO_2 capture in a multistage CFB: Part II: Riser with multiple cooling stages," *AIChE Journal,* vol. 63, no. 12, pp. 5280-5289, 2017/12/01 2017, doi: 10.1002/aic.15777.

[108] L. Zhu, Y. He, L. Li, and P. Wu, "Tech-economic assessment of second-generation CCS: Chemical looping combustion," *Energy,* vol. 144, pp. 915-927, 2018/02/01/ 2018, doi: https://doi.org/10.1016/j.energy.2017.12.047.

[109] E. Johansson, T. Mattisson, A. Lyngfelt, and H. Thunman, "Combustion of Syngas and Natural Gas in a 300 W Chemical-Looping Combustor," *Chemical Engineering Research and Design,* vol. 84, no. 9, pp. 819-827, 2006/09/01/ 2006, doi: https://doi.org/10.1205/cherd05024.

[110] B. Shi, W. Xu, W. Wu, and P.-C. Kuo, "Techno-economic analysis of oxy-fuel IGCC power plants using integrated intermittent chemical looping air

separation," *Energy Conversion and Management,* vol. 195, pp. 290-301, 2019/09/01/ 2019, doi: https://doi.org/10.1016/j.enconman.2019.05.006.

[111] W. Sakdasri, R. Sawangkeaw, and S. Ngamprasertsith, "Techno-economic analysis of biodiesel production from palm oil with supercritical methanol at a low molar ratio," *Energy,* vol. 152, pp. 144-153, 2018/06/01/ 2018, doi: https://doi.org/10.1016/j.energy.2018.03.125.

[112] J. Horowitz, J.-A. Cronin, H. Hawkins, L. Konda, and A. Yuskavage, "Methodology for Analyzing a Carbon Tax Methodology for Analyzing a Carbon Tax," *Office of Tax Analysis Working Paper,* vol. 115, 01/01 2017.

[113] M. Ishida, M. Yamamoto, and T. Ohba, "Experimental results of chemical-looping combustion with $NiO/NiAl_2O_4$ particle circulation at 1200^oC," *Energy Conversion and Management,* vol. 43, pp. 1469-1478, 2002.

[114] G. Huijun, S. Laihong, F. Fei, and J. Shouxi, "Experiments on biomass gasification using chemical looping with nickel-based oxygen carrier in a $25\ kW_{th}$ reactor," *Applied Thermal Engineering,* vol. 85, pp. 52-60, 2015/06/25/ 2015, doi: https://doi.org/10.1016/j.applthermaleng.2015.03.082.

[115] S. Yang, X. Liu, and S. Wang, "CFD simulation of air-blown coal gasification in a fluidized bed reactor with continuous feedstock," *Energy Conversion and Management,* vol. 213, p. 112774, 2020/06/01/ 2020, doi: https://doi.org/10.1016/j.enconman.2020.112774.

[116] S. R. Son and S. D. Kim, "Chemical-Looping Combustion with NiO and Fe_2O_3 in a Thermobalance and Circulating Fluidized Bed Reactor with Double Loops," *Industrial & Engineering Chemistry Research,* vol. 45, no. 8, pp. 2689-2696, 2006/04/01 2006, doi: 10.1021/ie050919x.

[117] H. Jin, T. Okamoto, and M. Ishida, "Development of a Novel Chemical-Looping Combustion: Synthesis of a Solid Looping Material of $NiO/NiAl_2O_4$," *Industrial & Engineering Chemistry Research,* vol. 38, no. 1, pp. 126-132, 1999/01/01 1999, doi: 10.1021/ie9803265.

[118] D. Ipsakis, E. Heracleous, L. Silvester, D. B. Bukur, and A. A. Lemonidou, "Kinetic modeling of NiO-based oxygen carriers for the sorption enhanced chemical looping steam CH_4 reforming," *Materials Today: Proceedings,* vol.

5, no. 14, Part 1, pp. 27353-27361, 2018/01/01/ 2018, doi: https://doi.org/10.1016/j.matpr.2018.09.051.

[119] T. Shen, S. Wang, J. Yan, L. Shen, and H. Tian, "Performance improvement of chemical looping combustion with coal by optimizing operational strategies in a 3 kW_{th} interconnected fluidized bed," *International Journal of Greenhouse Gas Control,* vol. 98, p. 103060, 2020/07/01/ 2020, doi: https://doi.org/10.1016/j.ijggc.2020.103060.

[120] O. y. Brandvoll and O. Bolland, "Inherent CO2 Capture Using Chemical Looping Combustion in a Natural Gas Fired Power Cycle," in *ASME Turbo Expo 2002: Power for Land, Sea, and Air*, 2002, vol. Volume 2: Turbo Expo 2002, Parts A and B, pp. 493-499, doi: 10.1115/gt2002-30129. [Online]. Available: https://doi.org/10.1115/GT2002-30129

[121] Y. Hu, G. Xu, C. Xu, and Y. Yang, "Thermodynamic analysis and techno-economic evaluation of an integrated natural gas combined cycle (NGCC) power plant with post-combustion CO2 capture," *Applied Thermal Engineering,* vol. 111, pp. 308-316, 2017/01/25/ 2017, doi: https://doi.org/10.1016/j.applthermaleng.2016.09.094.

[122] Z. Hamidouche, E. Masi, P. Fede, O. Simonin, K. Mayer, and S. Penthor, "Unsteady three-dimensional theoretical model and numerical simulation of a 120-kW chemical looping combustion pilot plant," *Chemical Engineering Science,* vol. 193, pp. 102-119, 2019/01/16/ 2019, doi: https://doi.org/10.1016/j.ces.2018.08.032.

[123] C. A. Tassinari, S. H. Bonilla, F. Agostinho, C. M. V. B. Almeida, and B. F. Giannetti, "Evaluation of two hydropower plants in Brazil: using emergy for exploring regional possibilities," *Journal of Cleaner Production,* vol. 122, pp. 78-86, 2016/05/20/ 2016, doi: https://doi.org/10.1016/j.jclepro.2016.01.077.

[124] S. Bastianoni, D. Campbell, R. Ridolfi, and F. Pulselli, "The solar transformity of petroleum fuels," *Ecological modelling,* vol. 220, no. 1, pp. 40-50, 2009.

[125] S. Sha and M. Hurme, "The solar transformity of heat and power in coproduction," *Ecological Engineering,* vol. 106, pp. 392-399, 09/01 2017, doi: 10.1016/j.ecoleng.2017.06.020.

[126] I. Andrić, N. Jamali-Zghal, M. Santarelli, B. Lacarrière, and O. Le Corre, "Environmental performance assessment of retrofitting existing coal fired power plants to co-firing with biomass: carbon footprint and emergy approach," *Journal of Cleaner Production,* vol. 103, pp. 13-27, 2015/09/15/ 2015, doi: https://doi.org/10.1016/j.jclepro.2014.08.019.

[127] Q. Yang, G. Q. Chen, S. Liao, Y. H. Zhao, H. W. Peng, and H. P. Chen, "Environmental sustainability of wind power: An emergy analysis of a Chinese wind farm," *Renewable and Sustainable Energy Reviews,* vol. 25, pp. 229-239, 2013/09/01/ 2013, doi: https://doi.org/10.1016/j.rser.2013.04.013.

[128] E. Buonocore, L. Vanoli, A. Carotenuto, and S. Ulgiati, "Integrating life cycle assessment and emergy synthesis for the evaluation of a dry steam geothermal power plant in Italy," *Energy,* vol. 86, pp. 476-487, 2015/06/15/ 2015, doi: https://doi.org/10.1016/j.energy.2015.04.048.

จุฬาลงกรณ์มหาวิทยาลัย

CHULALONGKORN UNIVERSITY

VITA

NAME	Watchara Uraisakul
DATE OF BIRTH	9 December 1987
PLACE OF BIRTH	Lampang
INSTITUTIONS ATTENDED	B.Sc and M.Sc Chemical Engineering, Chulalongkorn University
HOME ADDRESS	109/145, Moo 3, Tumbon Klongsuanploo, Ayutthaya 13000
PUBLICATION	1) CFD simulation of fuel reactor in chemical looping combustion 2) Hydrodynamics of dual circulating fluidized bed reactor for chemical looping combustion 3) Sustainability of natural gas chemical looping combustion from efficiency, economic and emergy analyses
AWARD RECEIVED	-

จุฬาลงกรณ์มหาวิทยาลัย
CHULALONGKORN UNIVERSITY